

**High resolution leaf fall monitoring
using hemispherical NIR imagery**

By

Jennifer Louise Alice Kirby

A thesis submitted to the University of Birmingham for the degree of

DOCTOR OF PHILOSOPHY

Word count: 43,777

Department of Geography,
School of Geography, Earth & Environmental Sciences,
University of Birmingham,

B15 2TT,

UK

July 2019

UNIVERSITY OF
BIRMINGHAM

University of Birmingham Research Archive

e-theses repository

This unpublished thesis/dissertation is copyright of the author and/or third parties. The intellectual property rights of the author or third parties in respect of this work are as defined by The Copyright Designs and Patents Act 1988 or as modified by any successor legislation.

Any use made of information contained in this thesis/dissertation must be in accordance with that legislation and must be properly acknowledged. Further distribution or reproduction in any format is prohibited without the permission of the copyright holder.

Abstract

'Leaves on the line' is a common phrase heard across autumn on the UK rail network. Leaves that have fallen onto the rail track coupled with adverse weather conditions such as drizzle, combine to create a gel layer on the rail head. This gel reduces the adhesion between the wheels of a train and the rail track. The reduction in adhesion leads to problems with acceleration and deceleration of the train as well as damage to the train itself, resulting in delays across the network; costing the UK rail industry over £300 million per year. Leaf fall and low adhesion forecasts allow the rail network to prepare for large leaf fall and low adhesion events.

One of the main inputs into a leaf fall forecast model is the percentage of leaves that have fallen in a given area. At the Met Office, this input is currently conducted by trained leaf fall observers. This research develops a new, alternative method to record leaf fall using a low-cost Raspberry Pi device in order to improve leaf fall observations at a high spatial and temporal scale. The device uses hemispherical images in the near-infrared spectrum to capture the change in leaf canopy from full canopy to bare tree. The Raspberry Pi device is comparable to the current best practice for hemispherical photography, the Nikon Coolpix camera and could be offered as an alternative to current leaf fall observations. This device was tested on Oak, Birch and Beech trees across two autumn seasons.

This research further tested the possibility of mounting the Raspberry Pi onto a train in order to capture data along a rail line; the initial testing showed that the Raspberry Pi device could capture images at 125mph and further discusses the next stages of development needed to make the device operational on the UK rail network.

Dedicated to the Kirbys, the Ridds, the Gannons and the Ents

For their support, dedication and inspiration

Acknowledgements

I would like to thank my supervisor Professor Lee Chapman for his guidance, advice and support throughout this PhD without which this project would not have been possible. I would also like to thank Dr Victoria Chapman as well as the leaf fall team at the Met Office for allowing me insight into how the leaf fall and low adhesion forecast model, discussed in this research, is conducted. I would also like to thank the Rail Safety and Standards Board for funding part of this project, specifically Giulia Lorenzini and Anup Chalisey for their time and encouragement throughout this project and the opportunities that they have given me to interact with the rail industry throughout this research. This interaction with the rail industry also allowed me to meet regularly with the Adhesion Working Group, a consortium of industry and university partners that meet to discuss the problems of rail adhesion, their help and enthusiasm was vital to the completion of this project. A special thank you must also be made to the Birmingham Institute of Forest Research for showcasing my research to the forestry community and promoting my work at conferences and to the Engineering Physical Science Research council for funding part of this project.

Experiments in this research were also conducted with the help of specific people throughout the PhD. A special thank you to Virgin Trains West Coast team for allowing me access to the train cab for the experiments conducted in chapter six, in particular the generous help of Michael Jacks and Russel Pearce. Experiments in chapter three of this project were completed using equipment and guidance from the Physics department at the University of Birmingham in particular the teaching and advice of David Hoyland, Graham Kirkby, Matthew Angling and John Bryant.

I would also like to thank Richard Johnson who was always around to help make and develop equipment for this PhD project. His wisdom, enthusiasm and happy attitude to engineering allowed the fast and resourceful development of the leaf fall recording device. Without him this project would not have been possible.

I was also like to thank the people who have helped with the completion of this PhD on a personal level. Firstly, my parents Helen and Paul Kirby; without their support throughout my education this research would not have been undertaken. I would also like to thank Karen and Phil Stern for always asking about my research and offering advice and support throughout my academic career. Charlotte Gannon, Christine Flowers, the entire Kirby, Ridd, Tipper and Dark families also deserve to be acknowledged for always asking about my research and offering an endless supply of support.

I would also like to thank my fellow PhD students in Room 425 for the coffee breaks, the long running lunches and the friendly encouragement all the students give to each other throughout the PhD process. In particular I would like to thank Helen Pearce and Katie Reilly for the breakfasts at Cherry Reds, the Costa Coffee runs, the supply of brain jelly sweets but most importantly their friendship throughout this process. I also need to thank the song "Into the West" from the Lord of the Rings soundtrack that was played on repeat throughout the most stressful parts of this PhD process.

Finally, I would like to thank Benjamin Gannon who has gone above and beyond what a partner needed to do in order to help me succeed in completing this project. During the four years of this PhD, Ben would wake up at 4 am and drive me to the rail station in order to get me to the Met Office leaf fall team in time for their autumn modelling sessions, he would also accompany me at sunrise to country parks in order for me to

conduct experiments in good lighting conditions using the Raspberry Pi device and would always be encouraging even when experiments went wrong or I forgot pieces of equipment. Without his time, support, encouragement and determination this project would not have been possible.

Thank you.

Contents Page

Abstract	ii
Dedication.....	iii
Acknowledgements	iv
Content Page.....	vii
List of Figures.....	xiii
List of Tables.....	xviii
Chapter One – Autumn effects on the UK rail network	1
1.1 Introduction.....	1
1.2 Vegetation and Railways	6
1.2.1 Types of vegetation around the rail network.....	12
1.3 Low Adhesion	14
1.4 The cost of Low Adhesion.....	16
1.5 Causes of Low Adhesion	18
1.5.1 The ‘Chemical’ Layer.....	20
1.5.2 The ‘Slippery’ Layer	20
1.6 Measuring Low Adhesion	23
1.7 Low Adhesion Safety and Performance Consequences	28
1.7.1 Station OVERRUNS and Station Stop Starts	30
1.7.2 Signals Passes At Danger (SPADs)	30
1.7.3 Wrong Side Track Circuit Failures (WSTCF)	31
1.7.4 Public Performance Measures (PPM)	33
1.8 Low Adhesion Mitigation and Management	37
1.8.1 Track Based Mitigation Tools	38

1.8.1.1	Water Jetting.....	38
1.8.1.2	Sandite and Sanding.....	39
1.8.1.3	Laser Treatment	40
1.8.2	Vegetation Mitigation	41
1.8.3	Vehicle and Driver Mitigation	42
1.8.4	Adhesion Management Tools	44
1.8.5	ACCAT system London Underground.....	45
1.9	Low Adhesion Forecast.....	46
1.10	Research Gap	53
1.11	Aims and Objectives	55
1.12	Thesis Outline.....	58
	Chapter One Summary.....	60
	Chapter Two – Review of leaf fall measurement techniques.....	61
2.	Introduction to Measurement Techniques.....	61
2.1	Direct Vegetation Measurement Techniques	62
2.1.1	Leaf Fall Observers.....	63
2.1.2	Harvest Sampling	63
2.1.3	Sap Sampling	65
2.1.4	Leaf Traps and Needle Point Sampling	66
2.2	Indirect Vegetation Measurement Techniques	67
2.2.1	Radiation Methods.....	68
2.2.2	Near-infrared Technology	69
2.2.3	Normalised Difference Vegetation Index (NDVI)	72
2.2.4	Remote Sensing in Forestry Research.....	73
2.2.5	Remote Sensing to Capture Change in Forest Over Large Areas.....	75

2.2.6	Ground Based Remote Sensing.....	77
2.2.7	Sky-View Factors	78
2.2.8	Hemispherical Digital Photography	83
2.2.9	Near-infrared Hemispherical Photography.....	84
2.3	Evolution of Scientific Equipment	86
2.4	The ‘Internet of Things’ and mobile phones as low-cost sensors	90
2.5	Raspberry Pi Advancement	94
2.5.1	Raspberry Pi Cameras	96
2.5.2	Raspberry Pi Software	99
2.6	Methodological Considerations.....	99
2.6.1	Direct Method Considerations.....	100
2.6.2	Indirect Method Considerations	101
2.6.3	Low-cost Sensor Considerations	102
	Chapter Two Summary	103
	Chapter Three– Development of a low-cost leaf fall sensor	104
3.1	Introduction.....	104
3.2	Mobile Phone Adaption	106
3.3	Nikon Coolpix Cameras and Fisheye Lenses	109
3.4	Adapting a Raspberry Pi	115
3.5	Comparison of Fisheye Lenses	115
3.6	Adapting a PI NoIR Camera to Take Hemispherical Images	119
3.7	Comparison of Nikon camera and PI NoIR Raspberry Pi Camera.	120
3.7.1	General Specifications.....	120
3.7.2	Distortion Analysis	122
3.8	Sky-View Factor Analysis	124

3.9 Near-Infrared Capabilities	127
3.10 Conclusions	127
Chapter Three Summary	129
Chapter Four– Designing an operational leaf fall device for an autumn field campaign	130
4.1 Review of Current Leaf Fall Recording Approaches	130
4.2 Hemispherical Imagery	131
4.3 Methodology	132
4.3.1 Camera Adaption	133
4.3.2 Firmware and Software	135
4.3.3 Study site and Data Collection	136
4.4 Results and Discussion	136
4.4.1 Automated Versus Manual Measurements	136
4.5 Leaf fall and the Weather	140
4.5.1 Wind Speed	140
4.5.2 Temperature	141
4.5.3 Rainfall	141
4.5.4 Antecedence	142
4.6 Conclusion	144
Chapter Four Summary	145
Chapter Five– Automatic data processing for integration of leaf fall data into a forecast model	146
5.1 Leaf Fall Techniques used by the Met Office	146
5.2 Methodology	149

5.3 Results and Discussion	160
5.3.1 Comparison of Threshold Analysis	160
5.3.2 Comparison of Sky-View Factor Techniques	162
5.4 Conclusion	165
Chapter Five Summary	167
Chapter Six– A blueprint for autumn monitoring systems	168
6.1 The Next Stages of the Raspberry Pi Monitoring System	168
6.2 In Situ Deployment of Leaf fall sensors	169
6.3 Mobile Monitoring	170
6.4 Safety Requirements of New Equipment on the UK Rail Network	172
6.5 Benefits and Challenges of using a Raspberry Pi Leaf Fall Sensor	174
6.5.1 The Effect of Motion Blur using a Raspberry Pi Device	175
6.5.2 Spatial Referencing and GPS Data Constraints	176
6.5.3 Mounting and Video Liability	179
6.6 Initial testing of the Raspberry Pi Device Onboard a Moving Train Result	180
6.7 Current Low-cost Sensors on the UK Railway and the Viability of Low-cost Sensor Innovation	184
6.8 Combination of Autumn Sensors and Sensor Innovation on the UK Railways	186
6.8.1 Moisture Sensors	187
6.8.2 Temperature Sensors.....	188
6.8.3 Contamination Sensors	189
6.8.4 Weather Stations	190

6.9 The Blueprint of the Autumn Rail Sensor Network.....	191
6.10 Recommendations for Future Research	194
6.11 Conclusion.....	196
Chapter Six Summary	198
Chapter Seven– Evaluation of the PhD and the original contribution to science	199
7.1 Aims and Objectives	199
7.1.1 Objective One	199
7.1.2 Objective Two	201
7.1.3 Objective Three.....	202
7.1.4 Objective Four.....	203
7.2 Original contribution to science.....	203
17.3 Conclusion	205
References	206
Appendix	234

List of Figures Captions

Chapter One Figures		
1.1	Operational weather management plan, taken from Figure 14 of the WRCCA strategy (<i>Network Rail, 2017a</i>).	4
1.2	(a) Structure of the UK rail network (<i>Office for Road and Rail, 2019</i>), (b) List of TOCs (<i>National Rail, 2019</i>).	5
1.3	Cost of weather-related events 2006 – 2016, taken from Figure 3 of the WRCCA strategy (<i>Network Rail, 2017a</i>).	6
1.4	Spending attributed to external vegetation management contractors from Network Rail (<i>Varley, 2018</i>).	7
1.5	Layers of Fe Ions and leaf components released into pockets of water bonding the leaf to the rail track under high pressure (<i>Ishizaka et al., 2017</i>).	22
1.6	Light rain falling on leaf film mixes pectin and Fe ions to form a pectin gel	22
1.7	Graph produced by Lewis et al. (2011) showing the difference between lab and field adhesion results using a pendulum rig and a tribometer.	24
1.8	(a) Adhesion coefficient recorded on a rail track, (b) Visual leaf contamination along the rail network (<i>Adhesion Working Group, 2018</i>).	26
1.9	Amount of SPADs, Overruns and WSTCFs from 2006 – 2018 during autumn (<i>Adhesion Working Group, 2018</i>).	32
1.10	(a) Wheel flat experienced on the Northern Line (<i>Northern Rail, 2018</i>), (b) Wheel flat experienced on the Piccadilly line in autumn 2016 (<i>Crawley et al., 2017</i>), (c) Graph showing the increase in number of trains removed from operation due to wheel flats from 2014 – 2017 (<i>Crawley et al., 2017</i>).	33
1.11	Network Rail PPM from 2006 – 2018 (<i>Network Rail, 2019b</i>).	34
1.12	Autumn delay report summary from London Underground for autumn 2016 (<i>Crawley et al., 2017</i>).	36
1.13	Measures against low adhesion events (<i>Adhesion Working Group, 2018</i>).	38

1.14	Depiction of the amount of action required when vegetation encroaches on the rail line (<i>Network Rail, 2018g</i>).	41
1.15	Autumn Adhesion index table produced by Met Desk for use in the Network Rail weather service throughout autumn (<i>Adhesion Working Group, 2018</i>).	47
1.16	Leaf Fall Matrix and Adhesion forecast produced by Met Desk showing levels of adhesion and daily leaf fall (<i>Adhesion Working Group, 2018</i>).	47
1.17	Met Office Forecast, taken from a Met Office (2018b) presentation as part of the RSSB (2018b) understanding adhesion forecasting conference.	49
1.18	Flow chart outlining the inputs and outputs of a typical forecast model including post season reviews and verification procedure.	51
Chapter Two Figures		
2.1	Spectral reflectance curve of vegetation (<i>GSP, 2016</i>)	70
2.2	(a) Reflectance of a leaf structure (<i>Carns, 2019</i>), (b) Photograph of vegetation captured in infrared (<i>Butcher, 2019</i>), (c) Photograph captured using a colour film (<i>Butcher, 2019</i>)	70
2.3	The Normalised Difference Vegetation Index calculation technique (<i>NASA, 2017</i>).	73
2.4	Schematic diagram of different Sky-view factors based on surrounding obstacles (<i>Hämmerle et al., 2011</i> adapted from <i>Oke 2002</i>).	78
2.5	Projection of an object in an image when using an equiangular fish-eye lens where O = Object, I = Image and $r = \frac{2r_o \delta}{\pi}$ (<i>Steyn, 1980</i>).	78
2.6	Series of concentric rings represented by dots in a hemispherical image used to calculate sky-view factor of the whole image (<i>Lindberg and Holmer, 2010</i>).	79
2.7	Variation in images from the original photograph (a) under different threshold limits (<i>Inoue et al., 2011</i>).	81

2.8	Raspberry Pi computer board with attached Raspberry Pi camera module (Nguyen et al., 2015).	97
Chapter Three Figures		
3.1	Flow chart showing the design process of a new leaf fall hemispherical device. The process is explored throughout chapter three.	105
3.2	(a) Mobile phone with a removed camera module, (b) Removed IR filter and a camera module, (c) close-up near-infrared image using a mobile phone camera, (d) 185° fisheye lens attached to an adapted mobile phone.	107
3.3	Evolution of hemispherical photography from 1964 - 2019	108
3.4	(a) FC-E8 Fisheye lens attached to a Coolpix camera Source: Reproduced with permission from Chapman et al. (2007), copyright © 2007 IEEE, (b) First2Savv 1850 fisheye camera attached to a Samsung Galaxy S5 Neo; (c) Perspex Dome used to measure distortion.	109
3.5	(a) Visual comparison of Nikon Coolpix camera, (b) smart phone camera with attached 185° fisheye lens, (c) smart phone camera with attached fisheye lens 198°, (d) smart phone camera with attached fisheye lens 180° and (e) smart phone camera with attached fisheye lens 235.	116
3.6	Comparison of radial distortion between different mobile fisheye lenses and Nikon Coolpix 4500 camera FC-E8 lens.	107
3.7	(a) 185° fisheye lens attached to base, (b) base component of Raspberry Pi fisheye module, (c) fisheye module attached to Raspberry Pi NoIR camera, (d) Camera module attached to a Raspberry Pi computer.	120
3.8	(a) Nikon Coolpix camera in a Perspex dome and (b) Raspberry Pi NoIR camera with fisheye attached under Perspex dome.	122
3.9	Radial Distortion of a Nikon Coolpix FC-E8 lens camera and a Raspberry Pi camera with attachable fisheye lens.	123
3.10	Visual variations in sky-view factors when comparing a Nikon Coolpix FC-E8 lens with an 185° Raspberry Pi NoIR camera.	125

Chapter Four Figures		
4.1	(a) Raspberry Pi, (b) Witty Pi 2, (c) Combined sensor with lithium battery, (d) IP65 waterproof enclosure.	134
4.2	Hemispherical images captured using an adapted Raspberry Pi and the corresponding SVF images, showing the reduction in leaf canopy over time.	137
4.3	Comparison between independent leaf fall observers and Raspberry Pi collected data.	139
4.4	Quantitative difference analysis between leaf fall captured on the Raspberry Pi and an independent leaf fall observer.	140
4.5	(a) Rate of change in percentage leaf fall over autumn 2017, (b) Weather conditions throughout autumn 2017.	143
Chapter Five Figures		
5.1	Sample of a Met Office leaf fall risk (<i>Crawley et al., 2017</i>).	148
5.2	Sample of a Met Office low adhesion forecast (<i>Crawley et al., 2017</i>).	148
5.3	A range of images captured using the Raspberry Pi NoIR camera highlighting the pink colour of leaves and the pink colour of light on the lens	152
5.4	Histogram of red pixels in a leaf canopy captured under ideal conditions produced using 'Image J' software (taken from a Beech image 2017).	153
5.5	(a) Scatter plot of pixel colour range in a typical tree canopy image, (b) Scatted plot of the colour range within an image once red threshold ranges had been applied (taken from a Beech image 2017).	155
5.6	(a) Scatter plot of colour range captured using a digital camera, (b) scatter plot of colour range using the same vegetation captured with a near-infrared Raspberry Pi camera.	156
5.7	(a) Leaf fall image captured using the Raspberry Pi NoIR camera, (b) leaf fall image that has been manually turned into a binary	157

	image using photo editing software, (c) binary image produced using automatic threshold code.	
5.8	Visual representation of the steps undertaken in the Python code produced on the Raspberry Pi computer	159
5.9	Comparison of manual threshold sky view factors and automatic thresholds sky view factors conducted on the Lindberg and Holmer (2010) sky-view calculator software	163
5.10	Rate of change for leaf fall images analysed using the manual approach and the automatic approach.	164
5.11	(a) Comparison of manual leaf fall threshold and automatic threshold calculated on the Lindberg and Holmer sky-view calculator, (b) comparison of automatic threshold images sky-view factor calculated using the Lindberg and Holmer (2010) calculator and automatic sky-view factor code produced on the Raspberry Pi.	164
Chapter Six Figures		
6.1	(a) - Adapted Raspberry Pi, (b) Raspberry Pi within a train cab, (c) Close up Raspberry Pi within the train cab, (d) Route of the Train from London Euston to Birmingham New Street.	181
6.2	(a) Hemispherical images captured along the rail route, (b) Sky-View factor images captured along the rail route.	182
6.3	Figure 6.3 – (1) Hemispherical image captured along the rail route showing vegetation alongside the track (2) Zoomed in photo of the tree shown in image 1 (3) zoomed in photo of a leaf on the tree from image 1 and 2.	183
6.4	Representation of an integrated data network consisting of weather stations, leaf fall monitors and moisture sensors.	192

List of Tables

Chapter One Tables		
1.1	The indirect effect vegetation can have on two major causes of weather-related delays.	9
1.2	Variation in characteristics of tree species for Oak, Birch and Beech	12
1.3	Areas of research focused on by the ADHERE program (<i>RSSB, 2019c</i>)	17
1.4	Coefficient of Friction for common railhead contamination (data taken from <i>Olofsson et al. 2016; Gallardo-Hernandez and Lewis, 2008</i>).	19
1.5	Variation in adhesion recordings taken from a train and a tribometer (<i>RSSB, 2008</i>).	26
1.6	Table adapted from AWG Manual 2018 (<i>Adhesion Working Group, 2018</i>).	27
1.7	List of low adhesion related accidents that caused passenger injuries.	29
1.8	Level of low adhesion experienced by train drivers and the action required over the GSM-R (<i>RSSB, 2019</i>).	42
1.9	Design specification for new apparatus to measure leaf fall on the rail lines.	54
1.10	The 'Rail Capability Plan' (<i>RSSB, 2017</i>).	56
Chapter Two Tables		
2.1	Low-cost sensors used in research.	88
2.2	List of studies using smartphone devices.	90

Chapter Three Table		
3.1	List of sample studies that use Nikon Coolpix cameras.	111
3.2	Studies using alternative cameras for hemispherical photography.	113
3.3	Mobile fisheye lenses specification.	117
3.4	Comparison of Coolpix cameras to Raspberry Pi cameras.	121
3.5	Sky-view factors of Nikon Coolpix camera adjusted FOV, Raspberry Pi NoIR camera, Nikon Coolpix unadjusted FOV and Raspberry Pi leaves only images.	126
Chapter Four Tables		
4.1	Dimensions of Raspberry Pi waterproof enclosure components.	133
Chapter Six Tables		
6.1	British Standards for new equipment on the rail network.	172
6.2	GPS devices that can be connected to the Raspberry Pi device to produce GPS data for each captured hemispherical image.	177

Chapter One

Autumn effects on the UK rail network

1.1 Introduction

There is a strong government led vision for the future of the UK railway industry; with an overall aim to create a fully integrated smart transport system that can be fully operational across the whole of the country (*Williams Rail Review, 2019*). Significant investment in the industry is anticipated between 2019 and 2024, with a plan to spend £47.9 billion in England and Wales (*Department for Transport, 2017a*) and a further £4.9 billion is planned for Scotland - excluding the investment in High Speed 2 and other major rail projects (*Railway Industry Association, 2019*). This highlights that innovation and investment in the UK rail industry remains a key focus of the UK Government. As stated in the Department for Transport 'Strategic Vision for Rail' report and the 'Rail Capability Plan', delays and passenger satisfaction are the driving reason for the need to innovate the current rail system (*Department for Transport 2018, Department for Transport, 2017c; RSSB, 2017*).

The rail industry plays a critical role in the UK economy and society; contributing £36.4 billion per year, facilitating 600,000 jobs across the nation and generating an annual tax revenue of £11 billion (*Oxford Economics, 2018*). 1.73 billion journeys on the rail network were made in 2018 alone (*Office of Rail and Road, 2019a; Department for Transport, 2017b; Department for Transport 2017d*) representing around a third (39%) of all public transport usage. The demand for rail transport has increased considerably over recent years, with rail usage in the UK increasing by 54% since 2002 (*Department for Transport, 2017a*) – the highest growth in Europe (*Williams Rail Review, 2019*).

The UK is currently one of the most congested rail networks in Europe, with utilisation on UK railways being 60% higher than the rest of Europe (*Railway Industry Association, 2019*) and is further expected to double in the next 25 years (*Oxford Economics, 2018*). This reduces the rail network's resilience (the ability to continue operation following unforeseen changes and disturbances to the rail line) (*Janić, 2018*). Network Rail, the UK rail infrastructure operator, has stated that delay reduction is a top priority with the aim to reduce delays by 15% by 2024 (*Network Rail, 2018a; Network Rail, 2018c*). However, in order to create solutions and innovative technology to improve the delays, the reasons for rail delays must be investigated.

Over 70% of rail delays are caused by knock-on effects with a delay on the route in one part of the country having the potential to delay a fleet hundreds of miles away. Therefore, understanding the cause of one delay that may in fact be the cause of several other issues along the rail network, and making any attempts to mitigate the initial delay has the potential to exponentially reduce the knock-on delays across the country (*Network Rail, 2018b; Jaroszweski et al. 2010*).

Network Rail (2018b) identify 10 key reasons for delays along a rail network; engineering works, knock-on-delays, signal failure, leaves on the line, landslips, flooding, snow and ice, buckling rail due to heat, vandalism and fatalities. Half of the delays listed by Network Rail are attributed to the weather and the environment with 40% of the weather-related delays occurring in the autumn and early winter (*Quinn et al., 2018; Network Rail, 2018b*). Over the last 10 years, 'adverse' weather-related issues have contributed to an average 2-3% reduction in PPM (Public Performance Measure) and have cost Network Rail around £50-100m (*Network Rail, 2018b*).

The climate in the UK is expected to become more extreme. In a high emission climate scenario, the UK winters by 2070 could be up to 4.2°C higher than today (*Met Office, 2018a*). Given the increase in temperature and extreme weather events, the problems associated with weather-related delays are likely to increase on the railways (*Network Rail, 2018b; Baker et al., 2010; Jaroszweski et al., 2010; Koetse and Rietveld, 2009; Thornes and Chapman, 2008; Thornes and Davis, 2002*).

In the rail industry, a weather-related risk is a weather-related event, such as flooding, that has the potential to cause problems on the rail network both operationally and economically. Figure 1.1 shows how weather-related risks are currently managed, highlighting the complex nature of preparation, response, recovery and mitigation. The rail industry is complex, being made up of stakeholders, privately owned companies and government bodies (Figure 1.3), all of which, have to work together in order to optimise weather-related responses (*Network Rail, 2017a*). In order to mitigate and reduce the delays on the rail line both the train operating companies (TOCs) and Network Rail have automatic fines associated with delays called 'Schedule 8' payments. These fines are automatically calculated by the Office for Road and Rail based on the type of delay and how the delay occurred on the rail network. 'Schedule 8' payments are calculated every 4 weeks for TOCs and Network Rail. Whilst there is variation year to year, Figure 1.2 shows that overall greatest costs are associated with wind and adhesion-related incidents, whilst flooding has the highest per incident cost (*Network Rail, 2017a*).

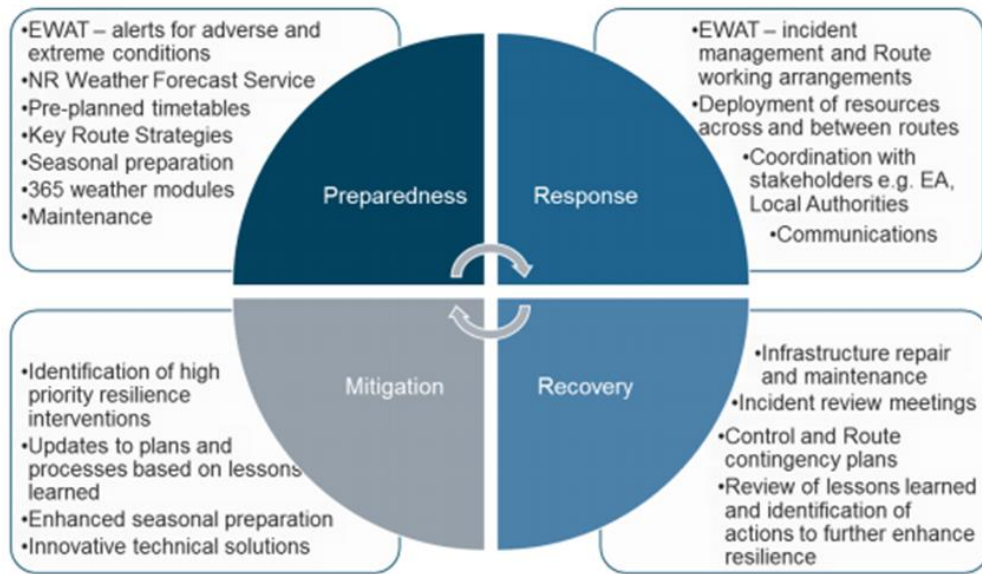


Figure 1.1 Operational weather management plan taken from Figure 14 of the WRCCA strategy (Network Rail, 2017a).

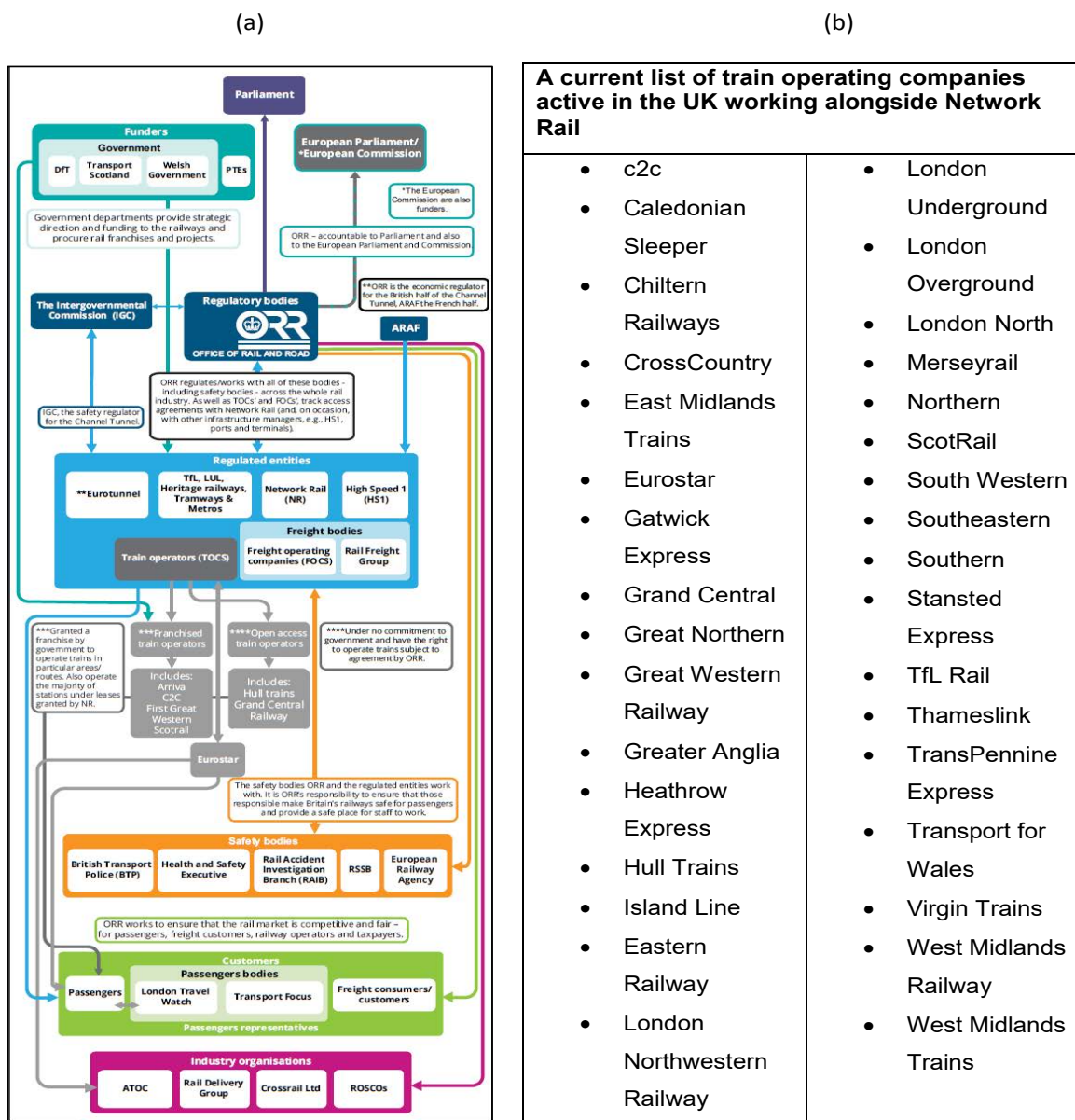


Figure 1.2 - (a) Structure of the UK rail network (*Office for Road and Rail, 2019*), (b) List of TOCs (*National Rail, 2019*).

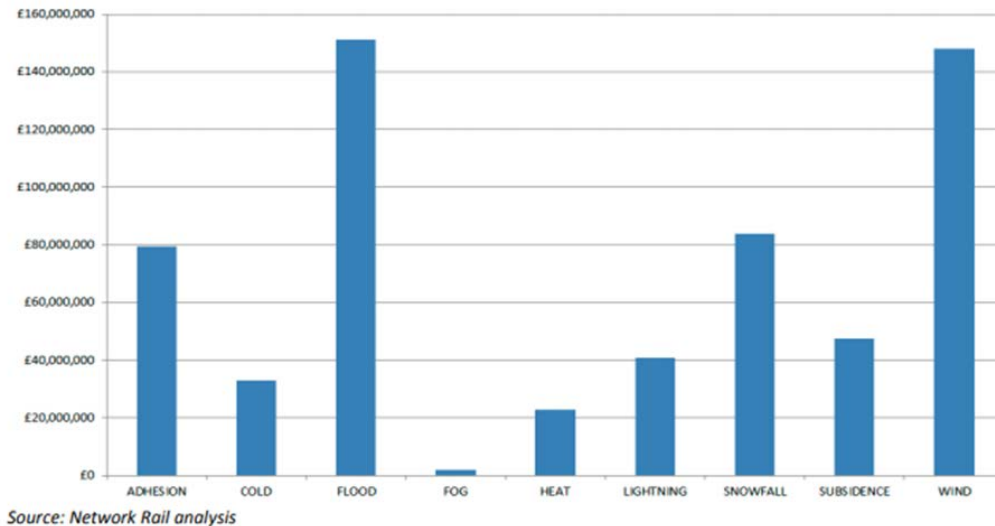


Figure 1.3 Cost of weather-related events 2006 – 2016 taken from Figure 3 of the WRCCA strategy (Network Rail, 2017a).

However, 40% of the causes of delays (rail buckling, landslips, flooding and adhesion) noted by Network Rail (2018b) can be attributed to hazards caused by lineside vegetation or lack of vegetation for example rail buckling increased in areas where there is lack of lineside vegetation which can act as shade on the railways. Yet the management of vegetation, similarly to weather-related issues is complex given the combination of public and privately-owned sectors that make up the rail industry (Figure 1.3). This underpins the need for increased research in this area.

1.2 Vegetation and Railways

The interaction between rail and vegetation has always been a complex issue, with Network Rail being the fourth largest landowner in the UK owning 52,000 hectares of land. A tension exists between the need to maintain a prosperous rail industry without compromising the natural landscape (Department for Transport, 2018b; Varley, 2018).

Indeed, the management of lineside vegetation remains a challenging task with 16,000 miles of lineside and approximately 6.3 million trees on the network (Varley, 2018).

Historically, vegetation was managed due to the risk of lineside fires from steam engines, but following the introduction of diesel engines in 1948 and the subsequent Beeching cuts (restructuring of the railways) in 1965, the management of vegetation was reduced (Varley, 2018). Figure 1.4 shows the current cost of lineside management to Network Rail between 2012 – 2018, accounting for a total of £217.26 million in the last six years alone. Whilst Figure 1.4 includes the cost of independent contractors who conducted vegetation management for Network Rail, it does not include internal costing as this is not included within the published accounts of Network Rail (Varley, 2018).



Figure 1.4 Spending attributed to external vegetation management contractors from Network Rail (m = millions) (Varley, 2018).

In 2017/18 there were 19,000 railway incidents *directly* related to vegetation resulting in 1,750 trains being cancelled for example falling tree branches, interaction with overhead wires and electrical faults (*Varley, 2018*); this does not account for indirect vegetation delay issues (see Table 1.1). Despite the incidents related to trees increasing over the last 9 years, in May 2018 Jo Johnson, then Minister for Rail, commissioned an independent review of Network Rail's vegetation strategy and thereafter suspended all tree clearance works (*Department for Transport, 2018b*). This review was driven on an environmental protection approach stemming from the growing public concern to protect British wildlife (*Department for Environment, Food and Rural Affairs, 2018*).

Table 1.1 – The indirect effect vegetation can have on two major causes of weather-related delays.

Delay Reason	Attribution to Vegetation
<p>Landslips - Landslips can be small in scale or range to large scale disruption events, such as the Hatfield Colliery landslip in South Yorkshire in 2013 (<i>Freeborough et al., 2016</i>).</p>	<p>Roots of trees act as anchors for the soil along the rail route holding the environmental infrastructure around the track together. When a tree and its roots are removed or the soil along the roots disturbed (for example during flood events) the embankment destabilises resulting in a landslip (<i>Scott et al., 2007</i>).</p>
<p>Flooding - The rail industry during periods of flooding can be completely shut down or cut off from the main network due to not being able to run trains through large areas of flooded track (<i>Pant et al., 2016</i>). The storm of the 28th June 2012 caused 10,000 delay minutes (number of minutes a train arrived late to its destination station) across the network and had knock-on effects into July (<i>Jaroszweski et al., 2015; Kendon et al., 2014</i>).</p>	<p>Flooding can again be exacerbated by the removal of vegetation. Tree roots can reduce the ground flow of water and encourage infiltration rather than surface flow of water reducing the impact of some flood events. The removal of tree roots along the track makes the soil less porous and results in large scale surface runoff, as well as the removal of leaves resulting in less interception around the rail line and hence an increase in flooding on the network (<i>Ellison et al., 2017</i>).</p>

It is important to note that whilst vegetation can cause delays on the rail network, it can also act as an important means to improve resilience. For example, trees reduce the effect of rail buckling by shading the track and reducing the temperature on the rail line. Hence, in a warming climate, this role of vegetation could become increasingly important as the existing design codes for laying track to withstand UK temperatures become stretched. Currently, prolonged periods of hot weather can result in blanket speed restrictions along specified rail routes and thus cause significant delays across the network (*Network Rail, 2017; Hooper and Chapman, 2012; Chapman et al., 2008*). The estimated cost of climate change on the railhead alone through buckling was predicted to be £26.1 million per summer by 2050 due to an increase in delay minutes and buckling treatment (*Dobney et al., 2008*).

From Table 1.1 it is clear that removal of vegetation can cause landslips by destabilising the embankment. The roots of the tree stabilise the embankment and thus there is a need to maintain the current lineside vegetation rather than removing it. The use of vegetation as a way of stabilising soil is referred to as bioengineering and is used as a way to stabilise embankments in both the rail and road transport network (*Forest Research, 2019*). Whilst trees could be removed, and the roots replaced by concrete, this would be costly and neither efficient nor eco-friendly.

As well as the potential to mitigate summer related delays, vegetation management is essential to maintain wildlife corridors, with the areas around rail lines often referred to as 'green corridors.' As lineside trees, grassland and shrubs are left largely undisturbed, they have become a habitat for British wildlife, including bird and mammal species (*Network Rail, 2017b*). Whilst there is less literature on the impact of railways

on wildlife compared to that related to the road transport network (*Popp and Boyle, 2017; Borda-de-Água et al., 2017; Dorsey et al., 2015*), there is nevertheless a growing public desire to protect this habitat (*Barrientos et al., 2018; Varley, 2018; Lucas et al., 2017*). The Varley (2018) review suggests that the protection of wildlife should be at the forefront of vegetation management. Whilst the loss of some habitats is inevitable along the rail network, given the scale of necessary vegetation removal work, the rail industry is expected to deploy a best practice approach when clearing in order to minimise impact on existing biodiversity. Such mitigation may include not removing vegetation during bird nesting season.

A key outcome of the Varley (2018) vegetation management review was a recommendation that Network Rail implement a 25-year government environment plan in order to meet the demand for a greener, more environmentally friendly nation (*Department for Environment, Food and Rural Affairs, 2018*). However, currently one of the major obstacles in developing an environmentally friendly rail network is that there is no standard approach to recording vegetation. Whilst vegetation management is well established, there are ambiguities around best practice (for example, the correct distance from rail track that vegetation needs to be in order to not cut it back). Likewise, recording methods in order to gain relevant data, are not clear. This need for new universal approaches to record vegetation at a high spatial resolution was echoed in the Varley (2018) vegetation management review and the Curley and Rainer (2010) autumn review report, documented in the Adhesion Working Group manual (*Adhesion Working Group, 2018*). In being able to capture the variation in species along the network, an up to date vegetation survey could be conducted (given that the majority of lineside species are less than 50 years old) which would help to enhance the current

knowledge of tree species in the area (Varley, 2018). This need for innovation in vegetation control is one of the driving factors behind this current PhD research and indicates a clear research gap for vegetation recording techniques.

1.2.1 Types of vegetation around the rail network.

It is important to note that whilst general vegetation management strategies are in place along the rail network the tree's that cause some of the most significant issues along the rail track (Oak, Birch, Beech) have variation in species and thus fall rates which can cause problems along the rail line at different times throughout autumn. The variation in species, growth rates, leaf morphology, leaf area index, specific leaf area and phenology is shown in table 1.2. Along the rail network trees are categorised into late and early falling species with Oak leaves being of particular interest due to the increased low adhesion that occurs in areas where these leaves fall.

Table 1.2 Variation in characteristics of tree species for Oak, Birch and Beech (Woodlands Trust, 2019; Natures Calendar, 2019; Safford et al., 1990).

Tree	Species	Growth Rates	Leaf Morphology	Leaf Area Index (Approx.)	Specific Leaf area (Approx.)	Phenology
OAK	Quercus robur (pedunculate oak)	Grow 20-40m tall	10 cm in length with 4-5 deep lobes per leaf with little to no stem.	5.1m ² -m ⁻² (OENL DAACA, 2019)	0.92 – 0.98 m ² g ⁻¹ (Van Hees, 1997)	Late falling leaf species

	Quercus petraea (Sessile Oak)	Grow 20- 40m in height	Long stalk with lobed leaves	4.67 – 5.8m ² -m ⁻² <i>(OENL DAACA, 2019)</i>	0.98 – 1.4 m ² g ⁻¹ <i>(Bruschi, 2010)</i>	Late falling leaf species
Birch	Paper Birch (Betula papyrifera)	Grow up to 30m in height	Triangular shaped leaf with jagged edge	2.58 -5.9 m ² -m ⁻² <i>(OENL DAACA, 2019)</i>	0.44-0.62 m ² g ⁻¹ <i>(Ashton et al., 1998)</i>	Mid – late falling species
	Silver Birch (Betula pendula)	Grow up to 30m in height	Triangular shaped leaf with jagged edge	1.2- 5.34 m ² -m ⁻² <i>(OENL DAACA, 2019)</i>	0.45 m ² g ⁻¹ <i>(Oksanen et al., 2005)</i>	Mid-season species falling leaves from October
Beech	Fagus sylvatica (Common Beech)	Grow to 40m tall	Short stalks with hairy leaf edges they are 4-9cm long and torpedo shaped	4.9-5.7 m ² m ⁻² <i>(OENL DAACA, 2019)</i>	1.288 m ² g ⁻¹ in a sunny environment <i>(Masarovicov á, 1990)</i>	Mid-season species falling leaves from October

1.3 Low Adhesion

During the autumn the main cause of delays on the rail network is due to low adhesion. Adhesion is often defined as how sticky a surface is (*Lacombe, 2005*) however in the railways it is essentially a measure of the 'slipperiness of a surface' and is defined as the measure of the ratio between braking force against the normal force of wheel-rail contact. As stated by the Adhesion Working Group (*2018*) the measure of adhesion is roughly equivalent to the maximum deceleration capability rate of a train as a percentage of gravitational deceleration (*Li et al., 2009; Arias-Cuevas, 2010*) – i.e. how quickly a train can brake in relation to how quick it is expected to brake on a given surface/ railhead. On a dry day when a train passes over a railhead the level of adhesion between the wheel and track should be above 0.15 (15% traction), however during autumn months the level of adhesion can drop to levels of 0.01, causing significant transport problems (*Olofsson et al., 2016; Rail Research Group 2015; Lewis et al., 2009*).

Low adhesion is exacerbated during the acceleration and braking of a train (*Chen et al., 2018; Gallardo-Hernandez and Lewis, 2008*). During braking, wheel slips occur, in which the speed of the train is faster than the wheel rotational speed. This causes track burn and damage to the wheel and rail, which is worsened during autumn when wheel slips are 40 times more likely to occur compared to other seasons (*Adhesion Working Group, 2018*). Wheel Slip Protection (WSP) systems are fitted to disc-braked rolling stock in which the brake is released and reapplied at appropriate times during a low adhesion event. This controls the speed of the wheel to just below the speed at which a wheel slip would occur and therefore reduces the occurrence of wheel slips during low adhesion areas along the railhead (*Adhesion Working Group, 2018; Network Rail, 2018d*).

Wheel slides occur when the wheel locks or spins at a rate lower than expected for the speed of the train (often defined as a wheel creep) and causes the wheel to slide along the rail track, this motion increases the temperature between the rail wheel interface causing the steel to melt or soften. This can lead to damage of both the wheel in terms of defects on the wheel itself and the railhead from rail burn caused by increased friction (*Adhesion Working Group 2018; White, 2018*). Wheel slides also cause wheel flats; this is caused by high vibrations during sliding resulting in breaks and damaged areas in the wheel. These can be costly to replace and cause trains to be non-operational until the wheel is repaired, thus increasing delays on the network (*Kolukirik and Bezgin, 2019; Sanchís et al., 2019; Chen et al., 2018; Wu and Thompson, 2002*). During autumn 2016, wheel flats on Northern Rail trains alone cost the company £2 million (*Northern Rail, 2018*).

1.4 The cost of Low Adhesion

RSSB estimate that autumn related issues cost the railway industry approximately £345 million per year (*RSSB, 2019b*) with an estimation of £3000 per minute on the London Piccadilly line alone (*Crawley et al., 2017*). This cost is made up of several different factors including: Public Performance Measures (PPM), cost of signals passed at danger (SPADs) and overruns, reduction in profit from leaf fall timetables, railhead treatment and mitigation techniques, lineside vegetation management, replacement train parts that have been damaged during autumn, cost of treatment train operation, staff training and incident responses, forecasting adhesion costs and the cost of bad publicity and loss of reputation due to poor reliability of trains during the autumn season (*Adhesion Working Group, 2018*).

In order to better understand the root cause of low adhesion and therefore improve mitigation and management techniques, RSSB developed a new research program called the ADHERE portfolio (*RSSB, 2018c*). Working with Network Rail, London Underground, TOCs, commercial suppliers and research organisations as well as academic research organisations in the UK and abroad, the ADHERE program was split into five key objectives as shown in Table 1.3. In June 2018 the ADHERE program launched a £300,000 competition to fund feasibility studies that focus on adhesion to be conducted over autumn 2018/2019, showing the industry and academic drive to improve low adhesion and its associated problems on the UK rail line (*RSSB, 2019b*).

Table 1.3 Areas of research focused on by the ADHERE program (RSSB, 2019c)

Areas of Research	Definition
Fundamental science and modelling	Improve low-adhesion and braking modelling as well as improving the knowledge behind why low adhesion causes delays.
Rail cleaning and re-contamination	To improve knowledge of railhead treatment and cleaning techniques and the effects of the treatments.
Driver behaviours	To improve drivers' performance and confidence during times of low adhesion on the railhead.
Changes to train design	Investigation of train-borne technologies such as magnetic track brakes.
Forecasting adhesion	Improving forecast reliability and observation capabilities to improve decision making during low adhesion leaf fall related events.

From Table 1.3 it is clear that many areas of research could be conducted around the low adhesion issue. There is a clear research gap in improving forecasting adhesion in terms of observation related recording techniques. This project is funded by RSSB in order to improve observation of leaf fall along the rail network and will focus on improving knowledge and understanding of how leaf fall is recorded and how this could be improved.

1.5 Causes of Low Adhesion

Low adhesion is caused by several factors including railhead contamination and the presence of low levels of moisture (Table 1.4). However, as discussed in 2018 by the ADHERE group one of the major challenges faced in the rail industry is that the root causes of adhesion are still poorly understood (RSSB, 2019c). Railhead contamination can be caused by many factors such as rust, oil, grease and even air pollution (Adhesion Working Group 2018; Olofsson et al., 2016; Gallardo-Hernandez and Lewis, 2008). One theory is that leaves which become trapped between the wheel-rail interface under intense pressure could lead to the formation of a gel on the track, these leaves produce a slippery coating on the railhead (Adhesion Working Group, 2018; Ward, 2010; Zhang et al., 2002) that can result in exceptionally low adhesion coefficients at less than 0.02 (Ishizaka et al. 2017; Olofsson et al., 2016; Gallardo-Hernandez and Lewis, 2008). Gallardo-Hernandez and Lewis (2008), using a twin disk rig under laboratory conditions, showed that the presence of leaves could even cause indents in disk services highlighting the damage that leaves alone on the railhead can cause.

Table 1.4 Coefficient of Friction for common railhead contamination (data taken from *Olofsson et al. 2016; Gallardo-Hernandez and Lewis, 2008*).

Substance	Coefficient of Friction (μ)	Potential Adhesion Level
Water	0.15	Medium
Oil	0.05	Low
Dry Leaves	0.04	Exceptionally low
Wet Leaves	Less than 0.02	Exceptionally low
Snow	0.03	Exceptionally low
Wet Rail	Less than 0.02	Exceptionally low

Low adhesion from leaf fall is ultimately determined by the properties within the leaf structure which control how the leaf litter interacts with the rail. Unlike other causes of low adhesion such as water or oil, which can run off the track or evaporate, leaves adhere to the track and form a smooth layer which can be difficult to remove (*Gallardo-Hernandez and Lewis, 2008; Olofsson, 2007; Zhu et al., 2014*). The length of time from when the leaf has fallen from the tree is also a factor in how the leaf will impact the rail head. Leaves that have begun to decay can begin to turn into a mulch and contain high levels of moisture which can lower the adhesion levels on the rail track and small levels of moisture within the leaf would be present. Therefore, when predicting leaf related issues on the rail track the timing in autumn and percentage of leaves already fallen would need to be considered in order to incorporate already fallen remobilised litter (*Brunel et al., 1994*).

The leaf layer on a typical track is usually split into two defined sections; a coated slippery layer and a chemical layer (*Cann, 2006; Gallardo-Hernandez and Lewis, 2008; Olofsson, 2007*).

1.5.1 The 'Chemical' Layer

The chemical layer forms a black flaky substance that is made from iron oxides, calcium, phosphorus and larger leaf particles (*Ishizaka et al., 2018; Olofsson, 2007; Cann, 2006; Zhu et al., 2014*). Due to the different proportions of calcium and phosphorus in various leaf species, the amount of chemical layer across different regions will vary dependant on the composition of flora around the track (*Olofsson, 2007*).

1.5.2 The 'Slippery' Layer

Cann (2006) suggests that the 'slippery layer' is predominantly made of Pectin. Pectin is a polysaccharide found within the leaf; the carbohydrate can form in up to 35% of cell walls. In contrast to within the leaf, Pectin found in the cell walls of woody matter, such as bark, is present at 5% (*Ridley et al., 2001; Cann, 2006; Willats et al., 2006; Mohnen, 2008*). When water is added to Pectin the substance turns into a gel, which when combined with the pressure and other components such as the amount of calcium present (*Willats et al., 2006*) results in the slippery layer. Therefore, a rail track presents favourable conditions for the Pectin from leaves to be crushed under wheels with the presence of water from the autumn weather conditions.

Like the chemical (black film) layer, the suggested Pectin layer (slippery layer) is difficult to remove and often removal from brushing is not adequate (*Hizaka et al., 2017; Olofsson, 2007; Cann, 2006*). As previously stated, Pectin bonds with water to form a gel and this hydrogen bonding creates a slippery surface however Pectin can also bond to hydrophobic surfaces (*Crockett et al. 2014*). Pectin can make electrostatic bonds onto surfaces such as rail tracks. These bonds are stronger than hydrogen

bonding and make it more difficult to remove the layer (*Crockett et al, 2014*). The bonding of Pectin and cellulose onto the surface remains in a gel structure during heavy loads (trains) passing over the track (*Zhang et al., 2002; Crockett et al., 2014*). Therefore, not only do more trains increase the number of leaves blown onto the line but they also increase weight and pressure needed to form more Pectin gel, exacerbating the low adhesion problem (*Crockett et al., 2014; Zhu et al., 2014*).

Whilst the suggested high level of Pectin within the leaf structure combined with water-soluble material from the leaves themselves are one potential cause of low adhesion created from leaf matter other theories have disagreed with the current literature on pectin being the cause of low adhesion (*Ishizaka et al., 2018; Cann, 2006; Ward, 2010; Arias-Cuevas, 2010; Zhu et al., 2014*). An alternative reason for leaf matter to cause low levels of adhesion (*Ishizaka et al., 2017*). Research conducted by Ishizaka et al. (*2018*), noted that the black film on a railhead, that is present under low adhesion measurements, contains a high proportion of iron oxides, phosphate and carbon. Moreover, this research showed that brown leaves and green leaves, when crushed and dissolved, produce a lower adhesion coefficient than that of pure Pectin suggesting that the reduction in adhesion could be due to the levels of iron oxides and organic matter in the leaf. Figure 1.5 and 1.6 taken from Ishizaka et al., (*2017*) shows how leaves can bond to the rail line in both the pectin theory and the black film iron bonding theory. Both of these theories suggest that leaf litter is blown on or remains on the rail head for longer periods of time. Once leaf abscission occurs winds can remobilise litter and blow it onto the track post leaf falling suggesting that low adhesion can occur throughout the autumn season based on wind speeds as well as fall rates (*Met Office, 2018*).

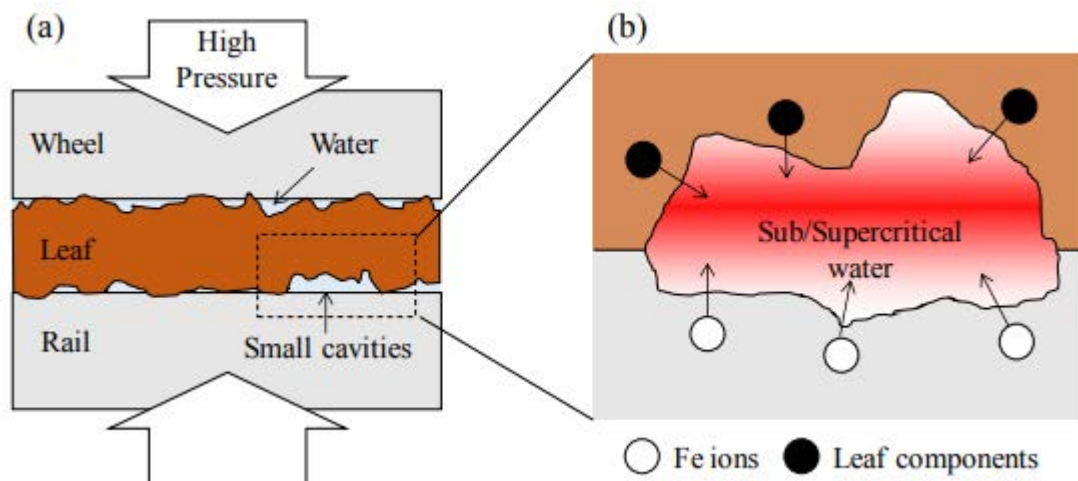


Figure 1.5 Layers of Fe Irons and leaf components released into pockets of water bonding the leaf to the rail track under high pressure (Ishizaka et al., 2017).

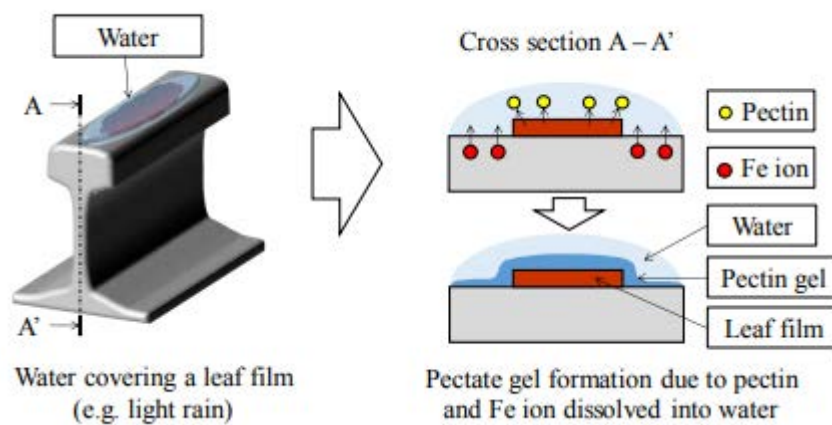


Figure 1.6 Light rain falling on leaf film mixes pectin and Fe ions to form a pectin gel (Ishizaka et al., 2017).

Low levels of moisture are caused by a number of meteorological phenomena such as light rainfall, drizzle, dew and mist/ fog. 'Wet Rail Syndrome' has been the focus of much research in recent years (Buckley-Johnstone et al., 2019; Adhesion working

Group, 2018; White et al., 2018). It is defined by RSSB (2014) as low adhesion due to low levels of moisture caused by dew, drizzle, frost and the transition from wet to dry rail on the track. 'Wet Rail Syndrome' contributes to exceptionally low adhesion episodes (adhesion coefficients around 0.02) when small amounts of water are present under both lab conditions and in the field. This reduction in friction between the rail head and the wheel of the train due to moisture can cause low adhesion incidents resulting in rail delays. It is important to note that wet rail can occur all year round in periods of low moisture levels. (*Olofsson et al., 2016; Zhu et al., 2014; Lewis et al., 2009; Li et al., 2009; Gallardo-Hernandez and Lewis, 2008*). T

1.6 Measuring Low Adhesion

British Rail in the late 70s and 80s conducted extensive research into measuring low adhesion due to an increased number of rail adhesion events (*Fulford, 2004*). Tribology (the study of friction) in the early 70s consisted of portable tribometers and friction rigs, for example the Amsler rig. However, there is a debate on the reliability of portable tribometers when compared to the actual size of a wheel rail interface. A tribometer train was invented that could test friction on a large scale, however due to the cost of the apparatus with little return in terms of accuracy the last measurement using this train was in 1996 (*Fulford, 2004; Poole, 1996*).

As the main method of measurement outlined in the 'Guidance on wheel/ rail low adhesion management' the tribometer is available for use in many forms; a pin and disk tribometer, a hand pushed tribometer and a top-of-rail and gauge-face tribometer to name a selection (*Harrison et al., 2002*). Whilst improvements to a tribometer that can be used in the field (*Areiza et al., 2015*) have been made, for example the

pendulum rig developed by Lewis et al. (2011), the majority of rail testing using the tribometer methods are time consuming and do not take in to account external factors such as weather conditions at time of testing (Lewis et al., 2011).

Alternatively, laboratory test rigs act as a solution for measuring low adhesion under test conditions. Low adhesion is measured between two wheels when various test solutions are added to the rig. This method can cause damage to the test wheels and each new product may require a new wheel to obtain credible results (Lu et al., 2005; Li et al., 2009; Arias-Cuevas et al., 2011; RSSB, 2016). Lewis et al. (2011) researched the differences of tribology measurements in the field and in the lab using a standard tribometer and a pendulum rig (Figure 1.7), showing that in reality modern tribometer measurements under the right conditions are comparable in both the laboratory and the field.

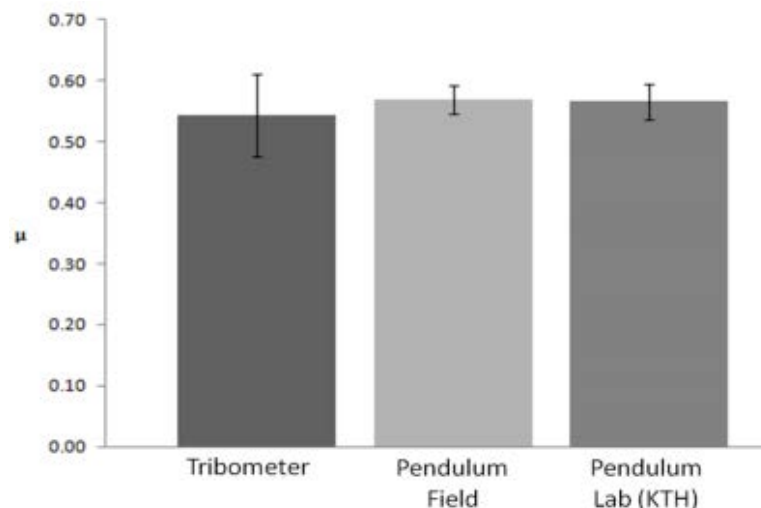


Figure 1.7 - Graph produced by Lewis et al., (2011) showing the difference between lab and field adhesion results using a pendulum rig and a tribometer.

Indirectly, low adhesion can be measured using a test train. Deceleration along a track can be recorded using Wheel Slip Protection (WSP) data that has been optimised to

detect low adhesion. Once wheel slip is detected the brake should be released, the longer it takes for a train to stop along a track the lower the low adhesion coefficient is between the track and rail (*Adhesion Working Group, 2018; RSSB, 2008*). Unfortunately, conditions are not constant on the rail line and data analysed by RSSB (*2008*), showed the difference in recording adhesion measured on a train and using a tribometer with the greatest differences occurring when leaf fall is present (Table 1.5). Currently, there are no conversion factors available between adhesion measured on a train and that measured using a tribometer due to the variation between results. Even though low adhesion along the track can be measured, there is no daily real time measurement of low adhesion along each rail track. Instead, reviews of the rail are undertaken after a significant event has occurred in order to assess the state of the rail; low adhesion recordings as well as photographs are taken, showing the amount of substance on the railhead as shown in Figure 1.8 (*Adhesion Working Group, 2018*). Table 1.6 shows the measurement criteria used when assessing the level of black film and in effect the level of low adhesion on the railhead.

Table 1.5 – Variation in adhesion recordings taken from a train and a tribometer (*RSSB, 2008*).

Rail condition	Train adhesion values			Portable tribometer values		
	Maximum	Minimum	Average	Maximum	Minimum	Average
Clean dry	0.60	0.13	0.23	0.70	0.30	0.50
Clean wet	0.20	0.05	0.12	0.30	0.13	0.21
Dry simulated leaf	0.17	0.07	0.14	0.66	0.33	0.46
Dry leaf	0.15	0.09	0.11	-	-	-
Wet simulated leaf	0.09	0.05	0.08	0.47	0.06	0.22
Dampened Leaf	0.06	0.01	0.05	-	-	-
Oil	0.14	0.08	0.12	0.30	0.15	0.24
Oil and water	0.08	0.03	0.06	0.21	0.13	0.16



Figure 1.8 - (a) Adhesion coefficient recorded on a rail track, (b) Visual leaf contamination along the rail network (*Adhesion Working Group, 2018*).

Table 1.6- Table adapted from AWG Manual 2018 (*Adhesion Working Group, 2018*).

Adhesion Level	Typical coefficient of friction (μ)	Description
High	Above 0.15 On a dry day 0.2– 0.4	Also known as ‘shiny rail’ where no braking problems should occur.
Medium	0.1-0.15	Damp rail with slight signs of contamination along the rail track
Low	0.05-0.09	Expected rail condition in damp morning conditions especially over the autumn period. Can be attributed to overnight rust of the railhead.
Exceptionally Low	Less than 0.05 (Rare occurrences can be as low as 0.01)	This is below the required level for a train to break and can cause serious problems. Usually due to leaf contamination in autumn, but can occur when other contamination is on the track e.g. oil.

1.7 Low Adhesion Safety and Performance Consequences

When low adhesion occurs on a section of the rail track it can cause multiple safety and performance issues, as it affects the ability of the train to accelerate and brake. The Rail Accident and Investigation Branch (RAIB) work with the Office for Road and Transport to investigate any problems across the rail line (*Office for Rail and Road, 2017*). There have been a number of incidents attributed to low adhesion that have caused significant injury in the past. For example, in November 1985, 40 passengers were injured (11 seriously injured) when two trains collided due to low adhesion at Copyhold Junction, Sussex. In a subsequent incident in November 1994, a low adhesion event caused serious injury to a driver when a train hit a buffer stop in Slough (*RAIB, 2007*). Table 1.7 is a summary of serious low adhesion related events in the last 10 years that have occurred on the UK rail network.

Table 1.7 - List of low adhesion related accidents that caused passenger injuries.

Date	Location	Accident
October 2015 <i>(RAIB, 2016)</i>	Shalesmoor Tram Stop	Two trams collided at Shalesmoor tram stop. This was due to a reduction in braking ability as a result of poor driving during low adhesion conditions. Several passengers were treated with minor injuries.
November 2013 <i>(RAIB, 2014)</i>	Chester Station	Station overrun caused a train to hit a buffer stop causing damage to the glass screen, the train and the platform. One passenger was taken to hospital and this incident was attributed to wet rail and leaves on the line.
January 2010 <i>(RAIB, 2011)</i>	Exeter St Davids Station	Two trains collided on platform one due to low adhesion on the rail track. This caused a train to not brake effectively when entering the station. Six passengers and three members of staff were injured, and minor damage was done to both trains.

Fortunately, there have been relatively few low adhesion events that have caused significant injury to passengers, but there are still a number of safety incidents that occur due to low adhesion. Due to safety issues, Network Rail has a number of measurable key performance indicators (KPIs) to ensure safety and performance (*Network Rail, 2019; Steer Davies Gleave, 2007*). A number of these relate to autumn and include the measurement of station overruns, station stop shorts, signals passed

at danger (SPADs) and wrong side track circuit failures (WSTCF). The approximate split of reported incidents during the leaf fall season is 60% WSTCFs, 37% station overruns and 3% SPADs (*Adhesion Working Group, 2018*).

1.7.1 Station Overruns and Station Stop Shorts

A station overrun occurs when a train fails to stop at a station. This is usually attributed to poor braking performance when entering the station due to low adhesion between the wheel and the rail track (*Adhesion Working Group, 2018; ATOC, 2016; RAIB, 2014*). A station overrun was the cause of the serious low adhesion event at Chester Station shown in Table 1.7. Station stop shorts occur when a train has applied its brakes too early and not the full number of doors can be opened to let passengers alight the train. These are known collectively as SSI - Station Stop Incidents (*RSSB, 2019d*). SSI can cause numerous issues; safety for passenger alighting, operational risk, investigation costs, delay repay costs and knock-on delay effects impacting whole route operation (*RSSB, 2011*). The number of station overruns during the autumn are shown in Figure 1.7, although station overruns can occur throughout the year due to other factors such as driver error (*Adhesion Working Group 2018; RSSB, 2019d*).

1.7.2 Signals Passed At Danger (SPADS)

A SPAD occurs when a train fails to stop even though a stop indicator is operational and showing that a train should stop. A category A SPAD represents the most significant risk to staff and passengers and occurs when a train has reached a fouling point - a critical point on the track where two trains could collide. There were 17 category A SPADs during the 2017/18-year period (*Office for Rail and Road; Network*

Rail, 2019). However, there has been a 90% reduction in SPAD occurrence since 1990 (*RSSB, 2019e*) and there is a drive by RSSB for the SPAD risk to be reduced significantly by 2035. The number of SPADS in the last 10 years can be seen in Figure 1.7.

1.7.3 Wrong Side Track Circuit Failures (WSTCF)

A WSTCF occurs when a passing train fails to activate a circuit. This means that there is a blockage in signal between the rail and track and therefore the presence of a train is not detectable (*Adhesion Working Group, 2018; Delay Attribution Board, 2018*). The circuit failures can occur during periods of low adhesion and can also be caused by the presence of sandite or sand (an adhesion mitigation factor discussed further in section 1.8) breaking the connection between wheel and track. Although over the last 10 years only 3% of WSTCF were attributed to the presence of sand (*RSSB, 2019f*), 97% of WSTCF were attributed to the presence of other railhead contamination such as rust and leaf matter (*RSSB, 2019c; Delay Attribution Board, 2018*). Despite leaf matter causing WSTCF, there is unlikely to be a low adhesion related event occurring during a WSTCF. This is because conditions typically have to be dry for a WSTCF to occur (*RSSB, 2019f; Adhesion Working Group, 2018*). The danger of a WSTCF is that a train can be signalled into an area that is already occupied by another carriage causing potentially fatal collisions (*Office for Road and Rail, 2017*). WSTCF are attributed to Network Rail (*Delay Attribution Board, 2018*) and the Network Rail standard (NR/L2/OCS/095) states that at any high-risk site (a site in which two WSTCFs have occurred) a risk assessment and removal plan must be made (*Network*

Rail, 2018e). Figure 1.9 shows the number of autumn related WSTCFs 2006 – 2016 (Adhesion Working Group, 2018).

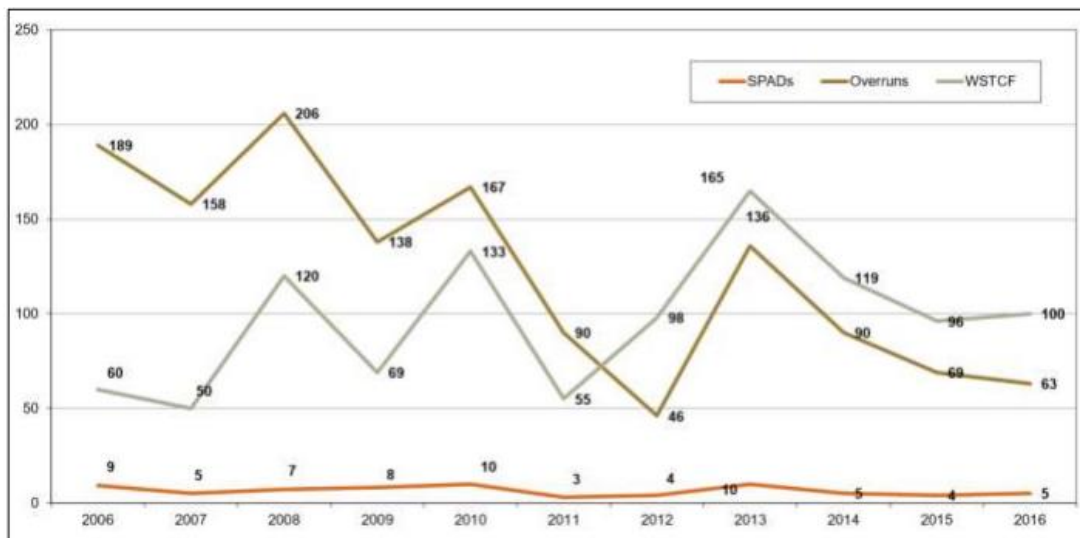


Figure 1.9 – Amount of SPADs, Overruns and WSTCFs from 2006 – 2018 during autumn (Adhesion Working Group, 2018).

Physical damage to the train can also be caused by low adhesion. Wheel flats (as discussed in section 1.3), caused by the spinning of the wheel, can create damage to the track as well as the wheel itself. This often results in carriage removal from operation leading to cancellations, delays on the line and passenger overcrowding (Thommesen et al., 2014). The number of wheel flats experienced by Northern Rail in the autumn of 2016 was a 100% increase in occurrences than that of the previous year (Northern Rail, 2018) and the Piccadilly Line noted that wheel flats increased dramatically over the autumn months. Figure 1.10 (a) shows a picture of a wheel flat experienced in autumn 2016 on a Northern Rail train (Northern Rail, 2018) whilst Figure 1.10 (b) shows a wheel flat experience on the Piccadilly rail line in autumn 2016 (Crawley et al., 2017). The increase in number of wheel flats during the autumn of 2016 (Figure 1.10 (c)) resulted in an investigation into autumn adhesion issues on the

Piccadilly line conducted by Crawley et al. (2017). A summary of the report is shown in Figure 1.12.

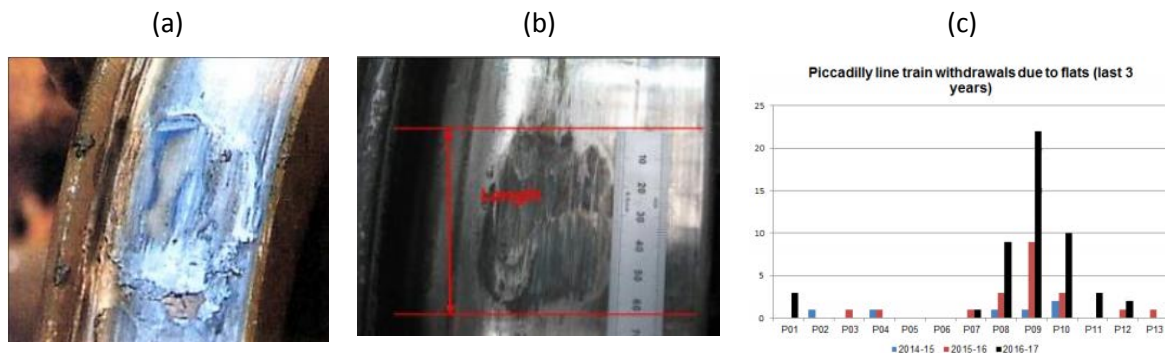


Figure 1.10 - (a) Wheel flat experienced on the Northern Rail (*Northern Rail, 2018*), (b) Wheel flat experienced on the Piccadilly line in autumn 2016 (*Crawley et al., 2017*) (c) Graph showing the increase in number of trains removed from operation due to wheel flats from 2014 – 2017 (*Crawley et al., 2017*).

1.7.4 Public Performance Measures (PPM)

In addition to safety issues, there are also performance related issues caused by low adhesion. Significant performance related problems that do not affect the safety of passengers, but can cause delays; often when the train accelerates and decelerates due to the lack of traction (*Lewis and Olofsson, 2009; Zhu et al., 2014*). The cumulative effect of this creates knock-on delays and signalling issues along the rail network (*Olofsson et al., 2007; Olofsson and Sundvall, 2004; Ward, 2010*). These performance measurements are also measured by Network Rail and are referred to as Public Performance Measures (PPM). Previous to an update in 2019, a PPM was defined as the percentage of trains arriving at a station on time or within 5 minutes of the expected arrival time or 10 minutes for long distance journeys. Figure 1.9 shows the PPM measured by Network Rail over the last 12 years; the percentage of trains arriving on time in the year has never risen above 93% and since 2011 there has been a general reduction in PPM (*Network Rail, 2019b*).

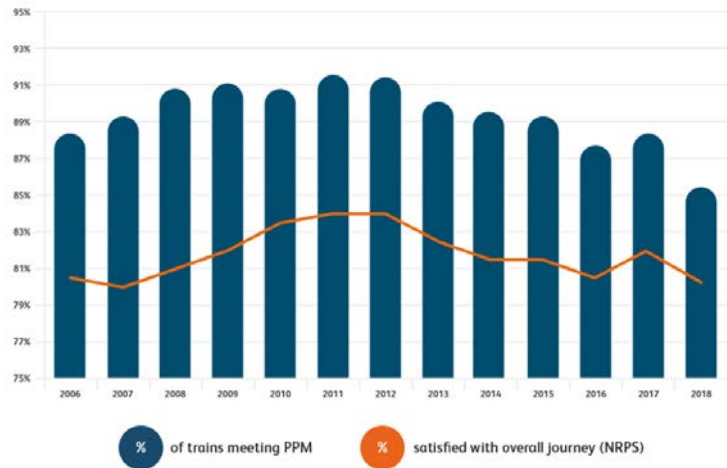


Figure 1.11 – Network Rail PPM from 2006 – 2018 (*Network Rail, 2019b*).

As of 2019, an additional measure of performance has been introduced. The PPM will now include punctuality at all station stops where measurable (currently 80% of stations have the technology to record train arrival time to the minute) rather than the end destination and will also include train cancellations as part of the performance measure (*Network Rail, 2019b*).

During the autumn period there is a reduction in PPM. This is attributed to the specific delays caused by low adhesion and autumn related weather and is known as the ‘autumn dip’ (*Office for Road and Rail and Network Rail, 2018; Department for Transport, 2018; Network Rail, 2010*). Northern Rail experiences an average autumn dip of 5% on PPM which equates to 131 extra trains failing to meet the Network Rail PPM standards, which are set each spring and autumn (*Northern Rail, 2019*).

Figure 1.12 shows the main conclusions drawn from an intensive review of issues found during an autumn period on the London Underground in 2016. Autumn cost the London Underground £20 million and resulted in an investigation into the causes and

reasons behind the poor performance period. Whilst low adhesion was deemed the cause of the London Undergrounds delays, other components of the leaves on the line issue were raised such as management strategies, capability of rolling stock and lack of preventative measures in reducing the effects of the poor adhesion on the rail track (*Crawley et al, 2017*). The London Underground S1165 'Landscape and Vegetation' standard states the types of vegetation permitted along the rail line. During the last vegetation survey in 2014, the investigation found that not all of the Piccadilly line met the required standard and had a large number of overhanging trees along the rail track. An automatic observation recording of tree species along a route could be beneficial, by producing a more regular vegetation survey, showing how different tree species will vary and grow over time and once again shows the need for a vegetation recording device across the rail network.

London Underground 2016 Case Study

In 2016 the low adhesion and leaf fall related issues on the Piccadilly Underground line cost £20 million in lost customer hours and prompted an independent incident report to be carried out investigating the severity of the delays. The report states that there are four key elements of an effective adhesion regime:

- Prevention; to retain adhesion at safe levels through vegetation control and early warning systems;
- Prediction; use of Met Office reports to trigger early warning indicators of poor adhesion days in the future;
- Containment; short term action to reduce low adhesion such as railhead cleaning techniques;
- Recovery; which is reducing the effects of a low adhesion event such as changes in train timetable.

The report stated that adhesion management schemes in 2016 were not 'adequately in place' for the London Underground Piccadilly line (*Crawley et al., 2017*). The investigation attributed the increase in low adhesion issues in part to the poor vegetation management around the Piccadilly line. Leaves on the line, mostly from Oak, Ash and Sycamore, reduced the adhesion coefficient on the track to 0.02. The tube stock in the UK are resistant to low adhesion at the 0.06 level and therefore were not equipped to resist leaf film induced low adhesion (*Adhesion Working Group, 2018; Crawley et al., 2017; Olofsson et al., 2016; Gallardo-Hernandez and Lewis, 2008*). Despite this, "assumptions" were made that low-adhesion due to leaf fall was deemed "minor" on this line. This assumption contradicted the Met Office warnings (*Crawley et al., 2017*).

Figure 1.12 – Autumn delay report summary from London Underground for autumn 2016 (*Crawley et al., 2017*).

1.8 Low Adhesion Mitigation and Management

The Mobile Operational Manager (MOM) is in charge of reacting to low adhesion events on the rail network. However, there are not universal practices to establish what a MOM or adhesion management team is required to do post low adhesion events. Most MOMs work Monday - Friday and therefore there is a reduced response over weekends when low adhesion events occur highlighting the need for a universal response approach across Network Rail and TOCs. The general response to a low adhesion report is to increase the level of adhesion on the track by applying sand by hand, sandite by a train, water jetting or adding adhesion gel as well as enforcing speeding restrictions in low adhesion reported areas however water jetting given that it is adding moisture to the track may result in wet-rail syndrome (*Adhesion Working Group, 2018; RAIB, 2014*). Therefore, alternative mitigation recording techniques and strategies are needed to reduce the risks caused by low adhesion. Figure 1.13 taken from the Adhesion Working Group (2018) adhesion manual, indicates the current mitigation strategies available to MOMs and evaluates their usefulness on a scale of 1 to 10; with train operated sanders, water jetting, sandite and WSP data being some of the most effective measures in low adhesion mitigation.

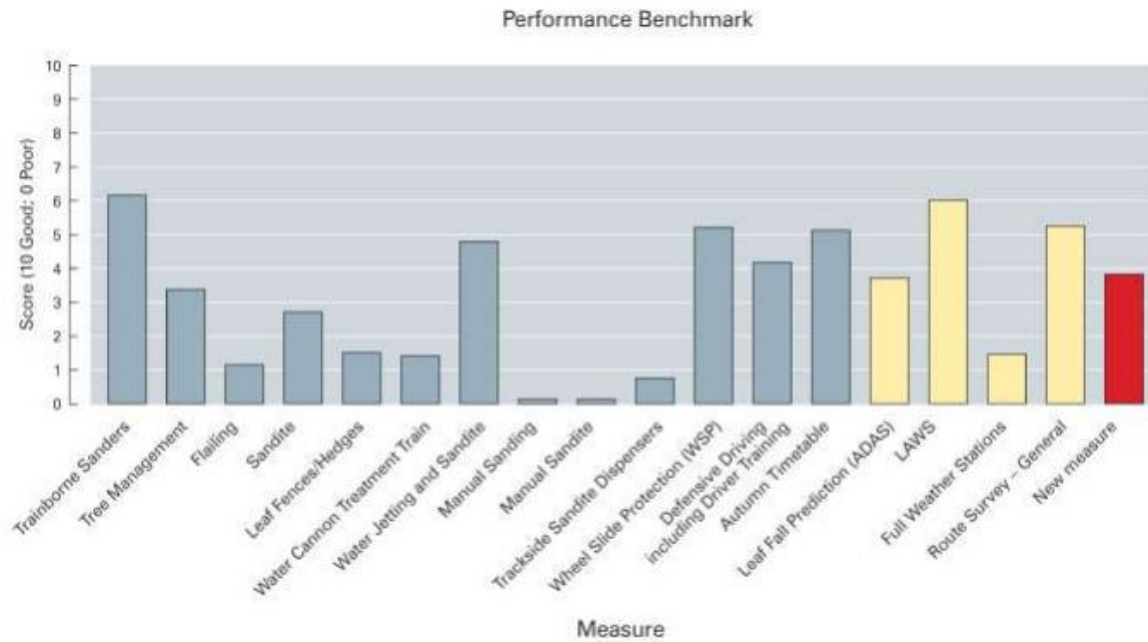


Figure 1.13 Measures against low adhesion events (*Adhesion Working Group, 2018*).

1.8.1 Track Based Mitigation Tools and Vegetation Management.

As shown in Figure 1.13, low adhesion on the railhead can be improved using a series of approaches; water jetting, sanding, laser technology, vegetation management and adhesion mitigation techniques (*Thommessen et al., 2014; Li et al., 2009; Lewis and Dwyer-Joyce, 2005*).

1.8.1.1 Water Jetting

Water jetting removes the leaf layer before it has time to chemically break down. This relies on visual detection of a leaf layer on the track. Scrubbers and water jets are attached to a slow-moving service train that cleans the track. This can be problematic as the service train is slow and needs to be done at a time of minimal traffic on the line. Water also increases the humidity which means there is a possibility of wet-rail

syndrome occurring on the track (*Buckley-Johnstone et al., 2019; Adhesion working Group 2018; White et al., 2018; Thommesen et al., 2014; Olofsson and Lewis, 2006*).

1.8.1.2 Sandite and Sanding

Adding sand to the rail line increases the adhesion between track and wheel (*Lewis and Dwyer-Joyce, 2005; Olofsson and Lewis, 2006; Zhu et al., 2014*). The additional sand can also increase the adhesion to pre-leaf fall levels (*Zhu et al., 2014*). The method to add sand to the track is a manual process which is controlled by the driver of the train however is applied automatically in emergency situations. Compressed air releases the sand from a hopper under the train. The sand is blown just under the wheel and can decrease the stopping distance of a train in low adhesion areas (*Lewis and Dwyer-Joyce, 2005*).

The main issue with using sand to increase adhesion is that it can cause wear on the track. The dents and scratches in the track can be expensive to remove and thus cost the rail company more money in clean up expenditure (*Zhu et al., 2014; Lewis and Dwyer-Joyce, 2005*). The use of sanding during wet weather conditions causes more damage to the rail track than using sand under dry conditions. Due to the time of year and average weather conditions, in which sanding would be used, the abrasion damage caused would be more severe to the track safety (*Lewis and Dwyer-Joyce, 2005; Olofsson et al., 2013*).

Sandite, which is a mixture of sand, water, gelling agent and stabiliser, can be used in sanding. Network Rail release Sandite on their cleaning trains, which can go up to 40 mph during cleaning (*Vasić et al., 2003; Olofsson and Lewis, 2006*). Sandite works in a similar way to sand, being released onto the track from a hopper, but has a longer

lasting effect as it is less likely to be blown from the rail tracks as easily as sand. However, if too much is applied the contact between the wheel and the track could be broken which could cause an electrical signalling failure. Sodium bicarbonate could be used as an alternative to both Sandite and sand, this compound is considered more environmentally friendly and does not damage substrate however it is not widely used (*Vasić et al., 2003*).

1.8.1.3 Laser treatment

The third way to remove leaves is the use of lasers (*Litchfield et al., 2006*). Laser beams work by releasing a high-intensity photon burst, sent at set intervals to a targeted surface at temperature above 100°C. However, if the laser pulse width is too long cleaning will not occur and too short a pulse width will damage the rail track (*Tam et al., 1998*).

There are two types of laser cleaning, 'steam laser cleaning' and 'dry laser cleaning.' Steam laser cleaning uses the laser to vaporize a thin liquid film made of water and ethanol which cleans the surface. Dry laser cleaning uses ultraviolet lasers to blast off contaminants and is more effective for removing organic film, such as the Pectin on rail tracks (*Tam et al., 1998; Bloisi et al., 2004; Vasić et al., 2003*). The laser beam on a rail track is manually operated and attached to trains that can reach 3 – 5 mph. If the photon burst is at too high intensity the beam could melt the metal rather than cleaning it. Due to the cost of laser treatment and the potential damage to the track, this cleaning type is not used in the UK (*Tam et al., 1998; Vasić et al., 2003*).

1.8.2 Vegetation Mitigation

Alternative methods for reducing leaves on the line use preventative methods rather than cleaning technology. Leaf fences around the track and vegetation management have been suggested in order to reduce leaves on the line (*Vasić et al., 2003*). As discussed in section 1.2, vegetation is extremely important for habitats and wildlife, yet there are regulations that attempt to reduce the effect of leaf fall on the rail network. Figure 1.14 shows the vegetation management regulations set out by Network Rail in a management report, the report shows the scale of intervention required based on the overhang distance of tree on the rail line (*Network Rail, 2018g*). This cut back strategy reduces direct fall of leaves on the line. However, given that there is a backlog of vegetation management around the rail (*Varley, 2018*) and that winds cause leaves to mobilise and move from one location to another, the cutting back of vegetation may not be an effective mitigation strategy. A large spatial scale recording of vegetation overhang would potentially improve this mitigation technique which again shows the need to develop a method of recording vegetation at a high spatial and temporal scale.

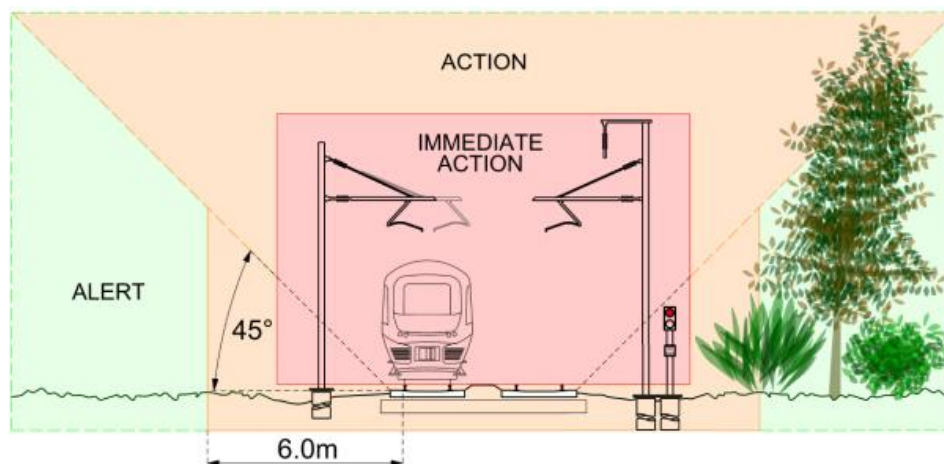


Figure 1.14 - Depiction of the amount of action required when vegetation encroaches on the rail line m = meters (*Network Rail 2018g*).

1.8.3 Vehicle and Driver Mitigation

In the UK, train drivers under the European Railway Traffic Management System (ERTMS) are required to anticipate low adhesion conditions and alter their driving to mitigate against potential impacts (RSSB, 2015). GSM-R (Global System for Mobile Communications- Railway) regulations require feedback from drivers on the track back to a central infrastructure manager who is required to warn other drivers of potential low adhesion areas (RSSB, 2019; RSSB, 2016a). The level of adhesion experienced that requires reporting by train drivers is shown in Table 1.8.

Table 1.8 – Level of low adhesion experienced by train drivers and the action required over the GSM-R (RSSB, 2019).

Level	Definition	Action by the driver
Good	Rail adhesion conditions are good.	No further action needed.
Expected	Rail adhesion is no worse than would be expected for the location and environmental conditions.	Adapt your driving to manage the conditions in line with your company's Professional Driving Policy. No need to report to the signaller.
Reportable	Rail adhesion is worse than would be expected for the location and environmental conditions.	Report to the signaller immediately.

Drivers are also expected to maintain a reduced speed during low adhesion areas and be aware of any reported low adhesion spots along the rail route. However, given the short time frame in which a low adhesion event can occur train drivers are not always able to mitigate against a low adhesion related fault on the line e.g. wheel slip (Adhesion Working Group, 2018). The Adhesion Working Group further publishes low adhesion awareness manuals specifically for train drivers in the 'Right Track' newsletter published by the Train Accident Risk Group. This aims to inform drivers of

up to date techniques on recognising low adhesion and aids training provided to drivers by independent TOCs.

Specifically, drivers are expected to use three key principles when operating a train during autumn (*Adhesion Working Group, 2018; ATOC 2000*):

1. Defensive driving - drivers should know the correct braking and traction mechanisms when driving in potential low adhesion environments as to cause unnecessary strain on the wheel/ rail interface, for example skid pan training (knowledge of what to do in the event of a skid on the rail track).
2. Know the route - drivers are expected to understand the current and forecasted conditions expected along the rail route that they are operating on and to know of historic key problem areas along the line.
3. Maintain a safe distance - reduced speed restrictions are in place over autumn including a reduction of vehicles on the line resulting in reduced timetables. Whilst unpopular with the public, drivers need to adhere to strict reduction regulations and adapt their speed and braking distances accordingly.

1.8.4 Adhesion Management Tools

On a train operational scale, there are several policies in place to mitigate low adhesion. As stated, some TOCs put in place a leaf fall timetable such as the West Midlands Railways and Northern by Arriva Rail. These are in place to reduce safety risks and allow drivers more time to accelerate and brake between station arrivals and departures (*West Midlands Railway, 2018; Northern Rail, 2018*). As part of the leaf fall timetable, TOCs may implement a 'skip, stop' timetable in which some of the rail stations that are usually stopped at during normal operations are removed at certain times of the day. Greater Anglia implements a 'request to stop' train timetable on certain rail routes during the autumn months in order to reduce delays on the network (*Greater Anglia, 2018*). This again allows a reduced speed to be operated on the rail route with minimal disruption to arrival time (*Niu et al., 2015; Jiang et al., 2017*). When a low-level adhesion event is reported, the new regulation requires the immediate visit to the low adhesion site in order to assess the courses and action required on the site (*Adhesion Working Group, 2018*).

1.8.5 ACCAT system London Underground

London Underground has a sophisticated approach to tackling adhesion in the form of the 'Adhesion Controllers Condition Assessment Tool' (ACCAT). The ACCAT system is an automatic low adhesion warning tool that integrates WSP activity, vegetation management, weather forecasts, lineside observations of 'wet rail syndrome' and leaf fall, site visits and treatment train data to provide a real time risk for running an ATO (Automatic Train Operation) in low adhesion areas. The ACCAT system triggers a reduced break rate of 0.55m/s^2 so that trains can still operate under hazardous conditions without a manual train driver. Despite the large quantity of information assimilated into the ACCAT system, there is still potential for improvement. With current work being conducted to develop a Mainline ACCAT, an improved vegetation observation technique that could feed in high spatial and temporal leaf fall data could improve the system's understanding of potential hazardous low adhesion due to leaf fall areas. The introduction of a new ACCAT for the Mainline highlights the need for a new method that records vegetation in real time to be built and implemented into the model on a short time scale (*Adhesion Working Group, 2018; Crawley, 2017*).

Overall, the biggest issue with most of the cleaning technologies discussed is that they rely on manually cleaning the track. These processes occur regularly however a better understanding of the prevailing weather conditions, leaf fall amounts and problem areas is needed in order to select the best time to clean the railhead. There are two main leaf fall forecasts currently used in the rail industry, operated by two companies; the Met Office and Met Desk.

1.9 Low adhesion forecasts

As well as the reliance on daily feedback from train drivers, TOCs must have a prediction service for low adhesion required by the GE/GN8540 low adhesion standards (*RSSB, 2015*). There are a variety of private and government weather forecast providers that provide leaf fall or low adhesion forecasts to the rail industry and each have a different approach, different forecast resolutions resulting in varying forecast outcomes.

Met Desk have been providing national low adhesion forecasts for Network Rail since the start of 2014 and is Network Rail's current National Weather provider. The autumn forecast produced by Met Desk allows a daily prediction of both leaf fall and low adhesion across the rail network. However, there is little available information on how the prediction of low adhesion and leaf fall forecasting is made. The service provides a start date and peak leaf fall times, weather conditions such as high wind risks and a 5-day predictive output of low adhesion risk on the rail route, which are updated twice a day. The risk of poor adhesion is colour coded, with green representing good adhesion and black very poor adhesion, as shown in Figure 1.15 (*Met Desk, 2018; Adhesion Working Group 2018*). There is also a written forecast describing the predicted weather and low adhesion in the 5 forecasted days, which gives an overall indication of factors contributing to adhesion for each day for specific regions (Figure 1.16). A daily average may not predict all low adhesion events over the typical autumn day due to the transient nature of low adhesion (*Adhesion Working Group, 2018*). The forecast is delivered to clients by both email and a dedicated weather portal.

Autumn Adhesion Index (AAI)	Adhesion Conditions	Probability of Overruns, SPADS & WSTCF	Possible scenarios
0 – 3	Good	Low	Below 2 the risk is low and will be confined mostly to high vegetation index areas (with close or overhanging trees). 3 will be due to moisture.
4 – 5	Moderate	Moderate	The risk is moderate with problems potentially in lower vegetation index areas.
6 – 8	Poor	High	There will potentially be more general problems due to higher leaf fall rates and / or greater leaf litter mobility.
9 - 10	Very poor	Very High	Potentially means general and widespread disruption due to leaf contamination. This situation is most likely to occur during the period around the 50% leaf fall date – normally the peak of the season – when combined with strong or storm force winds.

Figure 1.15 – Autumn Adhesion Index table produced by Met Desk for use in the Network Rail weather service throughout autumn (Adhesion Working Group, 2018).

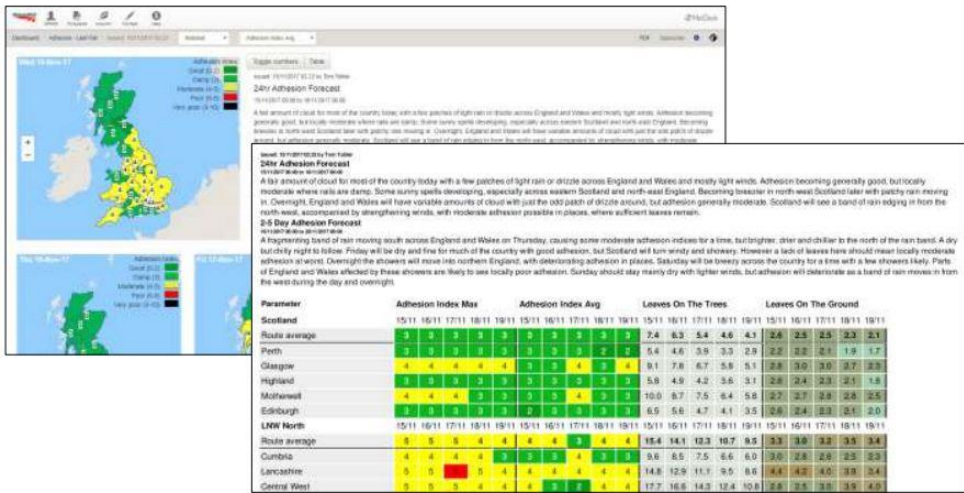


Figure 1.16 – Leaf Fall Matrix and Adhesion forecast produced by Met Desk showing levels of adhesion and daily leaf fall (Adhesion Working Group, 2018).

The Met Office also provide leaf fall, low adhesion and wind throw forecasts to various parts of the UK rail industry. The wind throw element of the forecast provides a risk of fallen branches and trees and is distributed to the rail industry when a significant wind throw risk is forecasted (Met Office, 2018b).

The Met Office also uses a colour coded risk indication system. There is a low risk (green), moderate risk (yellow), high risk (red) and very high risk (black) categories based on an index. The Met Office also provide a 10-day outlook and hourly summaries of leaf fall and low adhesion risk for a 48-hour period in order to capture the transient nature of the low adhesion forecast in time and space (*Met Office, 2018b*).

A key distinction of the Met Office approach, as discussed in the RSSB 'Understanding Adhesion Forecasting Conference' (2018) is the inclusion of a high-resolution perspective, having moved away from large area-based forecasts due to increases in accuracy (*Met Office, 2018b*). This means that Met Office forecasts are now derived at a 1/8th mile resolution and take into account a number of factors including species composition, density and proximity of vegetation to the rail track (*Met Office 2018b; RSSB, 2018b*). For drivers and route controllers delivering services, short term forecasts at station to station level are useful, whereas for more general decisions on whether to cancel engineering works, larger signal box areas forecasts are useful up to 10 days in advance. There is clearly a benefit of high-resolution forecasts in order to show the potential for highly varying levels of low adhesion along a small part of the rail track (Figure 1.17). However, it is clear that in order for this approach to be successful, high resolution vegetation data is needed for inclusions in the forecast model.

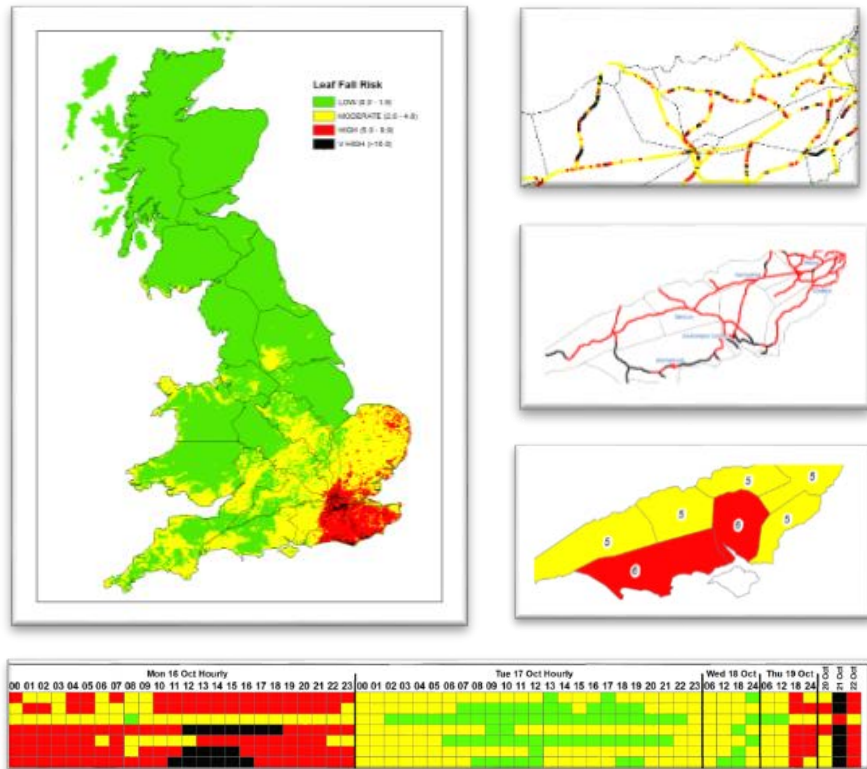


Figure 1.17 – Met Office Forecast - Taken from a Met Office (2018b) presentation as part of the RSSB (2018b) Understanding Adhesion Forecasting conference.

It is important to model leaf fall from different tree species due to the different timing of species fall, as this impacts the accuracy of a leaf fall forecast. For example, Oak is a much later falling species compared to Sycamore, Ash and Poplar. The Met Office records different leaf fall species along the rail track using trained leaf fall observers. The observer network is used to inform the Met Office forecast model on the rate at which vegetation will fall compared to a seasonal leaf fall average. Combined with information of vegetation along the lineside collected from vegetation surveys, the Met Office can predict bespoke leaf fall rates for different parts of the country (*Met Office, 2018b*). The leaf fall forecast also incorporates percentage leaf fall remaining on the trees and amount of leaf litter on the ground to predict how quickly vegetation can fall on or affect the railhead (*Met Office, 2018b*).

The meteorological component of the forecast determines wind-speed as well as a suite of parameters related to 'wet rail syndrome', such as dew, frost, light intermittent rain, drizzle, mist or fog in an area which is likely to result in low levels of adhesion due to moisture on the railhead. A number of models are used in the prediction of this element of the forecast including a weather forecast model and a rail surface temperature model. Due to the fundamental causes of low adhesion it is a highly transient phenomenon - both spatially and temporally, which makes it difficult to observe at high resolution using traditional methods. As such, low adhesion will vary considerably over even small sections of track (*Met Office, 2018b, Adhesion Working Group, 2018*).

In order to review the forecasts produced throughout the autumn, each forecast provider must produce a post-season review in which forecast accuracy is calculated by comparing incidents during forecasted poor adhesion days. This review is built into future low-adhesion management plans and fundamentally considers both the strengths and weaknesses of current operational methods (*Adhesion Working Group, 2018*). The review also allows forecast verification as the predicted outcome is compared to incidents along the track as well as observer data to validate the model. This verification compares the accuracy of the model throughout the autumn and can be reviewed by independent contractors to assess the usefulness of the current forecaster's operations. This post-season review could be improved if visual representation of the leaves on different tree species were given to validate the observations entered into leaf fall models and thus show evidence and justification for model outputs. Figure 1.18 summarises a typical leaf fall forecast model with inputs, outputs and review procedures.

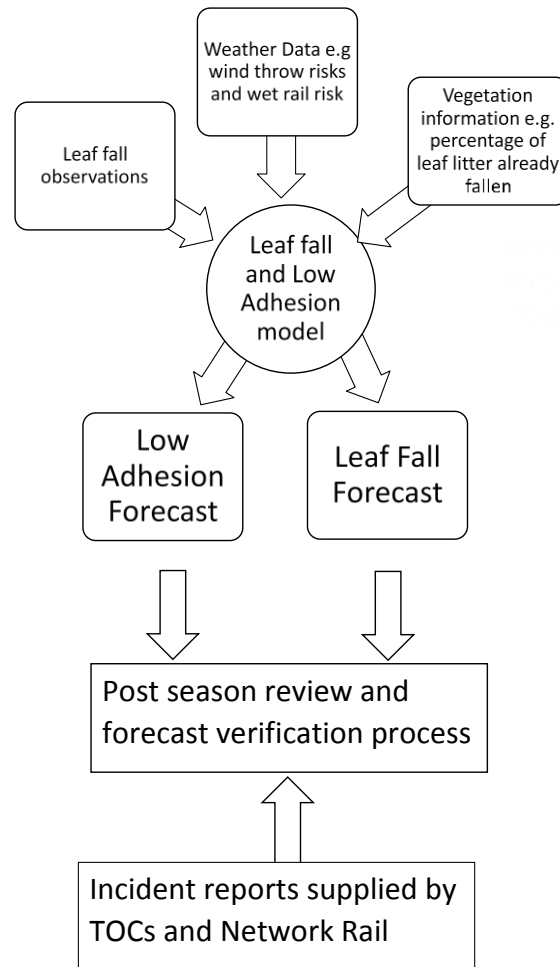


Figure 1.18 – Flow chart outlining the inputs and outputs of a typical forecast model including post season reviews and verification procedure.

There is a clear research gap in terms of reviewing vegetation management and its importance in the ‘adhesion riddle’ (RSSB, 2018b). To improve understanding of the fundamental causes of low adhesion further in an operational environment, a high-resolution approach to monitoring leaf fall and ‘wet rail syndrome’ is required.

Whilst work has been done on the development of a low-cost moisture sensor network to monitor ‘wet rail syndrome’ at a high resolution (Chapman et al., 2014) and currently under implementation by RSSB (RSSB, 2019g), to date there has been no ground-

based high resolution approach to leaf fall monitoring. There is a pressing need for collecting robust and objective data on leaf fall on an operational rail network. Despite long running Met Office and Met Desk leaf fall forecasts, currently, no forecast has a high spatial and temporal resolution observation input that is automatic and can capture leaf fall throughout the day.

Improving the resolution of the leaf fall observations would ultimately lead to improvements in the prediction of low adhesion to help industry mitigate against its effects. This would allow detailed information to be captured on some aspects of the leaf fall process that are not fully quantified such as the impacts of frosts on all species, or the effects of topography on leaf fall. Furthermore, a high-resolution approach in both time and space could be used as a standalone service to help detect how many leaves have fallen on a daily basis and also determine at the close of season when 100% fall had occurred. This could help with the planning of leaf fall mitigation such as railhead treatment trains, or feed into the adhesion management system. Alternatively, high amount of fall could lead to the implementation of localised speed restrictions across an area to reduce safety risks (*Adhesion Working Group, 2018; Crawley et al., 2017*). This potentially would reduce the operational cost of cleaning an entire route area and allow more attention in areas prone to low adhesion.

A further benefit of the high-resolution approach to leaf fall observations would be to validate leaf fall and low adhesion forecasts provided to the industry. There is currently no published independent review for leaf fall forecasting and low adhesion prediction accuracy although this is being addressed through the Adhere Adhesion Forecasting work package (*Adhesion Working Group, 2018; RSSB 2019c*). Leaf fall forecasters

such as the Met Office conduct sensitivity analysis however due to contractual obligations this is not discussed further in this thesis.

1.10 Research Gap

Overall, there is a clear research gap for improving observational capabilities of vegetation on the rail network. This work aligns with the Rail Technical Strategy (RTS, 2012) and the 'Network Rail 2013 Technical Strategy' (NRTS) (RSSB, 2017), which set out a strategic vision for UK railways for the next 30 years, as summarised in Table 1.9.

In particular, the development of a high-resolution leaf fall observation technology would align with the other rapid developments in smart technology and sensors to innovate in data collection. The increase in smart technology for passenger satisfaction also harnesses the current improvement and innovation of technology in the rail industry and includes the use of internet-connected sensors to relay information about the train system in real time, replacing lineside sensors with onboard technology in order to run trains closer together (thus improving capacity) and reducing disruption by adding pre-empting sensors to detect potential problems on the line (RSSB, 2017). This is part of a broader 'Strategic Vision Plan' which aims to modernise and improve the railways across the UK, with a £35 million investment in Wi-Fi technology for both customers and communication systems within the railways. In order to achieve this a design specification for a new apparatus has been agreed by RSSB and is shown in table 1.9

Table 1.9: Design specification for new apparatus to measure leaf fall on the rail lines

Specification requirement	Definition
Accuracy	The device should be comparable with the current best market option in recording leaf fall and reproduce similar observation values to what is expected throughout an autumn season. A decrease in daily leaf fall rather than a fluctuation of leaves or an addition of leaves on a tree.
High Spatial and temporal Scale	The device should have the potential of being implemented at a station to station level and be able to capture images daily
Automatic	The device should be able to run in isolation during the autumn season without the need for daily adaptation or human interaction
Non invasive	The device should not have to have contact with the rail track or be placed in a site that could cause danger to the public
Robust	The device should be able to withstand typical weather conditions expected in the UK autumn.

1.11 Aims and Objectives

As this opening chapter has articulated, this PhD is part of a much larger body of work to solve the problem of low adhesion. It aims to specifically focus on the leaf fall measurement component of the solution by developing a robust leaf fall sensor that can capture the change in leaf fall at a high temporal and spatial resolution. This aim will be met by the following objectives:

1. Investigate and develop low-cost imaging approaches to monitor vegetation
2. Using a prototype device, test the utility of the approach in measuring daily leaf fall over autumn
3. Demonstrate how the low-cost imaging approach can be scaled up in relation to current practices
4. Produce a broader blueprint to integrate the work within the wider research effort for understanding the fundamental causes of low adhesion

This work is funded by the Engineering Physical Sciences Research Council (EPSRC) but is also financially supported by the Rail Safety and Standards Board as a strategic piece of work within its broader 'Rail Capability Plan' (Table 1.10).

Table 1.10 – The ‘Rail Capability Plan’ (RSSB, 2017).

Key Strategies	How this will improve the rail industry
1. Running trains closer together	Increasing sensors on trains to identify their position in real time. A safety zone will be placed around each train and updated as the trains move through the rail network. This will increase the capacity of people on the network with more trains running at once. The replacing of lineside signalling with automatic sensors and train to train communication will improve rail safety. Further research is also needed into the ability for trains to brake in low adhesion areas and the automatic real time data sharing of this information with other trains on the track.
2. Minimal disruption to train service	The use of internet sensors to relay real time data across the rail network to pre-empt issues on the rail line. This increase in technology will also look at drone and satellite data and further monitor any potential problems before a disruption to the rail industry is caused.
3. Efficient passenger flow in transit	A redesign of current railway platforms will allow a smoother passenger flow through the station. This is in the form of smart ticketing, virtual assistants and up to date information for rail passenger whilst on their journey.
4. More value from data	Increase in real time useable data that can inform decision makers quickly and efficiently regarding all aspects of the rail network.
5. Energy efficiency	Despite already being more energy efficient than other major modes of transport, the rail sector is looking at improving the energy usage of current railways. This includes electrification of the rail line and the use of alternative fuel such as self-powered trains compared to traditional fossil fuels.
6. More space on trains	Reimaging of the inside of a train to better facilitate the changing demographics of train users. There is also the

	potential on certain train routes to run double-decker trains to increase passenger capacity.
7. Service time to the second	Development of on train monitoring systems to relay instant data about the positioning of the train.
8. Intelligent trains	Investing in smart technology where trains can regulate speed and mechanics based on where they are supposed to be and the problems on the tracks. This will reduce the need for lineside signals.
9. Personal customer Service	Development of communication technology that can interact with the customer on a journey by journey level. Showing up to date information on connecting trains and access to platforms.
10. Flexible freight	Redesigning the freight train carriers to improve the capacity on the network. This includes a structural redesign of carriages and an automated loading approach to optimise handling of items and reduce cost.
11. Low cost railways	To produce low cost and efficient sensors and train carriages to help increase the sustainability of the rail network.
12. Accelerated research, development and technology deployment	Working with research and development teams to reduce the time it takes to introduce new technology to railways. Including more cross-communication between different operating sectors within the railways.

Specifically, this research focusses on:

- Key strategy 2, by increasing technology usage around the network by developing low-cost internet connected leaf fall sensors;
- Key strategy 4, by increasing the use of real-time data along the network;
- Key strategy 8, by testing a prototype onboard device that can be added to the network in order to increase the possibility of intelligent trains. The use of intelligent

trains is also being explored by artificial intelligence on the railways which includes moisture monitoring;

- Key strategy 11, by reducing the need for expensive satellite data and replacing it with high resolution, cheap low-cost sensors across the network;
- Key strategy 12, by continuing the collaboration of industry and rail – with the help of the Met Office, the University of Birmingham and the EPSRC this research project has moved at a quick pace to develop and research innovative solutions to rail problems (*RSSB, 2017*).

1.12 Thesis outline

This thesis will be divided into 7 chapters as discussed below:

Chapter One - Autumn effects on the UK rail network, discusses the problems associated with autumn vegetation on the rail network including low adhesion and low adhesion incidents. The chapter concludes that there is a research gap in low-cost observation techniques in order to improve leaf fall forecast operation and validation.

Chapter Two - Review of leaf fall measurement techniques, investigates the different ways in which leaf fall can be recorded including direct and indirect measurements. The chapter discusses the use of using hemispherical photography and sky-view factors as ways to record tree canopies (amount of leaves above ground on a tree). The chapter further looks at the emerging technology known as the internet of things in order to record low-cost data and the potential to use this technique in leaf fall recording.

Chapter Three– Development of a low-cost leaf fall sensor, conducts research around the potential to use a mobile phone and alternatively a Raspberry Pi as a low-cost

hemispherical device. In this chapter a mobile fisheye lens is adapted to attach to a Raspberry Pi and tested against the current best market apparatus the Nikon Coolpix FC-E8 lens.

Chapter Four– Designing an operational leaf fall device for an autumn field campaign, tests the apparatus built in chapter 3 over two autumn seasons and with different tree species data. The output from the Raspberry Pi is compared to an independent leaf fall observer.

Chapter Five– Automatic data processing for integration of leaf fall data into a forecast model, develops an automatic leaf fall code which can capture a hemispherical image and produce a percentage of leaf fall automatically on the Raspberry Pi device in order to reduce manual operation of the leaf fall sensor. The output of the leaf fall code is compared to manually calculated leaf fall threshold data in order to compare and validate the data.

Chapter Six– A blueprint for autumn monitoring systems, discusses the future potential of the leaf fall sensor and tests the apparatus on a moving train. This chapter further sets out plans for a wider sensor network which incorporates other aspects of the leaf fall and low adhesion forecast discussed in chapter one.

Chapter Seven– Evaluation of the PhD and the original contribution to science, concludes the thesis by reflecting on the aims and objectives of the PhD and the contributions this research has made to the scientific community.

Chapter One Summary

The 'Leaves on the Line' problem occurs across the UK rail network due to a combination of leaf fall and weather conditions which result in a lowered adhesion coefficient between the rail track and the wheel of a train. During autumn, leaf fall prediction models aim to assist rail companies in highlighting days in which significant low adhesion may occur on the rail network. However, given the spatial nature of the problem, it is clear that high resolution models need to be utilised to better assist in the management of low adhesion and moisture detection.

Unfortunately, the current state-of-the-art in terms of observations is not conducive to facilitating this and there is a clear research gap to better develop techniques to observe the causes of low adhesion on the railway network. This research gap has led to the primary aim of this thesis which will explore the potential of low-cost imaging techniques to monitor leaf fall.

Chapter Two

Review of leaf fall and leaf fall measurements

2 Introduction to Measurement Techniques.

Vegetation is recorded across a wide range of scientific disciplines. In urban landscapes recording the amount of vegetation can be used as an indicator of air quality on a small spatial scale with an area of increased vegetation resulting in a reduction of urban air pollution (*Jayasooriya et al., 2017; Grote et al., 2016*). In hydrogeology the recording of vegetation around a stream can indicate the amount of external food sources for freshwater invertebrates as well as the river dynamics (*Weekes, 2018; Gurnell and Grabowski, 2016; Vannoppen et al., 2016*). In climatology the recording of different types of vegetation and the timings of leaf budding and leaf fall in an area can indicate long term climate change (*Ford et al., 2016; Nowacki and Abrams, 2015*). In forestry research the recording of vegetation can be used to assess the health of a forest, the amount of nutrients available within a forest canopy, the ecological diversity of an area as well as the effects of forest fires (*Chu et al., 2016; Lawley et al., 2016 ; Michez et al., 2016; Wang et al., 2016; Lévesque and King et al., 2002*). In the rail industry vegetation is monitored as a way of predicting leaf fall on the rail network (*Met Office, 2018b*) as well as providing a review of vegetation along a rail track (*Varley, 2018*). With the need to record vegetation across a plethora of scientific disciplines the way in which trees are recorded needs to be reviewed.

In this chapter both direct and indirect measurements for recording vegetation, with a specific focus on leaf fall (the amount of leaves fallen from a tree), will be discussed including: harvest sampling, sap sampling, leaf traps, radiation measurements, gap function analysis and the use of hemispherical imagery (*Bréda, 2003; Jonckheere et al., 2004; Liu et al., 2015*). Further to the methods in which leaf fall has been recorded, the current advancement in vegetation technology will be reviewed including, low-cost sensors and Raspberry Pi technology potential. This chapter will also discuss the methodological considerations needed when developing ways in which leaf fall could be recorded along a rail network.

2.1 Direct Vegetation Measurement Techniques

Direct leaf fall measurements are recording techniques that remove leaf litter from the ground or record measurements from the tree itself in order to determine the amount of leaves fallen from a tree. In general, direct leaf fall measurements require a combination of in field collection techniques and laboratory-based post analysis. The main four direct leaf fall measurement techniques are discussed in this section; harvest sampling, sap sampling, leaf litter traps and needle sampling. Currently, autumn leaf fall is estimated in numerous ways across the UK; leaf fall observers, forecast models, 'Citizen Science' projects and satellites are all used to estimate leaf fall during the autumn period (*Woodland Trust, 2017; Kosmala et al. 2016; Havens and Henderson, 2013*). However, as phenology is sensitive to changes in microclimate, there is a need to develop a way to record leaf fall over time at a high spatial and temporal scale.

2.1.1 Leaf fall Observers

Leaf fall forecasts, such as those produced by the Met Office and Met Desk (*Met Office, 2018; Crawley et al., 2017*), require accurate leaf fall information from a range of tree species and currently use a network of leaf fall observers (*Met Office, 2018*). However, no technique is currently fit for purpose to provide the required data at sufficient resolution. For example, on a national scale in the UK, untrained leaf fall observers contribute to an autumn phenology database managed by the Woodland Trust (2017). Volunteers add details pertaining to first leaf tinting, first leaf fall, full autumn tinting and bare tree of various species including, Horse Chestnut, Beech, Silver Birch and Elder. This database of 2,300 observers is used to collect and analyse trends in autumn phenology. Primarily this was to look at the effects of weather and climate on native species, beginning in 1999 (*Woodland Trust, 2017*). Despite the large number of observers across the UK in the Woodland Trust network, this database is not actually a record of daily leaf fall.

2.1.2 Harvest Sampling

One form of direct measurement is harvest sampling (*Bréda, 2003*). This technique relies on the collection of fallen leaves in a given area of woodland. Once the leaves have been collected, dried and weighed, the weight of the fallen leaves can be applied to allometric regression equations, these are equations based on the relationship between the size and height of a tree in relation to the volume of a tree (*Pastor et al., 1984; Clark et al., 2001*). Allometric regression equations use easily measured parameters such as tree height or trunk circumference to infer quantities that are more

difficult to measure such as the percentage of leaves remaining on the tree (*Karlik and McKay, 2002*).

The issues with using leaf harvesting and allometric equations occur at several stages. Firstly, litter in harvesting must be fresh and not contain any mulch or lingering litter as to avoid over weighing the fallen biomass (*Chambers et al., 2001*). Equations can be written to combine new and old leaf fall, however this can still increase overestimation of total or remaining leaves on the tree (*Clark et al., 2001*). Harvesting leaf litter and applying allometric equations to a mix species forest area is not extensively applied in current literature. This is due to allometric equations being species specific and therefore collecting mix leaf litter and entering the weight into an equation would be invalid (*Tobin et al., 2006*). Therefore, collecting leaf litter could be a laborious task in a mixed deciduous forest especially if the litter has begun to decay making identification difficult.

Further issues arise when using allometric equations and harvesting in an area of different aged trees (*Tobin et al., 2000*). Leaf foliage tends to decrease with the age of the tree. In order to assess woodlands, allometric equations would be needed for each species and then further equations depending on the age of the species (*O'Brien, et al., 1995, Peichl and Arain, 2007*). Harvesting relies on equations being conducted after the leaf litter is collected and weighed. The problems with sampling individual species and separating the age of the tree makes the harvesting method unsuitable for collecting instant leaf fall measurements.

2.1.3 Sap Sampling

Like harvesting methods, sap sampling uses direct measurements coupled with models to predict the leaf foliage of a given tree (*Waring et al.*, 1982; *Kodani et al.*, 2002; *Bréda*, 2003; *Liu et al.*, 2015). Sap sampling uses the pipe model theory in which the number of leaves on a given tree is proportional to the sap wood cross sectional area of the tree (*Shinozaki et al.*, 1964a; *Shinozaki et al.*, 1964b; *Waring et al.*, 1982). *Shinozaki* (1964a) based the theory on experiments looking at the correlation between number of branches as well as the area of a given tree branch to the number of leaves on each tree. The model shows that within a tree there is a system of pipes which start from the base of the tree and go to the tip of the branches. The number of these pipes can indicate the amount of leaves. As a tree grows, branches at close to ground level are lost. Mainly due to larger branches reducing sunlight and the dead branches leave disused pipes within the tree trunk (*Shinkozahki et al.*, 1964a).

Therefore, when measuring the number of pipes within the tree, the measurement must be taken just before the start of any branching. This makes measuring the tree species difficult. This approach was validated by felling a small number of species and then the results inferred on a wider population of mixed deciduous trees including popular UK species such as Birch. As well as the collection height, further complications arise when trying to collect samples from a range of tree species at different ages (*Tobin et al.*, 2006, *Shinkozahki et al.*, 1964b). One collection sample may not represent a whole forest or a range of trees along a rail track.

Furthering this work, *Waring et al.* (1982) were able to estimate leaf number based on the pipe theory using only the cross-sectional sapwood area of a tree at different heights. Unfortunately, the relationship between leaf area and number of pipes

decreases at breast height. This is due to the decreasing amount of transpiring tissue there and increased woody bark (*Bartelink et al., 1997; Waring et al., 1982*). As well as height sampling problems, the age of the tree also creates problems for the allometric relationships. This may be due to the increase height of tree altering the hydraulic mechanisms within the trunk of the tree (*McDowell, 2002*). In knowing the number of leaves expected to grow per tree, problem areas could be identified where large leaf number equals a large percentage of fall in autumn. However, this approach to leaf canopy measuring would not give a continuous leaf fall measurement over an autumn period.

2.1.4 Leaf Traps and Needle Point Sampling

Other forms of direct leaf fall measuring involve capturing leaf litter as it falls into traps or by needles on the ground (*Bréda, 2003; Jonckheere et al., 2004; McShane et al., 1983; Dufrêne and Bréda, 1995*). The trap measuring involves large mesh canopies or boxes placed around the tree which captures falling leaf litter. There is not a clear indication of the best way to lay the traps (*Jonckheere et al., 2004*) as it depends on individual tree species as to which collection method is more suitable (*McShane et al., 1983*). However, research has been conducted using transects, various height and placement designs and random placements methods (*McShane et al., 1983; Dufrêne and Bréda, 1995*). The trap method of collection has shown to be accurate (*McShane et al., 1983; Morrison, 1991*).

Similar to the harvesting method, the leaf litter is collected, weighed and then leaf area index can be calculated. This method reduces the error from other contaminants on the ground such as soil or mulch to calculate only for this season fallen leaves.

However, like the harvesting method, only trees of the same species can be captured in the traps (*Bréda, 2003; Jonckheere et al., 2004*).

An alternative to both harvesting and leaf traps when collecting leaf litter is the needle point method. The needle point approach to capturing leaf fall requires a large sampling area approximately 100 – 300 needles per area (*Bréda, 2003; Dufrêne and Bréda, 1995*). The needles are placed around the tree at equal measures. When the leaves fall a percentage of the total leaf fall will be captured directly on the needle (*Jonasson, 1988*). A regression equation can be applied to scale up the amount of leaves fallen onto the needle and the amount of leaves fallen in a given area (*Jonasson, 1988*). Like the other sampling methods this method does not show how fast the leaves fall at a giving time but rather over a collection period.

2.2 Indirect Vegetation Measurement Techniques

Indirect leaf fall measurements use other measurable parameters to infer the amount of vegetation in an area for example the amount of radiation from above and below a canopy can indicate canopy thickness and thus the relative amount of vegetation in an area (*Jonckheere et al., 2004*). Indirect methods vary both on the type of equipment used to capture the vegetation and the spatial scale in which vegetation can be recorded.

2.2.1 Radiation methods

Radiation methods infer leaf measurements from the transmission of radiation through the canopy to the ground (*Jonckheere et al., 2004; Weiss et al., 2004; Bréda, 2003*). More radiation will be present above a tree canopy in comparison to below the canopy due to the leaves absorbing the incoming radiation. The greater the number of leaves on a given tree, the less radiation can reach the ground surface (*Jordan, 1969*). The radiative transfer theory (*Ross, 2012*) uses the zenith angle, G function (fraction of foliage projected on the plane normal to the zenith angle) and leaf angle (*Bréda, 2003*) to calculate the leaf canopy (equation 2.1).

$$P(\theta) = e^{-G(\theta,\alpha)LAI/\cos(\theta)} \quad (2.1)$$

θ = Zenith angle

$G(\theta, \alpha)$ = G function

α = Leaf angle

$P(\theta)$ = gap function

LAI = leaf area index

Light scattering can cause errors with this method due to leaf angle, spacing between leaves and leaf clumping (*Schaefer et al., 2015; Weiss et al., 2004; Kodani et al., 2002; Gower et al., 1999; Jordan 1969*). However, measuring at various points below the tree canopy and above the canopy in transects can reduce the overall error for a tree species (*Behera et al., 2010*). Gap function is defined as the percentage of open sky that is not covered by canopies (*Welles and Cohen 1996; Stenberg et al., 1993*). The Gap function method assesses radiation below and above the canopy, reducing errors from clumping of leaves and leaf angle within a canopy (*Weiss et al., 2004; Gower et*

al., 1999). Equation 2.2 shows how to calculate the gap function which is independent of leaf angles (*Jonckheere et al.*, 2004; *Bréda*, 2003; *Welles and Cohen*, 1996).

$$LAI = \ln(P(\theta)) \cos \theta / G(\theta)$$

$$\theta = \text{Zenith angle} \quad G = \text{G function} \quad P(\theta) = \text{gap function} \quad (2.2)$$

The main assumptions of both radiative approaches are that the individual sizes of the leaves are small in comparison to the tree canopy and that leaves are randomly distributed. The gap function method further assumes that transmittance is equal to the gap function (*Bréda*, 2003).

2.2.2 Near-infrared Technology

Near-infrared images capture objects in the near-infrared spectrum; which is a wavelength between 0.7 – 1.2 μm (Figure 2.1). Vegetation in the visible spectrum appears green due to the chlorophyll absorbing energy from the blue and red wavelength and reflecting green wavelengths. However, in the near-infrared spectrum vegetation appears red due to the reflectance of mesophyll within the leaf (Figure 2.2). Due to the photosynthetic absorption properties of vegetation a near-infrared image can distinguish between the bark and leaves of a tree with the vegetation appearing bright red in colour and the bark appearing dark (Figure 2.2) which allows vegetation to be clearly identified (*Knipling*, 1970).

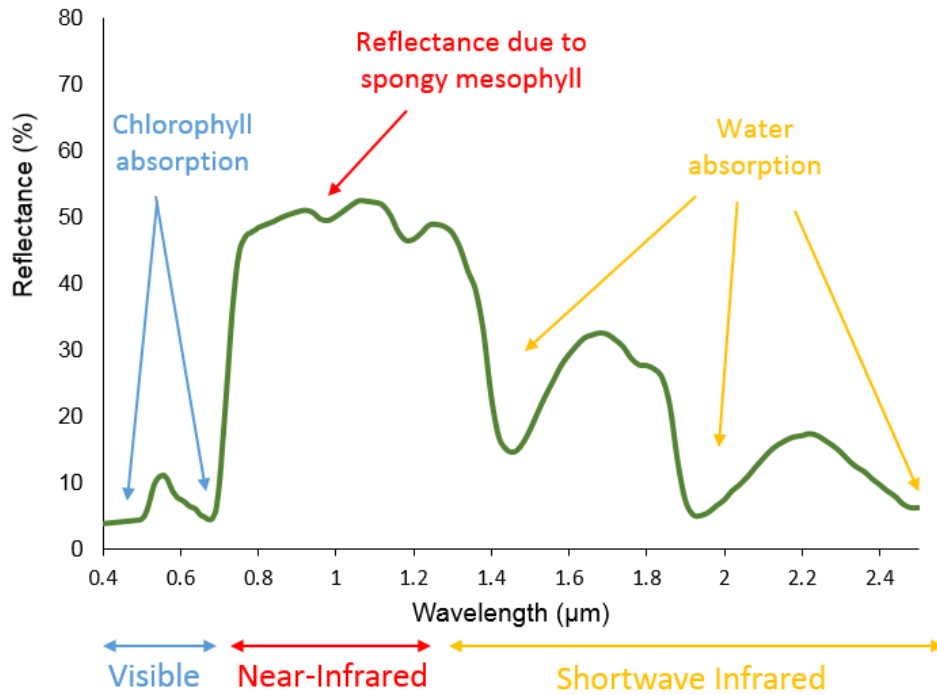


Figure 2.1 - Spectral reflectance curve of vegetation (GSP, 2016).

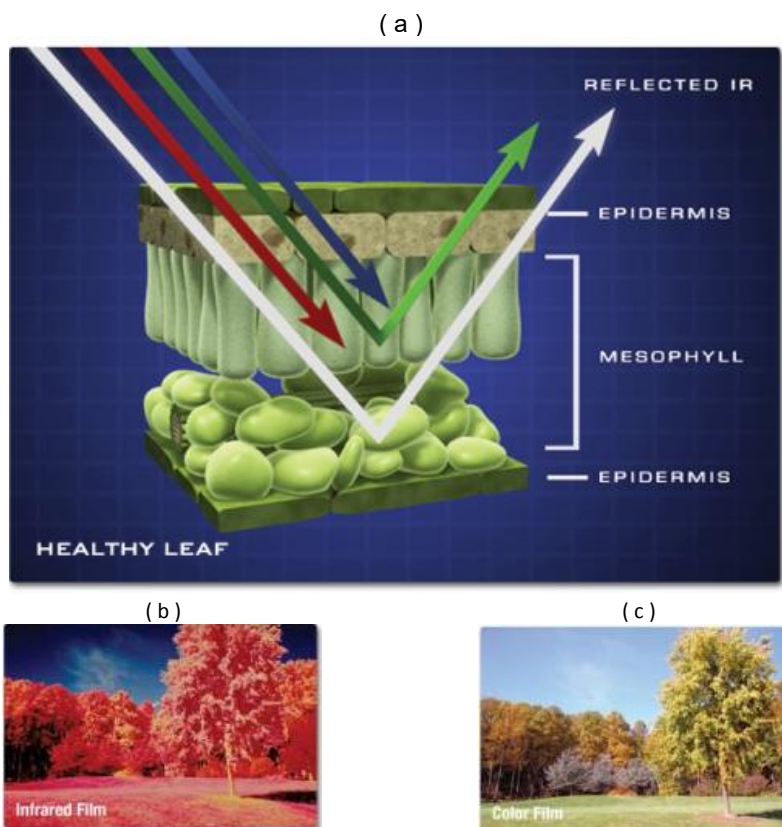


Figure 2.2 (a) Reflectance of a leaf structure (Carns, 2019), (b) Photograph of vegetation captured in infrared (Butcher, 2019), (c) Photograph captured using a colour film (Butcher, 2019).

Near-infrared imagery is usually used in vegetation indices captured from aerial photographs showing “greenery” over a large spatial scale (*Mattar et al., 2016; Liang et al., 2012; Fang et al., 2003*). Felderhof and Gillieson (2011) used aerial near-infrared images to capture vegetation reflectance of a tree canopy. This paper examined the approach of combining near-infrared captured images with satellite data to view tree health on a large spatial scale in which data captured informed where fertiliser was needed in order to improve vegetation growth rates in Canada. The use of near-infrared aerial photography was also utilised in Zarate-Valdez et al., (2012) paper in order to predict the leaf area index of almond plants, this research used the availability of satellite acquired near-infrared vegetation indices but also calibrated the data using hemispherical digital images.

Holmgren and Persson (2003) showed that the near-infrared technology combined with vegetation knowledge such as crown height, could also be used to distinguish between tree types - specifically deciduous and coniferous species. The paper also explores the ability for individual trees to be classified using near-infrared technology such as distinguishing between Norway Spruce and Scots Pine. The paper concluded that future research using near-infrared digital photography could improve the methodology and the classification accuracy of the aerial near-infrared imagery.

Hovi et al. (2016) again looked at the potential for near-infrared technologies to classify individual tree species looking specifically at Pine, Scott and Birch trees. Whilst the Hovi et al. (2016) showed that individual tree species could be classified it noted that there is a seasonal variation in reliability of data. With late summer recording of tree species resulting in less accurate classification, further research would explore this accuracy variation.

2.2.3 Normalised Difference Vegetation Index (NDVI)

NDVI is derived from satellite data that records the amount of vegetation in a given area (as shown in Figure 2.3). The principle of the approach uses near-infrared and visible radiation to detect the amount of vegetation at relatively high resolution. Due to the reflective properties of vegetation; if a high percentage of near-infrared radiation is reflected there is a high density of greenery in an area (*Houborg et al., 2007; Schwartz and Reed, 1999*). MODIS and EOS are satellites that calculated the NDVI on an 8-day time sampling period therefore correctional factors would need to be used when measuring a daily leaf fall change (*Zhang et al., 2003; Schwartz et al., 2002*). During autumn phenology (when leaves change colour due to the reduction of chlorophyll) the reflectance of vegetation decreases (*Gitelson and Merzlyak, 1994*). This results in a low NDVI even if there are leaves left on the tree canopy. Mitigation of this is still poorly understood (Liu, 2016) and therefore when recording changes in autumn leaf fall NDVI should not be used. Satellite data is also affected by weather conditions e.g. rain, cloud, haze (all prominent in the UK autumn) as well as complex land uses, such as urban parks and gardens, which can reduce the accuracy of the overall measurement (*Van Leeuwen et al., 2006; Schwartz and Reed, 1999*). Correctional factors mitigate this problem however different mitigation methods produce different NDVI for an area (*Brown et al., 2006; Justice et al., 2000*). Therefore, when assessing the reliability of NDVI in a leaf fall forecast or measurement more information on recording technique is required.

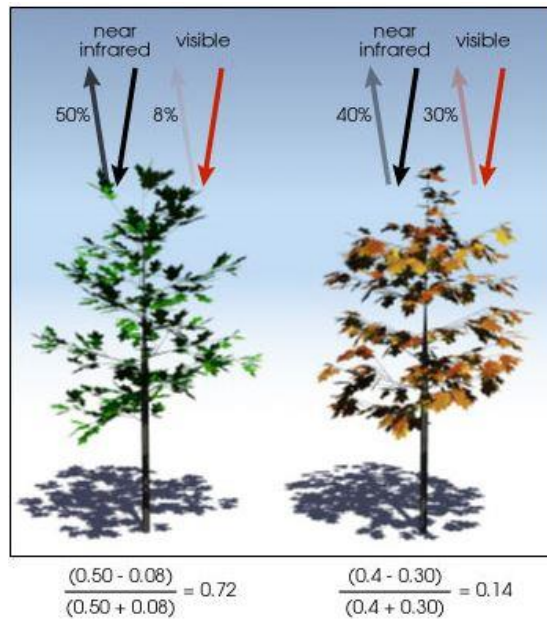


Figure 2.3 - The Normalised Difference Vegetation Index calculation technique (NASA, 2017).

2.2.4 Remote Sensing in Forestry Research

In forestry research, remote sensing has a long history of being used as a way to conduct forest inventories in which large areas of forest could be quantified and analysed using a combination of satellite imagery and ground observations. Such inventories could then be used to calculate how much wood is within one area that could then be used for timber or the amount of forest areas that could act as carbon stores (Tomppo et al., 2008; Köhl et al., 2006; Dong et al., 2003; Hyyppä et al., 2000; Wulder, 1998). Specifically, McRoberts and Tomppo (2016) reviewed the uses of remote sensing in order to construct an inventory of national forest resources within the US. McRoberts and Tomppo (2016) concluded that the use of remote sensing data was a quick and efficient method of capturing and analysing large areas of forest however, the next stage of forestry research sensing development required an advancement of digital remote sensing equipment in order to validate the data on a smaller spatial scale.

Further to wide scale inventories, remote sensing can also be used to analyse forest structure. LiDAR (Light Detection And Ranging) is often used when using remote sensing to assess the structure forest canopies and can be used to capture the horizontal and vertical spacing of a forest as well as the biomass within a forest canopy (*Lim et al., 2003*). The ability to measure the forest canopy at a three-dimensional scale is especially useful for ecologists as it can map out habitats for wildlife on a global scale (*Lefsky et al., 2002*). Hyde et al. 2006 used remote sensing data to assess wildlife habitats; the study noted that whilst remote sensing (with the most accurate technique being LiDAR) can be used to assess average canopy height and biomass, there is still the requirement of manual observations to verify the LiDAR data. However, using this technology is effective when looking a large spatial region and currently no other technology is available to accurately capture canopy distribution on a large scale. The paper further reports that accurate remote sensing of vegetation comes with additional costs and expertise such as; knowledge of an area including cost of data acquisition as well as correctional algorithms for removing atmospheric and topographical errors when capturing data.

2.2.5 Remote Sensing to Capture Change in Forests Over Large Areas

Remote sensing is also frequently used in the forestry community as a way to automatically capture emerging forest fires and log the changes in tree canopies during a fire event (*Yuan et al., 2017; Arnett et al., 2015; Yuan et al., 2015; Tang et al., 2015; Chowdhury et al., 2015*). *Chu et al. (2016)* used satellite data in order to capture the change in canopy coverage after a forest fire in a Siberian boreal forest, and the paper demonstrated that the use of satellite imagery showed the change in greenery over a large scale area and indicate forest regrowth post event, however satellite data often overestimated the actual recovery of a forest due to inaccuracy in vegetation indices. *Matin et al., (2017)* also used remote sensing with a combination of historical records and GIS data to evaluate the spatial patterns of forest fires over large regions and highlighted the benefit of remote sensing when developing yearly observation of tree canopies and building a database of largescale observations. Like *Chu et al. (2016); Hyde et al. (2006)* and *Matin et al. (2017)*, were unable to use remote sensing alone to draw conclusions of the vegetation over large spatial regions. The use of remote sensing and historical data can also be used when looking at changes in vegetation canopies in order to construct early warning systems when forest fires do arise. *Abdollahi et al. (2018)* used the MODIS satellite in order to detect changes in vegetation cover in Canada, combined with surface temperatures and atmospheric variables used remote sensing to construct a forest fire forecast and captured the potential severity of forest fires over a large spatial scale. This paper indicated the importance of having reliable observations of vegetation on a large scale when developing forecast methodology.

The use of remote sensing to capture the change in tree canopies pre and post an event such as the forest fire can also be applied on a seasonal scale. Remote sensing

can be used to capture the autumn phenology across different regions and has previously been used as a commercial tracker of the changing of leaf foliage in New England. During a New England autumn, the colour change of the maple leaves attracts a large number of global visitors. The use of remote sensing allows the 'leaf peeping' community (groups of tourists and businesses that travel to locations based on the changing colours of vegetation) to track the change in colour of the vegetation. On a longer timescale, remote sensing has been used to track the changes in foliage timing as a result of climate change in the northern hemisphere (*Salge, 2018*).

Using satellite and remote sensing data from 1982-2011, Liu et al. (*2016*) found that increasing temperatures due to climate change delayed the start of autumn phenology. Further work by Liu et al. (*2017*) analysed satellite data from 1982 to 2014 in order to analyse long term trends in vegetation, foliage during autumn and analysed trends in peak timings due to various weather conditions. The paper concluded that summer rainfall and temperatures had an effect on the timings of peak leaf fall. The use of long-term trends in this paper could also then be used as an input in future climate models to understand the effects of various climate scenarios on autumn vegetation.

2.2.6 Ground Based Remote Sensing

Radiation can also be modelled and measured using ground based remote sensing techniques, for example hemispherical imagery and plant canopy analysers such as the LAI- 2000 plant canopy analyser (*Liu et al., 2015; Bréda, 2003; Kodani et al., 2002; Welles and Cohen, 1996*). Satellites show the amount of vegetation over large areas allowing observations on a wide scale to be made. This is useful for long term climate change observations and forest fire surveillance (*Yuan et al., 2017*), however satellites are affected by atmospheric weather conditions and also do not capture the change in vegetation below the tree canopy (*Van Leeuwen et al., 2006*). However, the principles of remote sensing are not limited to space-based platforms. Hemispherical photography and LAI-2000 plant canopy analysers calculate sky-view factors (the amount of visible sky within an image) with low levels of bias (*Liu et al., 2015; Stenberg et al., 1993*). These devices take images of the tree canopy at ground level, allowing an observation of vegetation below the canopy to be captured. From the images a sky-view factor can be calculated. A similar method can also be performed from a digital camera with a fisheye lens attached. A fisheye lens is a wide angled lens, when added to a camera the lens produces a 180° hemispherical image which can be processed and analysed to calculate sky-view factors. (*Liu et al., 2015; Chianucci et al., 2015*).

2.2.7 Sky-View Factors

A sky-view factor is a dimensionless parameter that indicates the proportion of visible sky in an image and is represented as a value between 1 and 0 (Liu et al., 2015; Bréda, 2003; Chapman et al., 2001; Stein, 1980). A sky-view factor nearing 1 will indicate a full sky can be visible from an observer point such as an open field, however with increasing obstructions such as trees or buildings the visible sky would decrease and the sky-view factor will approach 0 as shown in Figure 2.4 (Oake, 2002).

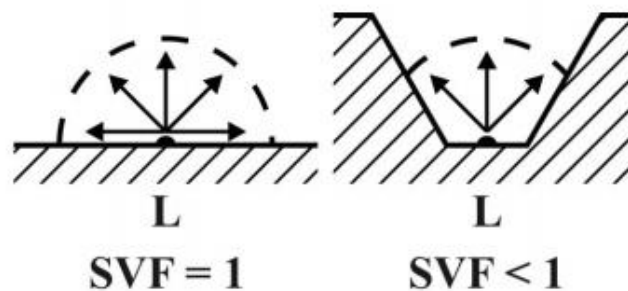


Figure 2.4 - Schematic diagram of different sky-view factors based on surrounding obstacles (Hämmerle et al., 2011 adapted from Oke 2002).

Steyn (1980), used a camera with an attached fisheye lens to calculate sky-view factors within an image. Figure 2.5 shows how an object is projected onto an image when using an equiangular fisheye lens and thus altering the amount of visible sky within an image.

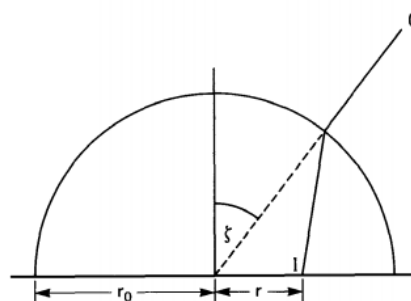


Figure 2.5 - Projection of an object in an image when using an equiangular fish-eye lens where O = Object, I = Image and $r = \frac{2r_0 z}{\pi}$ (Steyn, 1980)

Once the image has been taken the total sky-view factor is calculated by sectioning the image into rings of equal width and angular width as shown in Figure 2.6, within this the percentage of sky can be calculated (*Chapman et al., 2001; Steyn, 1980*) as shown in equation 2.3 (*Bernard et al., 2018*).

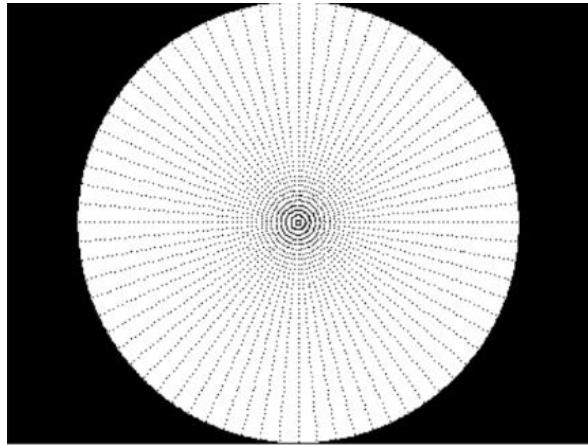


Figure 2.6 – Series of concentric rings represented by dots in a hemispherical image used to calculate sky-view factor of the whole image (*Lindberg and Holmer, 2010*).

$$SVF = 2\pi - \sum_d^{ND} S_{H_d'} \quad (2.3)$$

where d = is the number of concentric rings (azimuthal ray distortion) $S_{H_d'}$ =The percentage of sky hidden due to obstacles. Therefor SVF is the sum of each concentric rings ration between image and sky in order to construct a full hemispherical SVF of a given area (*Bernard et al., 2018*).

The sky-view factor is most commonly used in the scientific literature for urban climatological applications. In previous research, conducted in the 1980s and 1990s, sky view factors have been predominantly used in calculating urban geometry and was based on the ratio of building heights to widths calculated either geometrically or using photography (*Brown et al., 2001; Johnson and Watson, 1984; Watson and Johnson, 1987; Holmer, 1992*). Blennow (1995) began to speed up the rate in which fisheye photography could be analysed by scanning photographic negatives into a computer however, this sky-view analysis was still slow and took time to process the data. Grimmond et al. (2001) developed a rapid method to calculate sky-view factors in urban areas by using a digital camera and an FC-E8 attached fisheye lens, this decreased the time spent on collecting and analysing data. Chapman and Thornes (2004) built on the work by Grimmond et al. (2001) and Blennow (1995) by developing a real time method to calculate sky-view factors, but the accuracy of the method was limited by the computing power at the time of publication.

With increased computing power there has been an advancement in the speed in which sky-view factors can be calculated. A series of techniques are now available to calculate sky-view factors from images in near real time. These (discussed further in chapter 6) include software programs that have been developed to automatically calculate sky-view factors from digital images such as 'HemiView', 'Skyview', 'RayMan model' and the 'sky-view factor calculator' (*Matzarakis et al. 2010; Linberg and Holmer, 2010; Matzarakis et al. 2007; Jonckheere et al., 2004; Delta-T Devices Ltd, 1999*). However, there is still an issue of automated calculations of sky-view factors. This problem, first discussed in Chapman (2004), found that the use of automatic thresholds reduces the credibility of analysis. An automatic threshold converts a

hemispherical image into a binary image (black and white photograph) in order to calculate a sky-view factor. The problem of setting a threshold (number at which pixels in a certain colour range above that threshold number will turn black and every other pixel will turn white) is that some objects may be misclassified. This would result in some objects in the image being classified as sky when in fact they are part of a building or vegetation but lighter in colour than the threshold set. An example of how different thresholds can produce different binary images is seen in Figure 2.7 where sky has been classified as vegetation in 2.7(d) and vegetation has been classified as sky in Figure 2.7(e) (*Inoue et al., 2011*).

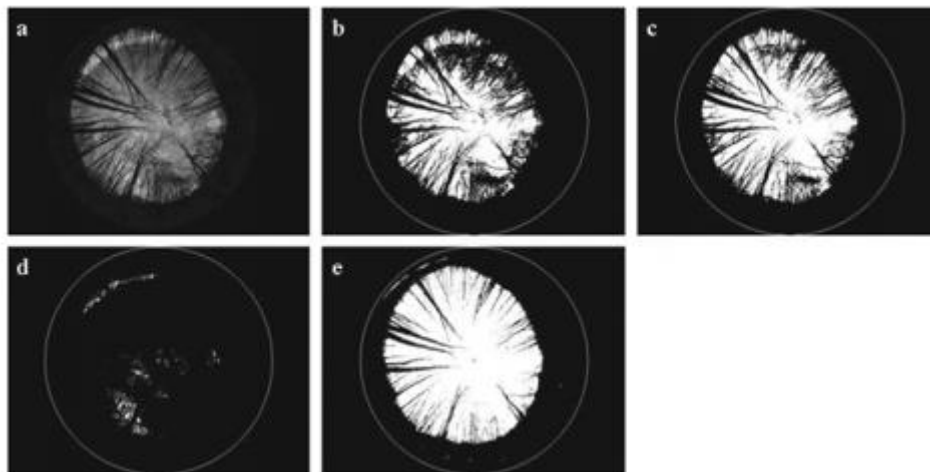


Figure 2.7 Variation in images from the original photograph (a) under different threshold limits (*Inoue et al., 2011*).

Using these approaches, sky-view factors have been used to determine temperature differences in urban areas and can be used to calculate the urban heat island effect. Svensson (2004) used fisheye photography captured at different height levels and used regression analysis to determine the link between air temperature and sky-view factors. The paper showed a strong relationship between images captured at ground level and temperature measurements. Despite strong correlations in temperature and sky view factors in the Svensson (2004) paper this is not always the case in other

research. Contrastingly, Blankenstein and Kuttler (2004) found weak correlation between air temperature and sky-view factors in urban areas. It is important to note the Blankenstein and Kuttler (2004) research was conducted over one year and in one European city, concluding that whilst the relationship between longwave radiation and sky-view factors is strong, the air temperature is determined more by micrometeorological factors such as wind through an urban canyon. Unger (2004), noted the discrepancy in literature when determining the relationship between temperature and sky-view factors. The research conducted by Unger (2004) ultimately found that a conclusion could be drawn from sky-view factors in relation to temperature, but only if an appropriate number of sites (covering a whole city) were measured. The relationship between the two variables was further confirmed in Unger (2009), Chen et al. (2012) and Wang and Akbari (2014).

In forestry research, sky-view factors can also indicate the change of leaves over a season; with the more sky visible the fewer leaves remaining on the tree. However, prior to calculating the change over a season, the initial calculation of full canopy is needed. Once the sky-view percentage is removed, the remaining objects within the photograph contain leaves and the bark, branches and twigs within the tree, known as 'wood-area index' (Liu et al., 2015; Chapman, 2007). The wood-area index is subtracted from total plant area index (the total remaining objects once the sky-view factor is subtracted) to give the leaf area index (Liu et al., 2015). Therefore, when calculating the change in leaf canopy over an autumn season, the bare tree sky-view factor would need to be calculated and then subtracted from the changing canopy in order to determine overall percentage change.

2.2.8 Hemispherical Digital Photography

The method again moved from film cameras to digital cameras in the late 90s (*Englund et al., 1999*). Thus, the main method used to determine leaf area index in tree canopies is a digital camera with an attached fisheye lens in which sky-view factors can be calculated to determine the amount of vegetation in an image (*Jonckheere et al., 2004; Chen et al., 1991*). Early work by Whitford et al. (1995) noted that hemispherical photography when analysing tree canopies overestimate leaf area index by up to 78% in dense forest canopies, however, when removing the area of bark and wood from the image the over estimation was reduced to 32%. This error has improved with the advancement of digital photography. Liu et al. (2013) used hemispherical digital photography to analyse the leaf area index below apple trees. The research showed that clumping of leaves in the captured images did not account for large overestimation errors and therefore used this to model evapotranspiration rates in leaf canopies.

As well as measuring leaf area, hemispherical photography has also been used in the winter months to determine canopy structure when there are no leaves present to distort an image. Reid and Essery (2013) used hemispherical photography to capture tree structures over the winter period. An automatic threshold was set to remove glare from sunlight and to create a bold outline of the tree trunk and branches. Combined with an algorithm to join bark together that had been removed due to sunspots on the lens, this method captured an accurate reflection of tree structure. This semi-automatic approach was still subject to manual alterations, but was effective at reducing estimation errors caused by capturing vegetation using hemispherical photography.

Research by Chianucci (2016) has suggested that digital canopy photographs (captured without a fisheye lens) are more accurate than using hemispherical

photographs as there is less distortion when capturing gaps in the canopy. This method was also used by Poblete-Echeverría et al. (2015) to analyse gap function and leaf area index in apple trees however hemispherical images and fisheye lens remains the dominant method when recording change in vegetation (Liu et al., 2015; Malenovský et al., 2010; Garrigues, et al., 2008; Frazer et al., 2001).

As with using hemispherical images in urban environments one of the main issues when analysing leaf area index is the automatic exposure and automatic threshold required to analyse the images (Jonckheere et al., 2004). Zhang et al., (2005) showed that images captured under different weather conditions required different levels of exposure from a digital camera in order to reduce estimation errors. A high exposure rate in which the sky appears white against foliage could be set based on a light meter next to a camera. This research showed the importance of contrast in hemispherical images. This increased contrast is also one of the main principles in capturing vegetation in the near-infrared spectrum.

2.2.9 Near-infrared Hemispherical Photography

Chapman (2007) showed that there is potential for the use of near-infrared digital cameras that could be accessible for researchers to use in the field at a ground level. Using this methodology, validation and comparisons of top down satellite produced vegetation indices such as the NDVI could be conducted using the same light spectrum. Whilst previous studies show the importance of near-infrared capturing, this was the first study to offer a customised, relatively low-cost apparatus to conduct research in the near-infrared spectrum using a digital camera. To convert a standard digital camera to a near-infrared camera the infrared blocking filter must be removed

and replaced with a cold place mirror and a plain clear glass filter. This can be done manually on an 'off the shelf' standard camera. The paper concluded that given the feasibility and cost of the equipment, this new apparatus has the potential to conduct NDVI measurements at a much larger spatial scale.

Osmond (2009) used the conversion technique of a standard digital camera approach laid out in Chapman's (2007) paper to research the leaf area index in urban areas. The research compared images captured using a regular camera and a near-infrared camera, concluding that in urban landscapes a near-infrared camera is better at capturing vegetation cover. This is because the leaves can be distinguished from non-vegetative material in the image such as background buildings. However further work from Osmond (2010) noted that different types of vegetation result in different levels of distinguishability from buildings in near-infrared photography with grassland being difficult to separate from building structure.

Sasaki et al. (2008) also conducted a comparative study between various near-infrared canopy measurement devices. Whilst vegetation indices were the most accurate in terms of showing the amount of green canopy under ideal conditions, the paper noted that high resolution near-infrared photographs were comparable to airborne laser scanners in the near-infrared. This research concluded that there is potential in future research for capturing and analysing more canopy structures using near-infrared digital photography alone.

Although now being used in research there are still some universal issues associated with near-infrared technology. Despite accounting for clumping and woody-leaf area ratios, hemispherical imagery and plant canopy analysers can still over or underestimate the leaf canopy if the image is taken on a slope in comparison to flat

surface (*Bréda, 2003; Walter and Torquebiau, 2000*). Further problems with this type of measurement technique is that, like satellites, it may be affected by weather conditions. On a cloudy or dull day, it can be difficult to distinguish the sky-view factor from the leaves on the trees due to the lack of incoming solar radiation visible in the infrared scale (*Chapman, 2007*) and on a wet day the raindrops may obscure the lens and therefore cause blurring on the captured image. However, during autumn weather conditions will be varied and can alter throughout the day. Therefore, ground up measurements, which are affected less than satellites and top down measurements, would best indicate leaf fall on a daily basis (*Kodani et al., 2002*).

2.3 Evolution of scientific equipment

Whilst direct methods can be used to verify the indirect methods discussed above, the advancement of technology has led to more accurate ways to record leaf fall resulting in less need for direct methods to be used. The evolution of scientific equipment occurs as new technology is available to conduct experiments in a cheaper or more reliable way. In tree canopy analysis, hemispherical imagery between 1989 and 1995 moved from film photography into digital photography (*Jonckheere, 2004*). This saved time on the process of photo development but also allowed more images to be taken and stored on a film camera. However, from 1995 there has been a decline in the rate of improvement of digital photography, with the Nikon Coolpix camera still the most used in tree canopy research and hemispherical data collection (*Chianucci et al., 2015; Liu et al., 2015; Chapman, 2007; Frazer et al., 2001; Jonckheere, 2004*).

Low-cost sensors are devices that can record variables in a scientific manner for a significantly lower cost than conventional or alternative monitors (*Chapman and Bell,*

2018). Any alternative low-cost sensor must be compared with the best available market option, the device doesn't have to be better than a high-end product but does have to record a similar range of outcomes to be considered viable (*Chapman and Bell, 2018; Heal et al. 1999*). In addition, low-cost sensors do not have to be custom built, they can be developed from technology that is conventionally used for alternative means for example Hut et al. (2010) adapted a remote controller from a Nintendo Wii videogame console to use as a water sensor for hydrological research.

One of the main benefits of low-cost sensors is their ability to produce a larger spatial and temporal network of sensing equipment. Due to the low cost of the equipment, more appliances can be distributed in an area, increasing the understanding of a given monitoring site (*Chapman and Bell, 2018; Hayes et al. 2008*). Table 2.1 shows how previous expensive technology is being replaced by low-cost sensors in order to increase spatial collection of data.

Table 2.1 Low-cost sensors used in research.

Author	Low-cost Sensor	Standard Sensor
<i>Chapman and Bell, 2018</i>	Road Service Temperature Sensor	A thermistor can be used to record temperature however currently there are no large spatial scale temperature monitors on either the road or rail network and high-resolution modelling is used in temperature prediction.
<i>Mead et al., 2013</i>	Electrochemical Air quality sensor costing (approximately £100s)	The UK AURN network (DEFRA, 2017) requires power cables and an enclosed infrastructure costing up to £80,000 (DEFRA, 2006).
<i>Wu et al., 2013</i>	Low-cost earthquake warning sensor for 10% of the cost of current sensors. Uses accelerometers to detect earthquakes.	Earthquake early warning system network made up of seismometers.

<i>Hayes et al., 2008</i>	Wireless sensor network for monitoring environmental toxic gases using low-cost colorimetric sensors.	Infrared laser differential absorption spectroscopy is used in portable monitoring stations to detect toxic gas (<i>Kolb et al., 2004</i>)
<i>Kizito et al., 2008</i>	Low-cost soil moisture sensors for a larger soil network.	Current technology uses time domain reflectometry costing approximately £900 (<i>Farnell, 2017</i>).
<i>Honicky et al., 2008</i>	Use of mobile phone GPS devices as environmental sensors by attaching environmental monitors onto mobiles.	The UK AURN network (<i>DEFRA, 2017</i>) requires power cables and an enclosed infrastructure costing up to £80,000 (<i>DEFRA, 2006</i>).
<i>van Emmerik et al., 2017</i>	Uses low-cost accelerometers to record the mass of tree species and canopy interception.	Previous research has calculated tree data using empirical methods and measuring of tree trunks rather than sensor data (<i>Stephenson et al. 2014</i>).

2.4 The 'Internet of Things' and mobile phones as low-cost sensors

The 'Internet of Things' (IoT), being such a broad term, incorporates many areas of science and can include sensors, data loggers, adapted Raspberry Pi's and mobile smartphones. If a small device (the thing) has the ability to connect to and send information via the internet, it is included in this general terminology (*Chapman and Bell, 2018; Atzori et al., 2010*).

The use of smartphones has increased in the last decade with more people using their smartphones for cameras, GPS and fundamentally a hand-held pocket computer (*Lane et al., 2010*). Given the connection to the internet and the portability of a mobile device; smartphones are considered an IoT sensor and are being used to collect scientific data (Table 2.2).

Table 2.2 List of studies using smartphone devices.

<i>Monteiro et al., 2016</i>	Used a smartphone attached to a quadcopter to record the altitude and pressure of the first hundred meters of the troposphere.
<i>Hussain et al., 2016</i>	Developed an app and a sensor that could be attached to a smartphone in order to detect the level of fluoride within water. This sensor (FSense) could be used in remote areas with the ability to transfer data of the inbuilt internet connection to a central air quality monitoring station.
<i>Kakria et al., 2015</i>	Developed a wearable sensor attached to an android smartphone that monitored heart rates. The app

	transferred heart rate data over the internet to track and monitor patients heart rates. An alert would be sent to the phone to warn patients of irregular heart rates as an early warning detection system for heart related problems.
<i>Snick et al., 2014</i>	Developed an optical add on camera module for a smartphone (Ispex) in order to capture atmospherically aerosol images. The Ispex add on was distributed to citizen scientists across the Netherlands whom attached the device to their smartphones and uploaded their images to an associated app; resulting in a high spatial and temporal resolution data set.
<i>de Frutos and Castro., 2014</i>	Developed a smartphone software program to conduct road inventories utilising the in-built camera and GPS system.
<i>de Nazelle et al., 2013</i>	Used the built in GPS system and a CalFit app (app that monitors personal activity such as running) within smartphones to track people's movement levels and personal exposure to air pollution.
<i>Petersen et al., 2013</i>	Developed a low-cost oximeter (measures oxygen in the blood using light emitting diodes) that could be attached to a smartphone and analysed using a bespoke smartphone app.
<i>Hasenfratz et al., 2012</i>	Attached an ozone sensor to a smartphone and developed an app that could record and store data on the

	mobile device resulting in a low-cost portable air pollution sensor (<i>Gas Mobile</i>).
<i>Stevens and Hondt., 2010</i>	Developed a smartphone app that could be used to detect noise levels in urban areas. Using citizen science volunteers, the NoiseTube app collected data using the built in GPS and microphone on the device as well as user inputs such as preserved level of noise e.g. loud. This data was instantly uploaded to the internet and a noise map of an areas was produced.

As well as mobile phones, an emerging literature on ubiquitous computing has developed in recent years. Computer systems have moved from desktop analysis tools to in situ recording devices. The Raspberry Pi can be used to monitor multiple factors at once, with a compatible and adaptable programming software and attachable monitoring ports, this low-cost device is beginning to emerge as the next technological advancement in environmental monitoring. Specifically, Ferdoush and Li (2014) researched the feasibility of the Raspberry Pi to act as a low-cost monitoring sensor that could act as a wireless sensor network. The paper states that the small 'credit-card' size computer was easy to configure, deploy and maintain. As one of the earlier papers discussing the role of Raspberry Pi's in future research, the paper was positive, stating that a Raspberry Pi could act as an environmental monitor and communicate over large spatial scales with other pieces of equipment to build a wireless, effective, robust and cheap network.

One of the major concerns with an IoT sensor is that once the device connects to the internet to send data it poses a risk of being hacked, however security coding and passwords at every available access point would reduce this problem (Atzori *et al.*, 2010). Furthermore, the change from old technology to new technology could cause problems in the long-term record of the recorded subject, e.g. leaf fall starting times (Gubbi *et al.*, 2013; Atzori *et al.*, 2010).

2.5 Raspberry Pi Advancement

Hajjii and Tso (2016) discussed the benefits of using a Raspberry Pi as a recording device. Building on the requirement of an IoT device to have the ability to connect to the internet, a Raspberry Pi can act as an internet provider. This ability to have a data dongle (a USB stick with built in 4G wi-fi) attached to the low-cost relatively small device makes the ability to collect and instantly log and transfer data in remote areas feasible. However, Hajjii and Tso (2016) did note that for large scale high intensity analysis the computing ability of the Raspberry Pi (at time of writing) was not at the same level as a desktop computer and further complications arise in energy consumption and battery power.

Basu et al. (2015) further developed the capability of the Raspberry Pi as a way of recording multiple environmental factors on one computer board alone. Given that a Raspberry Pi can be programmed to use multiple computer languages (e.g Python script and Java) it can therefore be compatible with multiple monitoring devices. Basu et al. (2015) used the Raspberry Pi computer board to connect together several pieces of monitoring equipment including a water quality Snode and an acoustic Doppler current profiler. Like in the research conducted by Hajjii and Tso (2016), this meant that the Raspberry Pi could collect, analyse and store data in situ without external inputs. The research further suggested that given the ease in which the Raspberry Pi could communicate with multiple monitoring devices and the relatively low-cost of the computer board, this type of equipment could be invaluable to university classroom teaching when it comes to the future of environmental monitoring equipment. The Raspberry Pi company itself has an ethos of teaching and developing easy and comprehensive instructions in order to make the Raspberry Pi a learning friendly tool

(*Raspberry Pi, 2018*) and thus lends itself well to future developments and adaptations in the technological industry.

Ibrahim et al. (2015) developed the Raspberry Pi further by showing the potential to access the small computer board remotely in order to control the environmental monitoring at various locations. Given the ability for the device to connect to the internet there is also the possibility of remotely accessing the device through the internet, in a two-way communication capacity. A software program (PuTTY) can be downloaded onto the Raspberry Pi that allows remote controlling ability. This is controlled by accessing the IP address of a Raspberry Pi and linking it with a remote sensor. Whilst this seems redundant when automatically sending and storing data it could be useful when errors occur or when additional monitoring is needed. This could also reduce the computing power needed if the device only needs to record conditions on demand rather than set timed intervals for example, recording air quality during an air pollution episode.

It was on the basis of monitoring air quality specifically that Kumar and Kurukshetra (2017) adapted a Raspberry Pi. Attaching sensors to monitor PM_{2.5}, carbon dioxide and carbon monoxide, the paper successfully created a fully automatic in-situ air quality monitor. The results of the air quality recordings around Delhi were compared to the local environmental control authority data. The paper concludes that whilst there is a 'trade off' between cost and accuracy, the Raspberry Pi computer board - in connection with sensor nodes - produces accurate findings, for example this paper showed the Raspberry Pi recorded a 1°C difference in air temperature to the expected air temperature.

Rather than remotely controlling the Raspberry Pi or using it as an in-situ measurement device, Vijayakumar and Ramya (2015) discussed the use of the computer board as a portable monitoring device. Focussing on water quality, the research conducted by Vijayakumar and Ramya (2015) adapted a Raspberry Pi to monitor physical and chemical properties of water. This adapted Raspberry Pi can send data over the internet to mobile devices or central servers but can also be used as monitoring equipment at different locations on a daily sampling route. Given the small size and light weight of the Raspberry Pi, the adapted computer could be carried easily making in both portable and instant in its data collecting abilities.

2.5.1 Raspberry Pi Cameras

The Raspberry Pi has also been adapted in order to create low-cost surveillance devices. Abaya et al. (2014) adapted a Raspberry Pi by adding a web cam to the computer board and using image processing software to capture both smoke and movement within a warehouse. When movement was detected on the web cam an email was sent from the Raspberry Pi to the manager of the warehouse. This research showed the potential for the Raspberry Pi to act as a real time observation device making real time low-cost CCTV feasible for small businesses.

Nguyen et al. (2015) further adapted the Raspberry Pi as an alternative to CCTV by using a compatible Raspberry Pi camera module attached to the Raspberry Pi computer board (Figure 2.8). The Raspberry Pi camera module when compared to CCTV footage has a clearer resolution, thus improving video monitoring from the current best market-available product. Capturing video footage on a Raspberry Pi also

allows the video files to be transferred via the internet to a smart phone or web browser allowing access to real time recordings.



Figure 2.8 – Raspberry Pi computer board with attached Raspberry Pi camera module (*Nguyen et al., 2015*).

As well as an alternative to CCTV the Raspberry Pi camera module has been used to record traffic flow. Kochláň et al. (2014) combined as Raspberry Pi computer board with a HD Raspberry Pi camera module. The Raspberry Pi recorded the change in images from no cars on the road to cars on the road using a threshold technique. Whilst this research into traffic monitoring using a Raspberry Pi was preliminary the research highlighted the potential for the Raspberry Pi camera to act as a low-cost energy efficient traffic monitoring system.

Wilkes (2016) further explored the adaptability of Raspberry Camera modules to record images in the UV range. Wilkes (2016) removed filters within the Raspberry Pi camera module using tweezers and chemical removal techniques to adapt the camera to capture in the UV range. This showed the potential for the Raspberry Pi camera to be used to record pollution emissions such as SO₂ emitted from stacks. Wilke's (2016)

research showed the adaptability of the Raspberry Pi computer board and the Raspberry Pi camera module in order to capture images at different light ranges.

The Raspberry Pi camera is also available in near-infrared (the Pi NoIR). The Pi NoIR camera module has been used to record wildlife and bird nesting boxes (*Prinz et al., 2016*). Given the vegetation reflectance capabilities in the near-infrared scale, the Pi NoIR cameras have also been used in phenology studies. Valle et al. (*2017*) used the Raspberry Pi NoIR camera to record the growth in lettuce plants under controlled conditions and Natividade et al. (*2017*) attached a Raspberry Pi module and a Raspberry Pi NoIR camera module to an unmanned aerial vehicle to record the health of vegetation over a farmland. This data could then inform farmers of crop areas needing more fertiliser based on the tree plant health recorded in the near-infrared spectrum. The use of Raspberry Pi NoIR cameras to record vegetation is an emerging discipline and there have been no studies combining the Raspberry Pi NoIR camera or a standard Raspberry Pi camera with a fisheye lens to produce hemispherical images.

2.5.2 Raspberry Pi Software

Another benefit of the Raspberry Pi monitor is the availability of open source software that can be used to conduct environmental monitoring. Lewis et al. (2016), similarly to Basu et al. (2015), used readily available environmental monitors (in this paper, air temperature, pressure and humidity sensors were used). The research expresses the ease in which open source Python-based code is available online to analyse the data captured using the Raspberry Pi, including script to run the environmental monitors at timed intervals. With the plethora of open source material and low-cost monitoring devices, the research notes the requirement to validate a Raspberry Pi alternative with the previous best market option. In terms of environmental monitoring equipment, the Raspberry Pi did compare to that of the market standard. The paper noted the need to calibrate the Raspberry Pi with other equipment but showed that the low-cost sensor could replace traditional equipment and improve on spatial and temporal scale monitoring in future research.

2.6 Methodological Considerations

This research has shown that there is a need to find a new way of recording vegetation around the rail track. RSSB and Network Rail are dedicated to improving the technology and smart sensors around the railways in order to move into a state-of-the-art smart railway system that reduces delays and improves passenger satisfaction. Chapter One also highlighted the need for an improved leaf fall forecast on a higher spatial and temporal scale in order to reduce the leaves on the line issues across British railways. Combining the need for a smarter railway and a new vegetation

monitoring device this chapter has looked at ways in which vegetation is currently monitored. The methodological considerations to building a new device are discussed in this section; direct, indirect and low-cost sensor method considerations are discussed below.

2.6.1 Direct Method Considerations

Leaf fall measurements need to be taken along a rail track through the autumn season. Direct methods such as harvesting and whole tree sampling would not be able to account for the diverse range of trees along the UK network (*Network Rail, 2016; Bréda, 2003; Karlik and McKay, 2002; Chambers et al., 2001*). Other sampling techniques, such as needle and leaf litter collection, measure the total leaf fall from one season and therefore could not measure real time rates of leaf fall change (*Bréda, 2003; Dufrêne and Bréda, 1995*). Further problems with directly measuring leaf fall are that direct measurements do not equate to an instant measurement of leaf fall. Allometric equations and lab analysis would need to be carried out on the collected material in order to obtain a leaf fall measurement (*Peichl and Arain, 2007; Bréda, 2003; Kodani et al., 2002; O'Brien et al., 1995; Waring et al., 1982*). Given that leaf fall on the UK rail network can change daily and the creation of low adhesion events can occur within hours, an indirect yet near real-time leaf fall recording technique is required.

2.6.2 Indirect Methods Consideration

Indirect methods such as hemispherical photography can record the change in leaf canopies on a daily a basis (*Chapman and Thornes, 2004; Chapman et al., 2001*) and, in comparison to satellites and direct methods, are better suited to recording the

change in leaf fall along the rail track. However, due to the overestimation a standard camera would cause when recording leaf fall, there is a need to covert cameras into near-infrared. This process can be done using digital cameras however is not readily available on the market and is expensive (*Liu et al., 2015; Chapman, 2007*).

Currently, digital cameras used in forestry research are not automated or have the ability to remain in the field for long periods of time. This may cause human errors as positioning the camera at the correct location and level on a daily basis would be difficult and an inefficient use of time. Given that the angle and placement of the camera are integral for monitoring the change of sky-view factor a stationary alternative is needed (*Bréda, 2003; Walter and Torquebiau, 2000*). Therefore, an automated device that can be left out in the field over autumn and record images in the near-infrared spectrum is required. As this device may be needed to record leaf fall across the UK along various rail tracks the cost of the device should be relatively low. A digital camera costing over £1000 would not be practical due to the quantity potentially needed and therefore when considering a feasible alternative, a low-cost solution idea is needed.

2.6.3 Low-cost Sensor Considerations

In the case of the rail network, leaf fall has not been previously measured by any hemispherical imagery equipment. The new technology would instead need to be compared to previous leaf fall recording techniques, in the case of the leaf fall forecasts a comparison would be needed between existing approaches and any new device (Chapter Four). Prior to this, the move from a digital camera to a low-cost sensor would also need to be compared (Chapter Three) building on comparative studies conducted to analyse the comparability of film to digital photography (*Jonchheere, 2004; Frazer et al. 2001; Englund et al., 2000*).

In addition to hacking and comparison to past science records, another key issue with an IoT sensor is data storage; the object would need to store a large quantity of data as well as sending the data results through the internet (*Gubbi et al., 2013*). Again, this issue could be reduced if the device self-deleted past records or alternatively memory cards, which can increase storage capacity, were attached to the device allowing larger long-term data to be stored throughout the autumn.

In the case of hemispherical images, the IoT sensor would need to be able to capture photos of the leaf fall and send the images back over the internet. Current ubiquitous technology such as a mobile phone could now potentially do this (*Corcoran et al., 2001*). Indeed, there is also now little distinguishing evidence between a high-resolution mobile phone camera and a digital camera (*Tsai et al., 2007*).

Chapter Two Summary

This chapter explored the various leaf fall measuring techniques used in forestry research that could potentially be used on the railway network. The conclusion is that the use of indirect measurements would be the most applicable for leaf fall measurement. Currently, the measurement of leaf fall in the forest community is mostly conducted using digital hemispherical imagery, with potential to harness the normally satellite-based multi-spectral approaches. From here, this thesis will build on the current trend of adapting and using emerging low-cost devices, which can relay data instantaneously over the internet, such as a Raspberry Pi or mobile smartphone to capture leaf fall. Given that leaf fall is currently not measured at high temporal or spatial resolution in any UK leaf fall forecast, an improvement in this forecast parameter will lead to an improvement in leaf fall forecasting. As well as being the principle input into a leaf fall forecast, in capturing leaf fall from a tree canopy rather than already fallen leaves or leaves on the rail head, this apparatus could show the amount of leaves left still to fall which is another key parameter in the leaf fall forecasting model and could further be used to indicate how many leaves are left post autumn forecasting season which could cause low adhesion issues further into the winter months of January and February. Using the Chapman (2007) methodology this thesis will further aim to modify and harness current technology in order to capture images in the near-infrared spectrum in order to reduce overestimation from clumping and send automatic tree canopy images instantly over the autumn season. This chapter has also highlighted that open source software that can calculate sky-view factors in captured images is now readily available.

Chapter Three

Development of a low-cost leaf fall sensor

This chapter is a modified version of a manuscript published in the Journal of Agricultural and Forest Meteorology in 2018 and can be found online; Kirby, J., Chapman, L. and Chapman, V., 2018. Assessing the Raspberry Pi as a low-cost alternative for acquisition of near infrared hemispherical digital imagery. *Agricultural and forest meteorology*, 259, pp.232-239.

My contribution to this manuscript involved conducting all parts of the research, including co-co-designing the project, collecting the data, analysing it and interpreting the results, as well as writing the manuscript. My supervisors collaborated by co-designing parts of the research project and providing crucial feedback on interpretation of results and drafts of the manuscript.

3.1 Introduction

A low-cost sensor is needed to record leaf fall around the UK rail network. With the emergence of low-cost devices and smartphones being used for scientific experiments an initial investigation of the feasibility of using a smartphone for recording vegetation was made. As discussed in chapter two, capturing vegetation in the near-infrared allows a clear distinction between vegetation and bark of a tree. The new equipment for the rail industry needs to be low cost (less than £100) in order to replicate the device at set intervals along a rail line, the device must be able to show a reduction in leaves from a tree overtime and be placed under specific tree species in order to run alongside or compare to current leaf fall observers. Whilst there is no design specification on weight, the device must be smaller than 12 inches to reduce the obstruction a recording device may cause along the rail network. Further to this the

device must be self-contained and waterproof without any visible wires. As there is no electronic device currently in operation the scope for this project is wide and as long as multiple devices can record vegetation on a high spatial scale (station to station level) then the design criteria will be met. The design specification advances in chapter six when future considerations of a recording device being placed on a train is explored. Given this broad specification a design development process was laid out in order to create a new device (figure 3.1)

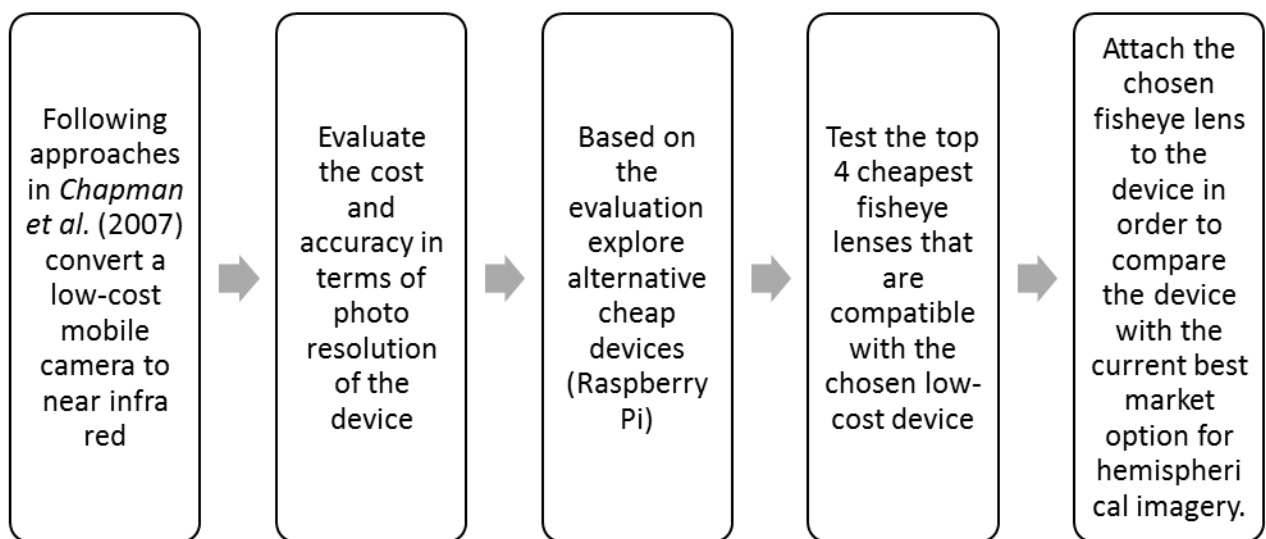


Figure 3.1 Flow chart showing the design process of a new leaf fall hemispherical device. The process is explored throughout chapter three.

Therefore, using the method set out in Chapman's (2007) paper when converting a Nikon Coolpix camera to near-infrared, this chapter explores the possibility of using the same approach to adapt a smartphone. Whilst chapter two showed that smartphone software can be adapted, this chapter focuses on adapting the hardware of a smartphone (the camera module) to capture near-infrared images. Due to the complex nature of adapting a mobile device (discussed in section 3.3), a Raspberry

Pi (also discussed in chapter two) was also adapted and then compared with a Nikon Coolpix camera (section 3.4 – 3.10).

3.2 Mobile Phone Adaption

The basic principles laid out in Chapman's (2007) paper to adapt a Nikon camera to take near-infrared imagery were also applicable when converting a mobile phone camera module. In principle, the removal of the infrared filter (needed by modern digital cameras due to the inherent capability to see beyond the visible spectrum) should allow the camera to capture images on the near-infrared spectrum.

The camera module was removed from the mobile phone and then opened at the edges to remove the outer casing as shown in Figure 3.2a. The base of the camera containing the infrared lens and the circuit board was cut open as shown in Figure 3.2b. This is a delicate procedure as any damage to the circuit board would render the camera unusable. Therefore, this process ideally needs to be conducted under a microscope and in a clean room. Once the lens and computer board were separated as shown in Figure 3.2b, the infrared filter can be removed from a camera module using a scalpel. The camera module can then be soldered back together with any loose connections being sealed with silver paint. This allowed conductivity between the camera circuit board and the lens to remain intact.

An example of the near-infrared imagery that can be obtained using this solution is shown in Figure 3.2c. The near-infrared image clearly picks up the structure of the leaf

in Figure 3.2c however once the fisheye lens is attached, the image becomes severely distorted (Figure 3.2d).

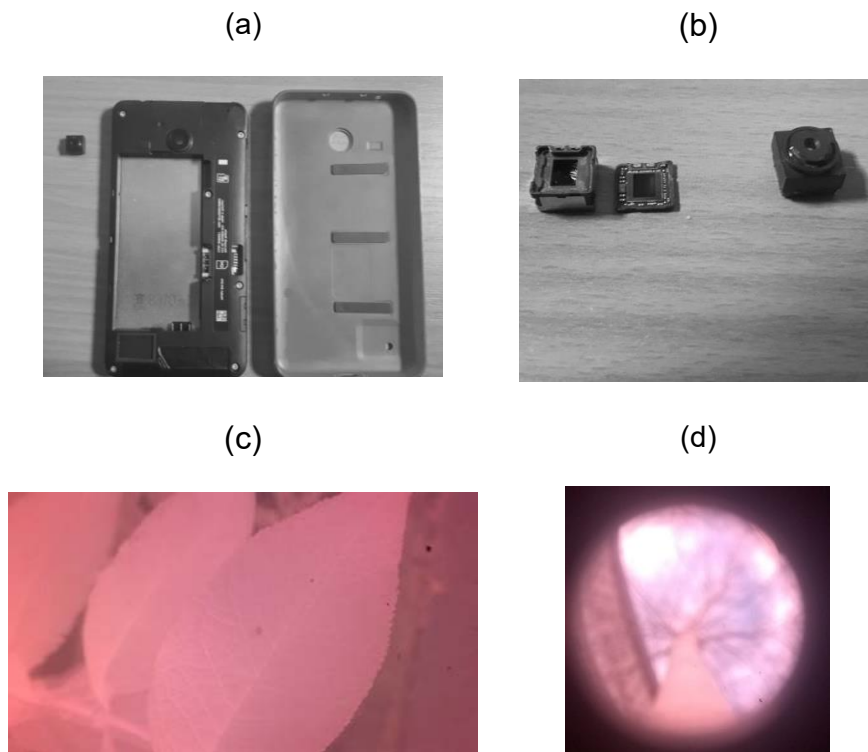


Figure 3.2 – (a) Mobile phone with a removed camera module, (b) Removed IR filter and a camera module, (c) close-up near-infrared image using a mobile phone camera, (d) 185° fisheye lens attached to an adapted mobile phone

An attempt to correct the distortion was made by adding a cold plate mirror into the camera module lens. As the cold plate mirror could only be purchased at 3mm thickness the cold plate mirror had to be filed down and then buffered. The mirror was buffered using a solution of Alumina Powders mixed with glycerol.

Then cold plate mirror was then super glued into the mobile camera module in place of the removed infrared lens. However, this process was unsuccessful as camera modules containing a cold plate mirror no longer produced images. This may be due to the inability to buffer the cold plate mirrors. A custom-made cold plate mirror of

adequate sizing would cost £500 per mirror which would no longer make a smartphone camera conversion technique a viable low-cost option.

Alternatively investing in specialist equipment that will only partially open the camera module leaving the metal connectors intact would also improve the image. This would allow the focusing technology of the camera module to remain undisturbed. Silver wires were also damaged that connected the camera module to the base containing the circuit board. Silver paint was used to reattach the connections however the focus remains poor for objects further away from the lens (Figure 3.2d).

The challenges of making the mobile phone into a near-infrared camera was too expensive to reproduce on a large scale. A mobile phone as an effective low-cost sensor may become more viable with the introduction of near-infrared mobile phones (FLIR, 2019). This would remove the need to adapt the camera module in a lab and could potentially make the sensor useable for the public. With the poor performance of an adapted mobile phone, an alternative approach was investigated. The following part of this chapter compares a Nikon camera to an unaltered mobile phone camera with an attached fisheye lens and further demonstrates the ability of a low-cost Raspberry Pi camera to act as an alternative to digital cameras. Thus, advancing the evolution of hemispherical imagery discussed in chapter 2, section 3.3 and shown in Figure 3.3.

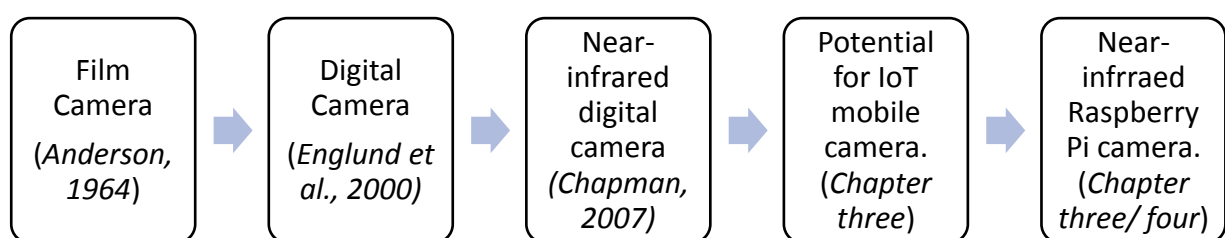


Figure 3.3 – Evolution of hemispherical photography from 1964 - 2019

3.3 Nikon Coolpix Cameras and Fisheye Lenses

Hemispherical imagery is commonly used to assist in the assessment of radiation budgets. Examples of use include below tree canopies, in urban areas or within riverine environments (*Hall et al., 2017; Liu et al., 2015; Chapman, 2007; Chapman et al.; 2007; Bréda, 2003; Ringold et al., 2003; Watson and Johnson, 1987*). Imagery is usually obtained using a camera equipped with a fisheye lens (Figure 3.4a) which allows the camera to take an approx. 180° hemispherical image (*Liu et al., 2015; Chianucci et al., 2015*). These images are then processed to analyse the amount of visible sky shown in the image (known as the sky-view factor). This can then be used in forestry research to quantify the health of a tree and to compare differences between tree canopies (*Schwalbe et al., 2009; Leblanc et al., 2005; Jonckheere et al. 2004*).



Figure 3.4 (a) FC-E8 Fisheye lens attached to a Coolpix camera Source: Reproduced with permission from Chapman et al. (2007), copyright © 2007 IEEE, (b) First2Savv 1850 fisheye camera attached to a Samsung Galaxy S5 Neo; (c) Perspex Dome used to measure distortion.

The use of fisheye imagery for this application can be dated back to the early work of Anderson (1964), but it was the advent of digital photography which saw the approach

become widely adopted. Following a number of scoping studies, which successfully compared results obtained from film cameras to the new generation of digital cameras (*Englund et al., 2000; Frazer et al., 2001; Hale and Edwards, 2002*), the new technology quickly became adopted by the scientific community. However, following the successful transition to mass digital photography, studies for the past two decades have become very reliant on the early digital cameras produced by Nikon (Table 3.1) such as the Coolpix 950 or 4500 (*Chianucci, 2016; Lang et al., 2009; Chapman, 2007; Zhang et al., 2002; Baret and Agroparc, 2004; Ishida, 2004*). Indeed, whilst research into hemispherical imagery has also been conducted using alternative cameras and equipment (Table 3.2), the Nikon Coolpix range equipped with the FC-E8 fisheye lens undoubtedly remains the most popular choice in research to date.

Table 3.1 - List of sample studies that use Nikon Coolpix cameras.

<i>Seasonal Changes in Canopy Structure</i>	
<i>Liu et al., 2015</i>	Used a Nikon Coolpix 4500 camera at sunset / sunrise to capture hemispherical images of tree canopies in order to investigate seasonal changes of tree canopies.
<i>Comparing Nikon Coolpix to film cameras and Leaf canopy analysers</i>	
<i>Malenovský et al., 2010</i>	Used a Nikon Coolpix 8700 to compare canopy analysers to hemispherical imagery.
<i>Garrigues et al., 2008</i>	Compares Nikon Coolpix 990 with LAI-2000 and AccuPAR.
<i>Frazer et al., 2001</i>	Compared a Nikon 950 to a film camera and highlighted the potential for blurred edges and colour distortion of a Coolpix camera but noted it can be used in calculating canopy gap measurements.
<i>Englund et al., 1999</i>	Compared a digital Nikon 950 and a film camera to find that low resolution images from the Nikon 950 were an adequate comparison to film cameras.
<i>Grimmond et al., 2001</i>	Compared a Nikon 950 Coolpix to a plant canopy analyser and found that the Nikon was an effective and easy approach to canopy analysis.
<i>Gap function Analysis and Estimation of tree canopies</i>	
<i>Hu et al., 2009</i>	Uses a Nikon 950 Coolpix camera to take hemispherical images to calculate gap size and shape within a tree canopy.
<i>Gap function Analysis and Estimation of tree canopies</i>	

<i>Zhang et al., 2005</i>	Researched the effect of exposure on calculating the leaf area index and gap function analysis using a Nikon Coolpix 4500.
<i>Lang et al., 2009</i>	Calculated gap function of canopies using a Nikon Coolpix 4500 and compared it to the Canon EOS 5D cameras.
<i>Chianucci, 2016</i>	Used a Nikon 4500 to compare gap functions in forested canopies.
<i>Danson et al., 2007</i>	A Nikon 4500 was used as a comparison to terrestrial laser scanning.
<i>Adaption or calibration of Nikon cameras</i>	
<i>Chapman, 2007</i>	Adapted a Nikon 4500 camera to make in near-infrared in order to better estimate sky-view factors and the woody bark index of tree canopies.
<i>Baret and Agroparc, 2004</i>	Used a Nikon 4500 in order to determine the optical centre of an image using a fisheye lens.
<i>Ishida, 2004</i>	Created threshold software for colour images from a Nikon 950 camera.

Table 3.2 - Studies using alternative cameras for hemispherical photography.

Studies	Camera used	Approach
<i>Kelly and Krueger, 2005</i>	HemiView 2.1 digital image system	Used a 20-megapixel SLR CMOS camera as part of the HemiView software (Delta T Devices) to record canopy structure in riparian environments
<i>Duveiller and Defourny, 2010</i>	Canon PowerShot A590 camera	Used a Canon PowerShot A590 camera to assess batch processing of hemispherical images
<i>Rich, 1990</i>	Canon T90 Minolta X700 Nikon FM2 Olympus OM4T	Comprehensive instructions on how to take hemispherical photography with a list of cameras suitable for research
<i>Urquhart, et al., 2014</i>	Allied Vision GE-2040C camera	Uses sky-view factors from a high dynamic range camera to calculate short term solar power forecasting
<i>Wagner and Hagemeyer, 2006</i>	Canon AE-1 camera	Used a Canon camera to estimate leaf inclination angles on tree canopies

The Nikon Coolpix range of cameras remain a key tool in forest climatology (Table 3.1 and Table 3.2). Unfortunately, the Coolpix range is no longer readily available (*Nikon, 2016*) with digital camera technology advancing considerably in the interim making models such as the Coolpix 4500 camera appear large and bulky with a relatively poor battery life and low image resolution (3.14 megapixels). However, even today, the FC-E8 fisheye lens remains one of the least distorted on the market (*Holmer et al., 2001*) and as such, the camera series remains very popular with researchers as a tried and tested means to collect hemispherical imagery (*Chapman, 2007*). A significant further advantage of the Coolpix range of cameras was the ability to easily convert the camera to take near-infrared (NIR) imagery. By adapting a camera in this way, it significantly enhances its functionality in the forest environment as due to the highly reflective nature of vegetation it becomes easier to distinguish this from woody elements and other features in imagery when taken in NIR; which can then be used to assess the health and density of tree canopies (*Chen et al., 1996; Turner et al., 1999; Chen et al., 2003*).

Overall, the Nikon Coolpix camera has reached the point where it is informally viewed as a standard device for this purpose, but with dwindling numbers now available for purchase on internet auction sites, there is a need to investigate new and more sustainable means to collect data in the long term. The approach explored in this chapter is to investigate whether a low-cost alternative can be developed using readily available off-the-shelf components.

3.4 Adapting a Raspberry Pi

The Raspberry Pi is a range of small computers designed to minimise the cost of computing and thus make it, and computer programming more generally accessible to a wide audience. After a prolific launch, it now has a worldwide following of developers focussed on producing generic code and peripherals for use in a range of applications. As an example, the computer can now be readily fitted with a Raspberry Pi camera and subsequently programmed to take images at set time intervals.

At the time of writing, the most popular Pi compatible camera available on the market is the Pi camera which comprises of a Sony IMX219 9-megapixel sensor. This is available either as a standard device or as a Pi NoIR camera where the infrared blocking filter (needed by modern digital cameras due to the inherent capability to see beyond the visible spectrum: *Chapman, 2007*) has been removed (*Raspberry Pi, 2016*). As outlined in the previous section, NIR capability improves the utility of the approach for use in forested environments.

3.5 Comparison of Fisheye Lenses

Unfortunately, a fisheye lens is presently not available that has been specifically designed for the Pi NoIR camera. However, due to the recent proliferation of smartphone photography, there is a wide range of fisheye lenses that are now available for smartphones which have the potential to be used. The key consideration here, as per Holmer et al. (2001), is to select a lens with minimal distortion to reduce error in later image analyses. This can be achieved by testing the equiangularity of the lens by calculating any distortions in the radial distance. As shown in Figure 3.5, the

aim is to acquire an image where the radial distance is directly proportional to the zenith angle (*Chapman, 2008*). Figure 3.5a shows how radial distortion was calculated by recording the distance between the projected dots in the image. In reality the dots between the image was 8cm apart, this distance is altered due to the distortion of the fisheye lens when captured using hemispherical photography.

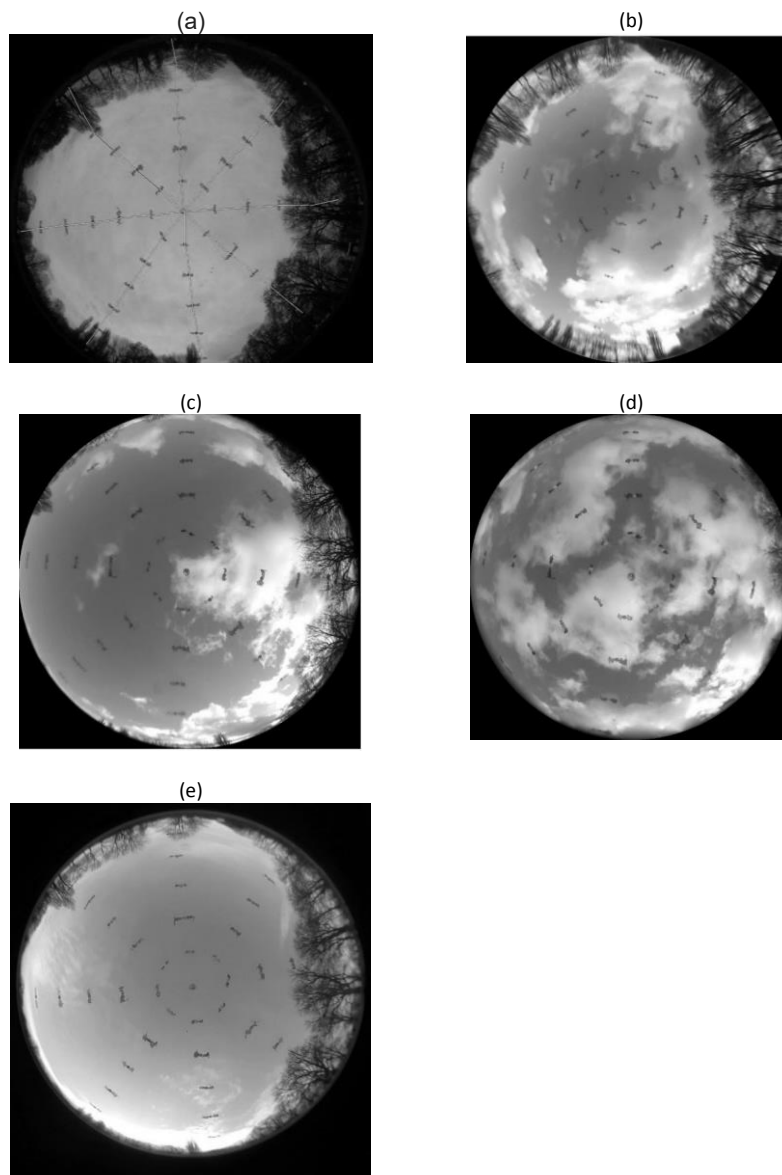


Figure 3.5 (a) Visual comparison of Nikon Coolpix camera, (b) smart phone camera with attached 185° fisheye lens, (c) smart phone camera with attached fisheye lens 198°, (d) smart phone camera with attached fisheye lens 180° and (e) smart phone camera with attached fisheye lens 235°.

A range of available fisheye lenses were tested for distortions based on the cheapness of the fisheye lens and the online reviews for each lens (Table 3.3). In this initial test, the fisheye lenses were clipped onto a Samsung Galaxy S5 Neo (Figure 3.5b) and placed under a large Perspex calibration dome marked at equal points along the sides using a compass (Figure 3.5c). A plumb bob was then used to position the device directly below the centre of the dome before a series of images were collected (Figure 3.5). Measurement distortions were then calculated using Image-J software (Figure 3.6).

Table 3.3 - Mobile fisheye lenses specification.

Product	Field of view	Cost (At time of writing)
Yarrashop fisheye lens	180	£7.99
First2Savv JTSJ-185-A01 fisheye lens	185	£8.99
AUKEY fisheye lens	198	£11.99
MEMTEQ universal fisheye lens	235	£10.99

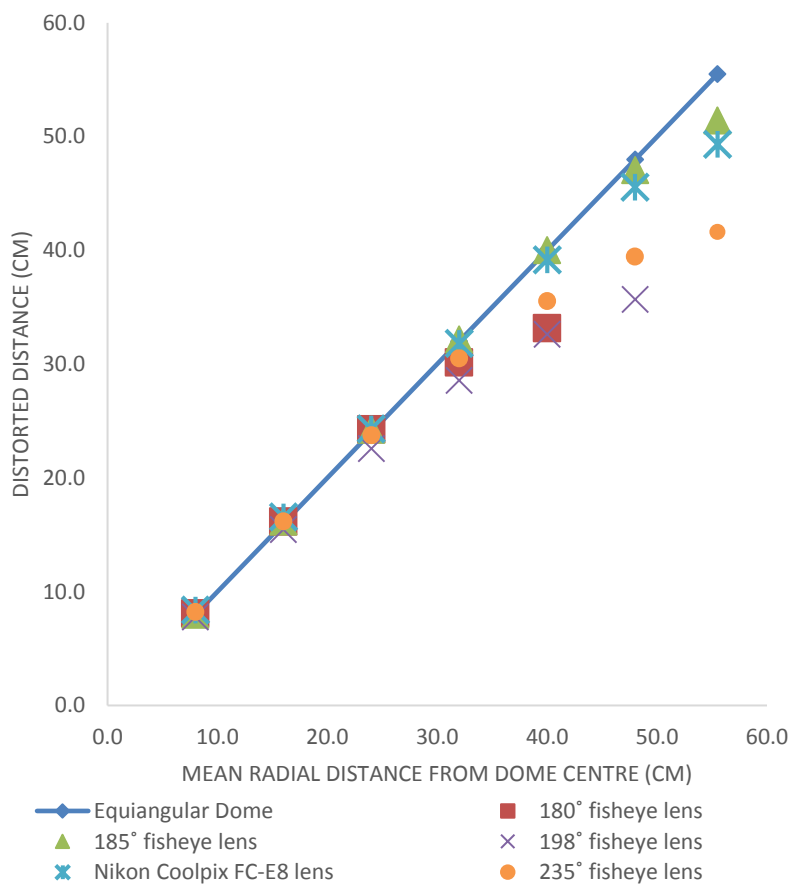


Figure 3.6 Comparison of radial distortion between different mobile fisheye lenses and Nikon Coolpix 4500 camera FC-E8 lens.

The distortion distance of each point on the image was calculated using a measuring tool on image j which equates pixels to a known distance. The distance between each point in the image was measure with image j software to create a distorted distance and this was plotted against the actual distance in reality (mean radial distance). The threshold for an acceptable comparison between the devices was that the same FOV should be present in the mobile fisheye lens and the FC-E8 lens and that the distortion from hemispherical image to reality should be similar (within 1 cm) of the current FC-E8 lens. The results show that the 185° fisheye lens (Figure 3.5 b) is most comparable with the Nikon Coolpix FC-E8 lens (Figure 3.5 a). It has a similar field of view (FOV) and despite a slight reduction in image clarity at high radial distances, the 185° lens

has the lowest level of distortion (Figure 3.6). However, comparisons between the Nikon Camera FC-E8 lens and other mobile fisheye lenses are not as favourable and all display clear distortions and/or significant reductions in FOV. For example, the 180° (Figure 3.5 d) camera captures the lowest FOV of the compared fisheye lenses (Figure 3.6). The 198° fisheye lens (Figure 3.5 c) has excellent clarity at high radial distances however has a lower FOV than reported and high levels of distortion (Figure 3.6). Conversely, the 234° fisheye lens (Figure 3.5 e) has a high FOV however has high levels of distortion, especially at high radial distances (Figure 3.6). Based on these analyses, the 185° fisheye lens was chosen for further investigation.

3.6 Adapting a Pi NoIR Camera to Take Hemispherical Images

In order to use the 185° fisheye lens with the Pi NoIR camera, a series of small adaptations are required. Whilst these adaptations could be achieved using 3D printing technology, this was achieved in this study using parts scavenged from the First2Savv 185° fisheye lens (Figure 3.7 a) and tubing from a Waveshare Raspberry Pi Camera Module Kit (Figure 3.7 b). The camera component of the Waveshare kit was removed, using a saw and drill, to leave a hollow tube. The tubing (Figure 3.7 b) was then tied and secured to the base of the Raspberry Pi NoIR camera using thin wire (Figure 3.7 c). The camera was then attached to the Raspberry Pi board using the connector port (Figure 3.7 d).

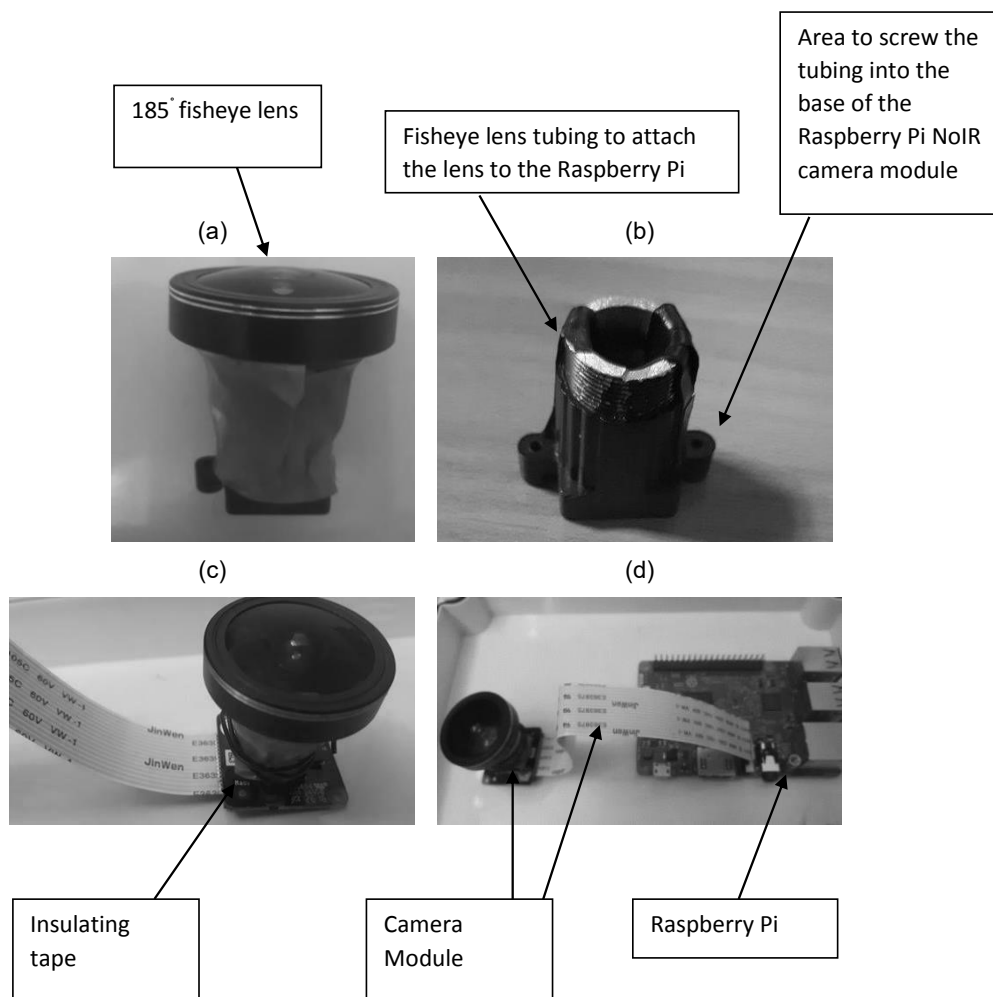


Figure 3.7 (a) 185° fisheye lens attached to base (b) base component of Raspberry Pi fisheye module, (c) fisheye module attached to Raspberry Pi NoIR camera (d) Camera module attached to a Raspberry Pi computer.

3.7 Comparison of Nikon camera and Pi NoIR Raspberry Pi camera.

3.7.1 General Specifications

Table 3.4 shows the specification comparison of both the Pi NoIR camera version 1 and 2, the Nikon Coolpix 4500 and the Nikon Coolpix 9000 camera. The most striking

difference between the models is the image resolution which clearly underlines the large advances in digital photography over the ensuing period. As has been demonstrated in the previous section, the reported FOV can vary with individual cameras (*Grimmond et al., 2001*) and therefore this has been estimated in this study using a mechanical clinometer. The adapted Pi camera FOV (164°) is less than the Nikon Coolpix FOV (176°) which is hypothesised to be a consequence of the added tubing (Figure 3.7 b) causing some distortion and loss of image at ground level.

Table 3.4 - Comparison of Coolpix cameras to Raspberry Pi cameras

	Nikon 900	Nikon 4500	Pi NoIR V1	Pi NoIR V2
Pixel range	1.2 megapixels	3.14 megapixels	5 megapixels	8 megapixels
Optical Zoom	3 x optical zoom lens	4 x optical zoom lens	N/A	N/A
Field of View	183° FC-E8 lens (176° using a mechanical clinometer)	183° FC-E8 lens (176° using a mechanical clinometer)	185° mobile fisheye lens (164° using a mechanical clinometer)	185° mobile fisheye lens (164° using a mechanical clinometer)
Dimensions	143 x 76.5 x 36.5mm (5.6 x 3.0 x 1.4 in.)	130 x 73 x 50mm (5.1 x 2.9 x 2.0 in.)	25 x 24 x 1mm	25 x 24 x 1mm
Cost	£100*	£200*	£25	£25

* Approximate second-hand price

3.7.2 Distortion Analysis

As hemispherical imagery is mostly used in the analysis of tree canopies, the loss of information at ground level (i.e. high radial distances) is less of a concern. It is at these extremities of the image where distortions are also more common and indeed one of the main attractions of the Nikon Coolpix range of cameras (*Holmer et al.*, 2001). Whilst an equiangular lens is not an essential requirement of a camera system for this application, it does ensure fewer corrections are required and minimises error in subsequent analysis. The distortions of the adapted fisheye lens are again tested by using the Perspex calibration dome (Figure 3.8).

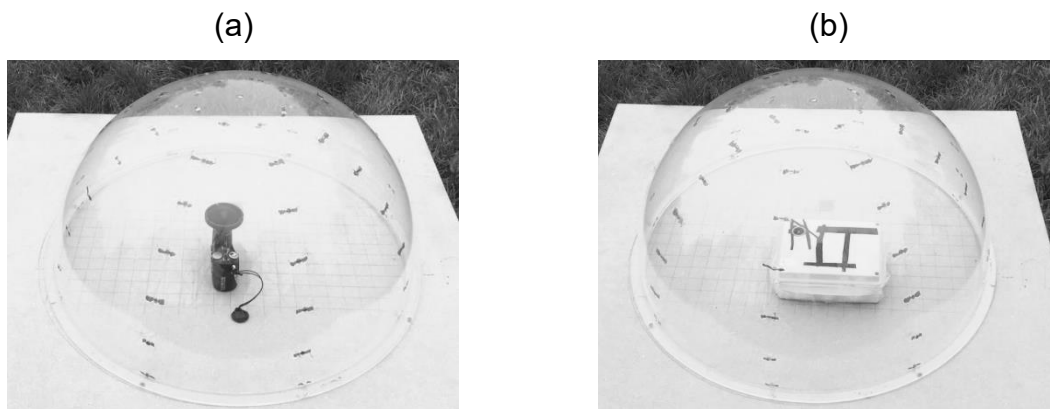


Figure 3.8 (a) Nikon Coolpix camera in a Perspex dome and (b) Raspberry Pi NoIR camera with fisheye attached under Perspex dome.

The FOV of the adapted Pi camera is demonstrated to be less than the Nikon camera however there is a greater level of distortion when using a Nikon Coolpix camera (Figure 3.9). This difference is likely due to the size of the equipment with the Nikon Coolpix camera being larger in size than the Pi camera lens (145 mm compared to

25mm). With respect to equiangularity, there is a strong correlation between radial distance distortions of the Nikon Coolpix FC-E8 lens camera and Raspberry Pi NoIR adapted fisheye camera at 99.9% confidence level (Figure 3.9).

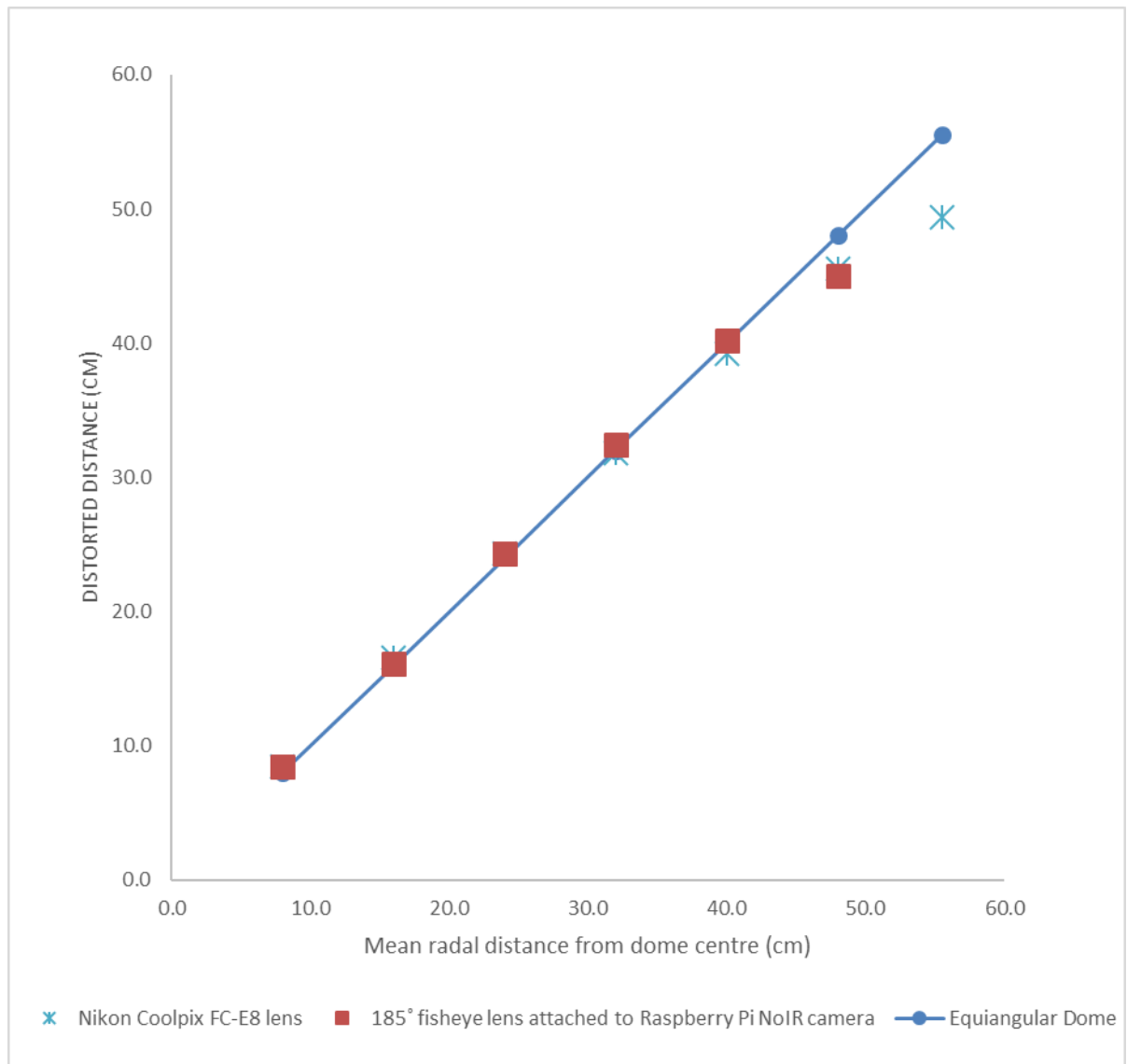


Figure 3.9 - Radial Distortion of a Nikon Coolpix FC-E8 lens camera and a Raspberry Pi camera with attachable fisheye lens.

3.8 Sky-View Factor Analysis

To further demonstrate the inter-device comparability, images were captured on both devices for sky-view factor analysis (Figure 3.10). The Images were then analysed using 'Sky-View Calculator' software developed by Lindberg and Holmer (2010) using a process where the image was converted to binary (Figure 3.10) divided into concentric annuli before calculating the number of white Pixels (sky) in each annulus and summed to produce a sky-view factor (*Holmer et al. 2001; Johnson and Watson, 1984; Steyn 1980*). Analyses were performed on the original imagery as well as images cropped to have the same FOV. In capturing the same FOV the Raspberry Pi's accuracy in terms of capturing the same amount of leaves in a given area could be tested. A similar FOV sky-view factor would indicate that pixel resolution on the raspberry pi device could capture similar levels of pixel resolution and thus individual leaves as the Nikon Coolpix camera. Table 3.5 shows that when the FOV is uncorrected, the Pi overestimates the sky-view factor as the edge of the image contains less leaves and thus a higher sky-view factor, but when this is corrected, the output is very similar and is significant at the 99.9% level. Leaf view factor (the area of vegetation in an image) is also calculated in Table 3.5. The leaf view factor (shown in figure 3.10) was calculated using the same software as the sky-view factor image however a threshold to remove the bark was conducted prior to uploading the image into the sky-view calculator software. A leaf view factor is easily calculated on a Raspberry Pi due to the near-infrared capturing of leaves (in making the leaves appear red the bark and wood stands out clearer than in a colour image). This leaf view factor removes overestimation from bark and wood and would better indicate purely a change in vegetation over time.

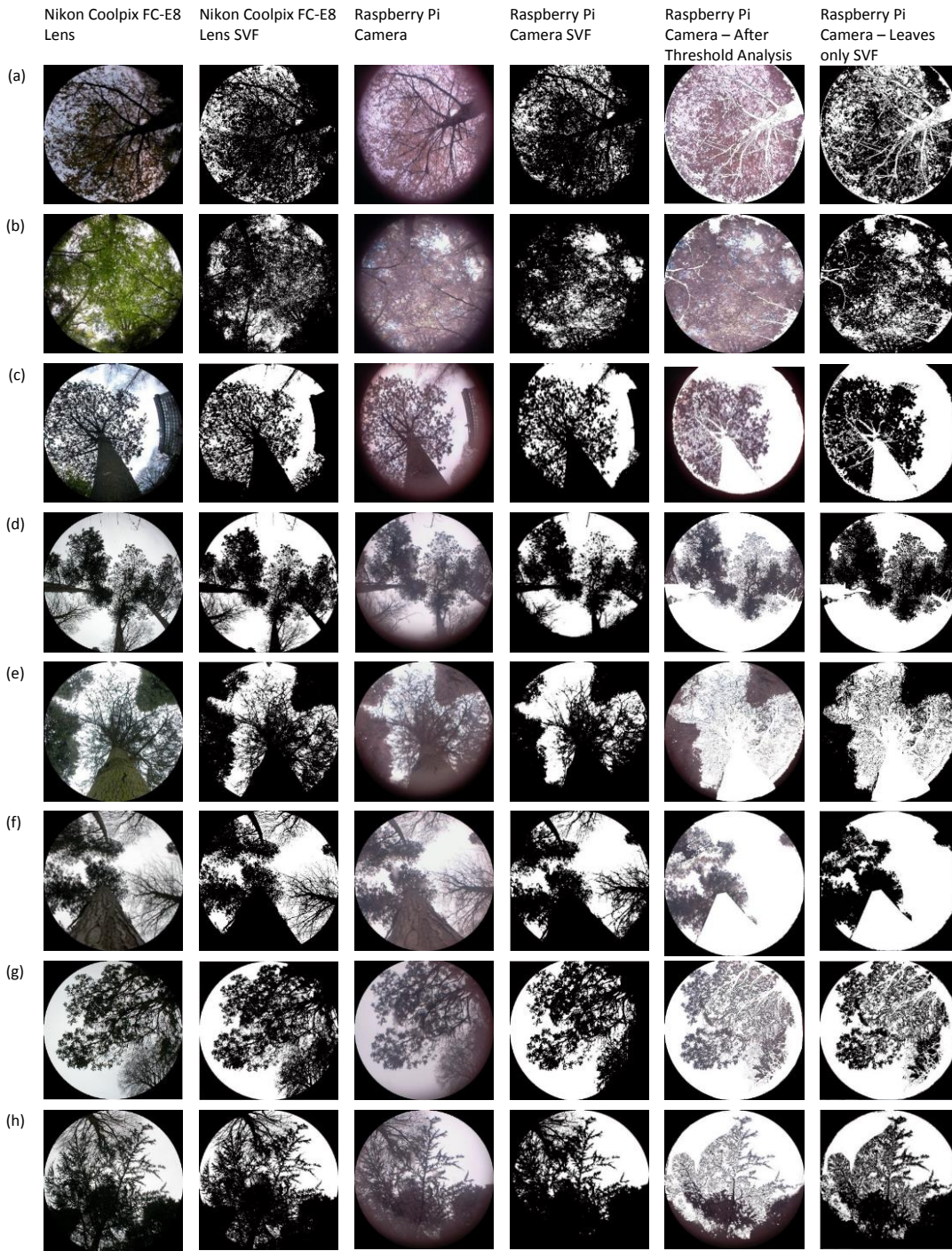


Figure 3.10 - Visual variations in sky-view factors when comparing a Nikon Coolpix FC-E8 lens with an 185° Raspberry Pi NoIR camera.

Table 3.5 – Sky-view factors of Nikon Coolpix camera adjusted FOV, Raspberry Pi NoIR camera, Nikon Coolpix unadjusted FOV and Raspberry Pi leaves only images.

Image	Sky-view factor			Leaf-view factor
	Nikon Coolpix Camera (Non-adjusted FOV)	Nikon Coolpix Camera (adjusted FOV)	Raspberry Pi Camera	
				Raspberry Pi camera – contribution of leaves
(a)	0.25	0.17	0.17	0.55
(b)	0.24	0.26	0.29	0.68
(c)	0.40	0.42	0.44	0.45
(d)	0.4	0.45	0.45	0.45
(e)	0.3	0.34	0.35	0.26
(f)	0.4	0.45	0.47	0.33
(g)	0.37	0.40	0.44	0.42
(h)	0.48	0.33	0.34	0.53

3.9 Near-Infrared Capabilities

In addition to hardware availability, the advantages of using a Raspberry Pi NoIR camera over a Nikon 4500 camera is the increase in resolution but also the in-built near-infrared (NIR) technology. Although it is also possible to convert the Nikon Coolpix camera to take NIR images (*Chapman, 2007*), this involves substantial effort which risks damaging the camera.

The capability of the Pi NoIR was confirmed in this study. A simple threshold analysis proved sufficient to remove all other aspects of the image except for vegetation (Figure 3.8). The differences in sky-view factor can then be calculated; from this a leaf-view calculation were made and presented in Table 3.5, indicating an approximation of leaf cover in the image and further highlights the utility of the camera in forestry applications.

3.10 Conclusions

The Nikon Coolpix camera range has provided a reliable 'standard' solution for obtaining hemispherical fisheye imagery for many years. However, whilst still fit for purpose, an alternative is needed to ensure a sustainable means of data collection moving forward. There is also the opportunity to take advantage of other improvements in digital photography, most notably the vastly improved resolution of modern imagery. This chapter has shown that comparable results can be provided with a low-cost image collection system using readily available components.

In addition to the advantages of improved resolution, the Pi NoIR camera provides an off-the-shelf NIR solution, making it perfect for use in forested environments and thus removing the need for further adaptation (i.e. removal of blocking filters and addition of cold mirrors: *Chapman, 2007*). However, fisheye lenses are not yet readily available and hence there is presently a need to carry out alternative adaptations such as those outlined in this chapter, or the use of simple 3D printing technology. However, the most positive result from this study is the direct comparability of the imagery (and subsequent results from sky-view factor analyses) obtained from the two techniques. Both systems have similarly low levels of distortion, but there are minor differences in relation to the FOV.

Further advantages of the Raspberry Pi approach are the computing capability of the device, which means it has internal logging capabilities and (once waterproofed) could be left in the field in time lapse mode for long periods at a time, even relaying imagery over the internet in real-time if communications are available. Overall, moving forward there are many advantages to using the Raspberry Pi, however the key conclusion is that a fit for purpose and dynamic solution for the collection of hemispherical imagery can be readily produced at a low cost.

Chapter Three Summary

This chapter has shown that it is possible to capture near-infrared hemispherical images from an adapted mobile phone and a Raspberry Pi device. Converting a mobile phone to near-infrared, at time of writing, to capture hemispherical images is deemed to complex and expensive to make it a viable alternative to an adapted digital camera. An alternate solution, the Raspberry Pi, has already been made near-infrared in the form of a Pi NoIR camera (an off the shelf alternative to individually altering a camera lens). Therefore, once adapted, by attaching a mobile fisheye lens it could capture hemispherical images as well as the market favourite Nikon Coolpix camera. The research has successfully created a new cheaper alternative approach to capturing hemispherical imagery which has similar levels of distortion but marginally less field of view. To further this research the technique, the technology would need to be tested over an autumn period to show how the device could capture changes in tree canopies over time.

Chapter Four

Designing an operational leaf fall device for an autumn field campaign

4.1 Review of Current Leaf Fall Recording Approaches

As discussed in chapter two, recording autumn leaf fall is important for a range of scientific disciplines including climatology, ecosystem recovery, river flood management and primary productivity in forestry (*Kosmala et al., 2016; Muotka and Laasonen, 2002; Molles et al., 1998; Day et al., 1996*). For example, whilst spring bud burst is usually analysed in relation to temperatures and changes in annual variability, leaf senescence can also be used as an indicator for climate change. Due to changes in climate, the average leaf fall season in Europe has started 0.3-1.6 days later per decade (*Menzel, 2002*). In addition to furthering our scientific understanding, there are also a number of applications that require a direct measurement of daily leaf-fall such as the leaf fall forecast required for the national railway networks.

As discussed in chapter two leaf fall observations are recorded regionally and not at the time frame required for a high temporal resolution leaf fall model. Therefore, to provide a step change in the number and quality of leaf fall observations, new approaches need to be explored. This chapter investigates the utility of a low-cost ground based hemispherical imaging device. Ground based sensing devices have the advantage of avoiding interference from clouds, aerosols and adverse weather conditions (*Chapman, 2007*). They also satisfy the need for a high spatial and temporal resolution in leaf forecasts by having an ability to measure leaf fall daily and be left in the field over time (*Crawley et al., 2017*).

4.2 Hemispherical Imagery

Hemispherical images have previously been used in forestry research to calculate tree canopy area and discussed in chapters two and three. This method infers amount of leaves from the transmission of radiation through the canopy to the ground (*Jonckheere et al., 2004; Weiss et al., 2004; Bréda, 2003*). Using the change in sky-view factor (with the assumption that the greater the sky-view factor, the fewer leaves are remaining on a tree) from a full canopy image and a bare tree image an estimation of percentage fall over time can be made.

However, whilst these techniques are well established, no standard instrumentation exists for collecting hemispherical imaging. As this application requires a large number of imaging devices to be deployed in a network across a large geographical area, it is imperative that a low-cost means of collecting data is investigated. Using the low-cost Raspberry Pi device built in chapter three; this chapter evaluates the use of this approach in assessing the changes in the tree canopy for the duration of an autumn season.

4.3 Methodology

4.3.1 Camera Adaptation

Chapter 3 showed that hemispherical imagery collected using a Raspberry Pi with a 185° 'First2Savv JTSJ-185-A01' mobile fisheye lens attached (Figure 4.1a) was comparable to the standard approach of using a Nikon Coolpix camera. However, in order to record the change in leaf fall over the autumn, the system had to be significantly refined to include power supply considerations and communications to enable the system to function effectively over an extended period in a remote location.

The adapted Raspberry Pi was connected to a Witty Pi 2 in-built clock system (Figure 4.1b) which allowed the Raspberry Pi to turn on and off at set times (*UUGEAR, 2018*). The Witty Pi clock system works by passing a small current through the adapted Raspberry Pi to keep a continuous low power supply; this was needed to ensure accurate timing and to turn the equipment on and off at set time intervals. With this approach, a 26800mAh lithium battery can be used to power the equipment for an hour of imaging per day for a three-week period.

With respect to communications, a dongle (small USB modem that can connect a device to the internet using 4G broadband technology) can be used to allow the Pi to transmit the captured images over the internet for locations where Wi-Fi is not readily available. As Wi-Fi networks were readily available, the inbuilt Wi-Fi sensor on the Pi was used to connect the device to the internet. The dimensions of individual components of the adapted Raspberry Pi are shown in Table 4.1 and the combined

equipment shown in Figure 4.1c. Finally, an IP65 waterproof enclosure was adapted for the fisheye lens to capture a hemispherical image. An opening was created for the lens and sealed with duct tape (Figure 4.1d).

Table 4.1 - Dimensions of Raspberry Pi waterproof enclosure components.

Product	Dimensions
Raspberry Pi	85.60mm × 56.5mm × 17mm
Witty Pi 2	65mm x 56 mm x 19 mm
Battery Pack (26800mAh Power Bank)	172mm x 80mm x 20mm
Pi NoIR camera	25mm x 24mm x 9mm
Adapted fisheye lens	25mm x 24mm x 30mm
Diameter of Fisheye lens	25mm
IP 65 waterproof enclosure	200mm x 155mm x 80mm

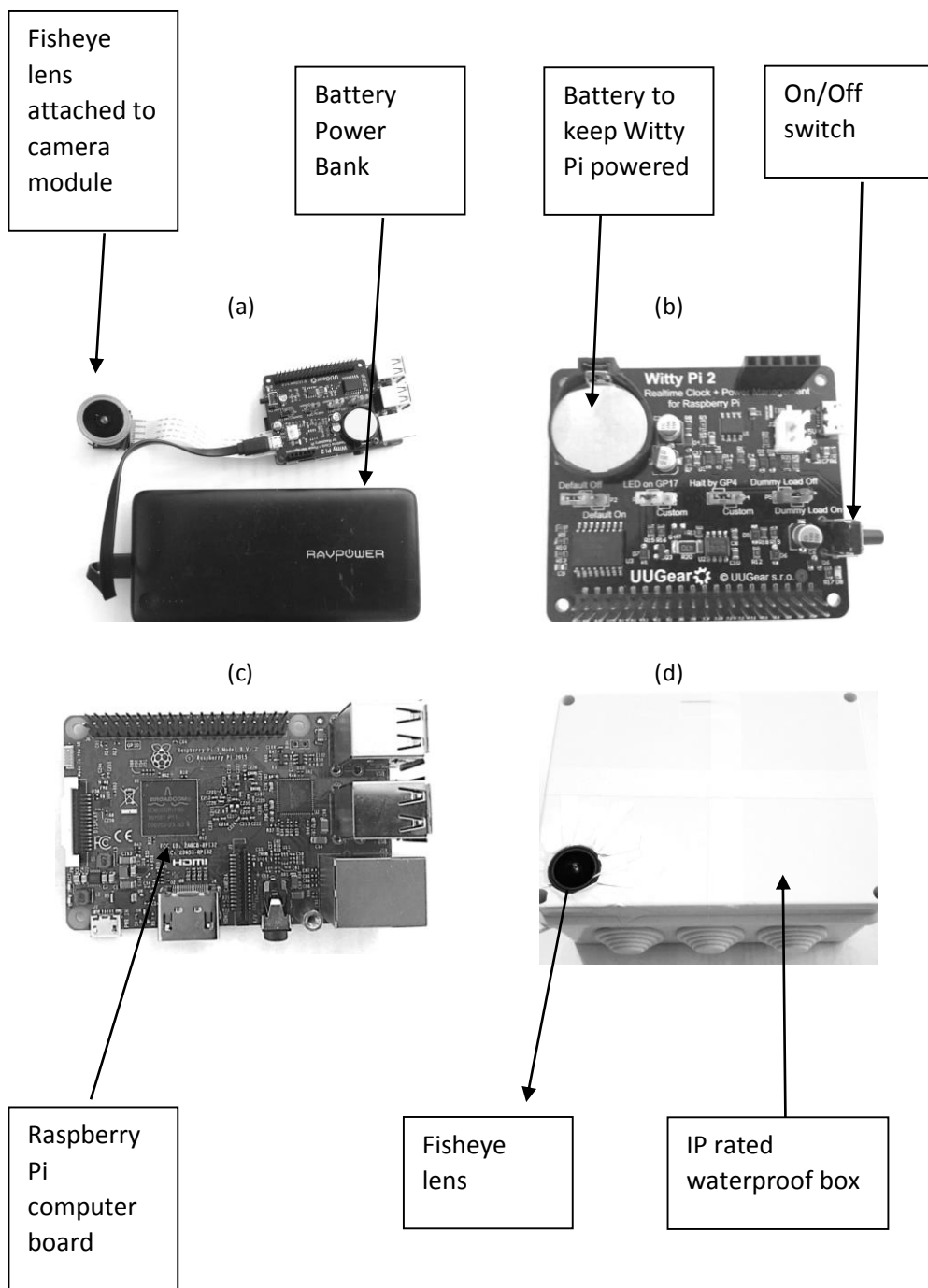


Figure 4.1 (a) Raspberry Pi, (b) Witty Pi 2, (c) Combined sensor with lithium battery, (d) IP65 waterproof enclosure.

4.3.2 Firmware and Software

The Witty Pi 2 system (*UUGEAR, 2018*) runs on an inbuilt code that turns the Raspberry Pi on and off at set time intervals, thus conserving battery power. A time-lapse crontab code (a type of code that can be set to run at designated time intervals for example every five minutes starting from when the Raspberry pi is turned on) was running on the Raspberry Pi capturing an image every five minutes. Finally, the Raspberry Pi was programmed to begin capturing images once it was turned on by the Witty Pi 2 system. The captured image was automatically emailed to a server to enable automated sky-view factor analysis.

Sky-view factors were calculated using the publicly available 'Sky-View Factor calculator' software (Lindberg and Holmer, 2010). The software analyses an image by first converting an image into binary and calculating the percentage of white pixels in a hemispherical image (*Holmer et al., 2001*). The sky-view factor is then calculated by using the annulus method (*Johnson and Watson, 1984; Steyn, 1980*). By coding the algorithm into MATLAB, the sky-view factor could be automatically calculated for any uploaded image. Percentage leaf fall was then calculated by comparing the rate of change of sky-view factor from image to image. 100% full canopy was set based on the first sky-view factor calculated from the first image taken at the start of the leaf fall season and 100% leaf fall was set based on the sky-view factor calculated from the image taken of the bare tree. From the two base values, the percentage leaf fall calculation of each image throughout the season can be made. The result is a measurement of leaf fall over the course of the season.

4.3.3 Study Site and Data Collection

Data was collected at a number of sites on the University of Birmingham campus, UK, during autumn 2017. The IP rated (waterproof) box was placed under three different species of tree: Oak, Beech and Birch (Figure 4.2). Each is a prominent native UK species making up a combined 33% of the 10 million trees along the UK rail network alone (*Crawley et al., 2017; Network Rail, 2018*). Data collection ran for the full autumn season from September 27th to December 20th. Note that the exact leaf fall season, typically September through to December, varies slightly each year depending on weather conditions (*Woodland Trust, 2017*).

4.4 Results and Discussion

4.4.1 Automated Versus Manual Measurements

Autumn 2017 provided a range of (normal) weather conditions e.g. heavy rain, sleet and snow through which the device performed robustly. To validate the Raspberry Pi's ability to capture accurate recordings of leaf fall, the percentage change in leaf fall was compared to the nearest regional Met Office trained observer recordings (Figure 4.3). It is important to note that the Met Office trained observer did not record the same trees as the ones captured using the Raspberry Pi. Instead, the regional Met Office observer records the average leaf fall of a collection of tree species in a region rather than individual trees. This means that the automated data is potentially more sensitive to sudden increases in leaf fall whilst the regional observers show a smooth decrease in leaf fall over time. However, the percentage leaf fall recorded on the device is comparable with the percentage change of all observed tree species.

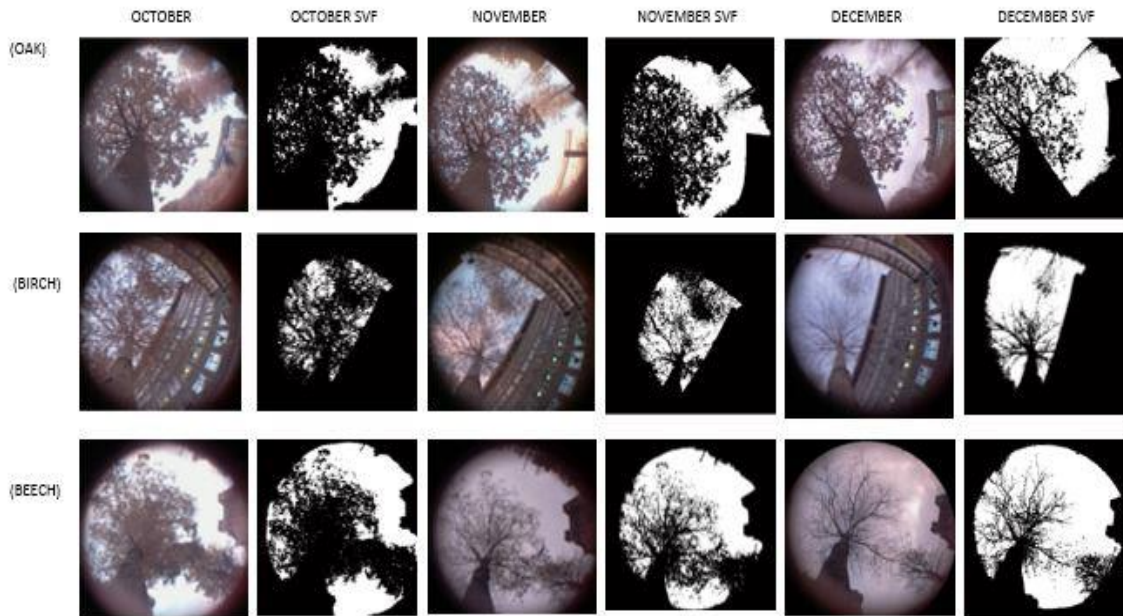


Figure 4.2 - Hemispherical images captured using an adapted Raspberry Pi and the corresponding SVF images, showing the reduction in leaf canopy over time.

The images captured from the Raspberry Pi visually show the general decline in leaf cover over autumn from full canopy to bare tree (Figure 4.2). Birch was the first observed tree species to reach 100% leaf fall, both on the automated device and the independent observer, with a sharp increase in leaf fall for Birch from 10/12/2017 – 15/12/2017, which coincided with freezing temperatures and snowfall in the region (Figure 4.5).

Beech reached 100% leaf fall by the 29/11/2017 (Raspberry Pi) and the 4/12/2017 (independent observer). Indeed, throughout the autumn the automatically recorded Beech remained one week ahead of the regional Met Office observer. This may be due to variations in microclimate of the area and the variation in leaf drop between individual tree species (*Rizwan et al., 2008; Peñuelas and Filella, 2009*). This recorded

delay illustrates the need for wider placement of automated devices in sheltered cuttings along the rail network. Similar to Birch, Beech automatic data recorded sharper increases in leaf fall which seemed to reflect changes in weather more so than the regional observer (Figure 4.5).

Oak reached just 67% leaf fall by December 2017 (Raspberry Pi) compared to 100% leaf fall according to the independent observer (Figure 4.3, Figure 4.4). This level of variation from a regional observation of oak to a single oak tree species highlight the need for a method that can assess tree species on a high spatial and temporal scale. The delay is likely due to the retention of oak leaves throughout autumn and winter on the individual Raspberry Pi recorded tree, which did not occur on a regional scale according to the leaf fall observer. This poses particular issues in autumn leaf fall observations when recording an individual tree species rather than a whole region (*Dixon, 1976*). This is one area of research in which the proposed approach could be particularly valuable enabling continued recording of leaves throughout the year and thus greatly improving scientific understanding of leaf retention. Further tests on a regional scale could also allow a comparison between regional observers and a regional Raspberry Pi network, however this was not possible during the current research period.

Figure 4.4 shows that the Birch and Beech recordings from the Raspberry Pi correlate above the 95% level with the independent leaf fall observer however the Oak correlates at the 69% level. This level of correlation in the oak shows the variation in single tree image capturing in comparison to a regional observer and highlights the need for a high spatial resolution leaf fall recording device.

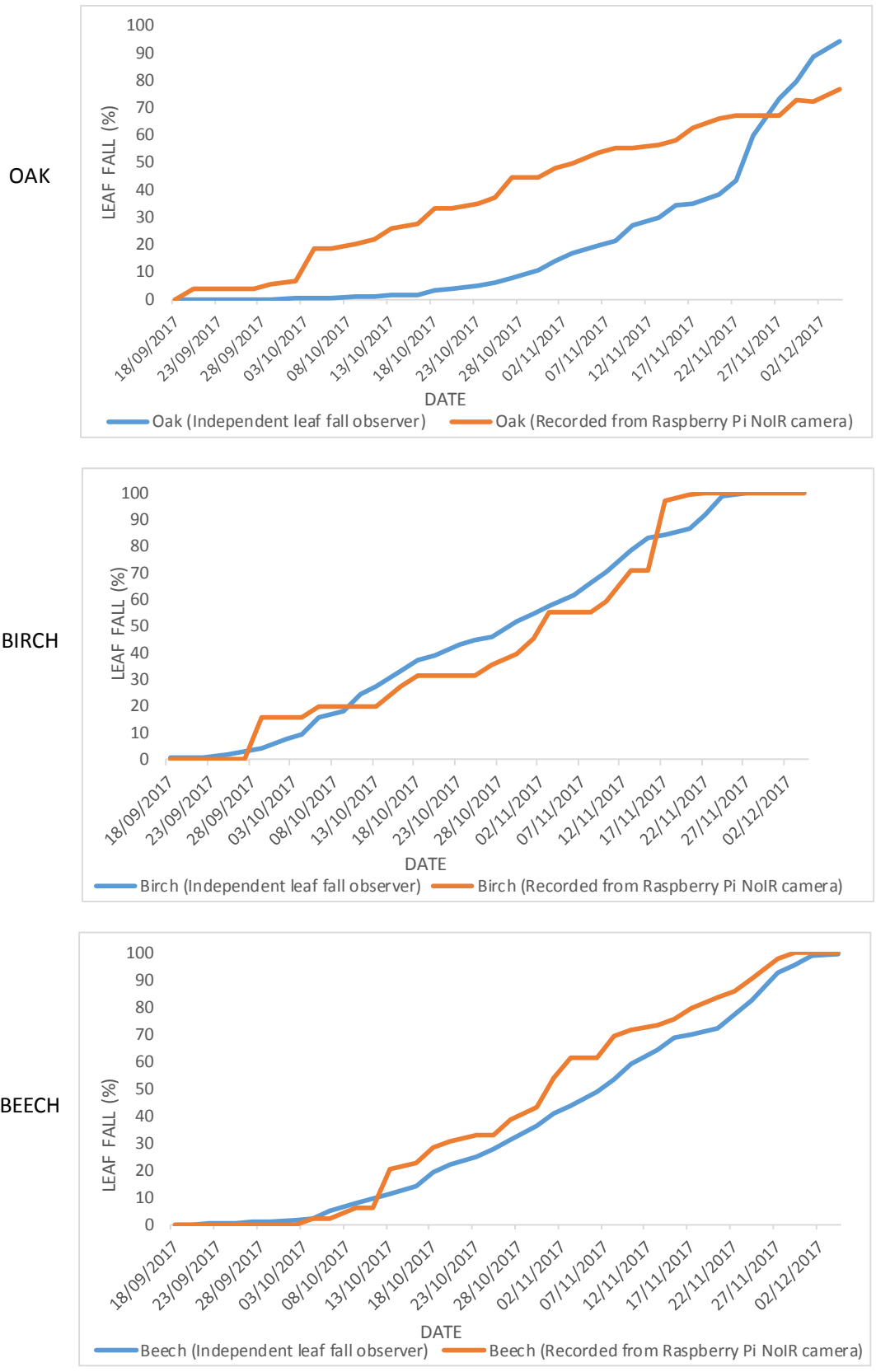


Figure 4.3 - Comparison between independent leaf fall observers and Raspberry Pi collected data.

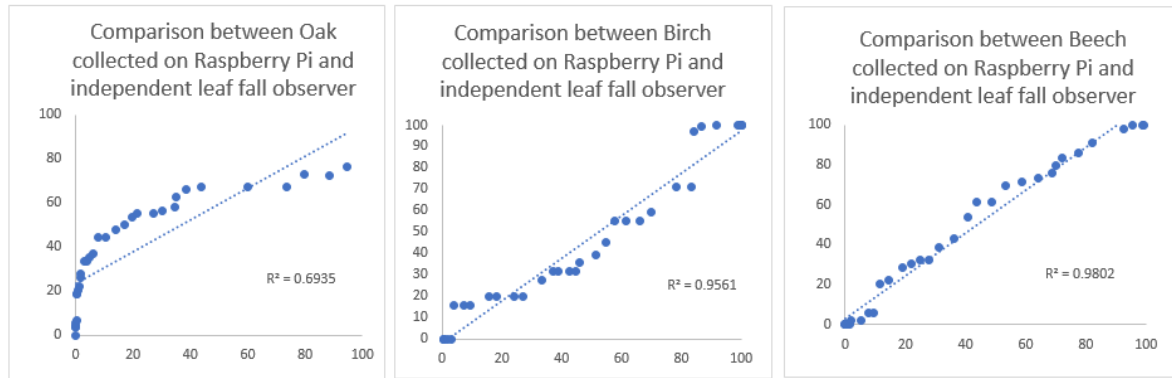


Figure 4.4 Quantitative difference analysis between leaf fall captured on the Raspberry Pi and an independent leaf fall observer.

4.5 Leaf Fall and the Weather

To understand the rates and timings of leaf fall recorded shown in Figure 4.3, the automatically recorded leaf fall data was compared to daily weather throughout the autumn. The four key weather variables that affect leaf fall; average wind speed, maximum gusts, rainfall and temperature were recorded and compared to the change in percentage leaf fall (*Gallinat et al., 2015*). Crucially all three species follow similar leaf fall patterns in response to weather related events.

4.5.1 Wind Speed

An increase in wind speed tends to lead to an increase in leaf fall (*Gallinat et al., 2015*). This is due to a greater force being placed upon the leaf, breaking the connection between branch and leaf. As the autumn season progresses, and leaf senescence has begun the strength of wind needed to remove leaves decreases. Acceleration of this process is also caused from the decrease in leaf canopy which previously acted

as a buffer for lower branches against wind effects (*Staelens et al., 2003*). Typically, Oak species seem more susceptible to changes in wind than Birch, potentially due to the differences in area and shape of leaves with some species being more aerodynamic than others (*Staelens et al., 2003*). This was shown in the automatic data collected, as leaf fall percentage remains low during a period of lower wind speeds (30/10/2017 - 6/11/2017) most noticeably in the recorded Beech species (Figure 4.5).

4.5.2 Temperature

Autumn leaf fall in deciduous woodland species can be delayed with higher than average temperatures (*Peñuelas and Filella, 2009*). The higher temperatures at the start of 2017 may have contributed to the delay in leaf drop of all recorded tree species (Figure 4.5) compared to the 'Natures Calendar' 2016 first leaf drop observations (*Woodland Trust, 2017*). However, rapid increases in leaf fall can occur after reductions in temperature, particularly frosts (Figure 4.5). This is most noticeable in the Birch tree data (Figure 4.4) with the sudden increase in leaf drop on the 18/11/2017 after a period of cold temperatures and heavy snowfall in the area (*Chmielewski et al., 2005; Norby et al., 2003*).

4.5.3 Rainfall

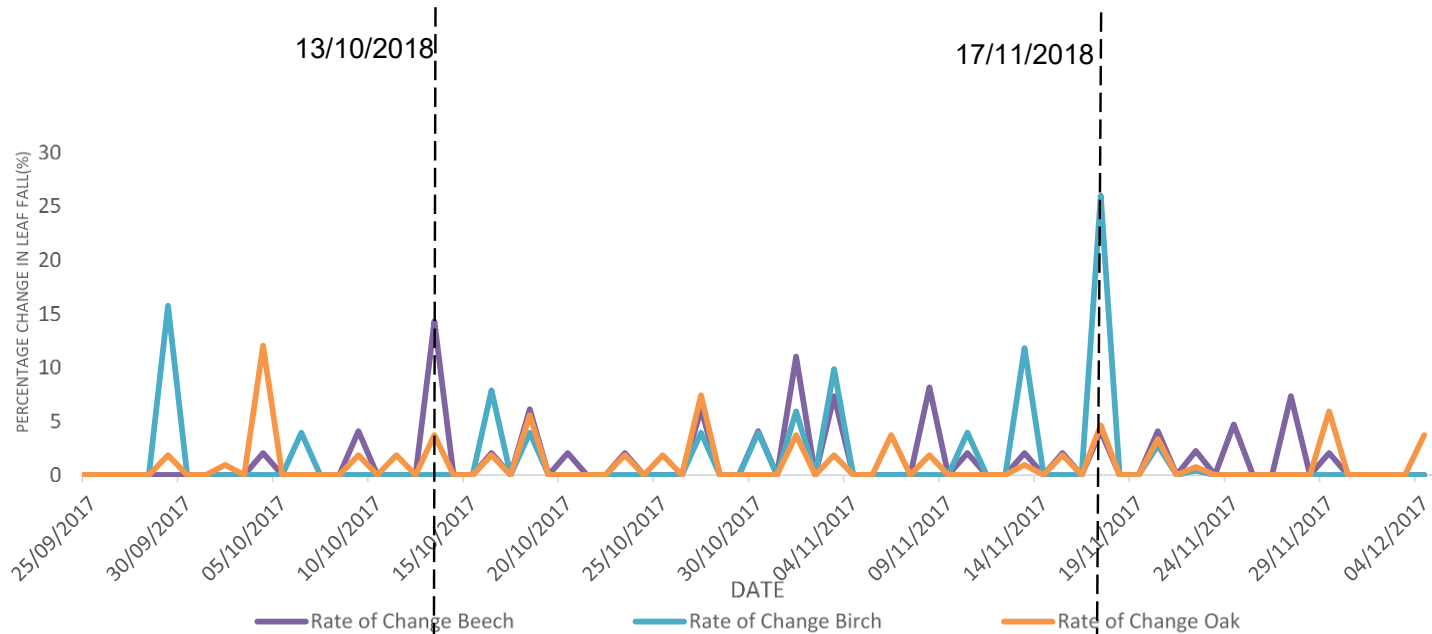
There are limited studies in existence on the effect of rainfall on autumn leaf fall, however, increased rain and soil moisture throughout the year can lead to delayed autumn senescence (*Estiarte and Peñuelas, 2015; Gordo and Sanz, 2010*). Rainfall shows less of an immediate pattern in the autumn 2017 collected data. After a period of high rainfall (19/10/2017, 4/11/2017 and 7/11/2017), the change in leaf fall

percentage for Birch is low or stable (Figure 4.5). A delayed response is also seen to a lesser extent in Beech trees (Figure 4.5), suggesting that different tree species respond to weather conditions at varying rates. This is evident in the Oak tree which correlates at the 0.01 significance level with rain for 2017. This may be due to the leaves being less affected by other weather conditions and thus a change in rainfall, and therefore pressure on the vegetation leads to an increased effect on leaf drop. However, further investigation is needed to assess the full extent of autumn leaf fall in relation to rainfall data.

4.5.4 Antecedence

A combination of weather is likely to have an effect on leaf fall rather than one isolated variable. High wind speeds coupled with low precipitation and cooler temperatures occurred during the start of the leaf fall season (13/10/2017) resulting in a high rate of fall for the Beech tree. However, a decrease in wind speed and a fall in temperature results in an increased leaf fall for Birch towards the end of the leaf fall season (Figure 4.5). Further research is needed over several years to statistically identify the combined effects of multiple variables. It is evident from Figure 4.5 that a combination of various weather conditions affects tree species at a different rate and therefore when recording leaf fall on a regional scale it is important to record a range of tree species throughout the autumn period.

(a)
 Comparison of
 the rate of
 change in leaf fall
 of Beech, Birch
 and Oak
 recorded on the
 Raspberry Pi
 device



(b)
 Rainfall,
 temperature and
 wind speed
 recordings for
 Autumn 2017.

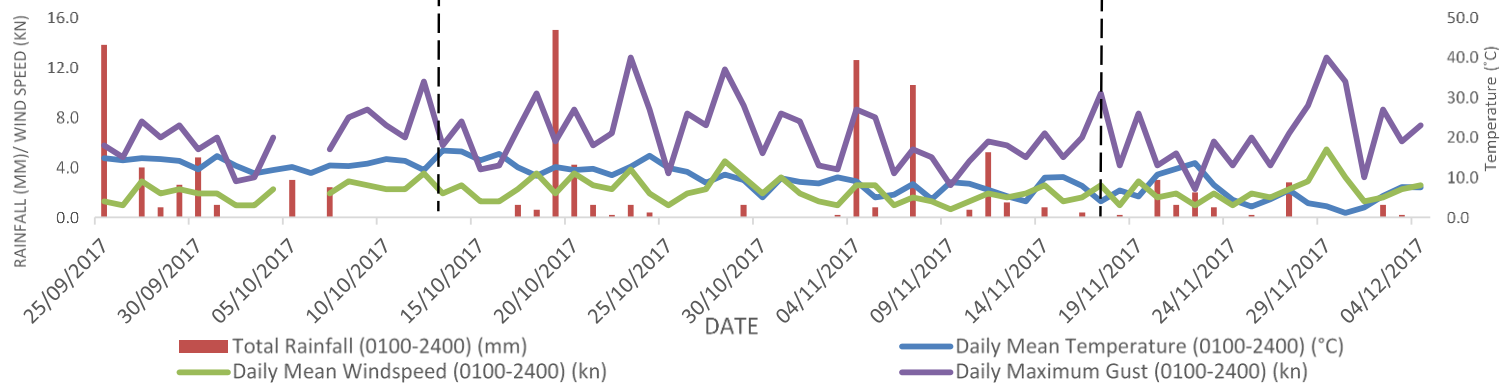


Figure 4.5 – (a) Rate of change in percentage leaf fall over autumn 2017, (b) Weather conditions throughout autumn 2017.

4.6 Conclusion

This chapter has evaluated a low-cost method to record leaf fall in-situ over an autumn period. An adapted Raspberry Pi device can remain operational in the field over an autumn season and connect using Wi-Fi or GSM communications to instantly relay recorded data. Variations in leaf canopy over time are clearly shown using a fisheye lens to capture hemispherical images. Using sky-view factor analysis, the images can be analysed to produce a change in percentage leaf fall from full canopy to bare tree. Whilst more data over a longer period of time would improve confidence levels in the long-term visibility of the Raspberry Pi, the current design has met the success criteria outline in chapter 3. The device is low-cost, can be placed outside at a high spatial scale and is relatively small in size. The data is comparable to current leaf fall observers and shows responses to variations in weather such as rain, temperature and wind speed. Although data collection over more autumn seasons is needed to further analyse the effect of weather conditions on autumn leaf fall, the approach has the potential to objectively replace observers in leaf-fall monitoring studies and networks.

Chapter Four Summary

This research tests the effectiveness of an adapted low-cost Raspberry Pi camera in recording the change in tree canopies over autumn. Oak, Beech and Birch trees were recorded in the field using the automated device which relayed captured hemispherical images in real-time over the internet. The sky-view factors of a sequence of images were calculated and used to highlight changes in the tree canopy (leaf fall) over time. Analysis showed that the objectively obtained Raspberry Pi data correlates with regional manual leaf fall observations. In addition, the role of the prevailing weather conditions can be analysed to quantify impacts on leaf fall.

Chapter Five

Automatic data processing for integration of leaf fall data into a forecast model

5.1 Leaf fall Techniques used by the Met Office

Leaf fall and low adhesion forecasting began as a result of severe delays on the UK rail network. As previously discussed, the Met Office have been producing leaf fall and low adhesion forecasts for the last 20 years in order to mitigate rail related problems caused during autumn. In order to improve the leaf fall predictions given to the railways the leaf fall model that produces the forecast has been redeveloped and designed over time with improvements in technology. Currently the leaf fall forecast model uses the following parameters: percentage leaf falls of certain tree species; forecasted weather conditions such as wind speed and moisture; amount and type of foliage along a rail route; and frost and storm warnings (*Met Office, 2018*). From these parameters the leaf fall (Figure 5.1) and low adhesion (Figure 5.2) forecast is produced at a high-resolution. As discussed in Chapter One, the forecast can predict leaf fall and low adhesion at a STANOX (e.g. station to station) resolution and is fundamentally used to predict the likelihood of autumn related issues on specific rail lines.

One of the main inputs into the leaf fall forecast model is the daily percentage leaf fall loss in an area. This input is provided by a network of Met Office trained observers who conduct manual observations each morning and then estimate the amount of leaf fall that has occurred from different tree species such as Oak, Beech and Birch on a regional scale across the UK. It is this element, which can be subjective, that has provided one of the primary motivations for this research in order to offer an alternative

solution to a manual observer. This is important as it permits an increase in objectivity over human observers as well as using new technology to increase the number of observations that can be made at once by using comparable low-cost sensors. So far, this research has designed and tested a low-cost device that could capture the change in leaf fall over the autumn season using hemispherical images (chapter three and chapter four). Chapter four further showed that using readily available programs such as the Lindberg and Holmer (2010) sky-view factor calculator, images captured on the low-cost device (Raspberry Pi) could be analysed and compared with the percentage leaf fall estimates from a regional Met Office observer for both late falling (Oak) and early falling species (Birch and Beech). Further testing in chapter four showed that the rate of change captured on the Raspberry Pi could be compared with changes in weather conditions such as frost and high winds. However, to ensure the robustness of analysis in these previous chapters, significant manual post processing of imaging has been required. This chapter continues this work by developing algorithms that have the potential to automate the process to a point that manual observations can be confidently replaced. Whilst this chapter focuses on the adaption of the Met Office forecast model, it is important to note that this input could be used for any leaf fall and low adhesion forecasting models.

This chapter presents a prototype code that calculates the percentage leaf fall from full canopy to bare tree using an automated threshold and sky-view factor calculations developed by Steyn (1980). The prototype code will be compared to manually analysed hemispherical images in order to test the reliability of an automatic threshold code.

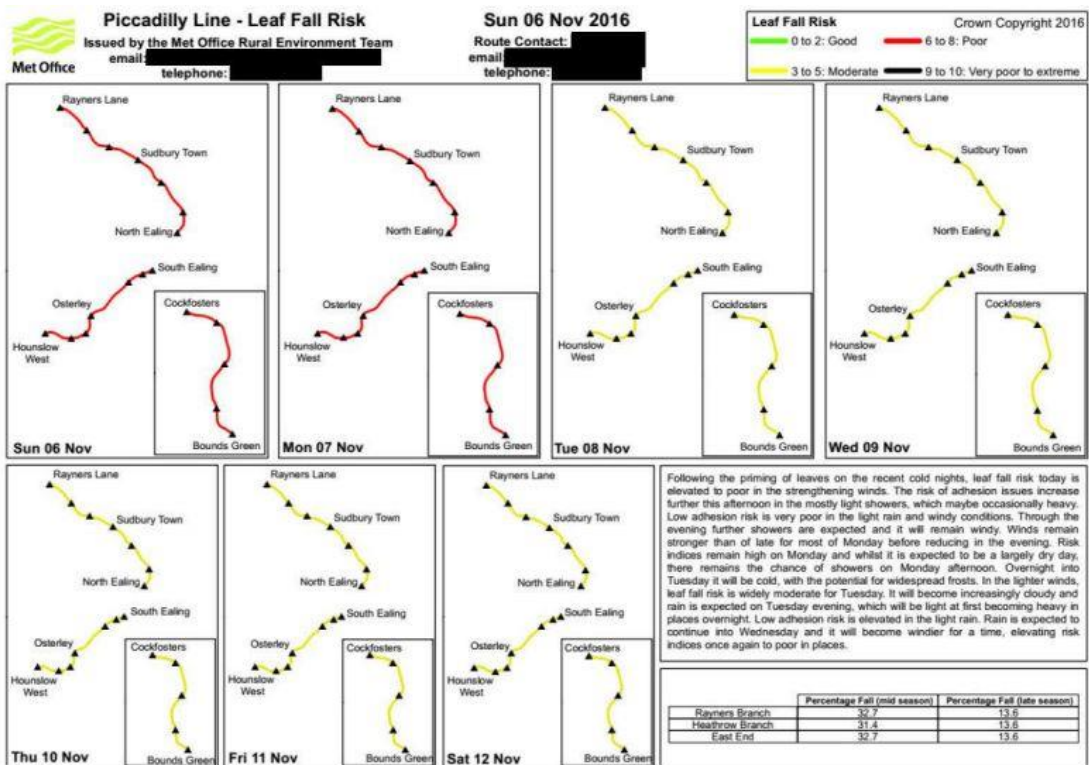


Figure 5.1 – Sample of a Met Office leaf fall risk (Crawley et al., 2017).

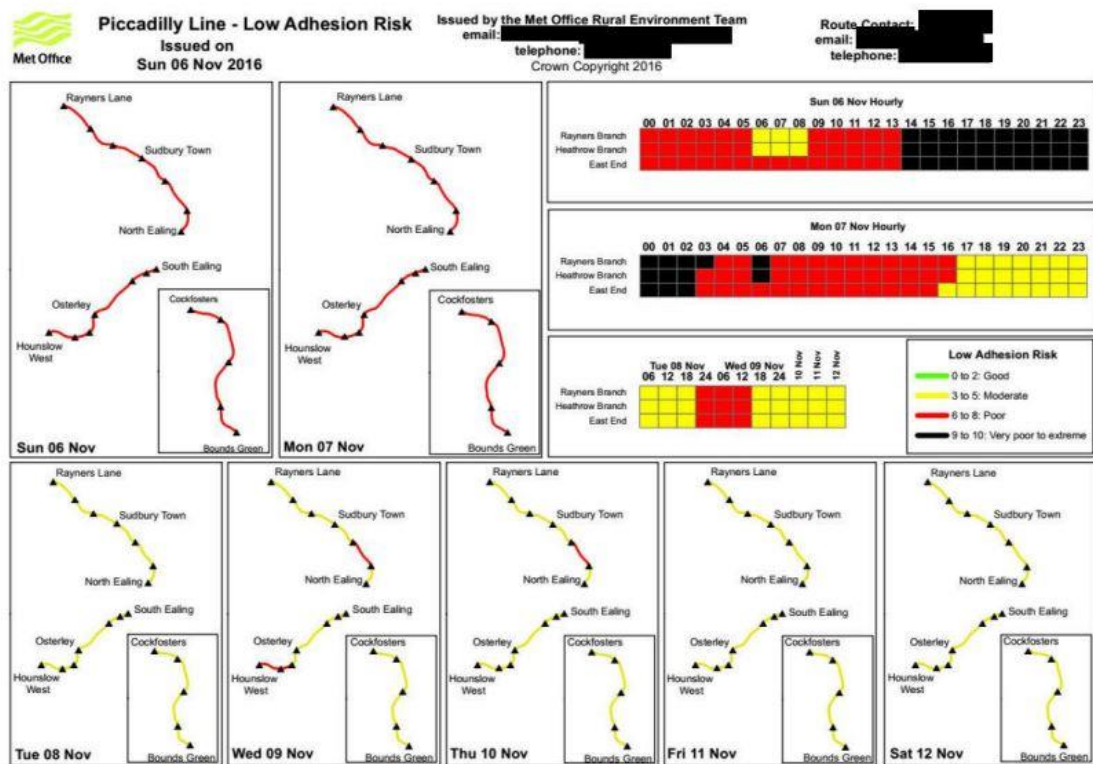


Figure 5.2 – Sample of a Met Office low adhesion forecast (Crawley et al., 2017).

5.2 Methodology

Whilst the Lindberg and Holmer (2010) 'sky-view factor calculator' can be readily used to post analyse data captured on the Raspberry Pi, it cannot be used in real time. Therefore, a bespoke real-time software would be beneficial to analyse the images directly on the Raspberry Pi rather than using third party software in the post autumn analysis. This software would be specifically designed to capture the changes in vegetation in the image sequence rather than the change in the visible sky in the image in order to reduce the effects of buildings or non-vegetation obstructions which may cause underestimation of leaf fall loss over time in captured images. The removal of post-processing would represent a significant step towards the operational use of the device; however, it does remove the potential for user-input when evaluating the robustness of the calculations.

There exists a range of different sky-view factor calculation codes which are readily available and could be used as a foundation for a new prototype code. For example, the RayMan model (Matzarakis *et al.* 2007; Matzarakis *et al.* 2010) and the Sky-helios method created by Matuschek and Matzarakis (2010) use a pixel threshold calculation in order to determine the percentage of sky-pixels in a raster image. Alternatively, the Arc-View sky-view factor – EXT and the Arc-View Steyn sky-view calculator (Gál *et al.* 2009; Hämmerle *et al.* 2011) use the mathematical principles first published by Steyn in 1980. These approaches were compared in research conducted by Hämmerle *et al.* (2011) and it was concluded that calculators that used the principles of Steyn's mathematical principles correlated more significantly than a raster-based pixel method. The Lindberg and Holmer (2010) sky-view factor calculator combines both the pixel

threshold, using a raster method similar to the RayMan model (*Matzarakis et al. 2007; 2010*), developed by Holmer et al. (*2001*) and the annulus method which uses the mathematical equations developed by Steyn (*1980*) and Johnson & Watson (*1984*).

Similar to the code produced by Lindberg and Holmer (*2010*), the prototype automatic Python code uses the combination of a threshold approach and mathematical equations. The code follows the mathematical approach laid out in Steyn's early sky-view factor work and adapted by several other sky-view calculators such as the BMSky-view calculator (*Gal et al. 2007*) and the Arc-View Steyn sky-view calculator (*Hämmerle et al., 2011*), which principally uses equation 5.1 (*Steyn, 1980; Barring and Mattson 1985*) to calculate sky-view factors in a hemispherical image as well as a pixel threshold technique used to specifically pick out the percentage of pixels labelled as vegetation.

$$SVF = \frac{1}{2 \cdot n} \sum_{i=1}^n \sin \left[\frac{\pi \left(i - \frac{1}{2} \right)}{2 \cdot n} \right] \cos \left[\frac{\pi \left(i - \frac{1}{2} \right)}{2 \cdot n} \right] \alpha i \quad (5.1)$$

Where n = the number of concentric rings in a hemispherical image and α is the width of the ring for the specific annulus (i)

Fundamentally, the code (appendix 1) analyses the image captured by the Raspberry Pi near-infrared camera module and returns a daily leaf fall percentage. The code was based on a pixel counting method, in which the fisheye lens image was converted into binary and then based on Chapmans (2001) paper split into 9 concentric rings to calculate a sky-view factor. A step by step process of the code is shown in figure 5.8.

One of the problems with using automated methods for the calculation of the sky-view factor is obtaining a consistent and reliable threshold to separate sky from non-sky pixels (*Chapman et al, 2014*). The collection of imagery is often restricted to 'ideal' conditions in which glare from light (the Sun) does not cause a red hue around the image. High sunlight glare can also be reflected from buildings and make the windows appear the same colour as vegetation. An example red haze caused by bright sunshine conditions can be seen in Figure 5.3. The restriction of ideal (overcast) conditions is not practical for an automatic image processing device as weather conditions in the UK autumn can vary with peaks of sunshine expected at certain times in the day. A way of reducing weather related issues is to capture the images during dawn or dusk when the sun is lower in the sky and thus reduces the potential for light reflectance and glare on the lens and ultimately distortion within the image.

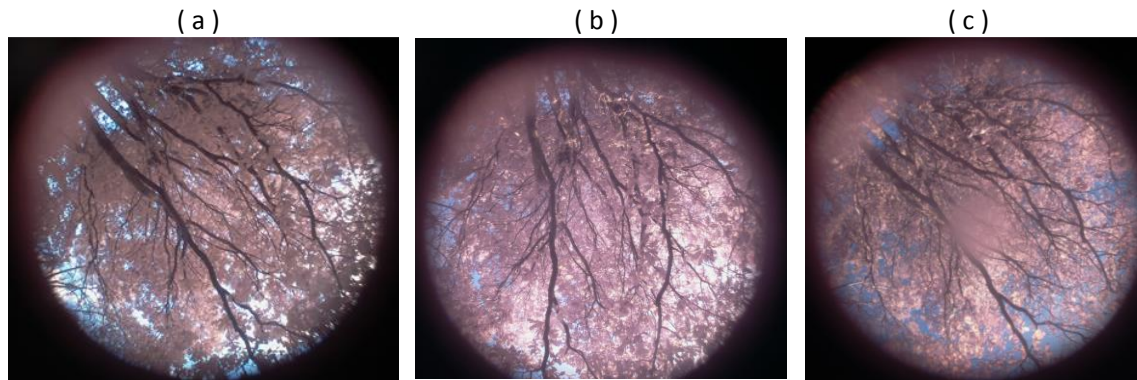


Figure 5.3 a, b and c show a range of images captured using the Raspberry Pi NoIR camera highlighting the pink colour of leaves and the pink colour of light on the lens

It is for this reason that this research has utilised the use of near-infrared to provide added information to aid in this process, in particular the ready classification of vegetation in the imagery. Due to the high reflectance properties of vegetation in near-infrared, leaves appear red in the captured image therefore a threshold to convert the image into vegetation / non-vegetation is set based on the red colour range within the image. The full range of colours can be seen in histograms produced using 'Image J' software (Figure 5.4), where a clear spike in red values above the 245 RGB range is evident, however there is a spike around the 80 – 120 RGB range as well. This is due to the blue sky and the bark colour within the photograph and therefore thresholding to select red only images could be made before the red peak at 245, removing other coloured material from the image.

However, due to the leaves in the image appearing in a range of red colours such as different shades of pink (as shown in Figure 5.4) a set threshold for "red" could not be applied. A Python code was needed to create a range of red / pink values that a pixel could fall into in order for it to be classified as vegetation. In order to adapt the Image

J values into a Python detectable list of red boundaries, licence free code produced by Rosebrock (2014) was used. This selects red, purple and pink colours from an image and could therefore be applied to the capturing of vegetation. The use of a range of threshold values is an improvement on the Chapman (2007) work in which only one value was used to threshold the near-infrared images. By advancing the threshold technique previously used in research this style of code improves on the previous scientific apparatus by capturing more vegetation in a range of colours; thus giving a more accurate sky-view factor. This code was designed to work on Python and specifically for use with a Raspberry Pi and thus easily assimilated into a sky-view factor code. The initial structure of the colour detection code used in Rosebrock (2014) was customised based on hue, saturation and value (HSV) colour scatter plots of a typical leaf canopy (Figure 5.5). The HSV range values can be converted using an online HSV to RGB converter to obtain the RGB boundary ranges needed in the automatic threshold code.

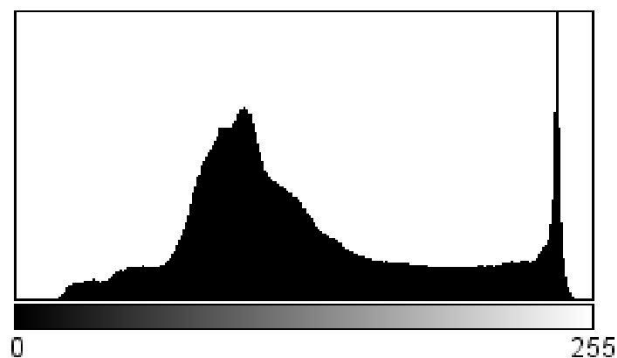


Figure 5.4 Histogram of red pixels in a leaf canopy captured under ideal conditions produced using 'Image J' software (taken from a Beech image 2017), (x axis= pixel colour value, y axis=number of pixels).

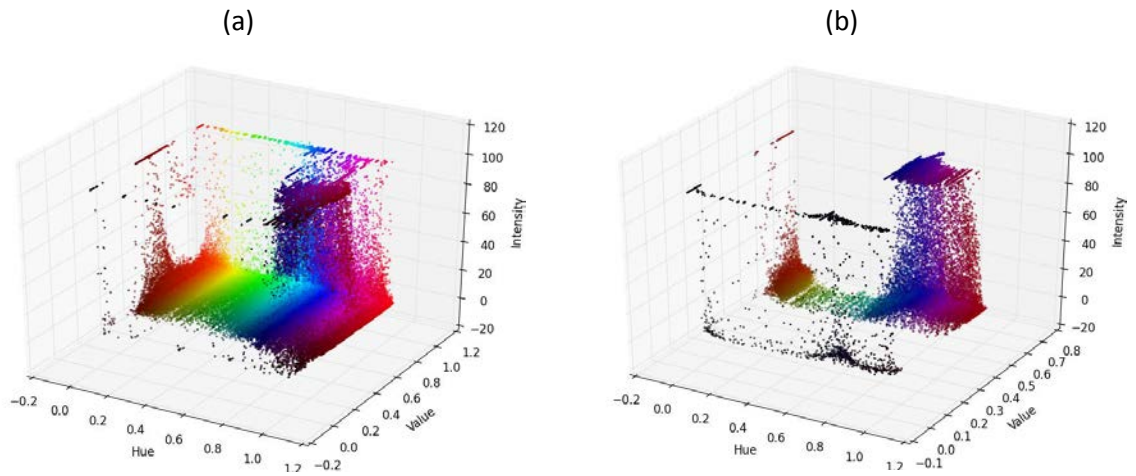


Figure 5.5 (a) Scatter plot of pixel colour range in a typical tree canopy image, (b) Scatted plot of the colour range within an image once red threshold ranges had been applied (taken from a Beech image 2017).

The boundaries in the automatic threshold range captured the HSV values in both the red and pink range displayed in the scatter plot (Figure 5.5a), allowing a large colour range of vegetation to be captured and the removal of pixels corresponding to non-vegetated components. The image produced after the removal of non-vegetative colours can be seen in Figure 5.5b.

The colour range captured in a typical Birch image was used in order to adapt the boundaries produced by Rosebrock (2014) and this pixel range was then used in all analysed images; which was a good representative for all other collected tree species images. The code converted pixels not in that set range to black hence the removal of light blue and green and the increase proportion of black pixels in Figure 5.5b. A set threshold on the converted image was then added to the code in order to produce a binary version of the image (i.e. turn the red/ pink pixels into white and the rest of the image black). This binary image was needed in order to calculate a sky-view factor.

Care needs to be taken during this process; near-infrared images can cause a red tinge on the lens creating a pink ring around the image (Figure 5.3) which can lead to overestimation of the leaves in an image. Whilst this code masks the image creating a circle around the hemispherical image some glare can intrude onto the photograph. However, the benefits of capturing in the near-infrared such as the clear distinction between bark and vegetation is more imperative than slight overestimation from light glare. The sky-view factor could also be applied to BGR images (BGR are used in Python rather than RGB images but the same principle applies) by adapting the threshold to capture in the green colour spectrum. However, due to senescence in autumn, the change in colour of the leaves would make capturing in the green spectrum alone not possible and alteration of the code over leaf tinting would be

needed. Figure 5.6 shows the comparison in colour range from an image capturing the same area of vegetation using a digital camera (5.6a) and a near-infrared image captured using the Raspberry Pi (5.6b) camera. From the figure it is clear that the green colour of vegetation is prominent using a standard digital camera (Figure 5.6a), but when the same image is captured using the near-infra red Raspberry Pi camera the vegetation turns pink in colour (Figure 5.6b).

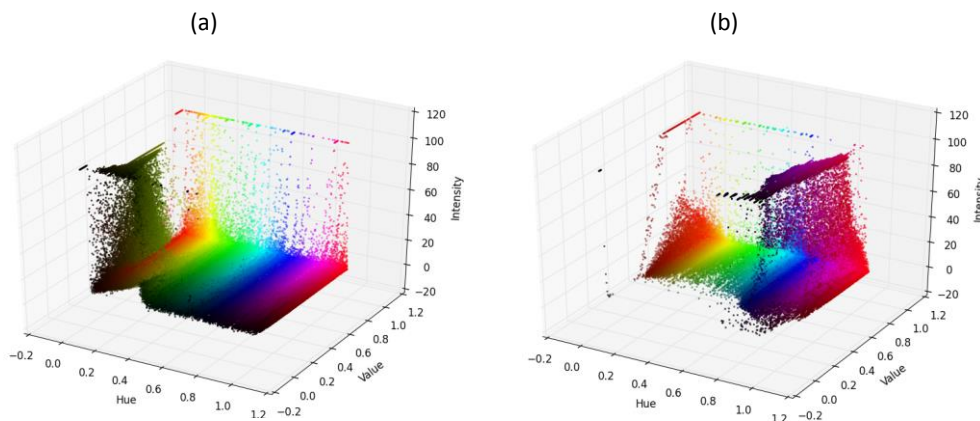


Figure 5.6 (a) Scatter plot of colour range captured using a digital camera, (b) scatter plot of colour range using the same vegetation captured with a near-infrared Raspberry Pi camera.

The red threshold boundaries were manually altered in an experimental trial and error approach to get the threshold that visually captured the most leaves per image. A visual comparison of an original captured oak 2016 image, the oak 2016 image that had been manually altered (leaves were coloured in white by hand on photo editing software) and the automatically produced threshold for oak 2016 are compared in Figure 5.7. There has been a slight loss of leaves in the automatic threshold however as shown in Figure 5.7 the majority of vegetation is captured.

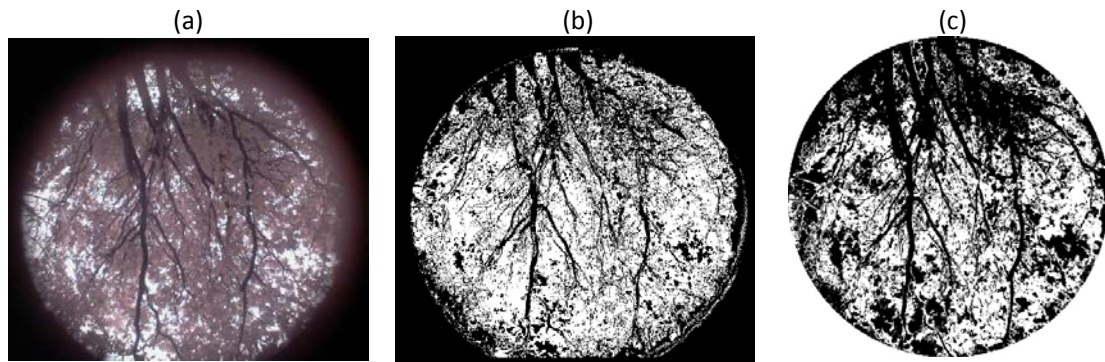


Figure 5.7 (a) Leaf fall image captured using the Raspberry Pi NoIR camera, (b) leaf fall image that has been manually turned into a binary image using photo editing software, (c) binary image produced using automatic threshold code.

The automatic threshold works on the images captured under ideal conditions. However, during unfavourable conditions such as light glare due to the time of day, slight overestimation of leaf fall could be made. This occurs when the colour of light glare on the lens is classified as leaf material. Capturing multiple images over the day, under different lighting conditions and calculating the average sky-view factor could reduce the interference caused by light conditions or cloud.

Once the image has been converted into binary the image is then cropped in order to analyse the hemispherical section of the captured image only, this reduces overestimation of sky-view factors from a FOV beyond 180 degrees as well as the pink tinge created due to light distortion.

A mask is then laid over the captured image in order to compare an image with no vegetation captured (effectively a black circle image) with the observed image captured on the Raspberry Pi camera. Using sky-view calculations from Steyn (1980), shown in Equation 5.1, the code splits the binary image into a series of annuli and calculates the

sky-view factors of each ring in order to offset the distortion caused by capturing images using a hemispherical lens (*Steyn, 1980; Barring and Mattson, 1985*). Once the sky-view factor has been calculated the code calculates the percentage leaf fall in each image (using the change in sky-view factor from full canopy, 0% fall, to bare tree, 100% fall, to convert into a percentage change over time). The percentage leaf fall is then saved as a .txt file alongside the time and date of the captured image. At set time intervals, using a crontab (a type of code that can be set to run at designated time intervals, for example every five minutes starting from when the Raspberry Pi is turned on as shown in appendix 2), the Raspberry Pi is programmed to capture a hemispherical image, run the sky-view factor Python code and send the .txt file to a designated server or email address. The process of the code can be seen in Figure 5.8.

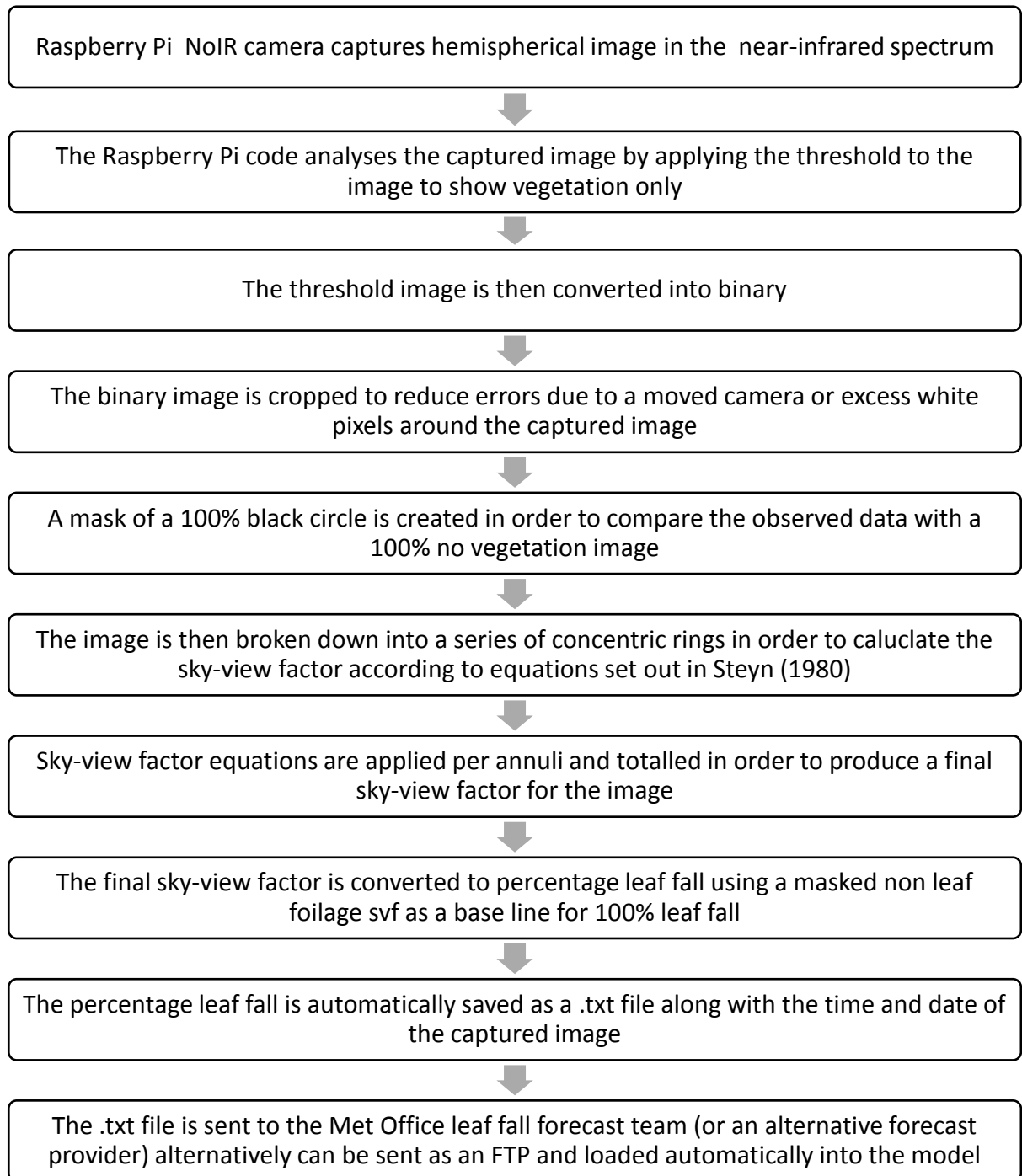


Figure 5.8 – Visual representation of the steps undertaken in the Python code produced on the Raspberry Pi computer.

5.3 Results and discussion

5.3.1 Comparison of Threshold Analysis

In order to compare the automated threshold code developed in this chapter with existing software, the same captured images for Oak, Beech and Birch used in figure 4.3 were analysed using the new approach. These could then be readily compared to the same images, that had been manually delineated (images in which leaves had been coloured white using photo editing software and non-vegetation coloured black) and processed using the Lindberg and Holmer (2010) sky-view calculator.

This comparison would then determine the viability of capturing vegetation using automatic threshold software. Figure 5.9 shows the variation in sky-view factors calculated manually and by the automatic threshold code.

For Oak (recorded in 2016), Beech and Birch, the automated code performs well but has a tendency to produce a slightly higher sky-view factor. It is thought that this overestimation of the amount of vegetation present in the hemispherical image is due to light glare during the start of the season and the reflectance of light on the buildings. Importantly, for this application, despite the slight overestimation, the sky-view factors show similar rate of change, as shown in Birch (2017) data where both sky-view factors increase rapidly towards the end of the season. Towards the end of the season the manual images sky-view factor read slightly higher than the automatic code, this is potentially due to light glare in the captured photograph resulting in a pink tinge on the image being classed as vegetation despite no vegetation being in the image. Whilst this light glare issue does not cause significant difference in sky-view factor, it is a

problem with automatic thresholding. Capturing multiple images throughout the day or programming the Raspberry Pi to capture images during low light conditions such as dawn, would reduce the light glare problems.

Oak (recorded in 2017) images produced using the automatic threshold calculator and the manually processed images produced a similar sky-view factor throughout the season, indicating the potential for the automatic code to be run without estimation errors. This shows the importance of placement, light conditions and surroundings when using automatic code as the Oak (2017) species was in a lowered area of ground near the university and sheltered from some of the light glare produced. The Oak (2017) species did not lose all of the leaves during the winter months and therefore the sheltered cutting and overhang of the leaves would block out some of the light glare from the images, again resulting in low estimation errors produced using the code.

The rate of change between the sky-view factors indicate when large amount of leaves fall over a set period. Figure 5.10 shows that the rate of change for the leaf fall species analysed for Birch, Beech and Oak are comparable with peaks occurring in both manual thresholding and automatic thresholding. This is essential for leaf fall observations as a sudden drop in leaves would indicate potential low adhesion events causing problems on the rail network.

The percentage leaf fall produced on the automatic threshold images and the manual images are similar as shown in Figure 5.11a. This similarity shows that the threshold image coding can be used over a season long campaign in varying weather and light conditions indicating that the threshold produced using the Raspberry Pi could be used as a viable automatic approach. However, further testing over multiple seasons and

locations would be needed to improve the statistical validation required to be certain of the code's viability. Despite the need for further testing over multiple seasons and places the initial findings are promising.

5.3.2 Comparison of Sky-View Factor Techniques

As well as the thresholding part of the code developed in this chapter, the actual code used to produce a sky-view factor needs to be comparable with current software techniques. The Lindberg and Holmer (2010) sky-view factors produced using the manual threshold images were compared with the automated sky-view factor code images. In order to test the practical viability of the two techniques, the percentage leaf fall produced from both techniques rather than the raw sky-view factors were analysed as raw sky-view factors using different techniques can vary by 20% (Hämmerle *et al.* 2011). The rate and percentage leaf fall need to be similar in order for the automatic code to be a viable alternative to the Lindberg and Holmer (2010) calculator. As show in Figure 5.10b, the percentage leaf fall across all images correlate and indicates that the prototype code could be used to calculate percentage leaf fall automatically over an autumn season.

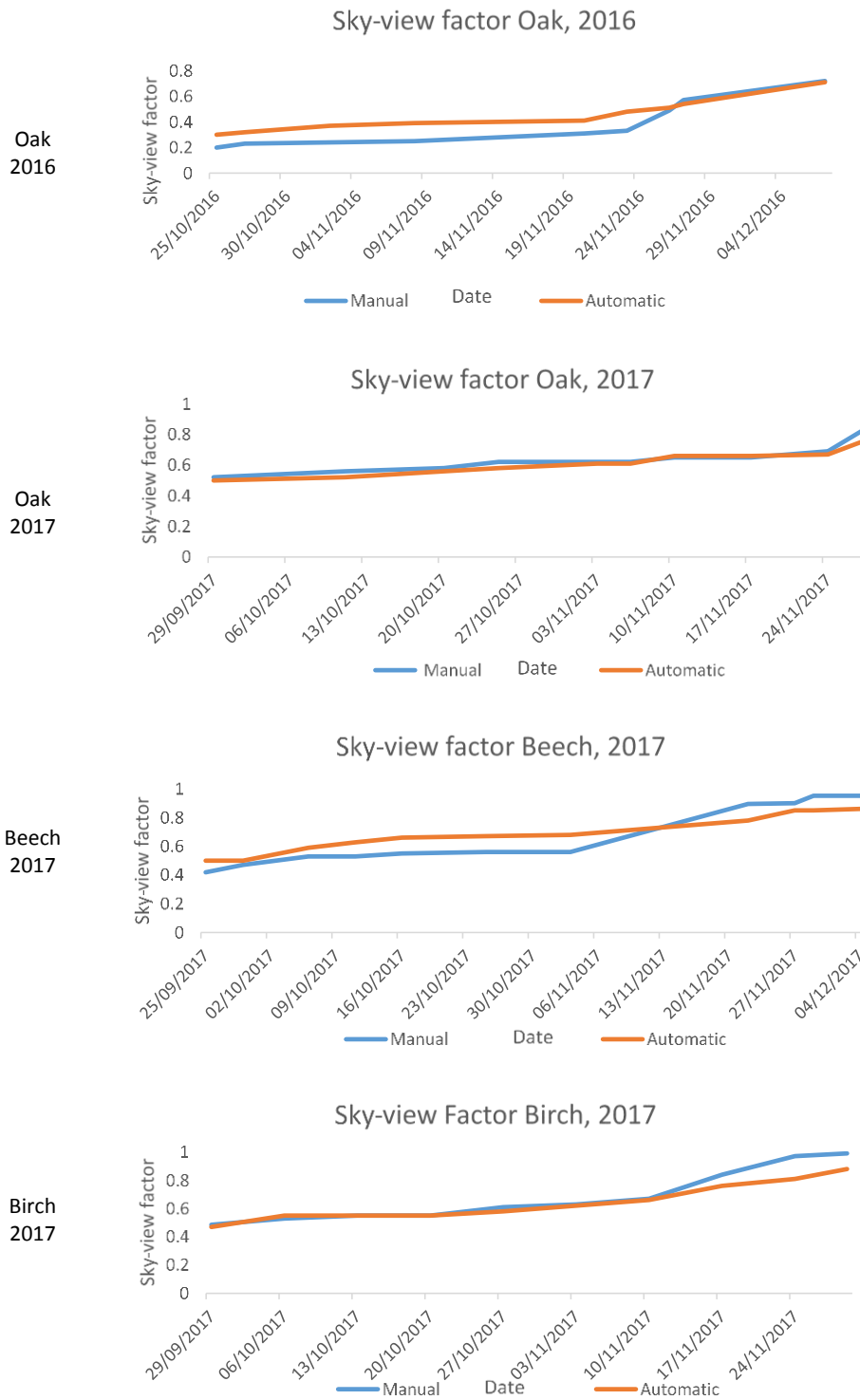


Figure 5.9 – Comparison of manual threshold sky view factors and automatic thresholds sky view factors conducted on the Lindberg and Holmer (2010) sky-view calculator software. See Figure 4.3 for leaf fall observer data.

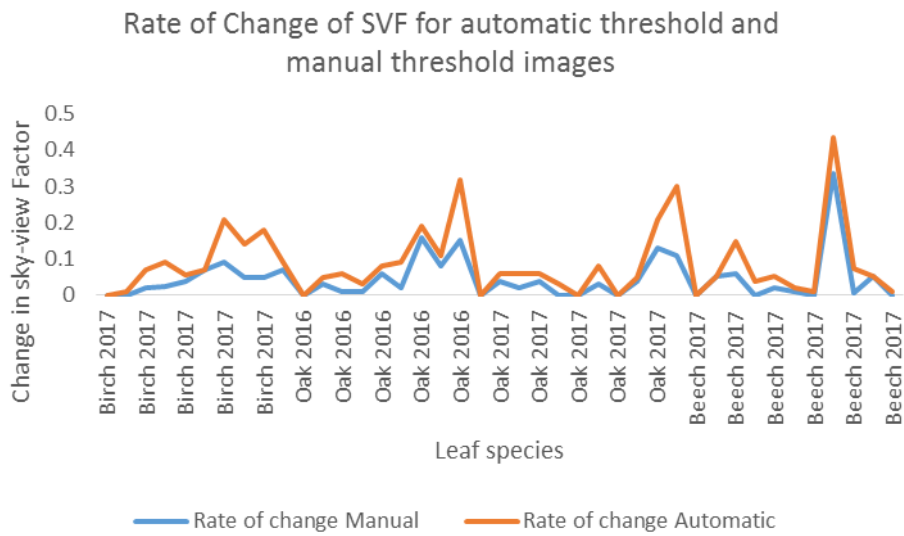


Figure 5.10 - Rate of change for leaf fall images analysed using the manual approach and the automatic approach.

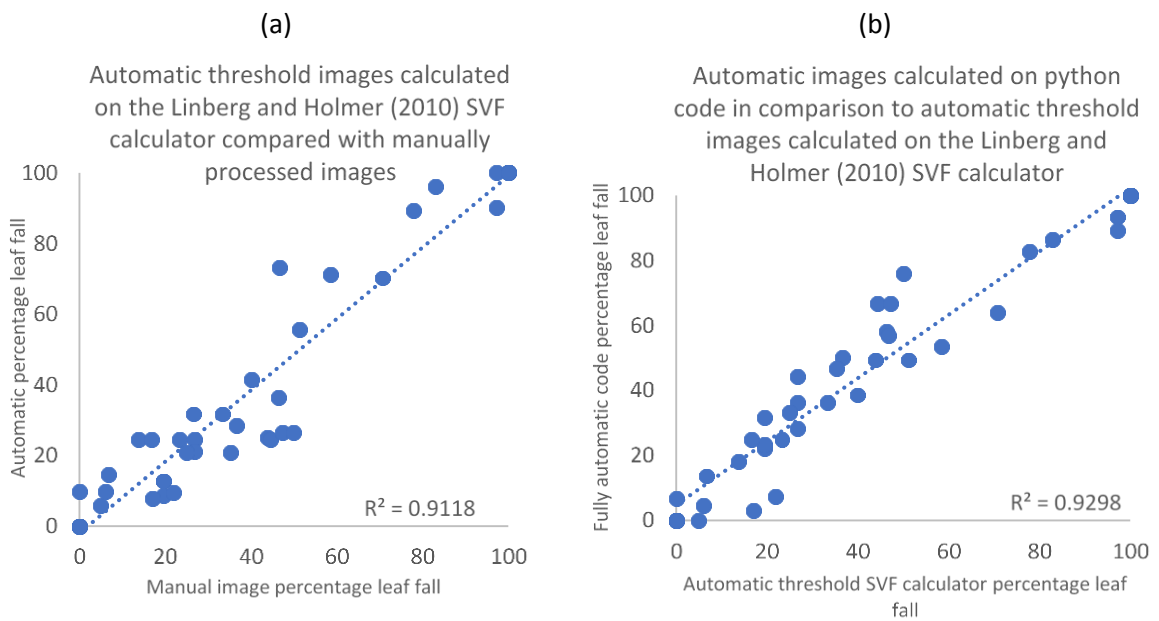


Figure 5.11 – (a) Comparison of manual leaf fall threshold and automatic threshold calculated on the Lindberg and Holmer sky-view calculator, (b) comparison of automatic threshold images sky-view factor calculated using the Lindberg and Holmer (2010) calculator and automatic sky-view factor code produced on the Raspberry Pi.

5.4 Conclusion

The results produced using the automatic threshold code are similar to the results produced by manual calculations using the Lindberg and Holmer (2010) sky-view factor calculator. Whilst chapter four showed that the hemispherical image approach could be used as a potential alternative to trained Met Office observers there was a need to make this approach automatic if it was to be successfully used. This chapter has showed that new coding technique can automatically produce results similar to that used in chapter four and therefore be used as a way to record leaf fall on the Raspberry Pi and be used as an alternative or alongside Met Office leaf fall observers (this feasibility of this is further discussed in chapter six).

Whilst the initial results are promising and show that a change in leaf fall percentage can be estimated with the created Python code on the Raspberry Pi based on threshold calculations and Steyn (1980) calculations, further testing is needed. Currently, buildings and light glare can cause problems with the use of automatic threshold code. For example, if the building captured in a hemispherical image appears in the same colour range as the vegetation under estimation of the percentage leaf fall can occur, and this was most noticeable in the Beech species data. Therefore, when picking a site location, potentially along a rail track, it would be important to carry out site visits and tests with the Raspberry Pi. This location testing should reduce potential problems for data capturing for example the Raspberry Pi device could be placed under sheltered cuttings along a rail track or where there are fewer buildings in the captured image.

The next stage in development of the automatic code is to test the data in real time in the field over a high spatial scale, e.g. a Raspberry Pi device at each platform along a high leaf fall problem route or alternatively test the potential for the Raspberry Pi to work on a moving platform such as a train in order to obtain data on a regional scale along a rail track. This increase in data at a regional scale would allow a comparison with a regional observer rather than data collected in one station. The increase in regional scale observation was not possible with the time frame of the current research, however chapter six does look at the potential to operationalise this research further to make it an industry usable product.

Chapter Five Summary

This chapter has developed a Python-based automatic code in order to analyse vegetation change within a hemispherical image rather than the typical sky-view factor code which records the change in the amount of sky visible in an image over time. In order to test the viability of the automatic based Python code the images produced using the code were compared with manually analysed images by running both sets of images through the Lindberg and Holmer (2010) sky-view factor calculator. The sky-view factors produced using the automatic threshold images and the manual images correlate and indicate that the threshold images could be used as an alternative to manually analysed images. However, overestimation at the start of the season and underestimation at the end of the season can occur due to light glare in the images. This estimation error could be corrected by increasing the number of images taken per day to reduce light glare effects, capturing images in low light conditions or alternatively manually altering the code in post processing to remove the light glare. The sky-view factors produced using the automatic code and the Lindberg and Holmer (2010) code also correlate and indicate that the automatic code can produce sky-view factors similar to that of marketable software. Future research would co-locate the leaf fall device with Met Office trained observers as well as testing the device across a larger spatial scale in order to validate the data with leaf fall observations and increase statistical validation to build on initial promising results.

Chapter Six

A blueprint for autumn monitoring systems

6.1 The Next Stages of the Raspberry Pi Monitoring System

As shown in chapter one, leaf fall is just one component of the 'leaves on the line' issue. In order to improve current low adhesion forecasts, an integrated approach of different sensors on the rail network is required. Low adhesion (adhesion levels below 0.9) is caused by a mixture of contamination on the rail head and moisture (wet rail). Therefore, sensors that can show leaf fall change, amount of contamination, moisture on the rail head and current weather conditions in real time are needed. This increased level of sensors could also be used to increase understanding of low adhesion and the causes of low adhesion in the field which will help to develop low adhesion strategies in the future.

This combination of sensors would allow train operators a real time view of the track. As discussed in chapter one, a train driver is responsible for safe driving during autumn. Currently a train driver has access to a leaf fall and low adhesion forecast however they do not have access to instant data on the rail line they are using. Given the transient nature of low adhesion and that it is not always a visual contamination on the track causing a loss in adhesion (wet rail); an instant data platform would allow the driver to make more informed decisions on his driving technique at a high spatial scale.

This chapter looks at the possibility of operationally using the Raspberry Pi leaf fall sensor (or equivalent) more broadly on the rail network as part of a bigger autumn

resilience monitoring solution. This could include locating sensors in situ or onboard trains to contribute to the 'digital rail plan' and innovation around the rail network. Overall, the chapter explores the potential for a wider sensor network that monitors environmental conditions on and around the rail network specifically for the monitoring of low adhesion.

6.2 In Situ Deployment of Leaf fall sensors

In order to monitor leaf fall at a high spatial scale, in-situ deployment of multiple leaf fall sensors would be required across the rail network. This could replace Met Office trained leaf fall observers who currently monitor leaf fall on a regional scale (*Met Office, 2018*) and act as an alternative leaf observation input for other leaf fall forecast providers. A Raspberry Pi leaf fall recording device could be placed at each station along the rail network; recording a range of tree species in the area such as Oak, Ash and Birch. Due to the low cost of building the Raspberry Pi leaf fall sensor coupled with the low running cost of the device (cost of accessing station Wi-Fi), it is possible to deploy a large network of Raspberry Pis'. The network of devices could be placed at each station, however given that currently there are 2570 stations in the UK (*National Rail, 2018*) the devices could alternatively be set at intervals along the track depending on the composition of vegetation in the area. If a station area along the network only has Oak trees surrounding the rail track, then one Raspberry Pi would be sufficient for that location. The amount of Raspberry Pi's could also vary depending on the individual rail line request. If a specified rail line between two stations has a high number of low

adhesion events in an autumn season the number of Raspberry Pi's in that area could increase in frequency.

6.3 Mobile Monitoring

As part of the 'Capability Delivery Plan' (RSSB, 2017) as well as the 'Digital Railway Plan' (Network Rail, 2017), the rail industry is aiming to move to a more advanced 'smart' train system in which data could be collected onboard a train in real time, increasing the amount of data collected on the rail network as well as reducing the need for trackside monitoring. Network Rail aims to increase sensors on trains rather than trackside monitoring implementing a digital railway structure as the normal industry practice by 2027 (Network Rail, 2017a) and therefore when designing new technology, the drive for onboard monitoring must be considered. Specifically, the reduction of trackside monitoring would improve safety and cost across the rail network (Network Rail, 2017a); for example, by removing the need for trained employees to deploy sensors close to the rail track. In placing the leaf fall sensor on a train this would reduce the need for trackside maintenance of equipment and thus reduce cost for the rail industry. The use of sensors on trains would also increase the spatial data collected over a set time period as a Raspberry Pi leaf fall device could capture the change in leaf fall across a train route in real time rather than extrapolating from a single location.

In addition to onboard monitoring, the use of in-situ measurements is still important along the rail network in terms of leaf fall observation. During autumn, sheltered cuttings and problem sites which often have a large area of overhanging trees will

benefit from a constant leaf fall observation in the area which can automatically show when large leaf falls occur. This would allow high resolution monitoring at problem sites without any obstruction due to over-head wires or bridges which could be captured onboard a moving train and allow a more accurate forecast in areas prone to low-adhesion issues. In-situ measurements can also be used in a post season review and act as validation for the moving train observations. Therefore, when designing a low adhesion and leaf fall monitoring network a combination of onboard sensors and in-situ measurements would be the preferred approach.

When building a device to be placed onboard a train both the regulations, as well as the current technology needed for the device to run, needs to be evaluated. The Rail Industry Standard RIS-0700-CCS regulates the internet and Wi-Fi availability on a train and suggests that new internet sensors may connect to onboard Wi-Fi systems making them more efficient in the future (*RSSB, 2014*). The UK Association of Train Operating Companies compiled a list of regulations and information regarding new equipment, which state that sensors on the roof of trains must be accessible and secured before going on an operational fleet. As there is already a precedent for new sensor technology to go on the roof of a train (*BSI, 2017*), low-cost sensor devices for leaf-fall monitoring, could feasibility be attached to a train once it has met safety standards.

This research designed an adapted Raspberry Pi (chapters 3 and 4) that could record leaf fall in real time and was comparable to current leaf fall observation techniques used by the Met Office. Although this device was initially designed for use in-situ at locations across the rail network, there is potential for the device to be further adapted

for onboard mounting thus providing a real-time track vegetation survey and a leaf fall prediction tool.

6.4 Safety Requirements of New Equipment on the UK rail network

With the knowledge that the increased availability of Wi-Fi on trains will make small sensor networks more plausible, the regulations on adding equipment onto trains needs to be further explored. Table 6.1 shows the main safety standards required before new equipment is attached to a train. An adapted Raspberry Pi has the potential to meet all of the safety standards once testing and adaption is performed.

Table 6.1 - British Standards for new equipment on the rail network.

Regulation	Description
BS EN50155:2007: Railway applications. Electronic equipment used on rolling stock – Updated to IEC 60571:2012	This is an electrical equipment standard stating that new equipment must be self-contained of specified size and height and not affect the train or be affected by the train. It states that new equipment must be able to endure temperatures between -40° and +85° and with approved ventilation. This regulation further states that the lifetime of any new equipment must be 20 years unless

	agreed otherwise with an easily maintained accessibility point.
BS EN50121-3-2:2006: Railway applications. Electromagnetic compatibility. Rolling stock. Apparatus	This regulation stipulates the amount of noise a new piece of equipment can make prior to being placed onto a train. This is to avoid interference radio communications such as hand-held radio transmitters.
BS EN61373:2010: Railway applications. Rolling stock equipment. Shock and vibration tests	To prove the viability of a new device, shock and vibration tests are needed, this will ensure that the equipment can be operational in the environment on top of a train.
BS EN45545-2:201: Railway applications. Fire protection on railway vehicles. Requirements for fire behaviour of materials and components	A fire safety test must be carried out on the container of new equipment and each individual part of the equipment to ensure that it is not flammable in standard conditions.

6.5 Benefits and Challenges of using a Raspberry Pi Leaf Fall Sensor

Due to funding and time constraints of this research, the safety testing listed in Table 6.1 was not able to be conducted. Therefore, for initial testing the Raspberry Pi was placed inside a train cab. In order for the Raspberry Pi device to stay in one position throughout testing the device was attached to the cab with tape and positioned with the camera facing the windscreen. The position of the camera was placed closest to the windscreen in order to avoid any potential obstructions, such as the driver, in the hemispherical image. The position of the Raspberry Pi device inside the train cab and how it was secured to the train is shown in Figure 6.1b and Figure 6.1c.

The adapted Raspberry Pi encased in a waterproof box (Figure 6.1b) was initially tested at speeds of 60 mph inside a car in order to demonstrate that the Raspberry Pi could capture clear images at high speeds. This is due to the nature of the Raspberry Pi NoIR camera, which takes a 5 second video and retains the last image frame in the video as its camera photo. This reduces any blurring which would have occurred when using a digital camera (*Raspberry Pi, 2018; Hata, 2003; Turner et al. 2001*). However, in order to make the Raspberry Pi sensor usable on a moving train other factors that could affect the quality of the data needed to be explored including; motion blur, spatial referencing, and position on the train itself.

6.5.1 The Effect of Motion Blur using a Raspberry Pi Device

One of the benefits of adapting a Raspberry Pi camera module over a digital camera is the reduction of motion blur. Motion blur occurs when an object is moving during the camera's exposure time in capturing a scene; for example, a car moving at high speed whilst taking a photo could look like a blur on the final photograph. The camera could also be moved during image capture which causes a blurry out of focus image to be produced (*Tiwari et al., 2013; Ji and Liu 2008*). The amount of blur produced depends on the speed and distance travelled by an object within the time of the camera capturing the image and the light conditions of the surrounding environment (*Sorel and Flusser 2008; Tico et al., 2006; Lee, 1990*).

Therefore, when designing a leaf fall sensor that would remain stationary over a fixed time period, motion blur was not originally considered. However, when designing a camera-based sensor to go onboard a moving train motion blur became a consideration. A digital fisheye camera would need corrective restoration of an image in order to remove the image blurs (*Tai et al., 2010; Sorel and Flusser 2008; Cho et al., 2007*). There are several ways to retrospectively restore an image, however it requires multiple images of the exact same environment. When onboard a train it would be difficult to capture the exact location with the same light conditions twice and therefore not plausible to correct a digital camera onboard a moving platform at this time.

The Raspberry Pi camera does not capture an image in the same way as a digital camera. Instead, the Pi camera records a video at 90 frames per second (*Raspberry Pi, 2014*) and saves the last frame of the video recording as a still image, hence the need to post process the Raspberry Pi image for motion blur is not required, irrespective of speed (*Raspberry Pi, 2018*). This rationale could also be applied to post analysing video data captured with a Raspberry Pi camera to look at a portion of a track over a set distance. The Raspberry Pi can be programmed to capture a set time of video, for example 5 minutes, and store the video instead of capturing a single image. Whilst this is not required for capturing images at 125 mph on a train it could be used in future research to look at longer sections of rail line.

6.5.2 Spatial Referencing and GPS Data Constraints

Spatial referencing is needed if the leaf fall sensor is to track leaf fall along various stages of a rail line. Spatial referencing gives the image a designated location which can be plotted in georeferencing software such as Arc Map (*Minami et al., 2000*). It allows the data to be compared to the same areas over time and allows the collected data to be compared to the vegetation surveys along the rail track in a given location (*Network Rail, 2017*).

The Raspberry Pi can be fitted with a GPS device (*Shinde and Mane, 2015; Prabha et al., 2014*) which will record the location of the Pi at set intervals along the rail journey. A GPS device can identify an objects location using GPS satellites, the GPS can triangulate a co-ordinate by sending and receiving signals from 3 or more satellites. Different GPS devices have different accuracy levels based on the detection ability of

the device to satellite data. Table 6.2 shows the types of GPS devices that are Raspberry Pi compatible which continue to keep the leaf fall sensor a low-cost product.

Table 6.2 – GPS devices that can be connected to the Raspberry Pi device to produce GPS data for each captured hemispherical image

GPS device compatible with Raspberry Pi devices	Cost
Raspberry Pi+ GPS expansion board (Uputronics, 2018)	£35.99
GlobalSat BU-353-S4 GPS (GlobalSat 2011; Amazon 2018)	£30.99
LoRa GPS HAT for Raspberry Pi (Dragino, 2018)	£32.65

During initial testing, the GPS recordings were time stamped and then matched with the time stamps allocated to the individual images captured along the rail route. This time stamp was based on the Raspberry Pi internal clock system. The time from the Raspberry Pi is calculated using the time provided by the internet rather than an internal clock. This ability to receive the time via an online clock system is more accurate as internal clocks may slow over time and result in a less accurate time stamp. However, this technique would need to be improved when recording leaf fall onboard a train on a daily basis. Whilst a low-cost device can record the GPS on the Raspberry Pi (Table 6.2) the difficulty would be capturing the exact same location each day along a rail track.

GPS devices need to connect to satellites in order to triangulate coordinate data and give an accurate reading of location. Research conducted by Sigrist, et al., (1999) showed that the tracking system can be affected by leaf canopies and therefore have a reduced precision accuracy. Whilst stationary locations may not require the use of GPS tracking built into the Pi, it is imperative to an onboard monitoring system. Whilst it is unlikely that no sky will be visible when capturing images from the top of a train cab there may be moments of reduced location recording efficiency. Whilst initial GPS tracking showed an accurate monitoring location along the UK rail route from London to Birmingham (Figure 6.1d) further research is needed into the efficiency of GPS data loggers on the roof of the train rather than inside the train cab.

Despite the potential for leaf canopies reducing the precision accuracy of GPS data, research has shown how the improvements of low-cost GPS technology has increased the overall accuracy of data loggers in a variety of weather conditions and locations making them comparable to high cost GPS equipment (*Forin-Wiart et al., 2015*). Further to this, the train itself records the locations and times of its journey internally, leading to a potential to calibrate the GPS logged data with the internal train tracking system. This would allow a more precise location to be allocated to each hemispherical captured image.

Further issues with capturing the exact location on a daily basis would be the time of day in which the image could be recorded. Trains can often be delayed and therefore matching a location with a time stamp would not be a viable option when designing a

code to match co-ordinates with images. One approach could potentially only capture images once the GPS records a certain area: for example, 2 miles outside of each station along a rail route. However, the lag time between the GPS recording a location and the Raspberry Pi capturing the location could alter based on computer speed. In order for the onboard monitoring system to be used, calibrations would be needed at each problem area or site that is being captured by the moving train and therefore an in-situ camera network is needed. Given the relatively low cost of each sensor, this combination of in-situ and onboard monitoring would be a feasible option.

6.5.3 Mounting and Video Liability

When recording video or capturing images along a rail track the positioning of the camera is extremely important. Due to regulations on recording train drivers in the cab environment, a camera placed inside the train must be facing outwards or not be able to capture the inside of the cab. This can then guarantee the privacy of the train driver. Currently, a forward-facing CCTV camera records outwards facing video from inside the cab for vegetation surveys and train surveillance (*Jenkins and Harvey, 2015; RSSB, 2010; Goddard, 2006*).

The cameras used inside the train cab are not fisheye lenses and therefore do not capture the inside of the train. The Raspberry Pi camera however, consisting of a fisheye lens, has the potential to capture the inside of the cab. As well as driver privacy issues, placing a Raspberry Pi inside the train can lead to objects distorting the hemispherical image such as windscreen wipers and glare from the train windscreen. Forward-facing CCTV must be placed in the cab in a position where it is not distorted

by windscreen wipers however this would be less plausible for the Raspberry Pi due to the fisheye lens capturing a hemispherical image (RSSB, 2010). In order to successfully capture the change in leaf fall along the rail track, minimal distortion is needed and therefore the placement of the sensor on top of the train would be the best option. This would allow a hemispherical image to be captured outside with the least internal impacts on the captured data.

Ultimately, a bespoke bracket would need to be made to fix the Raspberry Pi on top of a train. The bracket would have to be easily removed in order to access the Raspberry Pi for image processing and not interfere with any other equipment or sensors already placed on or around the train; RSSB recommended that the Raspberry Pi could be placed in the existing lamp bracket onboard older trains.

6.6 Initial testing of the Raspberry Pi device onboard a moving train result

Due to the safety and testing regulations (Table 6.1), the Raspberry Pi (Figure 6.1a) at this time was not placed on top of a moving train. Instead, the Raspberry Pi was placed inside a Virgin Voyager train cab (Figure 6.1b) running from London Euston to Birmingham New Street (reaching speeds of 120 mph) in the Spring of 2017 (Figure 6.1c, Figure 6.1d). A GPS device was attached to the Raspberry Pi box which recorded the location of the train along the route at specific time intervals. This GPS data could then be matched with the timestamped hemispherical images produced by the Raspberry Pi. If the Raspberry Pi was to be placed on the outside of a train cab, for

example attached by a bracket to the lamp area on top of a train roof, the integrated GPS system discussed in section 6.5.2 would be needed.

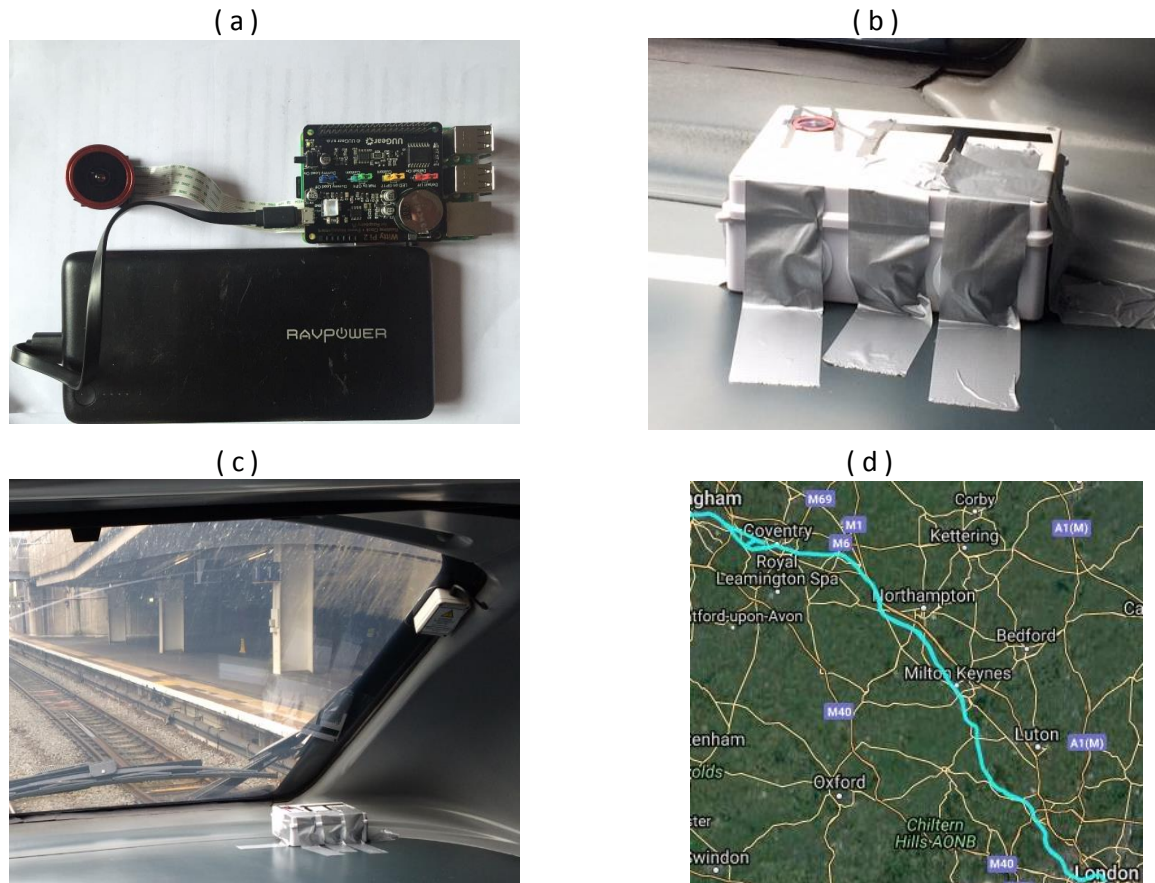


Figure 6.1 (a) - Adapted Raspberry Pi (b) Raspberry Pi within a train cab (c) Close up Raspberry Pi within the train cab (d) Route of the Train from London Euston to Birmingham New Street.

Due to the time of year that the data was collected and the lack of vegetation, the hemispherical images were analysed in the same way as chapters three and four, using a 'sky-view factor calculator' (*Lindberg and Holmer, 2010*) for each image along the rail line (Figure 6.2). The results showed clear distinctions in the images; bridges, trees and line side signals were all shown to reduce the sky-view factors of the rail

route. However, for an instant data analysis to take place the new approach designed in chapter five would be used to calculate sky-view factors for larger data sets in the autumn season. Figure 6.3 shows the ability of the Raspberry Pi to capture at a high resolution (identify singular leaves) along the rail track signifying the protentional for a track-based platform to record autumn leaf fall.

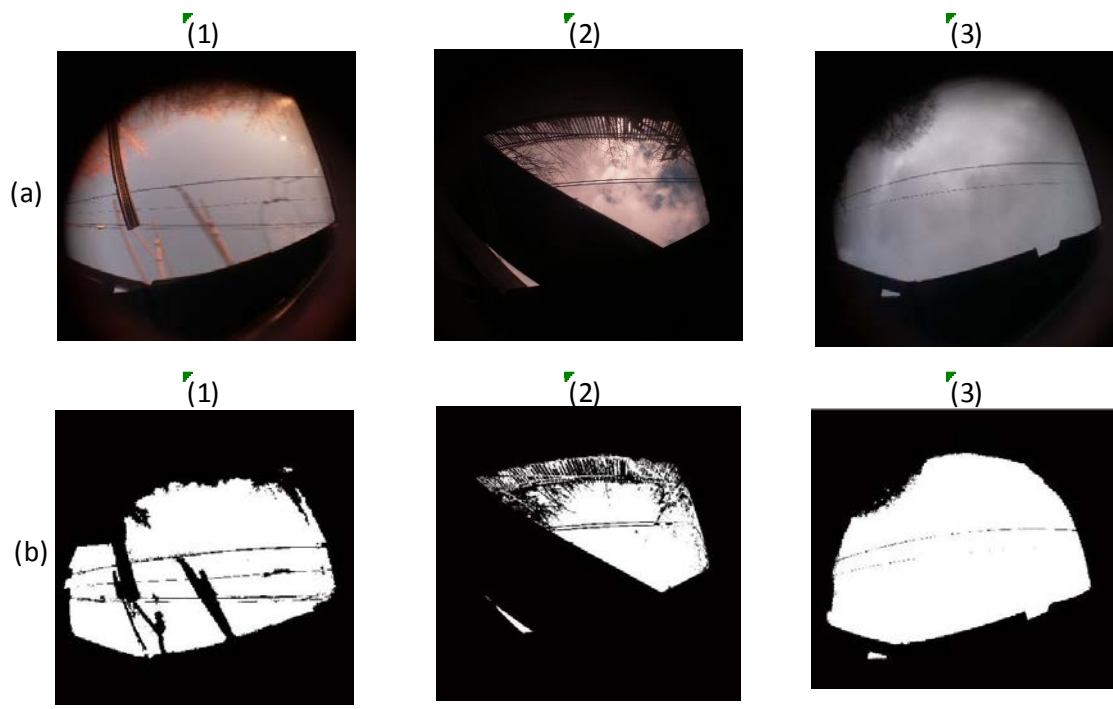


Figure 6.2- (a) Hemispherical images captured along the rail route, (b) Sky-View factor images captured along the rail route.

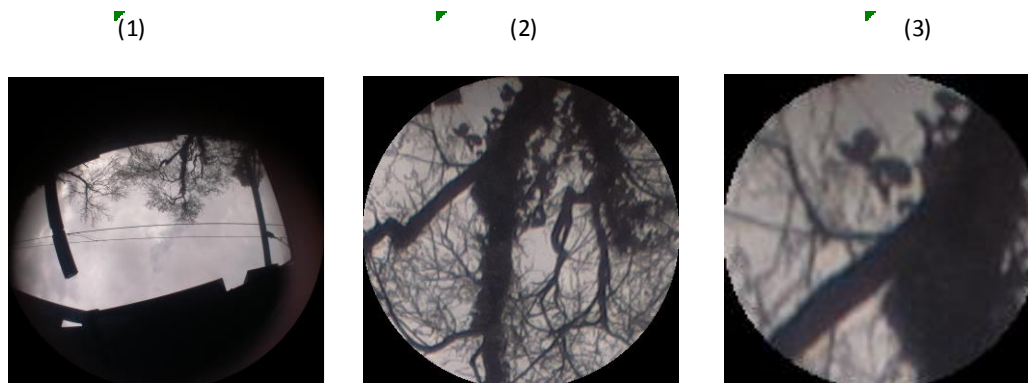


Figure 6.3 – (1) Hemispherical image captured along the rail route showing vegetation alongside the track (2) Zoomed in photo of the tree shown in image 1 (3) zoomed in photo of a leaf on the tree from image 1 and 2.

One of the limitations of this data collection came in the placement of the Raspberry Pi. Due to the main aim of this chapter being to assess the Raspberry Pi ability to capture images at 120 mph on a moving train, the placement of the Pi was inside the rail cab. This caused the least amount of disruption to the train and could easily be removed after the test was conducted. Therefore, unnecessary obstructions distorted some of the captured images such as windscreen wipers and window ledges. This problem would be removed with further testing on top of the train itself. Importantly the overall aim of the test was positive, and the Raspberry Pi camera has the potential to be a smart sensor capturing tree canopies onboard a train.

6.7 Current Low-cost Sensors on the UK Railway and the Viability of Low-cost Sensor Innovation.

Currently, UK trains are equipped with communication devices that can connect to static Wi-Fi connectors along the rail track indicating that a Wi-Fi sensor such as the Raspberry Pi leaf fall device could be added to the rail network. Low Power Wide Area Networks (LPWANs) are controlled and maintained by the Network Rail Telecoms organisation. This Wi-Fi integrated system relayed information to a central control platform from various sensors monitoring the condition of the rail network, for example track condition monitoring sensors (*Hodge et al., 2015*). Originally Network Rail Telecoms built a Fixed Telecom Network (FTN) to maintain communication along the rail route consisting of radio and mobile communications as well as a CCTV network. FTN consisted of a country-wide fibre network system along all of the main and secondary rail routes, this allowed high speed connectivity from mobile communications. However, with the move to a “digital railway” and the need to facilitate the transfer of data on an IP (internet protocol) system, a new communication structure was needed. FTNx (updated FTN which allows internet wireless connection of sensors) was laid alongside the original FTN network in 2013 (*Network Rail, 2018; Digital Rail, 2018; Kessel, 2015*). This allows a quicker data transfer and allows the ‘internet of trains’ to be explored with the ability to facilitate new Wi-Fi enabled digital sensors to be placed across the rail network.

The ‘Digital Rail Plan’ utilises the new FTNx network and works on a series of short, medium and long-term approaches to innovate the railways. The main aim of the

strategic plan is to increase onboard smart sensors to improve efficiency and reduce cost across the rail network. Currently, as part of this plan, European Train Control Systems (ETCS), sensors that allow trains to run closer together by monitoring location of trains along a track, are being tested on the Cambria line. Further to this 'Traffic Management Deployments', 'internet connected assimilation with crew' and DARWIN (real time data feed of timetables, cancellations and delays from all TOCs uploaded to the cloud and available as real time information) technology, is being tested on the Great Western route (*Digital Rail, 2018; Network Rail, 2018; National Rail, 2017*).

GSM-R (Global System for Mobile communication on Railways) was originally implemented to maintain the safety of the rail network through communication of drivers, operators, train support and passengers. However, the railways are moving toward a wireless network system that not only allows communication to occur but could also be harnessed to implement smart sensors across the rail network (*Fraga-Lamas et al., 2017*). This wireless technology and increased data transmittance is also part of RSSB's Innovation strategy and capability delivery plan. The innovation strategy consists of 12 categories including; 'intelligent trains', 'more value for data' and 'accelerated research', 'development and technology deployment' (RSSB, 2017).

Once initial testing has been undertaken on smart railway techniques, decisions can be made to further implement and improve the technology with the aim to make smart railways the business as usual approach by 2027. In the medium term (2019 – 2027) innovation business cases are available to continue to test and deploy smart railway applications, with a £450 million National Productivity Investment fund supported by

both government-run rail organisations and TOCs (*Digital Railways, 2018*). This increased interest in railway connectivity improvement and the move to internet integrated systems shows the potential for new sensors to be added to the network. The increase in small 'Internet of Things' devices has expanded in other areas of research and the move towards the 'Internet of Trains' seems the next logical stage for UK rail (*Fraga-Lamas et al., 2017*).

6.8 Combination of Autumn Sensors and Sensor Innovation on the UK Railways

Despite the ability to connect to a digital railway, there is a large variation in innovation and sensor technology types being considered and already implemented on and for the railways (*Hodge et al., 2015; RSSB, 2016*). An overview of the required autumn sensors in the rail industry and how they have been innovated is needed in order to explore why we need sensors and the variation in sensor types being used, including temperature sensors and moisture sensors.

A multi sensors approach is needed in order to reduce the cost of autumn rail delays on the UK network. This research has shown how the recording of leaf fall can be improved with an updated sensor however the inputs into the low adhesion forecast also include; moisture on the rail track and the accumulation of leaves (contamination) in an area as a proxy for the contamination of leaves on the actual rail line. Both of these parameters have the potential in future research to be improved by low-cost sensors and thus improve the overall leaf fall and low adhesion forecast.

6.8.1 Moisture Sensors

Drizzle and low levels of moisture, such as morning dew, increases low adhesion when present on the rail track. The phenomenon known as 'wet rail syndrome' can reduce traction on the rail head causing a loss in adhesion without the presence of any other contamination such as leaves (*White et al., 2018; Lewis et al., 2011; Lewis et al., 2009; Beagley, 1976*). Further to this, low adhesion increases when leaf fall mixes with small amounts of water which causes the leaves to form a gel-like substance. This gel reduces the traction between the wheel and rail causing severe problems for the rail network (*Chen et al., 2018; Wang et al., 2013; Gallardo-Hernandez and Lewis, 2008; Olofsson, 2007*). The need to detect instant low levels of moisture directly on the rail head is therefore needed rather than relying on the forecasted weather.

Chapman et al., (2016) conducted a feasibility study on the implementation of low-cost moisture sensors that could connect to the internet to relay moisture levels on the rail head in real time. Currently, a small number of leaf wet sensors, moisture sensors that detect water on a conductor through the change in electrical resistance, are available around the London central line but not the UK railway network (*Davis and Hughes, 1970*). This is potentially due to cost and the lack of ability to require the moisture data in real time. Chapman (2016) developed a low-cost alternative to current moisture sensors using a sensor head, originally designed to detect moisture in areas sensitive to water such as a computer server room, and a data logger with inbuilt Wi-Fi to instantly transmit recorded data. Whilst this low-cost sensor has been invented it is not yet widely used. In order to get an integrated data set of factors involved in the creation

of low adhesion, a large-scale trial would be needed into low-cost moisture sensors around the UK rail network.

6.8.2 Temperature Sensors

Temperature sensors are needed across the rail network to monitor both cold and hot temperature ranges. During the summer if the temperature rises above a set threshold the track is at risk of buckling, whilst in the winter freezing temperature can lead to ice and frozen rail (*Hodge et al., 2015; Dobney et al., 2009; Chapman et. al, 2008, Thornes and Davis 2002*). Mitigation and rail delay decisions due to temperature is carried out on a forecasted basis. Weather services, such as the Met Office, provide forecasts to 'Open Rail' (*Met Office, 2018; Thornes and Davis, 2002*) allowing train operating companies to make decisions based on predicted outcomes.

Chapman et al. (2008) notes the difficulty of obtaining access to railways and the extensive safety testing of new equipment needed to meet safety standards. However, with the emergence of low-cost sensors and less invasive equipment, there is potential to increase the temperature sensor points along the railways to increase the available observation of rail temperature and thus improve current forecasts.

6.8.3 Contamination Sensors

Contamination from oil, leaves or oxides on the railhead is a cause of low adhesion. The reduced friction on the rail track causing adhesion between the rail and the wheel of the train to decrease leading to problems with the wheel to rail interface such as loss of traction (*Olofsson et al., 2014; Lewis et al., 2014; Zhu et al., 2014; Cann, 2006; Olofsson and Sundvall, 2004*). Currently when an incident of low adhesion occurs, such as a wheel slip, it is reported, and the condition of the track is assessed. The plans in place for removing the contamination such as leaf removal or rail head cleaning can then be applied (*Crawley et al., 2017; Li and Ren, 2012*). Forecasts aim to prewarn TOCs of poor contamination days based on set parameters such as percentage leaf fall prediction and forecasted weather conditions (*Met Office a, 2018; Crawley et al., 2017*). However direct contamination sensors could give real time measurements of current contamination at a high spatial and temporal resolution.

This measurement could be achieved using reflectance sensors which would allow different levels of contamination on the rail head to be recorded. The rail track with no contamination appears shiny and has good reflectance however with increased contamination the rail track becomes darker and duller with low reflectance (*Li and Ren, 2012; Rose and Cho, 2009; Kenderian et al., 2006; Zumpano and Meo, 2006*). Therefore, a low-cost reflectance sensor, such as a dew point mirror, could be used as a proxy for contamination, with the greater reflectance recorded the less contamination on the rail head (*Chapman et al., 2016*). However, it is important to note that not all areas of the rail head have the same level of reflectance as some areas of the rail may be contaminated with rust whereas the rail head, due to the cleaning from passing trains, will be highly reflective (*Chapman et al., 2008*). Therefore, a base test of the rail

network would need to be conducted before the leaf fall season, so the contaminated rail could be compared to the 'pre-autumn' contamination levels.

6.8.4 Weather Stations

The rail network in the UK receives weather forecasts from the Met Office and Met Desk which informs TOCs of potential weather issues such as high wind speeds leading to branches on the line (*Crawley et al., 2017*). However, unlike on the highways network, there are limited bespoke rail weather stations. During winter, Highways England implements 250 environmental sensor stations along the road network recording temperature and road conditions in real time. This real time measuring informs highway maintenance when to use the gritters (*Highways England, 2017*). Due to the micrometeorology of the UK rail network, the current weather predictions are not at the needed spatial or temporal resolution and an autumn rail environmental sensor station could be implemented for the autumn season like the road winter implementation.

A network of low-cost weather stations is needed to improve real time knowledge of current temperatures, wind speeds and rainfall (all of which are needed in a low adhesion forecast model). The weather stations of a small collection of sensors, like the road networks sensors and unlike the recommended location of a Met Office weather station (*Met Office, 2016*) these smaller stations could be attached to railway stations of signalling areas along the rail network. This would enable collecting and transferring up to date data in real time.

6.9 The Blueprint of the Autumn Rail Sensor Network

The overall aim of low adhesion forecasting improvements is to have a low-cost integrated network of sensors recording temperature, moisture, wind speed, contamination on the rail head and leaves remaining on the trees around the rail track (*Met Office, 2018*). Low level moisture increases the risk of low adhesion by causing wet rail syndrome and coupled with leaves on the track creates a gel reducing adhesion on the rail head. Therefore, accurate sensor data showing low level moisture (such as drizzle or dew) in real time would improve low adhesion model inputs on a spatial and temporal time scale (*RSSB, 2014; White et al., 2018*). Temperature is another key input in forecasting low-adhesion on the rail line however, the temperature on the rail head may be different to the ambient temperature. Therefore, a frozen rail head (which will cause low adhesion) may not be predicted based on ambient air measurements alone (*Met Office, 2018*). Real time data recording of rail head temperatures like that of the moisture sensor could improve data collection again on a spatial and temporal scale. A combination of onboard and static leaf fall recording devices would need to be deployed in an autumn sensor network. This would allow problem sites such as sheltered cuttings along the rail line to be monitoring constantly as well as calibrating the onboard recording system. The onboard leaf fall recording system could be used to collect leaf fall data and also be used to conduct vegetation surveys in real time along the rail route. The combined collection of sensors (Figure 6.4) will allow an increase in data points across the UK network in real time data and thus improve the current low adhesion forecast models.

Whilst this PhD focuses on the development of the leaf fall sensors it is important to see how it would fit into an 'Internet of Trains' and 'digital railway' of the future. As devices are getting cheaper, smaller and more efficient the possibility of an improved digital low-adhesion and leaf monitoring network is plausible and most importantly needed in order to improve the current 'leaves on the line' issue.

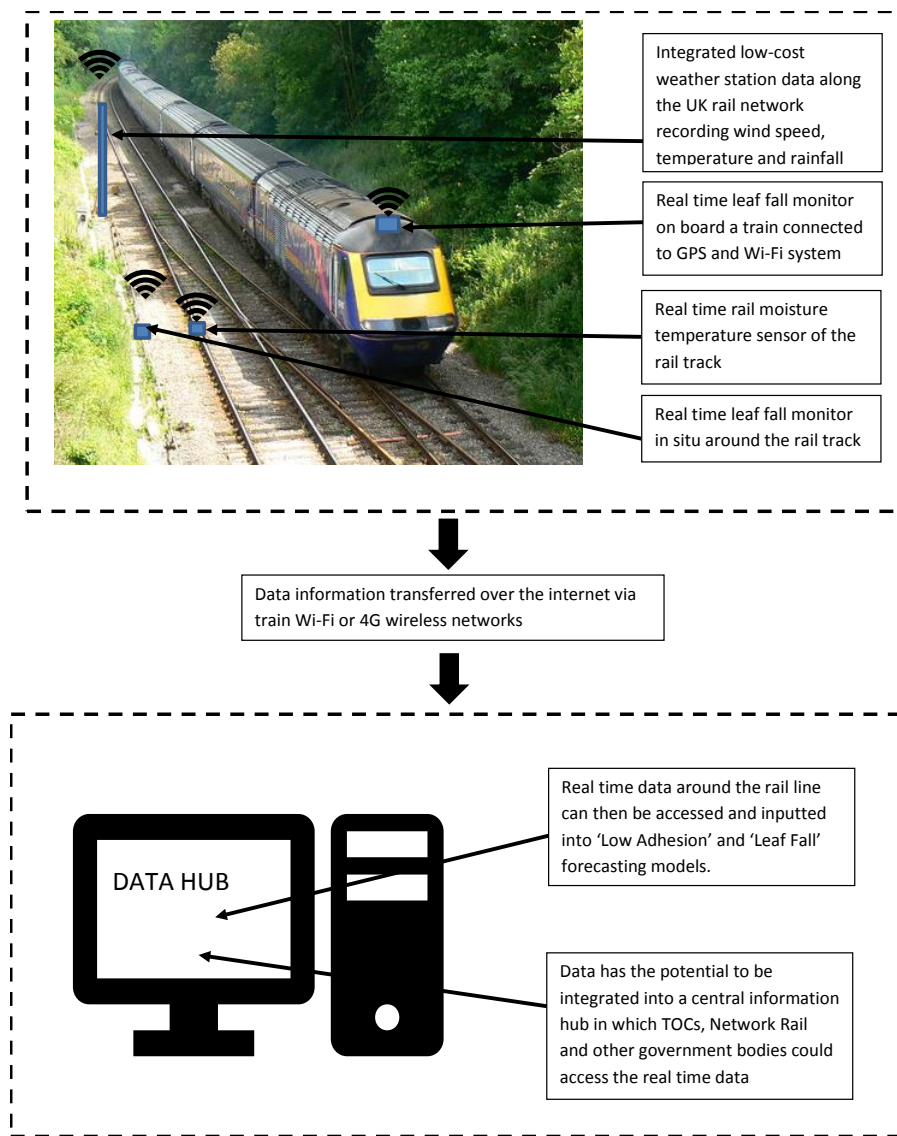


Figure 6.4 – Representation of an integrated data network consisting of weather stations, leaf fall monitors and moisture sensors.

It is clear from this research that hemispherical imagery can be used to calculate the variation in leaf fall across the rail network. The Raspberry Pi leaf fall device concept works well as a static device as shown in chapter four and has the potential to be adapted onto the train network. The idea behind adapting a device to capture hemispherical images could also be applied to other image capturing devices that already exists in train cabs and in rail research such as a 'GoPro' camera (*Gamon et al., 2015; Flammini et al., 2016; Rumpler et al., 2017*) or a CCTV device used to record track to comply with safety procedures. This adaptability could be explored in future research taking the prototype structure developed in this research and adapting it to alternative technology. This would allow the autumn leaf fall low-cost sensor network to be adapted to already existing infrastructure, potentially reducing the testing needed in adding a new device onto a train. Further research into adapting alternative devices is needed however the prototype Raspberry Pi leaf fall device opens up the possibility of alternative hemispherical image capturing devices that could be used to track change in leaf canopy over time.

6.10 Recommendations for Future Research

This research has designed, built (chapter three) and tested a leaf fall recording device in the field (chapter four) as well as its compatibility with current Met Office practices (chapter five). Further to this, chapter six has explored the potential of making this concept viable on an industry scale. Showing how low-cost sensors have previously been added to the rail network and conducted initial testing onboard a train from London to Birmingham. In order to advance the project further a series of recommendations have been made for future projects:

1. Regional in-situ scale testing – The Raspberry Pi leaf fall monitoring is cheap to make and robust in the field. In order for the next stage of testing to take place, a regional testing campaign is needed over two autumn seasons. This would take place on a regional scale, potentially placing a Raspberry Pi device at each station platform along a rail route. This research would involve a series of initial tests before autumn in order to ensure the correct thresholds for the Raspberry Pi code is set for each site and to evaluate the potential obstructions to vegetation at each site (chapter 5). This would allow data to be gathered on how leaf fall alters on a regional scale from the same tree species and then show how leaf fall alters along a rail track.
2. Continuous Vegetation train monitoring – This research has shown that a Raspberry Pi camera can capture images at high speed however due to the timing of the monitoring there was reduced vegetation in the images. Therefore, repeat train monitoring is needed. During this repeat monitoring it is recommended that the Raspberry Pi is mounted onto the top of the train rather

than in the train cab. Mounting the device on the top of the train is possible however due to funding constraints of the current project this was not possible at this time. This research would involve a series of safety tests such as extreme temperature and vibration testing in order for the device to comply with safety testing. Container design would also be required in order for the device to be successfully attached to the train roof.

3. An autumn field campaign of an in-situ combination of sensors is needed in order to record more aspects of low-adhesion on the railway. As low-cost moisture sensors and temperature sensors are readily available, this recommendation could be conducted during the same research time frame as the regional Raspberry Pi testing period and therefore the cost of deploying these extra sensors could be incorporated.
4. Further research is needed in order to make the combination sensors (section 6.7 and 6.8) train based. This would involve a series of safety tests as discussed in section 6.3. The testing for the combination sensors could be conducted at the same time as further Raspberry Pi based testing however, additional onboard testing would need to be conducted to determine the viability of recording the variables in the combination approach at high speeds.
5. Industry 'Forecast Model' evaluation – due to confidentiality procedures, access to a complete forecast model was not possible during this research. Therefore,

testing and validation of the Raspberry Pi leaf fall device was conducted using the Met Office model inputs and weather data. The research followed the principle that if the data produced from the leaf fall device is similar to the current best practice input used at the Met Office then the device is an alternative to leaf fall observers. However, it is recommended that further research should be conducted using industry forecast models by inputting the leaf fall results into a leaf fall forecast model and evaluating the output produced. Whilst it is expected that a similar input would produce a similar output from a leaf fall forecast model it would still be preferable that the captured data is tested.

6.11 Conclusion

This chapter has looked at the potential of adding a low-cost sensor to the UK railways in order to innovate autumn resilience. Rail industry safety testing showed that under this current research a full-scale train testing was not possible due to the need of safety rating of the Raspberry Pi at extreme temperatures and vibrations found on top of a train (*BSI, 2018*). In order to complete this testing further funding would be required and a new more robust IP rated container would need to be made. However, this research has shown the potential for a Raspberry Pi camera to be used onboard a moving train. Indicating that in the device could be used as an in-situ and a mobile means to collect leaf fall imagery at speeds up to 120mph. To improve the recording further, the Raspberry Pi would need to be attached to the roof of a train in order to reduce current distortion caused by windscreen wipers and the side of the train cab. Chapter 6 further explores ways to develop the current leaf fall device further and indicates that a low-cost sensor network is needed to collect instant data on the current

conditions of the rail line, such as; imaging solutions, moisture sensors and trackside monitoring stations.

Whilst this research is promising and shows the potential to increase data collection at the high spatial and temporal scale, in order to truly innovate the prediction of low adhesion on the UK rail network, an integrated approach is needed. The principal drivers of low adhesion such as moisture, rail contamination and leaf fall all need to be recorded. This chapter has looked at the potential to implement leaf fall sensors around the UK rail network. Automated data can be relayed in real time showing the change in leaf fall over time. However, in order to fully understand the leaves on the line issue, more sensors are needed in conjunction with the low-cost sensor developed in this PhD.

Chapter Six Summary

Low-cost sensors have been added to the UK rail network in a drive for a more innovative digital railway. To make a sensor a permanent fixture onboard a train, a series of rigorous safety testing is needed, including temperature and vibration testing. The leaf fall sensor Raspberry Pi device was placed inside a train cab and captured hemispherical images at set time intervals. The results of the study showed that the leaf fall sensor can capture images of the surrounding vegetation of a railway at speeds up to 120 mph. In order to geo-reference the data, a GPS device recorded the locations along the track. The Raspberry Pi clearly identified bridges, trees and line side signals as the train moved from London Euston to Birmingham New Street, however obstacles such as windscreen wipers obscured part of the image collection. This research is promising and shows the potential to increase data collection at the high spatial and temporal scale. However future research is recommended; regional testing of multiple Raspberry Pi devices are needed, safety testing in order for a Raspberry Pi device to be a permanent fixture onboard a train is required, a combined sensor approach could be tested in order to improve other inputs into a leaf fall and low adhesion forecast model, and ideally inputs from the new sensors would be integrated into an industry forecast model, such as the Met Office leaf fall forecast, in order to review the new products from data capture to outputted forecast.

Chapter Seven

Evaluation of the PhD and the original contribution to science

7.1 Aims and Objectives

This research has focused on developing a new approach to leaf fall monitoring on the rail network. The developed Raspberry Pi technology aims to improve leaf fall forecasting by increasing the temporal and spatial resolution beyond what is currently available from current leaf fall measurement techniques. This chapter will outline the four key objectives of this research and reinstates how those objectives were met. This chapter will also discuss the original contribution to science that this thesis has made.

7.1.1 Objective One: Investigate and develop a low-cost imaging approach to monitor vegetation

Chapter one of this thesis reviewed the current issues facing the UK rail industry, focusing on the problems associated with low adhesion and autumn rail delays. It was clear from this chapter that there was a research gap in terms of how vegetation is currently measured within the UK rail industry. A new low-cost device was needed to record vegetation at a high spatial and temporal resolution in order to improve current leaf fall forecasts and thus improve mitigation strategies implemented by the rail industry. Given the research gap defined in chapter one, there was a need to review the current ways in which leaf fall and vegetation is recorded across different scientific disciplines. Chapter two investigated both indirect and direct vegetation recording

devices and explored the possibility of using low-cost sensors in research. This chapter concluded that the best approach to recording vegetation along a rail track was an indirect hemispherical image approach that could utilise the advancement of smart technology and low-cost sensors emerging in the scientific discourse.

The development of the device was explored in chapter three by attempting to adapt a smartphone camera to capture images in the near-infrared. Using methods set out in Chapman's (2007) paper, a Nokia Lumon camera was successfully adapted to capture images in the near-infrared spectrum. However, the images captured using a converted mobile camera appeared blurred and out of focus; the equipment needed to enhance the image was too expensive to mass produce and would not allow the development of a low-cost sensor.

Chapter three further explored an alternative approach to the development of a low-cost sensor. A Raspberry Pi was adapted to take hemispherical images in the near-infrared spectrum. The device was then compared with the Nikon Coolpix camera (the most popular camera currently used to capture hemispherical images) to determine if the low-cost approach was a viable alternative to the current apparatus used in research. This thesis has shown that the Raspberry Pi is a viable alternative to digital photography and can be used to capture hemispherical leaf fall images.

7.1.2 Objective Two: Using a prototype device, test the utility of the approach in measuring daily leaf-fall over autumn

Whilst the Raspberry Pi was comparable to the Nikon Coolpix camera, further adaptations were needed to make it a viable device that could be used in the rail industry. Chapter four of this thesis tested the adapted Raspberry Pi approach for two autumn seasons. Data was collected in autumn 2016 and 2017; weather conditions such as heavy rain, snow and high winds did not affect the output of the Raspberry Pi device. Using sky-view factor software the percentage of leaf fall over time was able to be calculated on three tree species, Birch, Beech and Oak. In order to validate the percentage change captured on the Raspberry Pi, the data was compared with an independent Met Office observer and compared to daily weather data.

7.1.3 Objective Three: Demonstrate how the low-cost imaging approach can be scaled up in relation to current practices

Whilst using an already available sky-view factor calculator was adequate for testing the ability of the device to accurately capture leaf fall; further work was needed to make the device accessible for industry.

The device needed to capture the percentage change of leaf fall over autumn in real time. Chapter four showed that the device could capture an image in real time however the sky-view factors were calculated post season. Chapter five developed a leaf fall sky-view factor code that could automatically calculate the relative percentage vegetation left on a tree canopy and automatically send the percentage over the internet to a designated server. The percentage leaf-fall could automatically be inputted into a leaf-fall model in real time. The code was validated by comparing the output produced by the Raspberry Pi automatic threshold mechanism with manually processed images.

The fully automated in-situ low-cost device that captures and calculates leaf fall could be used to give higher spatial and temporal resolutions thus improving the leaf fall forecast inputs.

7.1.4 Objective Four: Produce a broader blueprint to integrate the work within the wider low adhesion research effort

Chapter Six researched the practicalities of putting new technology onto the rail network. An initial test indicated that the Raspberry Pi could be placed on top of a train to monitor the change in vegetation along a rail route. However, further research is needed to test the Raspberry Pi against current safety standards. Chapter six of this thesis also looked at the potential for future research and discussed a combined low-cost sensor approach in order to improve current leaf fall forecasts.

A low-cost leaf fall device is one of several low-cost sensors needed to improve the current leaf fall forecasts. This research has laid out a blueprint of a multi sensor network that could further improve leaf fall and low adhesion forecasting such as moisture and temperature sensors and suggests several areas of future research that could be conducted to continue to improve autumn data collection across the rail industry.

7.2 Original Contribution to Science

This PhD has made an original contribution to science in three key areas:

1. Developing a new low-cost portable hemispherical camera. Given that the existing camera used in hemispherical imagery, the Nikon Coolpix camera, can no longer be purchased, a viable alternative was needed. This research has developed an easily adaptable and buildable hemispherical Raspberry Pi camera that can be used for multi-disciplinary research. In particular its ability

to be left in the field for a long period of time would be beneficial for forestry research as well as the rail industry.

2. Investigated how leaf fall responds to different weather conditions. Chapter Four of this thesis tested the Raspberry Pi's device over autumn and showed how leaf fall can be affected by various weather conditions. For example, the Raspberry Pi captured the large fall in leaves that occurred after a period of snow in autumn 2017. Further contributions to knowledge could be made using this device by investigating autumnal weather patterns on vegetation over a longer time period. There is also the potential to look at the effects of weather on bud burst and other vegetation effects using this novel recording method.
3. Developing a new prototype leaf fall percentage leaf fall code. This research has improved on previous threshold using code when calculating sky-view factors in the near-infra red spectrum. The prototype code in this research uses a threshold range to capture colours in the red and purple spectrum rather than the previous technique of using one threshold value.

7.3 Conclusion

This research was principally funded by RSSB and the EPSRC in order to develop a new method for recoding leaf fall along the rail network. A novel way of automatically recoding leaf fall was needed in order to improve the temporal and spatial resolutions of current leaf fall capturing methods and thus improve current leaf fall forecasting models. The Raspberry Pi automatic leaf fall device can capture hemispherical images and automatically process them to show the change in leaf fall of a tree canopy from full tree to bare canopy. This research has designed, developed and tested the prototype device throughout two autumn seasons on a range of tree species.

The research further explores the potential for the leaf fall device to be implemented around the UK rail network. Given the Raspberry Pi's ability to be left in the field and send its data over the internet this low-cost device could be placed along every station in the rail network or at designated leaf fall hot spots and low adhesion rail sites.

This research has explored the problems associated with low adhesion on the rail line and given that leaf fall is only one component of the low adhesion issue, sets out a framework for future research and development.

References

- Abaya, W.F., Basa, J., Sy, M., Abad, A.C. and Dadios, E.P.**, 2014: Low cost smart security camera with night vision capability using Raspberry Pi and OpenCV. In *2014 International conference on humanoid, nanotechnology, information technology, communication and control, environment and management (HNICEM)* (pp. 1-6). IEEE.
- Aboelela, E., Edberg, W., Papakonstantinou, C. and Vokkarane, V.**, 2006: Wireless sensor network based model for secure railway operations. In *Performance, Computing, and Communications Conference, 2006. IPCCC 2006. 25th IEEE International* (pp. 6-pp). IEEE.
- Adhesion Working Group** 2018: Adhesion Working Group: Measuring Low Adhesion Manual <https://www.raildeliverygroup.com/component/arkhive/?task=file.download&id=469773735>
Accessed 2018
- Alemi, A., Corman, F. and Lodewijks, G.**, 2017: Condition monitoring approaches for the detection of railway wheel defects. *Proceedings of the Institution of Mechanical Engineers, Part F: Journal of Rail and Rapid Transit*, 231(8), pp.961-981.
- Amazon** 2018: GlobalSat BU-353-S4 USB GPS Receiver, <https://www.amazon.co.uk/GlobalSat-BU-353-S4-Receiver-SiRF-Black/dp/B008200LHW> accessed 2018
- Anderson, M.C.** 1964: Studies of Woodland light climate. *Journal of Ecology* 52, 27-41
- Arias-Cuevas, O.** 2010: Low adhesion in the wheel-rail contact. TU Delft, Delft University of Technology.
- Ashton, P.M.S., Olander, L.P., Berlyn, G.P., Thadani, R. and Cameron, I.R.**, 1998: Changes in leaf structure in relation to crown position and tree size of *Betula papyrifera* within fire-origin stands of interior cedar-hemlock. *Canadian Journal of Botany*, 76(7), pp.1180-1187.
- ATOC** 2000: Approved Code of Practice Train Driving – Basic Training, Assessment and Post Qualifying Monitoring <https://www.rssb.co.uk/rqs/oodocs/ATOCACOP003%20Iss%201.pdf>
[Accessed 2019](#)
- ATOC** 2016: ATOC Guidance Note Investigation of Station Stopping Incidents, <https://www.rssb.co.uk/rqs/oodocs/ATOCGN009%20Iss%203.pdf> [Accessed 2019](#)
- Atzori, L., Iera, A., & Morabito, G.** 2010: The internet of things: A survey. *Computer networks*, 54(15), 2787-2805.
- Azzoug, A. and Kaewunruen, S.**, 2017: RideComfort: a development of crowdsourcing smartphones in measuring train ride quality. *Frontiers in Built Environment*, 3, p.3.
- Baret, F. and Agroparc, S.** 2004: A simple method to calibrate hemispherical photographs. INRA-CSE, France (http://147.100.66.194/can_eye/hemis_calib3.pdf).

- Barke, D. and Chiu, W.K.**, 2005: Structural health monitoring in the railway industry: a review. *Structural Health Monitoring*, 4(1), pp.81-93.
- Barrientos, R., Ascensão, F., Beja, P., Pereira, H. and Borda-de-Água, L.**, 2018. Railway impacts on wildlife and flora: lessons for the 21st Century. *Frontiers in Ecology and Evolution*, 6, p.188.
- Bärring, L., Mattsson, J.O. and Lindqvist, S.**, 1985. Canyon geometry, street temperatures and urban heat island in Malmö, Sweden. *International Journal of Climatology*, 5(4), pp.433-444.
- Bartelink, H. H.** 1997: Allometric relationships for biomass and leaf area of beech (*Fagus sylvatica* L). In *Annales des Sciences Forestieres* (Vol. 54, No. 1, pp. 39-50). EDP Sciences.
- Basu, D., Purviance, J., Maczka, D., Brogan, D.S. and Lohani, V.K.**, 2015: Work-in-progress: high-frequency environmental monitoring using a Raspberry Pi-based system. In *122nd ASEE Annual Conference and Exposition, Seattle, WA, USA*.
- Beagley, T.M.**, 1976: The rheological properties of solid rail contaminants and their effect on wheel/rail adhesion. *Proceedings of the Institution of Mechanical Engineers*, 190(1), pp.419-428.
- Bedogni, L., Di Felice, M. and Bononi, L.** 2012: By train or by car? Detecting the user's motion type through smartphone sensors data. In *Wireless days (wd), 2012 IFIP*(pp. 1-6). IEEE.
- Behera, S. K., Srivastava, P., Pathre, U. V., & Tuli, R.** 2010: An indirect method of estimating leaf area index in *Jatropha curcas* L. using LAI-2000 Plant Canopy Analyzer. *Agricultural and Forest Meteorology*, 150(2), 307-311
- Berlin, E. and Van Laerhoven, K.**, 2013: Sensor networks for railway monitoring: Detecting trains from their distributed vibration footprints. In *Distributed Computing in Sensor Systems (DCOSS), 2013 IEEE International Conference on*(pp. 80-87). IEEE.
- Bernard, J., Bocher, E., Petit, G. and Palominos, S.**, 2018: Sky View Factor Calculation in Urban Context: Computational Performance and Accuracy Analysis of Two Open and Free GIS Tools. *Climate*, 6(3), p.60.
- Beugin, J. and Marais, J.**, 2012: Simulation-based evaluation of dependability and safety properties of satellite technologies for railway localization. *Transportation Research Part C: Emerging Technologies*, 22, pp.42-57.
- Blankenstein, S. and Kuttler, W.**, 2004. Impact of street geometry on downward longwave radiation and air temperature in an urban environment. *Meteorologische Zeitschrift*, 13(5), pp.373-379.
- Blennow, K.**, 1995. Sky view factors from high-resolution scanned fish-eye lens photographic negatives. *Journal of Atmospheric and Oceanic Technology*, 12(6), pp.1357-1362.
- Bogaert, J., Zhou, L., Tucker, C. J., Myneni, R. B., and Ceulemans, R.** 2002: Evidence for a persistent and extensive greening trend in Eurasia inferred from satellite vegetation index data. *Journal of Geophysical Research: Atmospheres*, 107(D11).
- Borda-de-Água, L., Barrientos, R., Beja, P. and Pereira, H.M.**, 2017. Railway ecology. In *Railway Ecology* (pp. 3-9). Springer, Cham.

- Bréda, N. J.** 2003: Ground-based measurements of leaf area index: a review of methods, instruments and current controversies. *Journal of experimental botany*, 54(392), 2403-2417.
- British Standards Institute** 2018: BS EN45545-2:2015, The British Standards Institution, London
- British Standards Institute** 2018: BS EN50121-3-2:2006, The British Standards Institution, London
- British Standards Institute** 2018: BS EN50155:2007, The British Standards Institution, London
- British Standards Institute** 2018: BS EN61373:2010, The British Standards Institution, London
- Brown, M. E., Pinzón, J. E., Didan, K., Morisette, J. T., & Tucker, C. J.** 2006: Evaluation of the consistency of long-term NDVI time series derived from AVHRR, SPOT-vegetation, SeaWiFS, MODIS, and Landsat ETM+ sensors. *IEEE Transactions on Geoscience and Remote Sensing*, 44(7), 1787-1793.
- Brown, M.J., Grimmond, S. and Ratti, C.,** 2001. *Comparison of methodologies for computing sky view factor in urban environments* (No. LA-UR-01-4107). Los Alamos National Lab., NM (US).
- Bruschi, P.,** 2010: Geographical variation in morphology of *Quercus petraea* (Matt.) Liebl. as related to drought stress. *Plant Biosystems*, 144(2), pp.298-307.
- Buckley-Johnstone, L.E., Trummer, G., Voltr, P., Meierhofer, A., Six, K., Fletcher, D.I. and Lewis, R.,** 2019. Assessing the impact of small amounts of water and iron oxides on adhesion in the wheel/rail interface using High Pressure Torsion testing. *Tribology International*, 135, pp.55-64.
- Butcher, G.,** 2019: NASA Reflected Near-Infrared Waves, https://science.nasa.gov/ems/08_nearinfraredwaves Accessed 2019
- Cann, P. M.** 2006: The “leaves on the line” problem—a study of leaf residue film formation and lubricity under laboratory test conditions. *Tribology letters*, 24(2), 151-158.
- Carns, J.,** 2019: NASA Reflected Near-Infrared Waves, https://science.nasa.gov/ems/08_nearinfraredwaves Accessed 2019
- Chambers, J. Q., dos Santos, J., Ribeiro, R. J., & Higuchi, N.** 2001: Tree damage, allometric relationships, and above-ground net primary production in central Amazon forest. *Forest Ecology and Management*, 152(1), 73-84.
- Chapman, L.** 2007: Potential applications of near-infrared hemispherical imagery in forest environments. *Journal of Agricultural and Forest Meteorology*, 143(1), 151-156.
- Chapman, L.** 2008: An introduction to upside-down remote sensing, *Progress in Physical Geography* 32 (5), 529-542
- Chapman, L., and Thornes, J. E.** 2004: Real-time Sky-View factor calculation and approximation. *Journal of Atmospheric and Oceanic Technology*, 21(5), 730-741.
- Chapman, L., Thornes, J. E. and Bradley, A. V.** 2001: Rapid determination of canyon geometry parameters for use in surface radiation budgets. *Theoretical and applied climatology*, 69(1-2), 81-89.

- Chapman, L., Thornes, J. E., Muller, J. P., and McMuldroy, S.** 2007: Potential applications of thermal fisheye imagery in urban environments. *IEEE Geoscience and Remote Sensing Letters*, 4(1), 56-59.
- Chapman, L., Thornes, J.E., Huang, Y., Cai, X., Sanderson, V.L. and White, S.P.** 2008: Modelling of rail surface temperatures: a preliminary study. *Theoretical and Applied Climatology*, 92(1-2), pp.121-131.
- Chapman, L., Warren, E., Chapman, V.,** 2016; Towards a high resolution 'Internet of Things' moisture detection system for railways - Final Feasibility Report;
<https://www.sparkrail.org/Lists/Records/DispForm.aspx?ID=24860> Accessed 2018
- Chen, H., Furuya, T., Fukagai, S., Saga, S., Murakami, K. And Ban, T.,** 2018: Influence of Leaves on the Adhesion between Wheel and Rail. *Quarterly Report of RTRI*, 59(1), pp.65-71.
- Chen, J. M.** 1996: Optically-based methods for measuring seasonal variation of leaf area index in boreal conifer stands. *Journal of Agricultural and Forest Meteorology*, 80(2-4), 135-163.
- Chen, J.M., Black, T.A. and Adams, R.S.,** 1991. Evaluation of hemispherical photography for determining plant area index and geometry of a forest stand. *Agricultural and forest meteorology*, 56(1-2), pp.129-143.
- Chen, L., Ng, E., An, X., Ren, C., Lee, M., Wang, U. and He, Z.,** 2012. Sky view factor analysis of street canyons and its implications for daytime intra-urban air temperature differentials in high-rise, high-density urban areas of Hong Kong: a GIS-based simulation approach. *International Journal of Climatology*, 32(1), pp.121-136.
- Chen, L., Ng, E., An, X., Ren, C., Lee, M., Wang, U. and He, Z.,** 2012. Sky view factor analysis of street canyons and its implications for daytime intra-urban air temperature differentials in high-rise, high-density urban areas of Hong Kong: a GIS-based simulation approach. *International Journal of Climatology*, 32(1), pp.121-136.
- Chianucci, F.,** 2016. A note on estimating canopy cover from digital cover and hemispherical photography. *Silva Fennica*, 50(1), pp.1-10.
- Chianucci, F., Macfarlane, C., Pisek, J., Cutini, A. and Casa, R.** 2015: Estimation of foliage clumping from the LAI-2000 Plant Canopy Analyzer: effect of view caps. *Trees*, 29(2), 355-366
- Chmielewski, F. M., Müller, A., and KÜchler, W.** 2005: Possible impacts of climate change on natural vegetation in Saxony (Germany). *International Journal of Biometeorology*, 50(2), 96-104.
- Cho, S., Matsushita, Y. and Lee, S.,** 2007: Removing non-uniform motion blur from images.
- Clark, D. A., Brown, S., Kicklighter, D. W., Chambers, J. Q., Thomlinson, J. R., & Ni, J.** 2001: Measuring net primary production in forests: concepts and field methods. *Ecological applications*, 11(2), 356-370.
- Colombo, R., Bellingeri, D., Fasolini, D., and Marino, C. M.** 2003: Retrieval of leaf area index in different vegetation types using high resolution satellite data. *Remote Sensing of Environment*, 86(1), 120-131.

Corcoran, P. M., Bigioi, P., & Steinberg, E. 2001: Wireless transfer of images from a digital camera to the Internet via a standard GSM mobile phone. *Consumer Electronics, IEEE Transactions on*, 47(3), 542-547.

Crawley, D., Perry C., Hailstone J., Johns S., Reynolds. 2017: Piccadilly Line Formal Investigation Report, Transport for London, Xanta Limited, <http://content.tfl.gov.uk/piccadilly-line-leaf-fall-report.pdf> Accessed 2017

Crockett, R., 2014: Friction and Adhesion of Polysaccharides. *Tribology Online*, 9(4), pp.154-163.

Danson, F. M., Hetherington, D., Morsdorf, F., Koetz, B., and Allgower, B. 2007: Forest canopy gap fraction from terrestrial laser scanning. *IEEE Geoscience and remote sensing letters*, 4(1), 157-160.

Davis, D.R. and Hughes, J.E., 1970: A new approach to recording the wetting parameter by the use of electrical resistance sensors. *Plant Disease Reporter*, 54(6), pp.474-479.

Day Jr, J.W., Coronado-Molina, C., Vera-Herrera, F.R., Twilley, R., Rivera-Monroy, V.H., Alvarez-Guillen, H., Day, R. and Conner, W., 1996: A 7 year record of above-ground net primary production in a southeastern Mexican mangrove forest. *Aquatic Botany*, 55(1), 39-60

de Frutos, S.H. and Castro, M., 2014: Using smartphones as a very low-cost tool for road inventories. *Transportation research part C: emerging technologies*, 38, pp.136-145.

De Nazelle, A., Seto, E., Donaire-Gonzalez, D., Mendez, M., Matamala, J., Nieuwenhuijsen, M.J. and Jerrett, M., 2013: Improving estimates of air pollution exposure through ubiquitous sensing technologies. *Environmental Pollution*, 176, pp.92-99.

DEFRA 2006: A Guide for Local Authorities Purchasing Air Quality Monitoring Equipment, https://ukair.defra.gov.uk/assets/documents/reports/cat06/0608141644-386_Purchasing_Guide_for_AQ_Monitoring_Equipment_Version2.pdf Accessed 2018

DEFRA 2017: Automatic and Rural network, <https://uk-air.defra.gov.uk/networks/network-info?view=aur> Accessed 2018

Delay Attribution Board 2018: Autumn Guidance http://www.delayattributionboard.co.uk/documents/Process_Guidance%20Documents/PGD18%20Autumn%20Good%20Practice%20Guide.pdf

Delta 2017: HemiView Forest Canopy Image Analysis System, <https://www.delta-t.co.uk/product/hemiview/> accessed 30/01/2018

Department for transport 2017a: Statement of Funds https://assets.publishing.service.gov.uk/government/uploads/system/uploads/attachment_data/file/650998/railways-act-2005-statement-of-funds-available-2017-web.pdf Accessed 2019

Department for Transport 2017b: Transport Statistics Great Britain 2017, https://assets.publishing.service.gov.uk/government/uploads/system/uploads/attachment_data/file/661933/tsgb-2017-report-summaries.pdf Accessed 2019

- Department for Transport** 2017c: Strategic Vision for Rail, <https://www.gov.uk/government/publications/a-strategic-vision-for-rail> Accessed 2018
- Department for Transport** 2017d: Rail Factsheet 2017 https://assets.publishing.service.gov.uk/government/uploads/system/uploads/attachment_data/file/663116/rail-factsheet-2017.pdf Accessed 2019
- Department for Transport** 2018: Rail passenger numbers and crowding on weekdays in major cities in England and Wales: 2017 https://assets.publishing.service.gov.uk/government/uploads/system/uploads/attachment_data/file/728526/rail-passengers-crowding-2017.pdf Accessed 2019
- Department for Transport** 2018b: Tree cutting review <https://www.gov.uk/government/news/rail-minister-launches-review-of-tree-cutting-alongside-rail-lines> Accessed 2019
- Dixon, K.** 1976: Analysis of Seasonal Leaf Fall in North Temperate Deciduous Forests. *Oikos*, 27(2), 300-306
- Dobney, K., Baker, C.J., Quinn, A.D. and Chapman, L.**, 2009: Quantifying the effects of high summer temperatures due to climate change on buckling and rail related delays in south-east United Kingdom. *Meteorological Applications: A journal of forecasting, practical applications, training techniques and modelling*, 16(2), pp.245-251.
- Dorsey, B., Olsson, M. and Rew, L.J.**, 2015. Ecological effects of railways on wildlife. *Handbook of road ecology*, pp.219-227.
- Dragino**, 2018: LoRa GPS hat, <http://www.dragino.com/products/module/item/106-lora-gps-hat.html> accessed 2018
- Dufrêne, E., & Bréda, N.** 1995: Estimation of deciduous forest leaf area index using direct and indirect methods. *Oecologia*, 104(2), 156-162.
- Duveiller, G., and Defourny, P.** 2010: Batch processing of hemispherical photography using object-based image analysis to derive canopy biophysical variables. *Proceedings of GEOBIA*, 1682-1777.
- Englund, S. R., O'brien, J. J., and Clark, D. B.** 2000: Evaluation of digital and film hemispherical photography and spherical densitometry for measuring forest light environments. *Canadian Journal of Forest Research*, 30(12), 1999-2005.
- Estiarte, M., and Peñuelas, J.** 2015: Alteration of the phenology of leaf senescence and fall in winter deciduous species by climate change: effects on nutrient proficiency. *Global change biology*, 21(3), 1005-1017.
- Fang, H., Liang, S. and Kuusk, A.**, 2003. Retrieving leaf area index using a genetic algorithm with a canopy radiative transfer model. *Remote sensing of environment*, 85(3), pp.257-270.
- Farnell** 2017: Reflectometer cost, http://uk.farnell.com/megger/tdr1000-3/reflectometer-time-domain/dp/2377742?ost=time+domain+reflectometer&mckv=sKX3v9hdL_dc%7Cpcrid%7C208734351755%7Ckword%7Ctime+domain+reflectometer%7Cmatch%7Cp%7Cplid%7C&CMP=KNC-

[GUK-GEN-CMDTY-Test Measurement Inspection-phrase&DM_PersistentCookieCreated=true&categoryId=700000005812&gclid=EAlaIqobChMirYC-o-eT51gIVCjwbCh0XuwTvEAAAYASAAEgIRL_D_BwE&isrcfnonsku=false&ddkey=http%3Aen-GB%2FEelement14_United_Kingdom%2Fsearch](http://www.guk-gen-cmdty-test-measurement-inspection-phrase&DM_PersistentCookieCreated=true&categoryId=700000005812&gclid=EAlaIqobChMirYC-o-eT51gIVCjwbCh0XuwTvEAAAYASAAEgIRL_D_BwE&isrcfnonsku=false&ddkey=http%3Aen-GB%2FEelement14_United_Kingdom%2Fsearch) accessed 2017

Felderhof, L. and **Gillieson, D.**, 2012. Near-infrared imagery from unmanned aerial systems and satellites can be used to specify fertilizer application rates in tree crops. *Canadian Journal of Remote Sensing*, 37(4), pp.376-386.

Ferdoush, S. and **Li, X.**, 2014: Wireless sensor network system design using Raspberry Pi and Arduino for environmental monitoring applications. *Procedia Computer Science*, 34, pp.103-110.

Filigrano, M.L., Corredera, P., Rodriguez-Plaza, M., Andres-Alguacil, A. and Gonzalez-Herraez, M., 2013. Wheel flat detection in high-speed railway systems using fiber Bragg gratings. *IEEE Sensors Journal*, 13(12), pp.4808-4816.

Filigrano, M.L., Rodriguez-Barrios, A., Gonzalez-Herraez, M., Corredera, P., Mart n-L pez, S., Rodríguez-Plaza, M. and Andrés-Alguacil, A., 2010: Real time monitoring of railway traffic using fiber Bragg grating sensors. In *2010 Joint Rail Conference* (pp. 493-500). American Society of Mechanical Engineers.

FLIR., 2019: Thermal camera for smartphones, <https://www.flir.co.uk/products/flir-one-gen-3/> Accessed 2019

Ford, K.R., Harrington, C.A., Bansal, S., Gould, P.J. and St. Clair, J.B., 2016: Will changes in phenology track climate change? A study of growth initiation timing in coast Douglas-fir. *Global change biology*, 22(11), pp.3712-3723.

Forest Research, 2019: Slope Stabilisation, <https://www.forestresearch.gov.uk/tools-and-resources/urban-regeneration-and-greenspace-partnership/greenspace-in-practice/benefits-of-greenspace/slope-stabilisation/> Accessed 2019

Fraga-Lamas, Paula, Tiago M. Fernández-Caramés, and Luis Castedo 2017: "Towards the internet of smart trains: a review on industrial IoT-connected railways." *Sensors* 17.6. 1457.

Frazer, G. W., Fournier, R. A., Trofymow, J. A., and Hall, R. J. 2001: A comparison of digital and film fisheye photography for analysis of forest canopy structure and gap light transmission. *Journal of Agricultural and forest meteorology*, 109(4), 249-263.

Freer-Smith, P.H. and Webber, J.F., 2017. Tree pests and diseases: the threat to biodiversity and the delivery of ecosystem services. *Biodiversity and Conservation*, 26(13), pp.3167-3181.

Gál, T., Lindberg, F. and Unger, J., 2009. Computing continuous sky view factors using 3D urban raster and vector databases: comparison and application to urban climate. *Theoretical and applied climatology*, 95(1-2), pp.111-123.

Gál, T.M., Rzepa, M., Gromek, B. and Unger, J., 2007. Comparison between sky view factor values computed by two different methods in an urban environment. *Acta Climatologica et Chorologica*, 40, pp.17-26.

- Gallardo-Hernandez, E. A., & Lewis, R.** 2008: Twin disc assessment of wheel/rail adhesion. *Wear*, 265(9), 1309-1316.
- Gallinat, A. S., Primack, R. B., and Wagner, D. L.** 2015: Autumn, the neglected season in climate change research. *Trends in ecology & evolution*, 30(3), 169-176.
- Ganti, R. K., Ye, F., and Lei, H.** 2011: Mobile crowdsensing: current state and future challenges. *IEEE Communications Magazine*, 49(11).
- Garrigues, S., Shabanov, N. V., Swanson, K., Morisette, J. T., Baret, F., and Myneni, R. B.** 2008: Intercomparison and sensitivity analysis of Leaf Area Index retrievals from LAI-2000, AccuPAR, and digital hemispherical photography over croplands. *Journal of Agricultural and Forest meteorology*, 148(8), 1193-1209.
- GDP** 2016: Vegetation Spectral Reflectance Curves, http://gsp.humboldt.edu/olm_2015/Courses/GSP_216_Online/lesson2-1/vegetation.html Accessed 2019
- Gitelson, A. A., Kaufman, Y. J., and Merzlyak, M. N.** 1996: Use of a green channel in remote sensing of global vegetation from EOS-MODIS. *Remote sensing of Environment*, 58(3), 289-298.
- Gitelson, A., & Merzlyak, M. N.** 1994: Quantitative estimation of chlorophyll-a using reflectance spectra: experiments with autumn chestnut and maple leaves. *Journal of Photochemistry and Photobiology B: Biology*, 22(3), 247-252.
- GlobalSat**, 2011: GPS User Manual, www.usglobalsat.com/store/download/688/WIN_UsersGuide.pdf Accessed 2018
- Goddard, E.**, 2006: Overview of signalling and train control systems. In *Electric Traction Systems, 2006. The 9th Institution of Engineering and Technology Professional Development Course on* (pp. 336-350). IET.
- Gordo, O. and Sanz, J. J.** 2010: Impact of climate change on plant phenology in Mediterranean ecosystems. *Global Change Biology*, 16(3), 1082-1106.
- Göteborg Urban Climate Group**, 2018: Sky-view Calculator, University of Gothenburg, <https://gvc.gu.se/english/research/climate/urban-climate/software/download>. Accessed 30/01/2018
- Gower, S. T., Kucharik, C. J., & Norman, J. M.** 1999: Direct and indirect estimation of leaf area index, f APAR, and net primary production of terrestrial ecosystems. *Remote sensing of environment*, 70(1), 29-51.
- Grimmond, C.S.B., Potter, S.K., Zutter, H.N. and Souch, C.**, 2001. Rapid methods to estimate sky-view factors applied to urban areas. *International journal of climatology*, 21(7), pp.903-913.
- Grote, R., Samson, R., Alonso, R., Amorim, J.H., Cariñanos, P., Churkina, G., Fares, S., Thiec, D.L., Niinemets, Ü., Mikkelsen, T.N. and Paoletti, E.**, 2016: Functional traits of urban trees: air pollution mitigation potential. *Frontiers in Ecology and the Environment*, 14(10), pp.543-550.

- Gubbi, J., Buyya, R., Marusic, S., & Palaniswami, M.** 2013: Internet of Things (IoT): A vision, architectural elements, and future directions. *Future Generation Computer Systems*, 29(7), 1645-1660.
- Gurnell, A.M. and Grabowski, R.C.**, 2016. Vegetation–hydrogeomorphology interactions in a low-energy, human-impacted river. *River Research and Applications*, 32(2), pp.202-215
- Hajji, W. and Tso, F.**, 2016. Understanding the performance of low power Raspberry Pi Cloud for big data. *Electronics*, 5(2), p.29.
- Hale, S. E.**, and **Edwards, C.** 2002: Comparison of film and digital hemispherical photography across a wide range of canopy densities. *Journal of Agricultural and Forest Meteorology*, 112(1), 51-56.
- Hall, R. J., Fournier, R. A., and Rich, P.** 2017: Introduction. In *Hemispherical Photography in Forest Science: Theory, Methods, Applications* (pp. 1-13). Springer Netherlands.
- Hämmerle, M., Gál, T., Unger, J. and Matzarakis, A.**, 2011. Comparison of models calculating the sky view factor used for urban climate investigations. *Theoretical and Applied Climatology*, 105(3-4), pp.521-527.
- Harrison, H., McCanney, T., & Cotter, J.** 2002: Recent developments in coefficient of friction measurements at the rail/wheel interface. *Wear*, 253(1), 114-123.
- Hasenfratz, D., Saukh, O., Sturzenegger, S. and Thiele, L.**, 2012: Participatory air pollution monitoring using smartphones. *Mobile Sensing*, 1, pp.1-5.
- Hata, D.** 2003: U.S. Patent No. 6,603,508. Washington, DC: U.S. Patent and Trademark Office.
- Havens, K., and Henderson, S.** 2013: Citizen science takes root. *American Scientist*, 101(5), 378.
- Hayes, J., Beirne, S., Lau, K.T. & Diamond, D.** 2008: Evaluation of a low-cost wireless chemical sensor network for environmental monitoring. In *Sensors, 2008 IEEE* (pp. 530-533). IEEE.
- Heal, M. R., O'donoghue, M. A., & Cape, J. N.** 1999: Overestimation of urban nitrogen dioxide by passive diffusion tubes: a comparative exposure and model study. *Atmospheric Environment*, 33(4), 513-524.
- Highways England** (2017) Highways England is geared up for winter, <https://www.gov.uk/government/news/highways-england-is-g geared-up-for-winter> accessed 2018
- Hodge, V.J., O'Keefe, S., Weeks, M. and Moulds, A.**, 2015. Wireless sensor networks for condition monitoring in the railway industry: A survey. *IEEE Trans. Intelligent transportation systems*, 16(3), pp.1088-1106.
- Holmer, B.**, 1992. A simple operative method for determination of sky view factors in complex urban canyons from fisheye photographs. *Meteorol. Z*, 1, pp.236-239.
- Holmer, B., Postgård, U. and Eriksson, M.** 2001: Sky view factors in forest canopies calculated with IDRISI. *Journal of Theoretical Applied Climatology*, 68(1), 33-40.
- Homo Malenovský, Z., Hanuš, J., To ko , I., Dvoř ov M., and Pokorný, R.** 2007: Comparaison of different ground techniques to map leaf area index of Norway spruce forest

canopy. In *Proceedings of the International Society for Photogrammetry and Remote Sensing (ISPRS)*

Honicky, R., Brewer, E.A., Paulos, E. and White, R. 2008: N-smarts: networked suite of mobile atmospheric real-time sensors. In *Proceedings of the second ACM SIGCOMM workshop on Networked systems for developing regions* (pp. 25-30). ACM.

Hooper, E. and Chapman, L., 2012. Chapter 5 The Impacts of Climate Change on National Road and Rail Networks. In *Transport and Climate Change* (pp. 105-136). Emerald Group Publishing Limited.

Houborg, R., Soegaard, H., & Boegh, E. 2007: Combining vegetation index and model inversion methods for the extraction of key vegetation biophysical parameters using Terra and Aqua MODIS reflectance data. *Remote Sensing of Environment*, 106(1), 39-58.

Hovi, A., Korhonen, L., Vauhkonen, J. and Korpela, I., 2016. LiDAR waveform features for tree species classification and their sensitivity to tree-and acquisition related parameters. *Remote sensing of environment*, 173, pp.224-237

Hu, L., Gong, Z., Li, J., and Zhu, J. 2009: Estimation of canopy gap size and gap shape using a hemispherical photograph. *Trees*, 23(5), 1101-1108.

Hung, C., Suda, Y., Aki, M., Tsuji, T., Morikawa, M., Yamashita, T., Kawanabe, T. and Kunimi, T., 2010: Study on detection of the early signs of derailment for railway vehicles. *Vehicle System Dynamics*, 48(S1), pp.451-466.

Hussain, I., Ahamad, K.U. and Nath, P., 2016: Low-cost, robust, and field portable smartphone platform photometric sensor for fluoride level detection in drinking water. *Analytical chemistry*, 89(1), pp.767-775.

Hut, R.W., Weijs, S.V. & Luxemburg, W.M.J., 2010: Using the Wiimote as a sensor in water research. *Water Resources Research*, 46(12).

Ibrahim, M., Elgamri, A., Babiker, S. and Mohamed, A., 2015, October. Internet of things based smart environmental monitoring using the Raspberry-Pi computer. In *2015 Fifth International Conference on Digital Information Processing and Communications (ICDIPC)* (pp. 159-164). IEEE.

Innovate UK 2016: Perpetuum, <https://www.gov.uk/government/case-studies/perpetuum-self-powered-rail-safety-technology-drives-jobs-growth>, accessed 2018

Inoue, A., Yamamoto, K. and Mizoue, N., 2011: Comparison of automatic and interactive thresholding of hemispherical photography. *Journal of Forest Science*, 57(2), pp.78-87.

Ishida, M. 2004: Automatic thresholding for digital hemispherical photography. *Canadian Journal of Forest Research*, 34(11), 2208-2216.

Ishizaka, K., Lewis, S.R. and Lewis, R., 2017. The low adhesion problem due to leaf contamination in the wheel/rail contact: Bonding and low adhesion mechanisms. *Wear*, 378, pp.183-197.

- Ishizaka, K., Lewis, S.R., Hammond, D. and Lewis, R.,** 2018. Chemistry of black leaf films synthesised using rail steels and their influence on the low friction mechanism. *RSC Advances*, 8(57), pp.32506-32521.
- Janić, M.,** 2018. Modelling the resilience of rail passenger transport networks affected by large-scale disruptive events: the case of HSR (high speed rail). *Transportation*, 45(4), pp.1101-1137.
- Jaroszweski, D., Chapman, L. and Petts, J.** 2010: Assessing the potential impact of climate change on transportation: the need for an interdisciplinary approach. *Journal of Transport Geography*, 18(2), pp.331-335
- Jaroszweski, D., Hooper, E., Baker, C., Chapman, L. and Quinn, A.,** 2015. The impacts of the 28 June 2012 storms on UK road and rail transport. *Meteorological Applications*, 22(3), pp.470-476.
- Jayasooriya, V.M., Ng, A.W.M., Muthukumaran, S. and Perera, B.J.C.,** 2017: Green infrastructure practices for improvement of urban air quality. *Urban forestry & urban greening*, 21, pp.34-47.
- Jenkins, D.P. and Harvey, C.,** 2015: KEEPING HUMAN FACTORS ON TRACK–THE DESIGN OF THE NEXT GENERATION INTERCITY EXPRESS TRAIN. In *Contemporary Ergonomics and Human Factors 2015: Proceedings of the International Conference on Ergonomics & Human Factors 2015, Daventry, Northamptonshire, UK, 13-16 April 2015* (p. 31). CRC Press.
- Ji, H. and Liu, C.,** 2008: Motion blur identification from image gradients. In *Computer Vision and Pattern Recognition, 2008. CVPR 2008. IEEE Conference on* (pp. 1-8). IEEE.
- Jiang, F., Cacchiani, V. and Toth, P.,** 2017. Train timetabling by skip-stop planning in highly congested lines. *Transportation Research Part B: Methodological*, 104, pp.149-174.
- Johnson, G. T., and Watson, I. D.** 1984: The determination of view-factors in urban canyons. *Journal of Climate and Applied Meteorology*, 23(2), 329-335.
- Johnson, G.T. and Watson, I.D.,** 1984. The determination of view-factors in urban canyons. *Journal of Climate and Applied Meteorology*, 23(2), pp.329-335.
- Jonasson, S.** 1988: Evaluation of the point intercept method for the estimation of plant biomass. *Oikos*, 101-106.
- Jonckheere, I., Fleck, S., Nackaerts, K., Muys, B., Coppin, P., Weiss, M., and Baret, F.** 2004: Review of methods for in situ leaf area index determination: Part I. Theories, sensors and hemispherical photography. *Agricultural and forest meteorology*, 121(1), 19-35.
- Justice, C., Belward, A., Morisette, J., Lewis, P., Privette, J., & Baret, F.** 2000: Developments in the validation of satellite sensor products for the study of the land surface. *International Journal of Remote Sensing*, 21(17), 3383-3390

Kakria, P., Tripathi, N.K. and Kitipawang, P., 2015: A real-time health monitoring system for remote cardiac patients using smartphone and wearable sensors. *International journal of telemedicine and applications*, 2015, p.8.

Kanjo, E.: 2010 Noisespy: A real-time mobile phone platform for urban noise monitoring and mapping. *Mobile Networks and Applications*, 15(4), 562-574.

Karlik, J.F. and McKay, A.H., 2002: Leaf area index, leaf mass density, and allometric relationships derived from harvest of blue oaks in a California oak savanna. In In: Standiford, Richard B., et al, tech. editor. Proceedings of the Fifth Symposium on Oak Woodlands: Oaks in California's Challenging Landscape. Gen. Tech. Rep. PSW-GTR-184, Albany, CA: Pacific Southwest Research Station, Forest Service, US Department of Agriculture: 719-729 (Vol. 184).

Kenderian, S.H.A.N.T., Djordjevic, B.B., Cerniglia, D. and Garcia, G., 2006: Dynamic railroad inspection using the laser-air hybrid ultrasonic technique. *Insight-Non-Destructive Testing and Condition Monitoring*, 48(6), pp.336-341.

Kendon, E.J., Roberts, N.M., Fowler, H.J., Roberts, M.J., Chan, S.C. and Senior, C.A., 2014: Heavier summer downpours with climate change revealed by weather forecast resolution model. *Nature Climate Change*, 4(7), p.570.

Kirby, J., Chapman, L., Chapman, V. 2018: Assessing the Raspberry Pi as a low-cost alternative for acquisition of near infrared hemispherical digital imagery, *Agricultural and Forest Meteorology*, 259, 232-239

Kizito, F., Campbell, C.S., Campbell, G.S., Cobos, D.R., Teare, B.L., Carter, B. & Hopmans, J.W., 2008: Frequency, electrical conductivity and temperature analysis of a low-cost capacitance soil moisture sensor. *Journal of Hydrology*, 352(3-4), pp.367-378.

Ko , Hodoň, M., Čechovič, L., Kapitu , J. and Jurečka, M., 2014: WSN for traffic monitoring using Raspberry Pi board. In 2014 Federated Conference on Computer Science and Information Systems (pp. 1023-1026). IEEE.

Kodani, E., Awaya, Y., Tanaka, K., & Matsumura, N. 2002: Seasonal patterns of canopy structure, biochemistry and spectral reflectance in a broad-leaved deciduous *Fagus crenata* canopy. *Forest Ecology and Management*, 167(1), 233-249.

Koetse, M.J. and Rietveld, P. 2009: The impact of climate change and weather on transport: An overview of empirical findings. *Transportation Research Part D: Transport and Environment*, 14(3), pp.205-221

Kolb, C.E., Herndon, S.C., McManus, J.B., Shorter, J.H., Zahniser, M.S., Nelson, D.D., Jayne, J.T., Canagaratna, M.R. & Worsnop, D.R. 2004: Mobile laboratory with rapid response instruments for real-time measurements of urban and regional trace gas and particulate distributions and emission source characteristics. *Environmental science & technology*, 38(21), pp.5694-5703.

Kolukirik, C. and Bezgin, N.O., 2019, March. Analysis of Dynamic Impact Forces on Railway Tracks Due to Wheel Flats. In *5th International Conference on Road and Rail Infrastructure*.

- Kosmala, M., Crall, A., Cheng, R., Hufkens, K., Henderson, S., & and Richardson, A. D.** 2016: Season Spotter: Using citizen science to validate and scale plant phenology from near-surface remote sensing. *Remote Sensing*, 8(9), 726.
- Kouroussis, G., Caucheteur, C., Kinet, D., Alexandrou, G., Verlinden, O. and Moeyaert, V.,** 2015: Review of trackside monitoring solutions: from strain gages to optical fibre sensors. *Sensors*, 15(8), pp.20115-20139.
- Kumar, S. and Jasuja, A.,** 2017, May. Air quality monitoring system based on IoT using Raspberry Pi. In *2017 International Conference on Computing, Communication and Automation (ICCCA)* (pp. 1341-1346). IEEE.
- Kumar, S. and Jasuja, A.,** 2017, May. Air quality monitoring system based on IoT using Raspberry Pi. In *2017 International Conference on Computing, Communication and Automation (ICCCA)* (pp. 1341-1346). IEEE.
- Lacombe, R.,** 2005. Adhesion measurement methods: theory and practice. CRC Press. Pp 3
- Lane, N. D., Miluzzo, E., Lu, H., Peebles, D., Choudhury, T., & Campbell, A. T:** 2010. A survey of mobile phone sensing. *IEEE Communications magazine*, 48(9).
- Lang, M., Kuusk, A., Möttus, M., Rautiainen, M., and Nilson, T.** 2010: Canopy gap fraction estimation from digital hemispherical images using sky radiance models and a linear conversion method. *Journal of Agricultural and Forest Meteorology*, 150(1), 20-29.
- Lawley, V., Lewis, M., Clarke, K. and Ostendorf, B.,** 2016: Site-based and remote sensing methods for monitoring indicators of vegetation condition: An Australian review. *Ecological Indicators*, 60, pp.1273-1283.
- Leblanc, S. G., Chen, J. M., Fernandes, R., Deering, D. W., and Conley, A.** 2005: Methodology comparison for canopy structure parameters extraction from digital hemispherical photography in boreal forests. *Journal of Agricultural and Forest Meteorology*, 129(3),187-207.
- Leccese, F., Cagnetti, M. & Trinca, D.,** 2014: A smart city application: A fully controlled street lighting isle based on Raspberry-Pi card, a ZigBee sensor network and WiMAX. *Sensors*, 14(12), pp.24408-24424.
- Lee, H.C.,** 1990: Review of image-blur models in a photographic system using the principles of optics. *Optical Engineering*, 29(5), pp.405-422.
- Lee, T. and Tso, M.,** 2016: A universal sensor data platform modelled for realtime asset condition surveillance and big data analytics for railway systems: developing a “Smart Railway” mastermind for the betterment of reliability, availability, maintainability and safety of railway systems and passenger service. In *SENSORS, 2016 IEEE* (pp. 1-3). IEEE.
- Lee, W., Lee, J., Henderson, C., Taylor, H.F., James, R., Lee, C.E., Swenson, V., Atkins, R.A. and Gemeiner, W.G.,** 1999: Railroad bridge instrumentation with fiber-optic sensors. *Applied optics*, 38(7), pp.1110-1114.

- Lévesque, J. and King, D.J.**, 2003: Spatial analysis of radiometric fractions from high-resolution multispectral imagery for modelling individual tree crown and forest canopy structure and health. *Remote Sensing of Environment*, 84(4), pp.589-602.
- Lewis, A.J., Campbell, M. & Stavroulakis, P.** 2016: Performance evaluation of a cheap, open source, digital environmental monitor based on the Raspberry Pi. *Measurement*, 87, pp.228-235.
- Lewis, A.J., Campbell, M. and Stavroulakis, P.**, 2016. Performance evaluation of a cheap, open source, digital environmental monitor based on the Raspberry Pi. *Measurement*, 87, pp.228-235.
- Lewis, A.J., Campbell, M. and Stavroulakis, P.**, 2016. Performance evaluation of a cheap, open source, digital environmental monitor based on the Raspberry Pi. *Measurement*, 87, pp.228-235.
- Lewis, R., & Dwyer-Joyce, R. S.** 2006: Wear at the wheel/rail interface when sanding is used to increase adhesion. *Proceedings of the Institution of Mechanical Engineers, Part F: Journal of Rail and Rapid Transit*, 220(1), 29-41.
- Lewis, R., Gallardo-Hernandez, E.A., Hilton, T. and Armitage, T.**, 2009: Effect of oil and water mixtures on adhesion in the wheel/rail contact. *Proceedings of the Institution of Mechanical Engineers, Part F: Journal of Rail and Rapid Transit*, 223(3), pp.275-283.
- Lewis, R., Gallardo-Hernandez, E.A., Hilton, T. and Armitage, T.**, 2009. Effect of oil and water mixtures on adhesion in the wheel/rail contact. *Proceedings of the Institution of Mechanical Engineers, Part F: Journal of Rail and Rapid Transit*, 223(3), pp.275-283.
- Lewis, S.R., Lewis, R. and Olofsson, U.**, 2011. An alternative method for the assessment of railhead traction. *Wear*, 271(1-2), pp.62-70.
- Lewis, S.R., Lewis, R., Richards, P. and Buckley-Johnstone, L.E.**, 2014: Investigation of the isolation and frictional properties of hydrophobic products on the rail head, when used to combat low adhesion. *Wear*, 314(1-2), pp.213-219.
- Li, Q. and Ren, S.**, 2012: A real-time visual inspection system for discrete surface defects of rail heads. *IEEE Transactions on Instrumentation and Measurement*, 61(8), pp.2189-2199.
- Li, Z., Arias-Cuevas, O., Lewis, R., & Gallardo-Hernandez, E. A.** 2009: Rolling–sliding laboratory tests of friction modifiers in leaf contaminated wheel–rail contacts. *Tribology letters*, 33(2), 97-109.
- Liang, S., Li, X. and Wang, J.**, 2012. Fraction of absorbed photosynthetically active radiation by green vegetation. *Advanced Remote Sensing: Terrestrial Information Extraction and Applications; Elsevier Inc.: Oxford, UK*, pp.383-414.
- Lindberg, F., and Holmer, B.** 2010: Sky View Factor Calculator, Göteborg Urban Climate Group, Department of Earth Sciences, University of Gothenburg
- Liu, C., Kang, S., Li, F., Li, S. and Du, T.**, 2013. Canopy leaf area index for apple tree using hemispherical photography in arid region. *Scientia horticultrae*, 164, pp.610-615.

- Liu, Z., Wang, C., Chen, J. M., Wang, X., and Jin, G** 2015: Empirical models for tracing seasonal changes in leaf area index in deciduous broadleaf forests by digital hemispherical photography. *Journal of Forest Ecology and Management*, 351, 67-77.
- López-Higuera, J.M., Cobo, L.R., Incera, A.Q. and Cobo, A.,** 2011: Fiber optic sensors in structural health monitoring. *Journal of lightwave technology*, 29(4), pp.587-608.
- Lu, X., Cotter, J., & Eadie, D. T.** 2005: Laboratory study of the tribological properties of friction modifier thin films for friction control at the wheel/rail interface. *Wear*, 259(7), 1262-1269.
- Lucas, P.S., de Carvalho, R.G. and Grilo, C.,** 2017. Railway disturbances on wildlife: types, effects, and mitigation measures. In *Railway Ecology* (pp. 81-99). Springer, Cham.
- Macucci, M., Di Pascoli, S., Marconcini, P. and Tellini, B.,** 2015: October. Wireless sensor network for derailment detection in freight trains powered from vibrations. In *Measurements & Networking (M&N), 2015 IEEE International Workshop on* (pp. 1-6). IEEE.
- Maisonnette, N., Stevens, M., Niessen, M. E., & Steels, L:** 2009. NoiseTube: Measuring and mapping noise pollution with mobile phones. In *Information technologies in environmental engineering* (pp. 215-228). Springer Berlin Heidelberg
- Masarovicová, E.,** 1990: Some ecophysiological features in sun and shade leaves of tall beech trees. *Biologia plantarum*, 32(5), p.374.
- Mattar, C., Santamaría-Artigas, A., Sobrino, J.A. and Jiménez-Muñoz, J.C.,** 2016. Soil Moisture Retrieved From a Combined Optical and Passive Microwave Approach: Theory and Applications. In *Satellite Soil Moisture Retrieval* (pp. 135-158).
- Matuschek, O., and Matzarakis, A :**2010 Estimation of sky view factor in complex environment as a tool for applied climatological studies. *Berichte des Meteorologischen Instituts der Albert-Ludwigs-Universität Freiburg*, 20, 534-539.
- Matzarakis, A., Rutz, F. and Mayer, H:** 2007. Modelling radiation fluxes in simple and complex environments—application of the RayMan model. *International journal of biometeorology*, 51(4), pp.323-334.
- Matzarakis, A., Rutz, F., and Mayer, H:** 2010 Modelling radiation fluxes in simple and complex environments: basics of the RayMan model. *International journal of biometeorology*, 54(2), 131-139.
- McDowell, N., Barnard, H., Bond, B., Hinckley, T., Hubbard, R., Ishii, H., Köstner, B., Magnani, F., Marshall, J., Meinzer, F. & Phillips, N.,** 2002: The relationship between tree height and leaf area: sapwood area ratio. *Oecologia*, 132(1), pp.12-20.
- McShane, M. C., Carlile, D. W., & Hinds, W. T.** 1983: The effect of collector size on forest litter-fall collection and analysis. *Canadian Journal of Forest Research*, 13(6), 1037-1042.
- Mead, M.I., Popoola, O.A.M., Stewart, G.B., Landshoff, P., Calleja, M., Hayes, M., Baldovi, J.J., McLeod, M.W., Hodgson, T.F., Dicks, J. & Lewis, A.** 2013: The use of electrochemical

sensors for monitoring urban air quality in low-cost, high-density networks. *Atmospheric Environment*, 70, pp.186-203

Menzel, A. 2002: Phenology: its importance to the global change community. *Climatic change*, 54(4), 379-385.

Met Office 2018b: Low Adhesion Forecast

<https://www.metoffice.gov.uk/services/transport/railways/low-adhesion-forecast> accessed 2018

Met Office (2016) Weather Stations, <https://www.metoffice.gov.uk/learning/making-a-forecast/first-steps/observations/weather-stations> Accessed 2018

Met Office 2018a: UKCP18 <https://www.metoffice.gov.uk/research/collaboration/ukcp> Accessed 2019

Met Office. 2018: Rail Weather Training <https://www.metoffice.gov.uk/training/industry/rail/rail-weather-training> accessed 2018

Michez, A., Piégay, H., Lisein, J., Claessens, H. and Lejeune, P., 2016: Classification of riparian forest species and health condition using multi-temporal and hyperspatial imagery from unmanned aerial system. *Environmental monitoring and assessment*, 188(3), p.146.

Minami, M., Sakala, M. and Wrightsell, J., 2000: *Using ArcMap* (p. 528). Redlands, CA: ESRI.

Mockel, S., Scherer, F. and Schuster, P.F., 2003: Multi-sensor obstacle detection on railway tracks. In *Intelligent Vehicles Symposium, Proceedings. IEEE* (pp. 42-46). IEEE.

Molles, M. C., Crawford, C. S., Ellis, L. M., Valett, H. M., and Dahm, C. N. 1998: Managed flooding for riparian ecosystem restoration. *BioScience*, 48(9), 749-756.

Monteiro, M., Vogt, P., Stari, C., Cabeza, C. and Marti, A.C., 2016: Exploring the atmosphere using smartphones. *The Physics Teacher*, 54(5), pp.308-309.

Morrison, I. K. 1991: Effect of trap dimensions on mass of litterfall collected in an Acer saccharum stand in northern Ontario. *Canadian Journal of Forest Research*, 21(6), 939-941.

Muotka, T., and Laasonen, P. 2002: Ecosystem recovery in restored headwater streams: the role of enhanced leaf retention. *Journal of applied Ecology*, 39(1), 145-156.

NASA 2017: Measuring Vegetation

https://earthobservatory.nasa.gov/Features/MeasuringVegetation/measuring_vegetation_2.php

Accessed 2017

National Rail. 2019: TOCs http://www.nationalrail.co.uk/tocs_maps/tocs/trainoperators.aspx

Accessed 2019

Natividade, J., Prado, J. and Marques, L., 2017, April. Low-cost multi-spectral vegetation classification using an Unmanned Aerial Vehicle. In *2017 IEEE International Conference on Autonomous Robot Systems and Competitions (ICARSC)* (pp. 336-342). IEEE.

Network Rail 2016: Leaves, <http://www.networkrail.co.uk/timetables-and-travel/delays-explained/leaves/> accessed 10/02/2016

Network Rail 2017: Vegetation Survey, <https://www.networkrail.co.uk/communities/environment/vegetation-management/>

Network Rail 2017a WRCA, <https://safety.networkrail.co.uk/wp-content/uploads/2017/02/NR-WRCCA-Strategy-2017-2019.pdf>

Network Rail 2018 g Lineside vegetation management, <https://cdn.networkrail.co.uk/wp-content/uploads/2018/05/Lineside-Vegetation-Management-Documentation.pdf> accessed 2019

Network Rail 2018a: Railway Upgrade Plan <https://cdn.networkrail.co.uk/wp-content/uploads/2017/08/Railway-Upgrade-Plan-Update-2017-2018.pdf>

Network Rail 2018b: Delays Explained, <https://www.networkrail.co.uk/running-the-railway/looking-after-the-railway/delays-explained/> accessed 23/04/2019

Network Rail 2018c: A better railway for a better Britain Strategic Business Plan 2019 – 2024, <https://cdn.networkrail.co.uk/wp-content/uploads/2018/02/Strategic-business-plan-high-level-summary.pdf>

Network Rail 2018d: <https://www.networkrail.co.uk/feeds/network-rails-leaf-busting-teams-prepare-to-keep-trains-moving-on-the-anglia-rail-network/>

Network Rail 2018f Standards Catalogue <https://www.networkrail.co.uk/wp-content/uploads/2018/04/Network-Rail-Standards-Catalogue.pdf>

Network Rail 2019 <https://www.networkrail.co.uk/who-we-are/how-we-work/performance/safety-performance/signals-passed-danger-spads-category/>

Network Rail 2019b: Public performance measure <https://www.networkrail.co.uk/who-we-are/how-we-work/performance/railway-performance/public-performance-measure-and-delay-responsibility/>

Network Rail. 2017b: Trees and the railways, <https://www.networkrail.co.uk/communities/environment/sharing-railway-wildlife/trees-and-the-railway/>

Nguyen, H.Q., Loan, T.T.K., Mao, B.D. and Huh, E.N., 2015: Low cost real-time system monitoring using Raspberry Pi. In *2015 Seventh International Conference on Ubiquitous and Future Networks* (pp. 857-859). IEEE.

Nikon, CoolPix 4500 product archive, 2017: <http://imaging.nikon.com/lineup/CoolPix/others/4500/> accessed 30/01/2018

Niu, H., Zhou, X. and Gao, R., 2015. Train scheduling for minimizing passenger waiting time with time-dependent demand and skip-stop patterns: Nonlinear integer programming models with linear constraints. *Transportation Research Part B: Methodological*, 76, pp.117-135.

Norby, R. J., Hartz-Rubin, J. S., and Verbrugge, M. J. 2003: Phenological responses in maple to experimental atmospheric warming and CO2 enrichment. *Global Change Biology*, 9(12), 1792-1801.

Northern Rail 2018: <https://dkf1ato8y5dsg.cloudfront.net/uploads/15/103/rssb-research-call-launch-presentation.pdf> Accessed 2019

Northern Rail 2019: Leaf fall time table <https://www.northernrailway.co.uk/news/latest-news/895-leaf-fall-timetable-change> Accessed 2019

Nowacki, G.J. and Abrams, M.D., 2015: Is climate an important driver of post-European vegetation change in the Eastern United States? *Global Change Biology*, 21(1), pp.314-334.

O'Brien, S. T., Hubbell, S. P., Spiro, P., Condit, R., & Foster, R. B. 1995: Diameter, height, crown, and age relationship in eight neotropical tree species. *Ecology*, 1926-1939

OENL DAACA., 2019: Global Database of Field-observed Leaf Area Index in Woody Plant Species, 1932-2011, https://daac.ornl.gov/cgi-bin/dsvviewer.pl?ds_id=1231 Accessed 2019

Office for Rail and Road 2017: Rail Statistics Compendium Great Britain 2016-17 Annual http://orr.gov.uk/_data/assets/pdf_file/0017/26108/rail-statistics-compendium-2016-17.pdf

Office for Rail and Road 2018: Health and Safety <https://orr.gov.uk/rail/health-and-safety/infrastructure-safety/signals-passed-at-danger> Accessed 2019

Office for Road and Rail 2017: Safety strategy https://orr.gov.uk/_data/assets/pdf_file/0018/6426/safety-strategy-chapter-5.pdf Accessed 2019

Office for Road and Rail 2019a https://orr.gov.uk/_data/assets/pdf_file/0005/39983/passenger-rail-usage-2018-19-q2.pdf Accessed 2019

Office for Road and Rail 2019b Overview of Rail https://orr.gov.uk/_data/assets/pdf_file/0008/16379/an-overview-of-the-rail-industry.pdf Accessed 2019

Oke, T.R., 2002. *Boundary layer climates*. Routledge. Pp 133

Oksanen, E., Riikonen, J., Kaakinen, S., Holopainen, T. and Vapaavuori, E., 2005: Structural characteristics and chemical composition of birch (*Betula pendula*) leaves are modified by increasing CO₂ and ozone. *Global Change Biology*, 11(5), pp.732-748.

Olofsson, U. 2007: A multi-layer model of low adhesion between railway wheel and rail. Proceedings of the Institution of Mechanical Engineers, Part F: Journal of Rail and Rapid Transit, 221(3), 385-389.

Olofsson, U. and Sundvall, K. 2004: Influence of leaf, humidity and applied lubrication on friction in the wheel-rail contact: pin-on-disc experiments. *Proceedings of the Institution of Mechanical Engineers, Part F: Journal of Rail and Rapid Transit*, 218(3), 235-242.

Olofsson, U., Sundh, J., Bik, U., & Nilsson, R. 2016: The influence of snow on the tread braking performance of a train: A pin-on-disc simulation performed in a climate chamber. Proceedings of the Institution of Mechanical Engineers, Part F: Journal of Rail and Rapid Transit, 230(6), 1521-1530.

- Olofsson, U., Zhu, Y., Abbasi, S., Lewis, R., and Lewis, S.** 2013: Tribology of the wheel–rail contact—aspects of wear, particle emission and adhesion. *Vehicle System Dynamics*, 51(7), 1091-1120.
- Osmond, P.** 2010: Hemispherical photography as a tool for urban sustainability evaluation and design. *OIDA International Journal of Sustainable Development*, 63-74
- Osmond, P.,** 2009, June. Application of near-infrared hemispherical photography to estimate leaf area index of urban vegetation. In *Extended Abstracts. The Seventh International Conference on Urban Climate, 29 June–3 July 2009* (pp. 4-pp).
- OXERA** 2014: Contribution of the UK rail to economy <https://www.oxera.com/wp-content/uploads/2018/07/Contribution-of-rail-to-the-UK-economy-140714.pdf.pdf>
- Oxford Economics** 2014: Economic Benefits from Air Transport in the UK <https://www.aoa.org.uk/wp-content/uploads/2014/11/Economic-Benefits-from-Air-Transport-in-the-UK.pdf.pdf>
- Oxford Economics** 2018: The Economic contribution of UK rail full report <http://oldsite.riagb.org.uk/wp-content/uploads/2014/07/The-Economic-Contribution-of-UK-Rail-Full-Report.pdf>
- Pastor, J., Aber, J. D., & Melillo, J. M.** 1984: Biomass prediction using generalized allometric regressions for some northeast tree species. *Forest Ecology and Management*, 7(4), 265-274.
- Peichl, M., & Arain, M. A.** 2007: Allometry and partitioning of above-and belowground tree biomass in an age-sequence of white pine forests. *Forest Ecology and Management*, 253(1), 68-80.
- Peñuelas, J. and Filella, I.** 2009: Phenology feedbacks on climate change. *Science*, 324(5929), 887-888.
- Perpetuum**, 2018: Rail Applications, <https://perpetuum.com/rail-applications/> accessed 2018
- Petersen, C., Chen, T., Ansermino, J. and Dumont, G.,** 2013: Design and evaluation of a low-cost smartphone pulse oximeter. *Sensors*, 13(12), pp.16882-16893.
- Poblete-Echeverría, C., Fuentes, S., Ortega-Farias, S., Gonzalez-Talice, J. and Yuri, J.,** 2015. Digital cover photography for estimating leaf area index (LAI) in apple trees using a variable light extinction coefficient. *Sensors*, 15(2), pp.2860-2872.
- Poblete-Echeverría, C., Fuentes, S., Ortega-Farias, S., Gonzalez-Talice, J. and Yuri, J.,** 2015. Digital cover photography for estimating leaf area index (LAI) in apple trees using a variable light extinction coefficient.
- Popp, J.N. and Boyle, S.P.,** 2017. Railway ecology: Underrepresented in science?. *Basic and Applied Ecology*, 19, pp.84-93.

Potter, C. and Urquhart, J., 2017. Tree disease and pest epidemics in the Anthropocene: A review of the drivers, impacts and policy responses in the UK. *Forest Policy and Economics*, 79, pp.61-68.

Prabha, S.S., Antony, A.J.P., Meena, M.J. and Pandian, S.R., 2014: Smart cloud robot using raspberry Pi. In *Recent Trends in Information Technology (ICRTIT), 2014 International Conference on* (pp. 1-5). IEEE.

Prinz, A.C., Taank, V.K., Voegeli, V. and Walters, E.L., 2016. A novel nest-monitoring camera system using a Raspberry Pi micro-computer. *Journal of Field Ornithology*, 87(4), pp.427-435.

Quinn, A.D., Ferranti, E.J., Hodgkinson, S.P., Jack, A.C., Beckford, J. and Dora, J.M., 2018: Adaptation Becoming Business as Usual: A Framework for Climate-Change-Ready Transport Infrastructure. *Infrastructures*, 3(2), p.10.

RAIB 2012: Exeter St Davids

https://assets.publishing.service.gov.uk/media/547c8ff4e5274a4290000193/R102010_100621_Exeter_St_Davids.pdf Accessed 2019

RAIB 2014: Chester

https://assets.publishing.service.gov.uk/media/547c8fa740f0b6024400014f/R262014_141124_Chester.pdf Accessed 2019

RAIB 2016: Shalesmoor

https://assets.publishing.service.gov.uk/media/57a9b26840f0b608ab00000a/R172016_160809_Shalesmoor.pdf

RAIB, 2007: Report 25 (Part3)/2006 January 2007,

https://assets.publishing.service.gov.uk/media/547c906840f0b602440001ad/R252006_070108_Part_3_Adhesion_Review.pdf

Railway Industry Association, 2019 Williams review response

https://www.riagb.org.uk/RIA/Newsroom/Press_Releases/Rail_review.aspx Accessed 2019

Raspberry Pi 2016: <https://www.RaspberryPi.org/products/Pi-noir-camera/>, Accessed 2017

Raspberry Pi 2018: Pi NoIR camera V2, <https://www.raspberrypi.org/products/pi-noir-camera-v2/> Accessed 2018

Reid, T.D. and Essery, R.L.H., 2013. New methods to quantify canopy structure of leafless boreal birch forest from hemispherical photographs. *Open Journal of Forestry*, 3(02), p.70.

Rich, P. M. 1990: Characterizing plant canopies with hemispherical photographs. *Remote sensing reviews*, 5(1), 13-29.

Rifat, A.A., Ahmed, R., Yetisen, A.K., Butt, H., Sabouri, A., Mahdiraji, G.A., Yun, S.H. and Adikan, F.M., 2017: Photonic crystal fiber based plasmonic sensors. *Sensors and Actuators B: Chemical*, 243, pp.311-325.

Ringold, P. L., Sickle, J., Rasar, K., and Schacher, J. 2003: Use of hemispheric imagery for estimating stream solar exposure. *JAWRA Journal of the American Water Resources Association*, 39(6), 1373-1384.

Rizwan, A. M., Dennis, L. Y. and Chunho, L. I. U. 2008: A review on the generation, determination and mitigation of Urban Heat Island. *Journal of Environmental Sciences*, 20(1), 120-128.

Rolling–sliding laboratory tests of friction modifiers in leaf contaminated wheel–rail contacts. *Tribology letters*, 33(2), 97-109.

Rose, J.L. and Cho, Y., 2009: A guided wave approach to defect detection under shelling in rail. *NDT & E International*, 42(3), pp.174-180.

Rosebrock. A (2014) OpenCV and Python Color Detection, <https://www.pyimagesearch.com/2014/08/04/opencv-python-color-detection/> Accessed 2019

Ross, J. 2012: The radiation regime and architecture of plant stands (Vol. 3). Springer Science & Business Media.

RSSB 2016: Rail technology strategy solutions catalogue <https://www.rssb.co.uk/Library/research-development-and-innovation/rail-technical-strategy-solutions-catalogue.pdf> accessed 2018

RSSB 2016a: GSM-R <https://www.rssb.co.uk/rgs/rulebooks/RS523%20GSM-R%20Iss%201.pdf> Accessed 2019

RSSB 2017: Rail Capability Plan, <https://www.rssb.co.uk/rts/Documents/2017-01-27-rail-technical-strategy-capability-delivery-plan-brochure.pdf> Accessed 2018

RSSB 2018a: Adhesion Working Group <https://www.rssb.co.uk/groups-and-committees/rssb-board/technical-strategy/technical-leadership-group/system-interface-committees/vehicle-track-system-interface-committee/adhesion-research-group> Accessed 2018

RSSB 2018c: <https://www.rssb.co.uk/rgs/standards/RIS-3119-TOM%20Iss%202.pdf> Accessed 2019

RSSB, 2010 Guidance on the Fitment and Functionality of Forward and Rear Facing Cameras on Rolling Stock, <https://www.rssb.co.uk/rgs/standards/GMGN2606%20Iss%201.pdf> Accessed 2018

RSSB., 2008: Rail safety and standards board, GM/GN2642 Issue One, Guidance on Wheel / Rail Low Adhesion Measurement, <https://www.rssb.co.uk/rgs/standards/GMGN2642%20Iss%201.pdf>

RSSB., 2012: The future railway the industry's rail technical strategy 2012 supporting railway business <https://www.rssb.co.uk/Library/Future%20Railway/innovation-in-rail-rail-technical-strategy-2012.pdf> Accessed 2018

RSSB., 2014: Key train requirements, <https://www.rssb.co.uk/library/groups-and-committees/2014-09-report-key-train-requirements.pdf>

RSSB., 2015: GE/GN8540 Guidance on Low Adhesion between the Wheel and the Rail – Managing the Risk Issue Two: June 2015 Rail Industry Guidance Note for GE/RT 8040

RSSB., 2018: Adhesion <https://www.rssb.co.uk/improving-industry-performance/adhesion>

- RSSB.**, 2018b: Forecasting adhesion, <https://rssb.wavecast.io/forecasting-adhesion/projects>
[Accessed 2019](#)
- RSSB.**, 2019: Changes to low adhesion reports <https://www.rssb.co.uk/Pages/rule-book-changes-poor-adhesion-and-when-to-report-it.aspx> Accessed 2019
- RSSB.**, 2019b: ADHERE library <https://rssb.wavecast.io/forecasting-adhesion/library> Accessed 2019
- RSSB.**, 2019c ADHERE <https://www.rssb.co.uk/Pages/adhere.aspx> Accessed 2019
- RSSB.**, 2019d: Causes, risk and mitigation of station stopping incidents (T595)
<https://www.sparkrail.org/Lists/Records/DispForm.aspx?ID=9699> Accessed 2019
- RSSB.**, 2019e: Signals Past at Danger, <https://www.rssb.co.uk/Pages/signals-passed-at-danger.aspx>
- RSSB.**, 2019f: T1046 Research brief. <https://www.rssb.co.uk/library/research-development-and-innovation/research-brief-T1046.pdf>
- RSSB.**, 2019g Low-cost moisture systems. <https://www.rssb.co.uk/Pages/research-catalogue/COF-TAR-01.aspx> Accessed 2019
- Safford, L.O., Bjorkbom, J.C. and Zasada, J.C.**, 1990: *Betula papyrifera* Marsh. paper birch. *Silvics of North America*, 2(654), p.158.
- Salge, J.**, 2018: 2018 New England Fall Foliage Forecast, <https://newengland.com/today/seasons/fall/2018-new-england-fall-foliage-forecast/> Accessed 2019
- Sanchís, R., Cardona, S. and Martínez, J.**, 2019. Determination of the Vertical Vibration of a Ballasted Railway Track to Be Used in the Experimental Detection of Wheel Flats in Metropolitan Railways. *Journal of Vibration and Acoustics*, 141(2), p.021015.
- Sasaki, T., Imanishi, J., Ioki, K., Morimoto, Y. and Kitada, K.**, 2008. Estimation of leaf area index and canopy openness in broad-leaved forest using an airborne laser scanner in comparison with high-resolution near-infrared digital photography. *Landscape and Ecological Engineering*, 4(1), pp.47-55.
- Sasaki, T., Imanishi, J., Ioki, K., Morimoto, Y. and Kitada, K.**, 2008. Estimation of leaf area index and canopy openness in broad-leaved forest using an airborne laser scanner in comparison with high-resolution near-infrared digital photography. *Landscape and Ecological Engineering*, 4(1), pp.47-55.
- Schaefer, M. T., Farmer, E., Soto-Berelov, M., Woodgate, W., & Jones, S.** 2015: Overview of ground-based techniques for estimating LAI. AusCover Good Practice Guidelines: A technical handbook supporting calibration and validation activities of remotely sensed data product, 90-122.

- Schwalbe, E., Maas, H. G., Kenter, M., and Wagner, S.** 2009: Hemispheric image modeling and analysis techniques for solar radiation determination in forest ecosystems. *Journal of Photogrammetric Engineering and Remote Sensing*, 75(4), 375-384.
- Schwartz, M. D., & Reed, B. C.** 1999: Surface phenology and satellite sensor-derived onset of greenness: an initial comparison. *International Journal of Remote Sensing*, 20(17), 3451-3457.
- Schwartz, M. D., Reed, B. C., & White, M. A.** 2002: Assessing satellite-derived start-of-season measures in the conterminous USA. *International Journal of Climatology*, 22(14), 1793-1805.
- Sharma, K., Maheshwari, S., Solanki, R. and Khanna, V.,** 2014, September. Railway track breakage detection method using vibration estimating sensor network: A novel approach. In *Advances in Computing, Communications and Informatics (ICACCI, 2014 International Conference on* (pp. 2355-2362). IEEE.
- Sheeren, D., Fauvel, M., Josipović, V., Lopes, M., Planque, C., Willm, J., and Dejoux, J. F.** 2016: Tree species classification in temperate forests using Formosat-2 satellite image time series. *Journal of Remote Sensing*, 8(9), 734.
- Shinde, P.A. and Mane, Y.B.,** 2015, January. Advanced vehicle monitoring, and tracking system based on Raspberry Pi. In *Intelligent Systems and Control (ISCO), 2015 IEEE 9th International Conference on* (pp. 1-6). IEEE.
- Shinozaki, K., Yoda, K., Hozumi, K., & Kira, T.** 1964 b: A quantitative analysis of plant form-the pipe model theory: II. Further evidence of the theory and its application in forest ecology. *Japanese journal of ecology* 14(4), 133-139.
- Shinozaki, Kichiro, Kyoji Yoda, Kazuo Hozumi, & Tatu Kira.** 1964a: "A quantitative analysis of plant form-the pipe model theory: I. Basic analyses." *Japanese journal of ecology*, 14,(3). 97-105.
- Smith K.** 2015: Network Rail uses Vibrations to monitor track, *International Rail Journal*, <http://m.railjournal.com/index.php/track/network-rail-uses-vibrations-to-monitor-track.html> Accessed 2018
- Snik, F., Rietjens, J.H., Apituley, A., Volten, H., Mijling, B., Di Noia, A., Heikamp, S., Heinsbroek, R.C., Hasekamp, O.P., Smit, J.M. and Vonk, J.,** 2014: Mapping atmospheric aerosols with a citizen science network of smartphone spectropolarimeters. *Geophysical Research Letters*, 41(20), pp.7351-7358.
- Staelens, J., Nachtergale, L., Luyssaert, S. and Lust, N.** 2003: A model of wind-influenced leaf litterfall in a mixed hardwood forest. *Canadian Journal of Forest Research*, 33(2), 201-209.
- Stephenson, N.L., Das, A.J., Condit, R., Russo, S.E., Baker, P.J., Beckman, N.G., Coomes, D.A., Lines, E.R., Morris, W.K., Rüger, N. & Alvarez, E.,** 2014: Rate of tree carbon accumulation increases continuously with tree size. *Nature*, 507(7490), pp.90-93.
- Stevens, M. and D'Hondt, E.,** 2010: September. Crowdsourcing of pollution data using smartphones. In *Workshop on Ubiquitous Crowdsourcing* (pp. 1-4).
- Steyn, D. G.** 1980: The calculation of view factors from fisheye-lens photographs: Research note. 254-258

- Svensson, M.K.**, 2004. Sky view factor analysis—implications for urban air temperature differences. *Meteorological applications*, 11(3), pp.201-211.
- Tai, Y.W., Du, H., Brown, M.S. and Lin, S.**, 2010: Correction of spatially varying image and video motion blur using a hybrid camera. *IEEE Transactions on Pattern Analysis and Machine Intelligence*, 32(6), pp.1012-1028.
- Tandon, N. and Choudhury, A.**, 1999: A review of vibration and acoustic measurement methods for the detection of defects in rolling element bearings. *Tribology international*, 32(8), pp.469-480.
- Thommesen, J., Duijm, N. J., & Andersen, H. B.** 2014: *Management of low adhesion on railway tracks in European countries*. DTU Management Engineering.
- Thornes, J. E., Davis, B. W.** 2002: Mitigating the impact of weather and climate on railway operations in the UK. In *Railroad Conference, 2002 ASME/IEEE Joint* (pp. 29-38). IEEE.
- Thornes, J., & Chapman, L.** 2008: The Next Generation Road Weather Information System: A new paradigm for road and rail severe weather prediction in the UK. *Geography Compass*, 2(4), 1012-1026.
- Tichý, L.** 2015: Field test of canopy cover estimation by hemispherical photographs taken with a smartphone. *Journal of Vegetation Science*.
- Tico, M., Trimeche, M. and Vehvilainen, M.**, 2006: Motion blur identification based on differently exposed images. In *Image Processing, 2006 IEEE International Conference on Image processing* (pp. 2021-2024). IEEE.
- Tien, C.L., Lin, H.Y. and Su, S.H.**, 2018: High Sensitivity Refractive Index Sensor by D-Shaped Fibers and Titanium Dioxide Nanofilm. *Advances in Condensed Matter Physics, 2018*.
- Tiwari, S., Shukla, V.P., Singh, A.K. and Biradar, S.R.**, 2013: Review of motion blur estimation techniques. *Journal of Image and Graphics*, 1(4), pp.176-184.
- Tobin, B., Black, K., Osborne, B., Reidy, B., Bolger, T., & Nieuwenhuis, M.** 2006: Assessment of allometric algorithms for estimating leaf biomass, leaf area index and litter fall in different-aged Sitka spruce forests. *Forestry*, 79(4), 453-465.
- Tsai, M. J., Lai, C., & Liu, J.** 2007: Camera/mobile phone source identification for digital forensics. In *Acoustics, Speech and Signal Processing, 2007. ICASSP 2007. IEEE International Conference on* (Vol. 2, pp. II-221). IEEE.
- Tucker, Compton J., Jorge E. Pinzon, Molly E. Brown, Daniel A. Slayback, Edwin W. Pak, Robert Mahoney, Eric F. Vermote, and Nazmi El Saleous.** 2005: An extended AVHRR 8-km NDVI dataset compatible with MODIS and SPOT vegetation NDVI data, *International Journal of Remote Sensing* 26, (20) 4485-4498.
- Turner, D. P., Cohen, W. B., Kennedy, R. E., Fassnacht, K. S., and Briggs, J. M.** 1999: Relationships between leaf area index and Landsat TM spectral vegetation indices across three temperate zone sites. *Remote sensing of environment*, 70(1), 52-68.
- Turner, E. L., Hill, W. A., and Wilson, D. L.** 2001: U.S. Patent No. 6,198,505. Washington, DC: U.S. Patent and Trademark Office.

Unger, J., 2004. Intra-urban relationship between surface geometry and urban heat island: review and new approach. *Climate research*, 27(3), pp.253-264.

Unger, J., 2004. Intra-urban relationship between surface geometry and urban heat island: review and new approach. *Climate research*, 27(3), pp.253-264.

Unger, J., 2009. Connection between urban heat island and sky view factor approximated by a software tool on a 3D urban database. *International Journal of Environment and Pollution*, 36(1), pp.59-80.

Unger, J., 2009. Connection between urban heat island and sky view factor approximated by a software tool on a 3D urban database. *International Journal of Environment and Pollution*, 36(1), pp.59-80.

Uputronics, 2018: Raspberry Pi GPS expansion board,
https://store.uputronics.com/index.php?route=product/product&path=60_64&product_id=81
accessed 2018

Urquhart, B., Kurtz, B., Dahlin, E., Ghonima, M., Shields, J. E., and Kleissl, J. 2014: Development of a sky imaging system for short-term solar power forecasting. *Atmospheric Measurement Techniques Discussions*, 7, 4859-4907.

UUGEAR. 2018: Witty Pi 2 manual, http://www.uugear.com/doc/WittyPi2_UserManual.pdf
Accessed 2018

Valle, B., Simonneau, T., Boulord, R., Sourd, F., Frisson, T., Ryckewaert, M., Hamard, P., Brichet, N., Dautat, M. and Christophe, A: 2017. PYM: a new, affordable, image-based method using a Raspberry Pi to phenotype plant leaf area in a wide diversity of environments. *Plant methods*, 13(1), p.98.

Van Emmerik, T., Steele-Dunne, S., Hut, R., Gentine, P., Guerin, M., Oliveira, R.S., Wagner, J., Selker, J. & van de Giesen, N., 2017: Measuring Tree Properties and Responses Using Low-Cost Accelerometers. *Sensors*, 17(5), p.1098.

Van Hees, A.F.M., 1997: Growth and morphology of pedunculate oak (*Quercus robur* L) and beech (*Fagus sylvatica* L) seedlings in relation to shading and drought. In *Annales des Sciences Forestières* (Vol. 54, No. 1, pp. 9-18). EDP Sciences.

Van Leeuwen, W. J., Orr, B. J., Marsh, S. E., and Herrmann, S. M. 2006: Multi-sensor NDVI data continuity: Uncertainties and implications for vegetation monitoring applications. *Remote sensing of environment*, 100(1), 67-81.

Vannoppen, W., Poesen, J., Peeters, P., De Baets, S. and Vandevorde, B., 2016. Root properties of vegetation communities and their impact on the erosion resistance of river dikes. *Earth Surface Processes and Landforms*, 41(14), pp.2038-2046.

Varley 2018: Valuing nature
https://assets.publishing.service.gov.uk/government/uploads/system/uploads/attachment_data/file/759698/valuing-nature_a-railway-for-people-and-wildlife-the-network-rail-vegetation-management-review.pdf

Vijayakumar, N. and Ramya, R., 2015, March. The real time monitoring of water quality in IoT environment. In *2015 International Conference on Innovations in Information, Embedded and Communication Systems (ICIIECS)* (pp. 1-5). IEEE.

Vijayakumar, N. and Ramya, R., 2015, March. The real time monitoring of water quality in IoT environment. In *2015 International Conference on Innovations in Information, Embedded and Communication Systems (ICIIECS)* (pp. 1-5). IEEE.

Wagner, S., and **Hagemeier, M.** 2006: Method of segmentation affects leaf inclination angle estimation in hemispherical photography. *Journal of Agricultural and Forest Meteorology*, 139(1), 12-24.

Walter, J. M. N., & Torquebiau, E. F. 2000: The computation of forest leaf area index on slope using fish-eye sensors. *Comptes Rendus de l'Academie des Sciences-Series III-Sciences de la Vie*, 323(9), 801-813.

Wang, M.M., Chen, H.S., Fu, T.G., Zhang, W. and Wang, K.L., 2016: Differences of soil nutrients among different vegetation types and their spatial prediction in a small typical karst catchment. *Ying yong sheng tai xue bao= The journal of applied ecology*, 27(6), pp.1759-1766.

Wang, P., Zhao, Z., Xu, C., Wu, Z. and Luo, Y., 2010: Design and implementation of the low-power tracking system based on GPS-GPRS module. In *Industrial Electronics and Applications (ICIEA), 2010 the 5th IEEE Conference on* (pp. 207-210). IEEE.

Wang, W.J., Wang, H., Wang, H.Y., Guo, J., Liu, Q.Y., Zhu, M.H. and Jin, X.S., 2013: Sub-scale simulation and measurement of railroad wheel/rail adhesion under dry and wet conditions. *Wear*, 302(1-2), pp.1461-1467.

Wang, Y. and Akbari, H., 2014. Effect of sky view factor on outdoor temperature and comfort in Montreal. *Environmental Engineering Science*, 31(6), pp.272-287.

Wang, Y. and Akbari, H., 2014. Effect of sky view factor on outdoor temperature and comfort in Montreal. *Environmental Engineering Science*, 31(6), pp.272-287.

Ward, C. P., Goodall, R. M., Dixon, R., & Charles, G. 2010: Condition monitoring of rail vehicle bogies. In *Control 2010, UKACC International Conference on* (pp. 1-6). IET.

Waring, R. H., Schroeder, P. E., & Oren, R. 1982: Application of the pipe model theory to predict canopy leaf area. *Canadian Journal of Forest Research*, 12(3), 556-560.

Watson, I. D., and **Johnson, G. T.** 1987: Graphical estimation of sky view-factors in urban environments. *Journal of Climatology*, 7(2), 193-197.

Watson, I.D. and Johnson, G.T., 1987. Graphical estimation of sky view-factors in urban environments. *Journal of climatology*, 7(2), pp.193-197.

Weekes, L., FitzPatrick, Ú., Kelly, F., Matson, R. and Kelly-Quinn, M., 2018: A review of the Irish River Vegetation Database: informing future river macrophyte surveying. In *Biology and Environment: Proceedings of the Royal Irish Academy* (Vol. 118, No. 2, pp. 81-112). Royal Irish Academy.

- Weiss, M., Baret, F., Smith, G. J., Jonckheere, I., & Coppin, P.** 2004: Review of methods for in situ leaf area index (LAI) determination: Part II. Estimation of LAI, errors and sampling. *Agricultural and Forest Meteorology*, 121(1), 37-53.
- Welles, J. M., & Cohen, S.** 1996: Canopy structure measurement by gap fraction analysis using commercial instrumentation. *Journal of Experimental Botany*, 47(9), 1335-1342.
- West Midlands Railways** 2018: Leaf fall time table <https://www.westmidlandsrailway.co.uk/about-us/news-desk/improved-leaf-fall-timetable-cross-city-commuters-autumn>
- Wheeler, L.N., Pannese, E., Hoult, N.A., Take, W.A. and Le, H.,** 2018: Measurement of distributed dynamic rail strains using a Rayleigh backscatter based fiber optic sensor: Lab and field evaluation. *Transportation Geotechnics*, 14, pp.70-80.
- White, B.,** 2018. *Using Tribo-Chemistry Analysis to Understand Low Adhesion in the Wheel-Rail Contact* (Doctoral dissertation, University of Sheffield).
- White, B.T., Nilsson, R., Olofsson, U., Arnall, A.D., Evans, M.D., Armitage, T., Fisk, J., Fletcher, D.I. and Lewis, R.,** 2018: Effect of the presence of moisture at the wheel–rail interface during dew and damp conditions. *Proceedings of the Institution of Mechanical Engineers, Part F: Journal of Rail and Rapid Transit*, 232(4), pp.979-989.
- Whitford, K.R., Colquhoun, I.J., Lang, A.R.G. and Harper, B.M.,** 1995: Measuring leaf area index in a sparse eucalypt forest: a comparison of estimates from direct measurement, hemispherical photography, sunlight transmittance and allometric regression. *Agricultural and Forest Meteorology*, 74(3-4), pp.237-249.
- Wilkes, T., McGonigle, A., Pering, T., Taggart, A., White, B., Bryant, R. and Willmott, J.,** 2016: Ultraviolet imaging with low cost smartphone sensors: Development and application of a raspberry Pi-based UV camera. *Sensors*, 16(10), p.1649.
- Willats, W.G., Knox, J.P. and Mikkelsen, J.D.,** 2006: Pectin: new insights into an old polymer are starting to gel. *Trends in Food Science & Technology*, 17(3), pp.97-104.
- Woodland Trust.** 2017: Natures Calendar Autumn Seasonal Report, <https://naturescalendar.woodlandtrust.org.uk/media/1681/2016-autumn.pdf> Accessed 2017
- Woodlands Trust.,** 2019: A-Z of British Trees <https://www.woodlandtrust.org.uk/trees-woods-and-wildlife/british-trees/a-z-of-british-trees>
- Wu, T.X. and Thompson, D.J.,** 2002. A hybrid model for the noise generation due to railway wheel flats. *Journal of Sound and Vibration*, 251(1), pp.115-139.
- Wu, Y.M., Chen, D.Y., Lin, T.L., Hsieh, C.Y., Chin, T.L., Chang, W.Y., Li, W.S. & Ker, S.H.** 2013: A high-density seismic network for earthquake early warning in Taiwan based on low-cost sensors. *Seismological Research Letters*, 84(6), pp.1048-1054.
- Xia, F., Yang, L. T., Wang, L., & Vinel, A.** 2012: Internet of things. *International Journal of Communication Systems*, 25(9), 1101.

- Zarate-Valdez, J.L., Whiting, M.L., Lampinen, B.D., Metcalf, S., Ustin, S.L. and Brown, P.H.,** 2012. Prediction of leaf area index in almonds by vegetation indexes. *Computers and electronics in agriculture*, 85, pp.24-32.
- Zhang, W., Chen, J., Wu, X., & Jin, X.** 2002: Wheel/rail adhesion and analysis by using full scale roller rig. *Wear*, 253(1), 82-88.
- Zhang, X., Friedl, M.A., Schaaf, C.B., Strahler, A.H., Hodges, J.C., Gao, F., Reed, B.C. and Huete, A.** 2003: Monitoring vegetation phenology using MODIS. *Remote sensing of environment*, 84(3), .471-475.
- Zhang, Y., Chen, J.M. and Miller, J.R.,** 2005. Determining digital hemispherical photograph exposure for leaf area index estimation. *Agricultural and Forest Meteorology*, 133(1-4), pp.166-181.
- Zhang, Y.J. and Lee, S.,** 2008: Modelling Rail Temperature with Real-Time Weather Data. *Surface Transportation Weather and Snow Removal and Ice Control Technology*, p.37.
- Zhu, Y., Olofsson, U. and Nilsson, R.** 2014: A field test study of leaf contamination on railhead surfaces. Proceedings of the Institution of Mechanical Engineers, Part F: Journal of Rail and Rapid Transit, 228(1), pp.71-84.
- Zipper, S.C., Schatz, J., Singh, A., Kucharik, C.J., Townsend, P.A. and Loheide II, S.P.,** 2016: Urban heat island impacts on plant phenology: Intra-urban variability and response to land cover. *Environmental Research Letters*, 11(5), p.054023.
- Zumpano, G. and Meo, M.,** 2006: A new damage detection technique based on wave propagation for rails. *International journal of solids and structures*, 43(5), pp.10

Appendix One

Prototype Sky-View factor code using a multi colour threshold approach

#Import mathematic code software programs available in python

1. import numpy as np
2. import argparse
3. import numpy, Image
4. import PIL
5. import math
6. import cv2
7. from array import array
8. import matplotlib.pyplot as plt
9. import matplotlib.image as mpimg
10. import PIL.ImageDraw as ImageDraw, PIL.Image as Image, PIL.ImageShow as ImageShow
11. from PIL import Image
12. from collections import Counter
13. import time, os, fnmatch, shutil
14. t = time.localtime()
15. date=time.strftime('%b-%d-%Y_%H%M',t)

#load captured image into the python code

16. #load timelapse image
17. #gray one channel
18. def rgb2gray(rgb):
19. return np.dot(rgb[...,:3], [0.299, 0.587, 0.114])
20. #load timelapse image convert to binary
21. imga = Image.open("timelapse.jpg")
22. img = np.array(imga)

#Define red boundary threshold and create a binary image

23. #pick out leaf pixels
24. # define the list of boundaries this was done on image j looking at pixel range of leaves
this can be altered in analysis based on light glare and building obstruction
25. boundaries = [
26. ([30, 25, 255], [90, 66, 255]),
27. ([96, 28, 4],[255, 88, 50]),
28. ([35, 136, 255], [72, 164, 255]),
29. ([90, 90, 65], [165, 130, 110])]
30. for (lower, upper) in boundaries:
 - a. lower = np.array(lower, dtype = "uint8")
 - b. upper = np.array(upper, dtype = "uint8")
31. mask = cv2.inRange(img, lower, upper)
32. output = cv2.bitwise_and(img, img, mask = mask)
33. cv2.imwrite("redimage.jpg", np.hstack([output]))
34. #convert to binary
35. image1=Image.open("redimage.jpg")

```

36. gray = image1.convert('L')
37. bw=np.asarray(gray).copy()
38. bw[bw< 50]=0 #black pixels
39. bw[bw> 50]=255 #whie pixelsd
40. imbw= Image.fromarray(bw)

```

#Make binary image into an array in order to calculate percentage of pixels and save image

```

41. tester=numpy.asarray(imbw)
42. #Change into a numpy array
43. npimage=np.array(tester)
44. mask=tester>0
45. coords=np.transpose(np.nonzero(mask))
46. y0,x0 = coords.min(axis=0)
47. y1,x1 = coords.max(axis=0)
48. cropped=tester[y0:y1,x0:x1]
49. cv2.imwrite("timelapse-time"+ ".jpg", np.hstack([cropped]))

```

Create annulus mask based on Chapman (2001) 9 ring recommendation and calculate total black pixels in masked image

```

50. #creating hemispherical rings and mask of image
51. #image a
52. im = Image.new("RGB", (2000,2000))
53. width = 2000
54. height = 2000
55. ax, ay = im.size
56. eX, eY = 2000, 2000 #Size of Bounding Box for ellipse
57. bbox=(ax/2 - eX/2, ay/2 - eY/2, ax/2 + eX/2, ay/2 + eY/2)
58. draw = ImageDraw.Draw(im)
59. draw.ellipse((bbox),fill=(255,255,255))
60. mask=im>0
61. npimage=np.array(im)
62. inverta=cv2.bitwise_not(npimage)
63. cv2.imwrite("inverta"+ ".jpg", np.hstack([inverta]))
64. background=(Image.open("timelapse-time.jpg").convert("L"))
65. foreground=(Image.open("inverta.jpg").convert("L"))
66. foreground_width=2000
67. foreground_height=2000
68. background_resizea=background.resize((foreground_width,foreground_height),Image.ANTIALIAS)
69. bga=np.array(background_resizea)
70. fga=np.array(foreground)
71. resulta=np.maximum(bga,fga)
72. Image.fromarray(resulta).save("resulta.jpg")
73. TP = width * height
74. im_gray = cv2.imread("inverta.jpg", cv2.CV_LOAD_IMAGE_GRAYSCALE)
75. thresh=127
76. imginvert=cv2.threshold(im_gray,thresh,255, cv2.THRESH_BINARY)[1]
77. blackpix = cv2.countNonZero(imginvert)

```

```

78. pixelstot1= TP - blackpix
79. pixelstotw = TP - pixelstot1
80. pixelresultw_a=cv2.countNonZero (resulta)
81. test= (float (pixelresultw_a - pixelstotw))/(float (pixelstot1)))
82. part1= (float (pixelstot1)- (float (pixelresultw_a - pixelstotw)))

‘ repeat process for each annuli (a-i)

83. #image b
84. im = Image.new("RGB", (2000,2000))
85. ax, ay = im.size
86. eX, eY = 1800, 1800 #Size of Bounding Box for ellipse
87. bbox=(ax/2 - eX/2, ay/2 - eY/2, ax/2 + eX/2, ay/2 + eY/2)
88. draw = ImageDraw.Draw(im)
89. draw.ellipse((bbox),fill=(255,255,255))
90. mask=im>0
91. npimage=np.array(im)
92. invertb=cv2.bitwise_not(npimage)
93. cv2.imwrite("invertb"+ ".jpg", np.hstack([invertb]))
94. backgroundb=(Image.open("timelapse-time.jpg").convert("L"))
95. foregroundb=(Image.open("invertb.jpg").convert("L"))
96. foreground_width=2000
97. foreground_height=2000
98. background_resizeb=background.resize((foreground_width,foreground_height),Image.A
    NTIALIAS)
99. bgb=np.array(background_resizeb)
100. fgb=np.array(foregroundb)
101. resultb=np.maximum(bgb,fgb)
102. Image.fromarray(resultb).save("resultb.jpg")
103. TPb = width * height
104. im_grayb = cv2.imread("invertb.jpg", cv2.CV_LOAD_IMAGE_GRAYSCALE)
105. thresh=127
106. imginvertb=cv2.threshold(im_grayb,thresh,255, cv2.THRESH_BINARY)[1]
107. blackpixb = cv2.countNonZero(imginvertb)
108. pixelstotb= TPb - blackpixb
109. pixelstotwb = TPb - pixelstotb
110. pixelresultw_b=cv2.countNonZero (resultb)
111. testb= (float (pixelresultw_b - pixelstotwb))/(float (pixelstotb)))
112. part1b= (float (pixelstotb)- (float (pixelresultw_b - pixelstotwb)))
113. #image c
114. im = Image.new("RGB", (2000,2000))
115. bx, by = im.size
116. cX, cY = 1600, 1600 #Size of Bounding Box for ellipse
117. bbox=(bx/2 - cX/2, by/2 - cY/2, bx/2 + cX/2, by/2 + cY/2)
118. draw = ImageDraw.Draw(im)
119. draw.ellipse((bbox),fill=(255,255,255))
120. mask=im>0
121. npimage=np.array(im)
122. invertc=cv2.bitwise_not(npimage)
123. cv2.imwrite("invertc"+ ".jpg", np.hstack([invertc]))

```

```

124.     background=(Image.open("timelapse-time.jpg").convert("L"))
125.     foregroundc=(Image.open("invertc.jpg").convert("L"))
126.     foreground_width=2000
127.     foreground_height=2000
128.     background_resizec=background.resize((foreground_width,foreground_height),I
mage.ANTIALIAS)
129.     bgc=np.array(background_resizec)
130.     fgc=np.array(foregroundc)
131.     resultc=np.maximum(bgc,fgc)
132.     Image.fromarray(resultc).save("resultc.jpg")
133.     TPc = width * height
134.     im_grayc = cv2.imread("invertc.jpg", cv2.CV_LOAD_IMAGE_GRAYSCALE)
135.     thresh=127
136.     imginvertc=cv2.threshold(im_grayc,thresh,255, cv2.THRESH_BINARY)[1]
137.     blackpixc= cv2.countNonZero(imginvertc)
138.     pixelstotc= TPc - blackpixc
139.     pixelstotwc = TPc - pixelstotc
140.     pixelresultw_c=cv2.countNonZero (resultc)
141.     testc= (float (pixelresultw_c - pixelstotwc)/(float (pixelstotc)))
142.     part1c= (float (pixelstotc)- (float (pixelresultw_c - pixelstotwc)))
143.     #image d
144.     im = Image.new("RGB", (2000,2000))
145.     bx, by = im.size
146.     cX, cY = 1400, 1400 #Size of Bounding Box for ellipse
147.     bbox =(bx/2 - cX/2, by/2 - cY/2, bx/2 + cX/2, by/2 + cY/2)
148.     draw = ImageDraw.Draw(im)
149.     draw.ellipse((bbox),fill=(255,255,255))
150.     mask=im>0
151.     npimage=np.array(im)
152.     invertd=cv2.bitwise_not(npimage)
153.     cv2.imwrite("invertd"+ ".jpg", np.hstack([invertd]))
154.     backgroundd=(Image.open("timelapse-time.jpg").convert("L"))
155.     foregrounddd=(Image.open("invertd.jpg").convert("L"))
156.     foreground_width=2000
157.     foreground_height=2000
158.     background_resized=background.resize((foreground_width,foreground_height),I
mage.ANTIALIAS)
159.     bgd=np.array(background_resized)
160.     fgd=np.array(foregrounddd)
161.     resultd=np.maximum(bgd,fgd)
162.     Image.fromarray(resultd).save("resultd.jpg")
163.     TPd = width * height
164.     im_grayd = cv2.imread("invertd.jpg", cv2.CV_LOAD_IMAGE_GRAYSCALE)
165.     thresh=127
166.     imginvertd=cv2.threshold(im_grayd,thresh,255, cv2.THRESH_BINARY)[1]
167.     blackpixd= cv2.countNonZero(imginvertd)
168.     pixelstotd= TPd - blackpixd
169.     pixelstotwd = TPd - pixelstotd
170.     pixelresultw_d=cv2.countNonZero (resultd)

```

```

171.     testd= (float (pixelresultw_d - pixelstotwd))/(float (pixelstotd))
172.     part1d= (float (pixelstotd)- (float (pixelresultw_d - pixelstotwd)))
173.     #image e
174.     im = Image.new("RGB", (2000,2000))
175.     bx, by = im.size
176.     cX, cY = 1200, 1200 #Size of Bounding Box for ellipse
177.     bbox =(bx/2 - cX/2, by/2 - cY/2, bx/2 + cX/2, by/2 + cY/2)
178.     draw = ImageDraw.Draw(im)
179.     draw.ellipse((bbox),fill=(255,255,255))
180.     mask=im>0
181.     npimage=np.array(im)
182.     invert=cv2.bitwise_not(npimage)
183.     cv2.imwrite("invert"+" .jpg", np.hstack([invert]))
184.     background=(Image.open("timelapse-time.jpg").convert("L"))
185.     foreground=(Image.open("invert.jpg").convert("L"))
186.     foreground_width=2000
187.     foreground_height=2000
188.     background_resizee=background.resize((foreground_width,foreground_height),I
image.ANTIALIAS)
189.     bge=np.array(background_resizee)
190.     fge=np.array(foregrounde)
191.     resulte=np.maximum(bge,fge)
192.     Image.fromarray(resulte).save("resulte.jpg")
193.     TPe = width * height
194.     im_graye = cv2.imread("invert.jpg", cv2.CV_LOAD_IMAGE_GRAYSCALE)
195.     thresh=127
196.     imginverte=cv2.threshold(im_graye,thresh,255, cv2.THRESH_BINARY)[1]
197.     blackpixe= cv2.countNonZero(imginverte)
198.     pixelstote= TPe - blackpixe
199.     pixelstotwe = TPe - pixelstote
200.     pixelresultw_e=cv2.countNonZero (resulte)
201.     teste= (float (pixelresultw_e - pixelstotwe))/(float (pixelstote))
202.     part1e= (float (pixelstote)- (float (pixelresultw_e - pixelstotwe)))
203.     #image f
204.     im = Image.new("RGB", (2000,2000))
205.     bx, by = im.size
206.     cX, cY = 1000, 1000 #Size of Bounding Box for ellipse
207.     bbox =(bx/2 - cX/2, by/2 - cY/2, bx/2 + cX/2, by/2 + cY/2)
208.     draw = ImageDraw.Draw(im)
209.     draw.ellipse((bbox),fill=(255,255,255))
210.     mask=im>0
211.     npimage=np.array(im)
212.     invertf=cv2.bitwise_not(npimage)
213.     cv2.imwrite("invertf"+" .jpg", np.hstack([invertf]))
214.     backgroundf=(Image.open("timelapse-time.jpg").convert("L"))
215.     foregroundf=(Image.open("invertf.jpg").convert("L"))
216.     foreground_width=2000
217.     foreground_height=2000

```

```

218.     background_resizef=background.resize((foreground_width,foreground_height),I
mage.ANTIALIAS)
219.     bgf=np.array(background_resizef)
220.     fgf=np.array(foregroundf)
221.     resultf=np.maximum(bgf,fgf)
222.     Image.fromarray(resultf).save("resultf.jpg")
223.     TPf = width * height
224.     im_grayf = cv2.imread("invertf.jpg", cv2.CV_LOAD_IMAGE_GRAYSCALE)
225.     thresh=127
226.     imginvertf=cv2.threshold(im_grayf,thresh,255, cv2.THRESH_BINARY)[1]
227.     blackpixf= cv2.countNonZero(imginvertf)
228.     pixelstotf= TPf - blackpixf
229.     pixelstotwf = TPf - pixelstotf
230.     pixelresultw_f=cv2.countNonZero (resultf)
231.     testf= (float (pixelresultw_f - pixelstotwf)/(float (pixelstotf)))
232.     part1f= (float (pixelstotf)- (float (pixelresultw_f - pixelstotwf)))
233.     #image g
234.     im = Image.new("RGB", (2000,2000))
235.     bx, by = im.size
236.     cX, cY = 800, 800 #Size of Bounding Box for ellipse
237.     bbox=(bx/2 - cX/2, by/2 - cY/2, bx/2 + cX/2, by/2 + cY/2)
238.     draw = ImageDraw.Draw(im)
239.     draw.ellipse((bbox),fill=(255,255,255))
240.     mask=im>0
241.     npimage=np.array(im)
242.     invertg=cv2.bitwise_not(npimage)
243.     cv2.imwrite("invertg"+ ".jpg", np.hstack([invertg]))
244.     backgroundg=(Image.open("timelapse-time.jpg").convert("L"))
245.     foregroundg=(Image.open("invertg.jpg").convert("L"))
246.     foreground_width=2000
247.     foreground_height=2000
248.     background_resizeg=background.resize((foreground_width,foreground_height),I
mage.ANTIALIAS)
249.     bgg=np.array(background_resizeg)
250.     fgg=np.array(foregroundg)
251.     resultg=np.maximum(bgg,fgg)
252.     Image.fromarray(resultg).save("resultg.jpg")
253.     TPg = width * height
254.     im_grayg = cv2.imread("invertg.jpg", cv2.CV_LOAD_IMAGE_GRAYSCALE)
255.     thresh=127
256.     imginvertg=cv2.threshold(im_grayg,thresh,255, cv2.THRESH_BINARY)[1]
257.     blackpixg= cv2.countNonZero(imginvertg)
258.     pixelstotg= TPg - blackpixg
259.     pixelstotwg = TPg - pixelstotg
260.     pixelresultw_g=cv2.countNonZero (resultg)
261.     testg= (float (pixelresultw_g - pixelstotwg)/(float (pixelstotg)))
262.     part1g= (float (pixelstotg)- (float (pixelresultw_g - pixelstotwg)))
263.     #image h
264.     im = Image.new("RGB", (2000,2000))

```

```

265.     bx, by = im.size
266.     cX, cY = 600, 600 #Size of Bounding Box for ellipse
267.     bbox =(bx/2 - cX/2, by/2 - cY/2, bx/2 + cX/2, by/2 + cY/2)
268.     draw = ImageDraw.Draw(im)
269.     draw.ellipse((bbox),fill=(255,255,255))
270.     mask=im>0
271.     npimage=np.array(im)
272.     inverth=cv2.bitwise_not(npimage)
273.     cv2.imwrite("inverth"+ ".jpg", np.hstack([inverth]))
274.     backgroundh=(Image.open("timelapse-time.jpg").convert("L"))
275.     foregroundh=(Image.open("inverth.jpg").convert("L"))
276.     foreground_width=2000
277.     foreground_height=2000
278.     background_resizeh=background.resize((foreground_width,foreground_height),I
mage.ANTIALIAS)
279.     bgh=np.array(background_resizeh)
280.     fgh=np.array(foregroundh)
281.     resulth=np.maximum(bgh,fgh)
282.     Image.fromarray(resulth).save("resulth.jpg")
283.     TPh = width * height
284.     im_grayh = cv2.imread("inverth.jpg", cv2.CV_LOAD_IMAGE_GRAYSCALE)
285.     thresh=127
286.     imginverth=cv2.threshold(im_grayh,thresh,255, cv2.THRESH_BINARY)[1]
287.     blackpixh= cv2.countNonZero(inginverth)
288.     pixelstoth= TPh - blackpixh
289.     pixelstotwh = TPh - pixelstoth
290.     pixelresultw_h=cv2.countNonZero (resulth)
291.     testh= (float (pixelresultw_h - pixelstotwh))/(float (pixelstoth))
292.     part1h= (float (pixelstoth)- (float (pixelresultw_h - pixelstotwh)))
293.     #image i
294.     im = Image.new("RGB", (2000,2000))
295.     bx, by = im.size
296.     cX, cY = 400, 400 #Size of Bounding Box for ellipse
297.     bbox =(bx/2 - cX/2, by/2 - cY/2, bx/2 + cX/2, by/2 + cY/2)
298.     draw = ImageDraw.Draw(im)
299.     draw.ellipse((bbox),fill=(255,255,255))
300.     mask=im>0
301.     npimage=np.array(im)
302.     inverti=cv2.bitwise_not(npimage)
303.     cv2.imwrite("inverti"+ ".jpg", np.hstack([inverti]))
304.     backgroundi=(Image.open("timelapse-time.jpg").convert("L"))
305.     foregroundi=(Image.open("inverti.jpg").convert("L"))
306.     foreground_width=2000
307.     foreground_height=2000
308.     background_resizei=background.resize((foreground_width,foreground_height),I
mage.ANTIALIAS)
309.     bgi=np.array(background_resizei)
310.     fgi=np.array(foregroundi)
311.     resulti=np.maximum(bgi,fgi)

```

```

312.     Image.fromarray(resulti).save("resulti.jpg")
313.     TPi = width * height
314.     im_grayi = cv2.imread("inverti.jpg", cv2.CV_LOAD_IMAGE_GRAYSCALE)
315.     thresh=127
316.     imginverti=cv2.threshold(im_grayi,thresh,255, cv2.THRESH_BINARY)[1]
317.     blackpixi= cv2.countNonZero(imginverti)
318.     pixelstoti= TPi - blackpixi
319.     pixelstotwi = TPi - pixelstoti
320.     pixelresultw_i=cv2.countNonZero (resulti)
321.     testi= (float (pixelresultw_i - pixelstotwi))/(float (pixelstoti))
322.     part1i= (float (pixelstoti)- (float (pixelresultw_i - pixelstotwi)))
323.     #Ttot -Tobs / ring radius2 stein equations

# Calculate the difference in masked black ring and image, using equation 2.3 calculate the
# Sky view factor for each ring

324.     #SVF RING EQUATIONS
325.     #Ringa = imagea - imageb
326.     ring1= part1 - part1b
327.     radiusringa= ((math.pi * (1000*1000)) - (math.pi * (900*900)))
328.     part2= ring1/radiusringa
329.     part3= part2/(2*math.pi)
330.     z1=numpy.cos(90)
331.     svfmax=(numpy.pi/2)*((numpy.sin(numpy.pi * ((1-0.5)/(2 * 9))))*
    (numpy.cos(numpy.pi * ((1-0.5)/(2 * 9)))))
332.     totSVF= svfmax * part3
333.     #ring b
334.     ringb= part1b - part1c
335.     radiusringb= ((math.pi * (900*900)) - (math.pi * (800*800)))
336.     part2b= ringb/radiusringb
337.     part3b= part2b/(2*math.pi)
338.     z1=numpy.cos(90)
339.     svfmax=(numpy.pi/2)*((numpy.sin(numpy.pi * ((2-0.5)/(2 * 9))))*
    (numpy.cos(numpy.pi * ((2-0.5)/(2 * 9)))))
340.     totSVFb= svfmax * part3b
341.     #ring c
342.     ringc= part1c - part1d
343.     radiusringc= ((math.pi * (800*800)) - (math.pi * (700*700)))
344.     part2c= ringc/radiusringc
345.     part3c= part2c/(2*math.pi)
346.     z1=numpy.cos(90)
347.     svfmax=(numpy.pi/2)*((numpy.sin(numpy.pi * ((3-0.5)/(2 * 9))))*
    (numpy.cos(numpy.pi * ((3-0.5)/(2 * 9)))))
348.     totSVFc= svfmax * part3c
349.     #ring d
350.     ringd= part1d - part1e
351.     radiusringd= ((math.pi * (700*700)) - (math.pi * (600*600)))
352.     part2d= ringd/radiusringd

```

```

353.     part3d= part2d/(2*math.pi)
354.     z1=numpy.cos(90)
355.     svfmax=(numpy.pi/2)*((numpy.sin(numpy.pi * ((4-0.5)/(2 * 9))))*
      (numpy.cos(numpy.pi * ((4-0.5)/(2 * 9))))))
356.     totSVFd= svfmax * part3d
357.     #ring e
358.     ringe= part1e - part1f
359.     radiusringe= ((math.pi * (600*600)) - (math.pi * (500*500)))
360.     part2e= ringe/radiusringe
361.     part3e= part2e/(2*math.pi)
362.     z1=numpy.cos(90)
363.     svfmax=(numpy.pi/2)*((numpy.sin(numpy.pi * ((5-0.5)/(2 * 9))))*
      (numpy.cos(numpy.pi * ((5-0.5)/(2 * 9))))))
364.     totSVFe= svfmax * part3e
365.     #ring f
366.     ringf= part1f - part1g
367.     radiusringf= ((math.pi * (500*500)) - (math.pi * (400*400)))
368.     part2f= ringf/radiusringf
369.     part3f= part2f/(2*math.pi)
370.     z1=numpy.cos(90)
371.     svfmax=(numpy.pi/2)*((numpy.sin(numpy.pi * ((6-0.5)/(2 * 9))))*
      (numpy.cos(numpy.pi * ((6-0.5)/(2 * 9))))))
372.     totSVFf= svfmax * part3f
373.     #ring g
374.     ringg= part1g - part1h
375.     radiusringg= ((math.pi * (400*400)) - (math.pi * (300*300)))
376.     part2g= ringg/radiusringg
377.     part3g= part2g/(2*math.pi)
378.     z1=numpy.cos(90)
379.     svfmax=(numpy.pi/2)*((numpy.sin(numpy.pi * ((7-0.5)/(2 * 9))))*
      (numpy.cos(numpy.pi * ((7-0.5)/(2 * 9))))))
380.     totSVFg= svfmax * part3g
381.     #ring h
382.     ringh= part1h - part1i
383.     radiusringh= ((math.pi * (300*300)) - (math.pi * (200*200)))
384.     part2h= ringh/radiusringh
385.     part3h= part2h/(2*math.pi)
386.     z1=numpy.cos(90)
387.     svfmax=(numpy.pi/2)*((numpy.sin(numpy.pi * ((8-0.5)/(2 * 9))))*
      (numpy.cos(numpy.pi * ((8-0.5)/(2 * 9))))))
388.     totSVFh= svfmax * part3h
389.     #ring i
390.     ringi= part1i
391.     radiusringi= ((math.pi * (200*200)) - (math.pi * (100*100)))
392.     part2i= ringi/radiusringi
393.     part3i= part2i/(2*math.pi)
394.     z1=numpy.cos(90)
395.     svfmax=(numpy.pi/2)*((numpy.sin(numpy.pi * ((9-0.5)/(2 * 9))))*
      (numpy.cos(numpy.pi * ((9-0.5)/(2 * 9))))))

```

```

# Sum the total sky-view factors in each annuli in order to get a total SVF for the image

396.      totSVFi= svfmax * part3i
397.      SVFtotal= totSVF + totSVFb + totSVFc + totSVFd + totSVFe + totSVFf + totSVFg +
          totSVFh + totSVFi
398.      originalSVF = 0.432
399.      svfmask = 0.701
400.      maskedcanopy = (svfmask/originalSVF)*100
401.      maskedcanopy2 = (maskedcanopy - 100)

#Converting to percentage leaf fall

# (sky-view factor / full canopy svf from first image of the season) *100

402.      phase1= ((SVFtotal/originalSVF)*100)
403.      phase2 = (phase1 - 100)
404.      percentagefall = ((phase2/ maskedcanopy2)*100)
405.      outputSVF=str(percentagefall)
406.      dates= str(date)

# create output .txt file to send to local server or email address

407.      with open ('SVF.txt', 'a') as f:
408.      f.write('\n' + outputSVF + " DATE " + dates)

```

Appendix Two

Email code (shell script) for the Raspberry Pi carried out using a CRONTAB code

```

#!/bin/bash

DATE=$(date +"%Y-%m-%d_%H%M")

#capture and save image

raspistill -o timelapse.jpg

#run python script in appendix 1

python thesiscode.py

#email or set up FTP for the output of python code

echo "autumnpi $date" | mpack -s timelapse SVF.txt timelapse.jpg enteremailaddresshere

```

